UNIVERSITY OF CALIFORNIA
RIVERSIDE

Supramolecular Cages with Endohedral Functionality

A Dissertation submitted in partial satisfaction
of the requirements for the degree of

Doctor of Philosophy

in

Chemistry

by

Ana Soledad Gamboa

December 2013

Dissertation Committee:

Dr. Richard J. Hooley, Chairperson
Dr. Christopher Y. Switzer
Dr. Thomas H. Morton

The Dissertation of Ana Soledad Gamboa is approved:

Committee Chairperson

University of California, Riverside

Acknowledgements

Too many people to list (I would hate to accidentally omit people that should be included if I were to have mentioned names.) Suffice to say… I would like to thank everybody that 1) made this thesis possible and 2) had an influential role in my microcosm during my time here, and furthered the evolution of my world view.

I had a beautiful time here.

I love this place.

Thank you Richard.

Dedicated to:

My parents

Jonathan

Sekhmet

Saturn

and…

to *Mein Liebe Fiend.*

ABSTRACT OF THE DISSERTATION

Supramolecular Cages with Endohedral Functionality

by

Ana Soledad Gamboa

Doctor of Philosophy, Graduate Program in Chemistry
University of California, Riverside, December 2013
Professor Richard J. Hooley, Chairperson

One of the ultimate goals within the field of supramolecular chemistry is to mimic the molecular recognition and catalytic activity of enzymes. Enzymes are more effective catalysts compared to human-made catalysts in terms of reaction specificity, rate of reaction, and capacity for substrate regulation, largely due to the characteristics (shape, size, electron density, functional groups) of the interior of the enzyme where the catalytic activity takes place. Supramolecular chemists can achieve this goal by creating assemblies with endohedral functionality that can mimic the interior cage-like nature of enzymes, mimic the asymmetric nature of enzyme active sites, and mimic the allosteric and cooperative nature of enzymes. This thesis takes steps towards achieving that goal by synthesizing and studying cages with endohedral functionality. Particularly, 1) self-assembled transition metal-ligand cages with (and without) endohedral functionality, 2) polyazacryptand cages with homo and hetero dinuclear metallation, and 3) allosterically regulated hydrogen bisulfate anion binding of a series of azacryptand ureas.

TABLE OF CONTENTS

Supramolecular Cages with Endohedral Functionality

Chapter 2: TREN Cages with Endohedral Functionality

Chapter 3: Synthesis and Study of Tripodal Azacryptand-Ureas

Chapter 6: Experimental Section

List of Figures

Chapter 1: Supramolecular Cages with Endohedral Functionality

Chapter 2: TREN Cages with Endohedral Functionality

Chapter 3: Synthesis and Study of Tripodal Azacryptand-Ureas

List of Tables

Chapter 3: Synthesis and Study of Tripodal Azacryptand-Ureas

Chapter 5: Metal-Ligand Self-Assemblies with Linear and V-Shape Ligands

Chapter 6: Experimental Section

Chapter 1

Supramolecular Cages with Endohedral Functionality

Overview

This dissertation focuses on the synthesis, characterization, molecular recognition and reactivity of supramolecular cages with endohedral functionality.

1.1. Introduction

Supramolecular chemistry is the study of self-assembly and the formation of bonds to form large discrete complexes from relatively simple subunits. The forces that dictate the spatial organization of a supramolecular complex vary from weak intermolecular forces to strong covalent bonding. Weak forces include hydrogen bonding, hydrophobic forces, metal coordination, π-π interactions, van der Waals forces, salt bridges and electrostatic effects.[1]

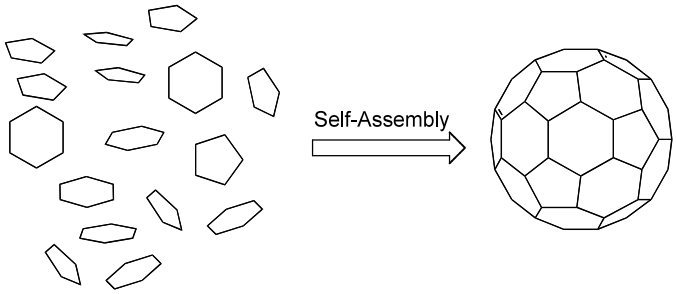

Figure 1.1: Self-assembly is the spontaneous and reversible organization of molecules into larger, more complicated arrangements. This concept is analogous to scattered hexagonal and pentagonal pieces of a soccer ball spontaneously assembling to form the shape of a ball.[2]

Several supramolecular complexes with biological importance are made from a repeated series of simple and identical building blocks. A well-known example of this is apoferritin, a protein that is self-assembled from twenty-four identical subunits by weak interactions such as hydrogen-bonding, π-π interactions and Van der Waals interactions. Apoferritin has octahedral symmetry and an internal cavity with a volume of approximately 230 nm^3, it can hold up to 4500 iron atoms as ferric hydrous oxides.[3]

Cyclodextrin, carcerands and hemi-carcerands are supramolecular structures that were previously common to study.[4] Over the past few decades, studies on self-assembled architectures via metal-ligand connections, hydrogen bonds, or dynamic covalent bonds have become common.[5] Self-assembled complexes have been shown to have a wide variety of uses, particularly the ability to stabilize highly reactive species (like the pyrophoric white phosphorus),[6] or to catalyze various reactions (*e.g.* unimolecular rearrangements, C-H activation and Diels-Alder reactions with unusual selectivities),[7] which will be discussed further on in this chapter. Like many enzymes, supramolecular metal organic cage complexes have an enclosed cavity capable of encapsulating suitably sized guests.

There are two models for enzyme-substrate binding; the lock and key model and the induced fit model.[8] The lock and key model is antiquated and overly simplistic, because the proteins are conformationally dynamic in solution, yet it remains useful for explaining binding phenomena. The lock is represented as the active site of the enzyme, and the key is the substrate. Just like a lock and a key, only a substrate of a specific size and shape can fit in the appropriate enzyme.

The induced fit model takes into account the flexible nature of enzymes, where the active site is able to modify its size and shape by varying degrees to accommodate the optimized binding of a substrate. Consequently, this allows the substrate to alter the properties of an enzyme by having modified its shape. A large part of an enzyme's efficiency is due to its ability to selectively recognize and bind a substrate. Enzymes often bind their substrates to be catalyzed in a self-contained interior cavity. The interior conditions of the enzyme (a synergistic combination of size, shape, space, functional group availability and proximity and electronic effects) give rise to the enzyme's substrate selectivity, reaction selectivity, stereoselectivity and overall catalytic capability.

The coenzyme Cytochrome P450 for example, binds to oxygen and uses it as a substrate to oxidize C-H bonds.[9] Consequently, developing supramolecular structures that mimic enzymes is one approach to improving the ability to control the rate and selectivity of chemical reactions.[4a, 10]

The chemical reactivity that takes place in most cage structures is largely limited to single molecule rearrangements, and examples of two or more molecules combining to react are very rare.[11] Other than irregular distributions of electron density, the interior cavities of these clusters are largely devoid of facets that would promote chemical reactions to occur. Enzymes, however, contain various functional groups in their interior cavities that actively take part in enabling reactions to occur.

Even though self-assembly has been a topic of study for the past few decades, to date there have been relatively few examples of self-assembled complexes with endohedral functionality. This chapter will provide an overview of the design, reactivity

and molecular recognition of supramolecular cage structures with endohedral functionality.

1.2. Design of Supramolecular Functionalized Cages

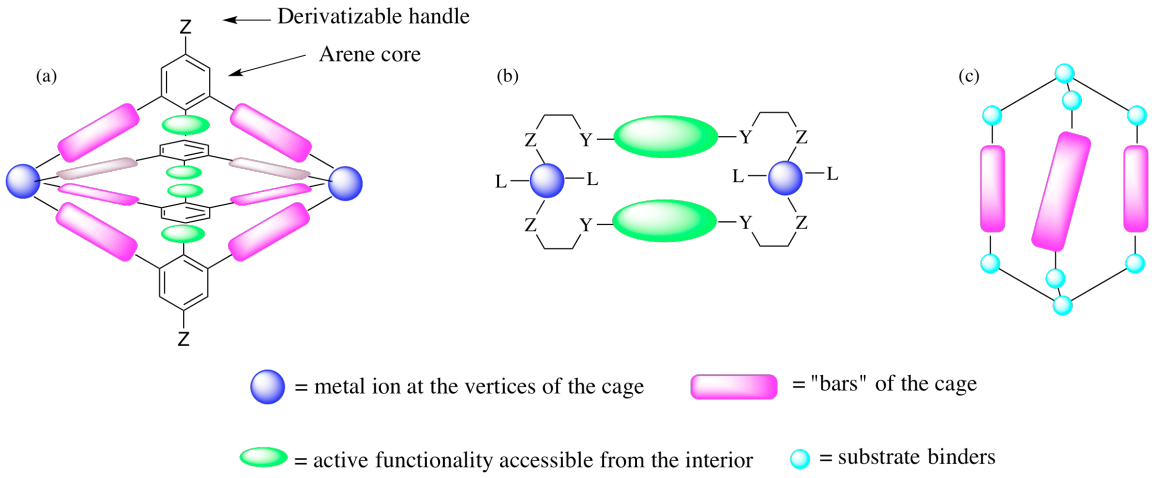

Figure 1.2: a) Endohedral functionality incorporated into the "building block" that is accessible inside the cage. b) Cage with an active site on the wall, and c) Cage with interior binding sites.

In order to properly mimic enzymes, it is necessary to synthesize supramolecular cages with endohedral functionality that actively engage in molecular recognition and/or catalysis. Water-soluble artificial cages are preferred because they provide the supramolecular cage structure with a similar environment to enzymes. This has several favorable consequences: 1) a great range of guests can be studied because the interior core of these cages are hydrophobic, thereby minimizing guest competition from the solvent 2) organic substrates are often insoluble in water, and the hydrophobic interior core of a cluster can provide an environment for organic reactions to occur under mild aqueous conditions.

There are three main strategies currently used to introduce endohedral functionality to a macrocyclic cage:

1) Incorporating a functional group on the cage where the endohedral functionality points inwards (*e.g.* ureas, amines, etc.)

2) Using the walls of the cage as an active species (*e.g.* porphyrin rings, metal salen complexes, etc.)

3) Incorporating a binding pocket in the interior of the cage with functionalities that can bind to substrates that can act as the active functionality, or be active functionality themselves (*e.g.* amines and imines.)

These strategies will be discussed further in the chapter.

1.2.1. Transition Metal-Ligand Self-Assembly

Over the last twenty-five years, studies in transition metal-ligand self-assembly has been on the rise, producing various polyhedra.[1b] The shape of these metal-ligand self-assemblies can be controlled by the metal coordination geometry and the approach angle of the metal coordinating group. For practical purposes, transition metal-ligand self-assembly will be defined as:

> *(a) self-assembling units [that] are held together by coordinative interactions; (b) the assembling of subunits into larger aggregates is selective- the subunits bind cooperatively to form the most stable aggregate; (c) the aggregates can be recognized by their properties that differ from those of the individual components; (d) the aggregates are discrete rather than infinite.*[1a]

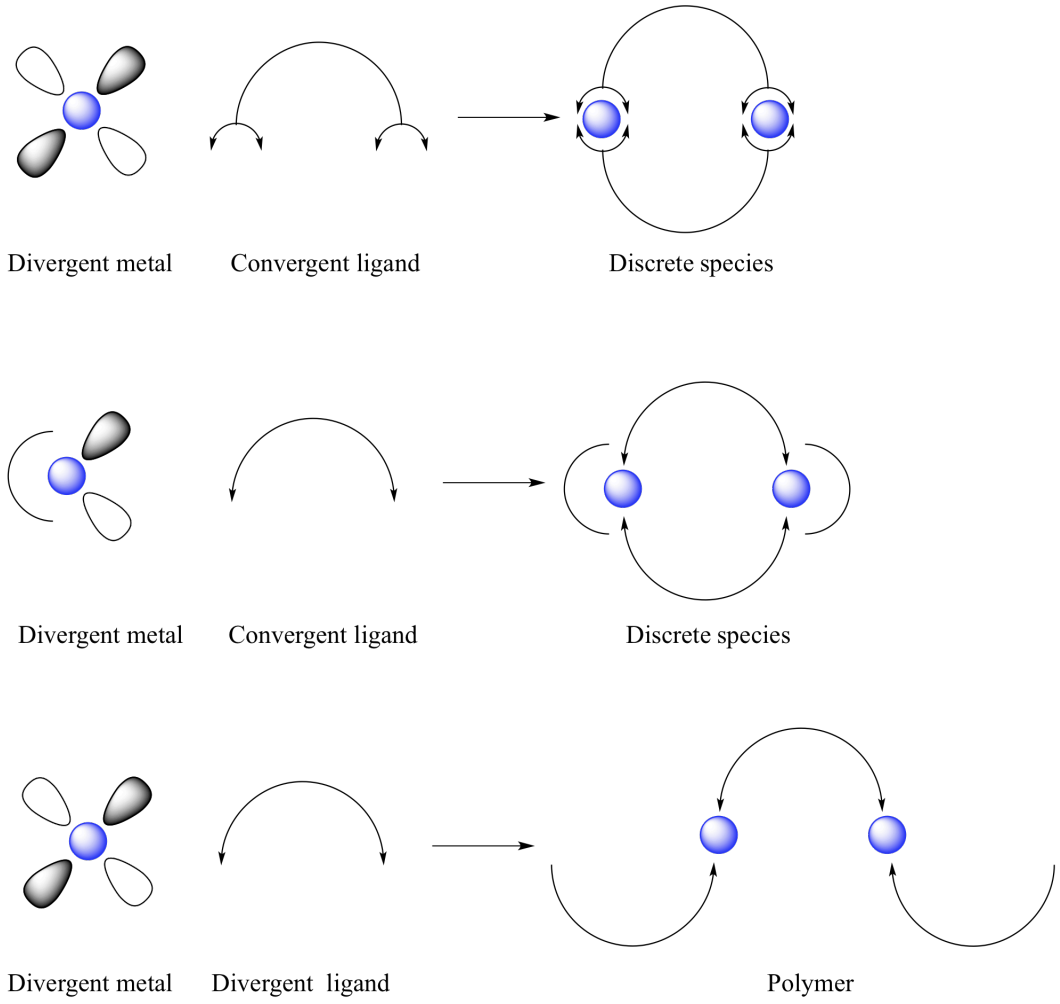

Figure 1.3: The formation of a discrete species or a polymer can be controlled based on the approach angle of the metal coordinator.[12]

There are three general approaches to transition metal-ligand self assembly, which will be discussed in this chapter. They are the molecular library approach, the symmetry interaction approach, and the weak-link approach. Mechanically bonded supramolecular structures will not be discussed since they stray from the topic of this thesis, but the interested reader can be referred to the article titled *Molecular Machines.*[13]

1.2.2. The Symmetry Interaction Approach

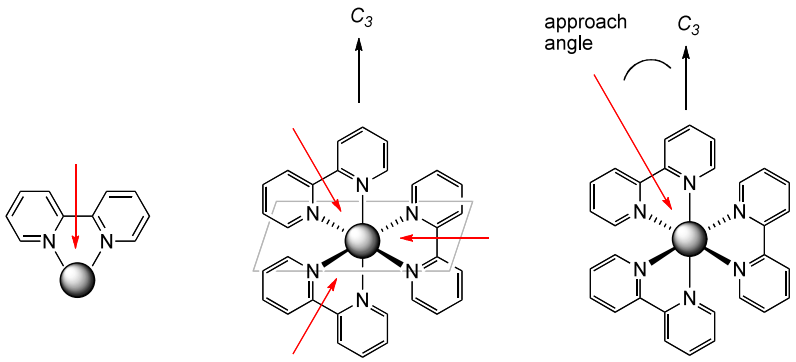

Figure 1.4: The symmetry interaction approach: a) Coordination vector for a bidentate ligand. b) Chelate plane (orthogonal to the axis of symmetry.) c) Shown here for an octahedral metal with a C_3 axis of symmetry, the approach angle for a bidentate chelator.[1a]

This model uses ligands with multi branched chelating ligand and "naked" metal ions to form a thermodynamically favored supramolecular complex. Higher binding constants are obtained due to the chelation effect than with monodentate ligands.[1a] The shape of the supramolecular complex is dependent on:

1) The coordination geometry and coordination number of the metal center.

2) The orientation of the coordinating vector (the vector that bisects a multidentate chelating group in the direction towards the metal center.)

3) The ligand's approach angle in relation to the metal (the angle between the metal coordination vector and the major axis of symmetry of the supramolecular complex.)

In principle, it is possible to form ligand-metal supramolecular complexes of any symmetry. To illustrate what role these principles play in the design of a polyhedron, examine the design of a M_2L_3 triple helicate and an M_4L_6 tetrahedral complex.

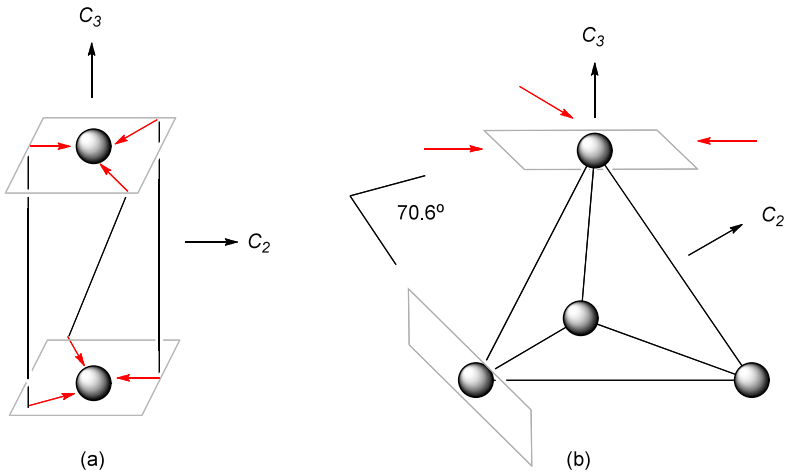

Figure 1.5: a) M_2L_3 D_3 helicate and b) M_4L_6 tetrahedron cage.[1a]

The simplest multi-metal ligand-metal supramolecular cage is the M_2L_3 triple helicate. Two metals form at opposite ends of the cage and are bridged by C_2 symmetric ligands. To form a M_2L_3 triple helicate having D_3 symmetry using the symmetry interaction approach, the cage complex must have three identical C_2 symmetric ligands that are perpendicular to the axis of highest symmetry (C_3) in the cage, and the two chelate planes must be parallel.

Another cage with the same metal:ligand ratio as the M_2L_3 cage is the M_4L_6 tetrahedron where six ligands form the edges of the tetrahedron and four metal ions function as the vertices of the polyhedron. All metal coordinating vectors must lie within the plane of chelation, a theoretical angle of 70.6° must exist between the two chelating vectors within the same ligand. It has also been calculated that the closer the approach angle is to 35.3° the higher the likelihood of a M_4L_6 cage being formed instead of a M_2L_3 cage.[1a]

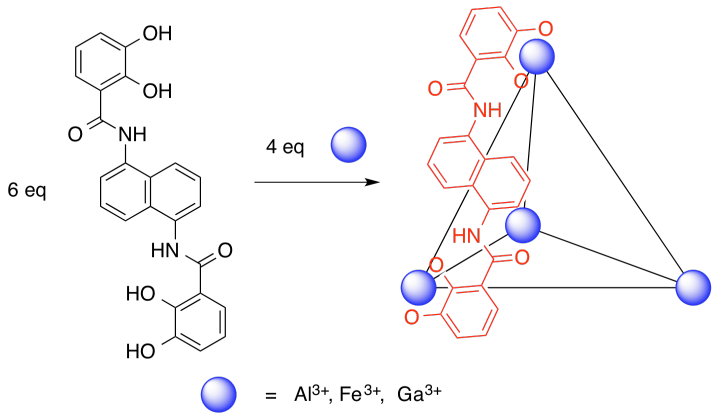

Figure 1.6: M_4L_6 tetrahedron cage.[14]

An interesting and extensively studied M_4L_6 cage with *bis*-bidentate catechol amide ligands that was made via the symmetry interaction approach is one shown in **figure 1.6**. The cage is chiral, and depending on the chiralities at the metal vertices, the cluster cage can have C_3 (ΔΛΛΛ/ ΛΔΔΔ), S_4 (ΔΔΛΛ/ΛΛΔΔ), or T (ΛΛΛΛ/ΔΔΔΔ) symmetry. The molecular recognition and catalytic activity of this tetrahedral cage will be discussed later on in this chapter.

Another interesting example of an M_4L_6 tetrahedron cage is the one shown in **figure 1.7**. The cage was formed via "multi component self-assembly", a method of self-assembly where multiple subcomponents self-assemble to form a polyhedron, as opposed to two building blocks, *e.g.* an intact ligand and a metal salt. This particular cage is formed in water with 4,4'-diaminobiphenyl-2,2'-disulfonic acid, and 2-formylpyridine as subcomponents with iron sulfate and a base.[15]

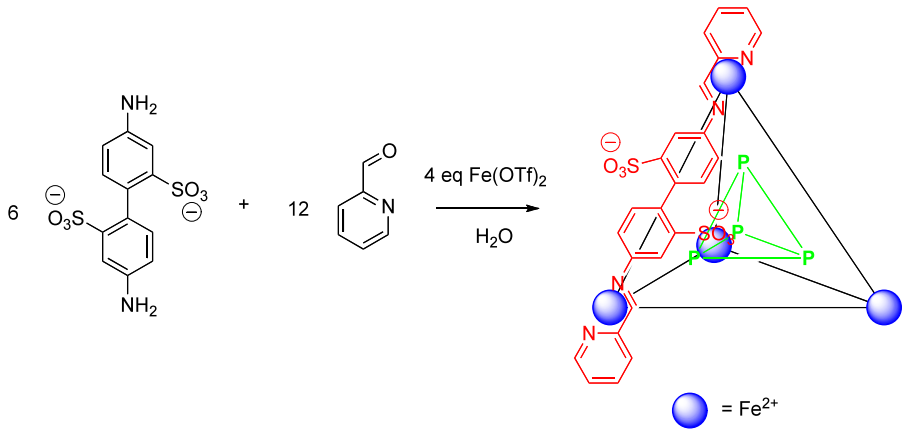

Figure 1.7: M_4L_6 tetrahedron cage with white phosphorus as a guest.

This cage is water soluble, and its hydrophobic interior makes it a suitable host to bind hydrophobic guests. This cage forms a host-guest complex with cyclohexane when it is present during the self-assembly process in water. Despite cyclohexane's volatility, it is so tightly bound in the cage that cyclohexane did not evaporate under vacuum. Upon addition of acid, the cage decomposes to starting material, thereby liberating the guest, and the host-gust complex is re-assembled upon addition of base. Upon addition of *tris*(aminoethyl)amine, the cage irreversibly disassembles to 2-formyl pyridine and Fe(II) react with *tris*(aminoethyl)amine to form a mononuclear Fe(II) complex. The driving force for this imine exchange is both enthalpic and entropic. The electron poor arylamine is replaced by an electron rich alkylamine, thereby increasing the overall number of molecules formed.

The same cage can bind pyrophoric white phosphorus (P_4) as a guest, where it becomes air stable upon encapsulation. P_4 is stable in the interior of the cavity due to size restrictions of the cage on the transition stage of the reaction between O_2 and P_4.[6]

1.2.3. Molecular Library Approach

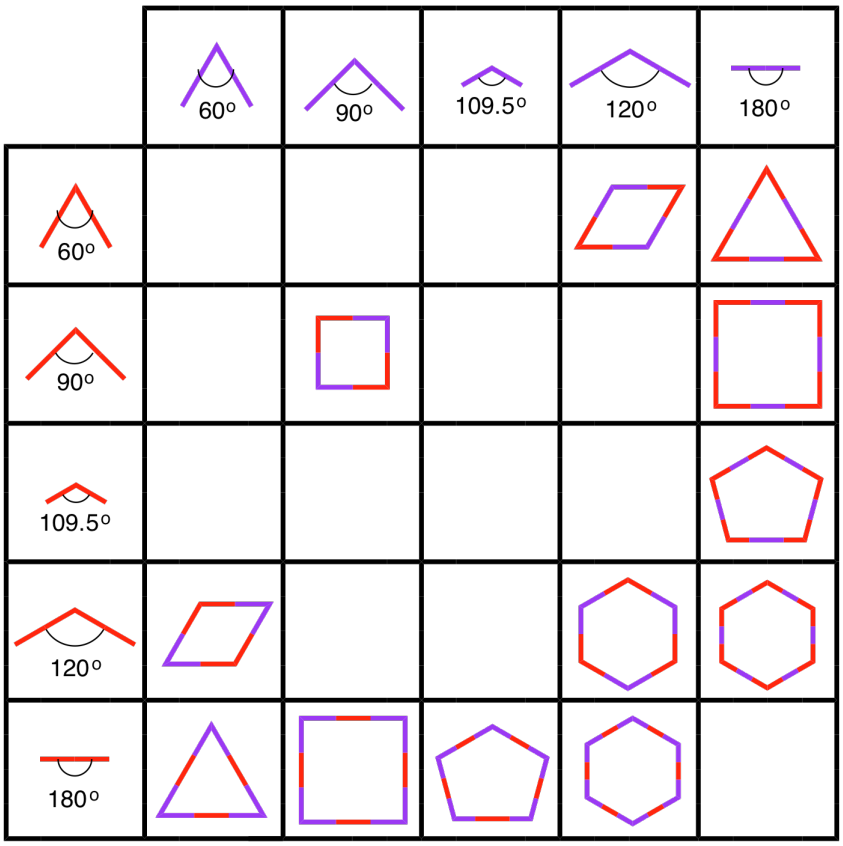

Figure 1.8: A library of the possible 2D polyhedra that can be formed via the systematic combination of ditopic subunits with fixed angles.[1a]

The molecular library approach, also known as the directional bonding approach, entails the self-assembly between multi-branched monodentate ligands and metal centers that can create a wide variety of 2D and 3D macrocycles. This approach has two

requirements for self-assembly; first, the ligands must be sufficiently rigid with well-defined metal coordinating angles and secondly, the appropriate ratio of ligand to metal must be used. If ditopic metal coordinating groups are used, then 2D macrocycles will be obtained. To obtain 3D macrocycles, at least one of the ligands has to have three binding sites (see **figure 1.8**.)

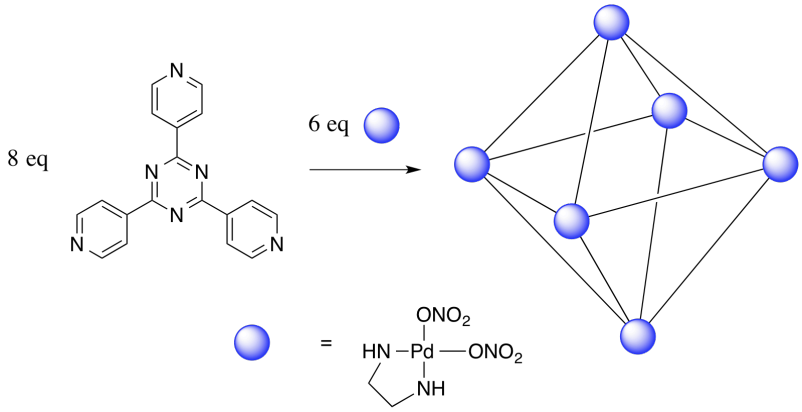

Figure 1.9: Formation of a 3D octahedron.

A well-studied octahedron cage that was assembled via the molecular library is shown in **figure 1.9**.[16] It is also an example of the molecular paneling approach, which is a term coined to describe the formation of 3D polyhedra by using panel-like organic ligands with more than two metal coordinating sites that are paneled together by an appropriate metal.[17] The nature of the *cis*-protected $Pd(en)_2(NO_3)_2$ allows for the two nitrate ligands that are 90° in relation to each other to be displaced by pyridine metal coordinating groups, thereby biasing the formation of a convergent discrete cage complex as opposed to a divergent polymer (**figure 1.3**.) This cationic cage (overall charge of 12+) is stable, water soluble, and has been found selectively to undergo bimolecular recognition with flexible alkanes and large planar aromatic molecules,[18] encapsulate

peptides[19] and host catalysis[7] that occurs in the interior. The catalytic activity of this octahedron cage will be discussed later on in this chapter.

1.2.4. Weak Link Approach

The weak link approach (WLA) entails the use of hemilabile ligands and transition metals to form structurally flexible supramolecular assemblies.[20] The bidentate metal coordinating group of the hemilabile ligands have different affinities for the metal center. When the hemilabile ligand initially coordinates to the metal, the kinetic product, a "closed" sandwich-like structure is formed. This closed structure can be opened up via the selective displacement of the weaker metal-ligand bond via the addition of a stronger ligand (*e.g.* the ancillary ligand) leading to the formation of the thermodynamically controlled product, an "open" structure that allows space for guests to be recognized.

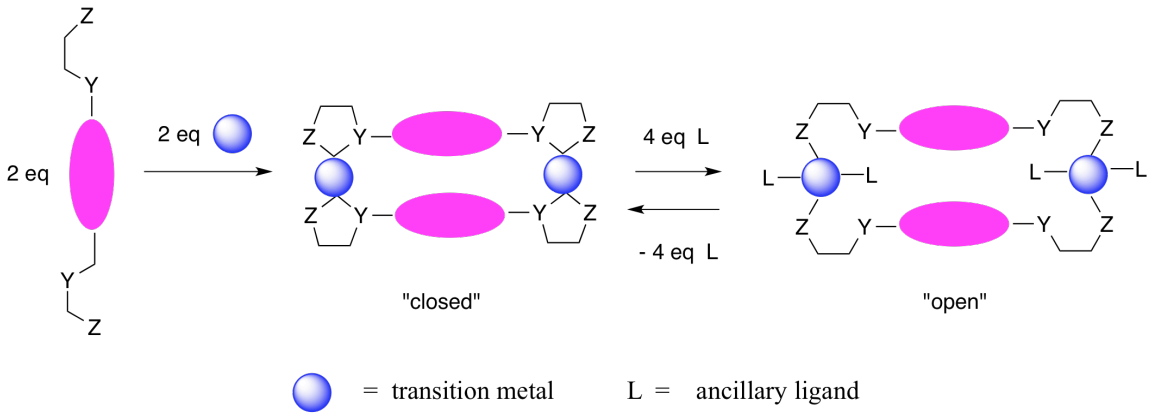

Figure 1.10. Formation of supramolecular macrocycles via the WLA.

The designed properties of this kind of supramolecular macrocycle, where conformational changes can be controlled by external factors have led to applications in

allosteric catalysis, molecular sensing, and host-guest chemistry,[20a] as will be discussed further in this chapter.

1.2.5.1. Non-Transition Metal Based Self-Assembly

The thermodynamically controlled self-assembly of cages that do not require the use of a transition metal as a structural unit are typically done via hydrogen bonds, van der Waals forces and charge-charge interactions, or the use of imines, boronate esters, and disulfides as dynamic covalent bonds. This chapter will briefly cover hydrogen bonds and imine bonds in the self-assembly of supramolecular cages. The interested reader can be referred to the following references for the other strategies not covered.[21]

1.2.5.2. Hydrogen Bonding Self-Assembly

The hydrogen bond is the interaction between an electronegative atom (e.g. nitrogen and oxygen) and a hydrogen atom. It is an important non-covalent interaction in the formation of supramolecular assemblies due to its strength (1 to 7 kcal/mol) and geometric directionality. Hydrogen bond donors have a hydrogen atom attached to an electronegative atom, thereby inducing a partial positive charge on the hydrogen. A hydrogen bond acceptor is an electronegative atom that is attracted to the electropositive hydrogen, thereby forming a hydrogen bond.

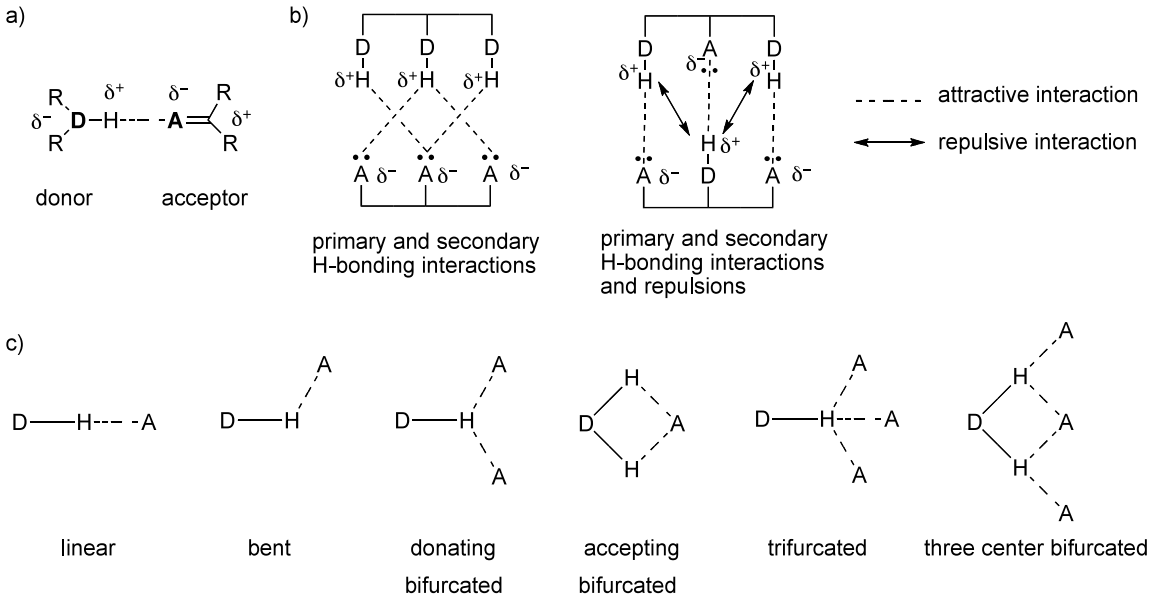

Figure 1.11: a) A hydrogen bond between a donor and acceptor pair, where the donor atom in this example can be a nitrogen and the acceptor atom can be oxygen. B) Primary and secondary interactions and repulsions in molecules with multiple hydrogen bonding sites c) Types of hydrogen bonding geometries.[12]

Because of the fixed geometries of hydrogen bonding systems, designing hydrogen bonded self-assembled systems can be done with some ease. Self-assembly of hydrogen bonded dimeric cages have been observed with cyclodextrins, carcerands, calix[4]arenes.[22] Further discussion on this topic can be found in Chapter 3, where the discussion on the synthesis and study of tripodal azacryptand ureas will be discussed.

1.2.5.3. Imine-Based Self-Assembly

Azomethine linkages are an effective method used in the construction of macrocycles. These reactions entail the condensation of primary amines with aldehydes which form imine bonds (Schiff bases) as the thermodynamic product and water as the byproduct.[23]

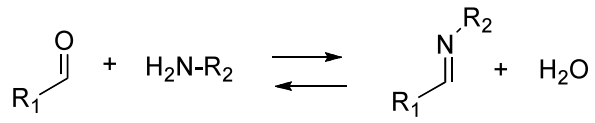

Figure 1.12: The reversible formation of the imine bond.

Because of the reversible nature of the imine bond, they are commonly used in dynamic combinatorial chemistry (DCC). More often than not, imines can be readily reduced (more often than not) to their corresponding amine by using sodium cyanoborohydride or sodium borohydride.

Due to the presence of lone pair electrons on the nitrogen atom, imines and amines can coordinate to transition metal ions. This can be a useful scaffold to incorporate endohedral functionality in a macrocycle, which we will be discussed later in this thesis.

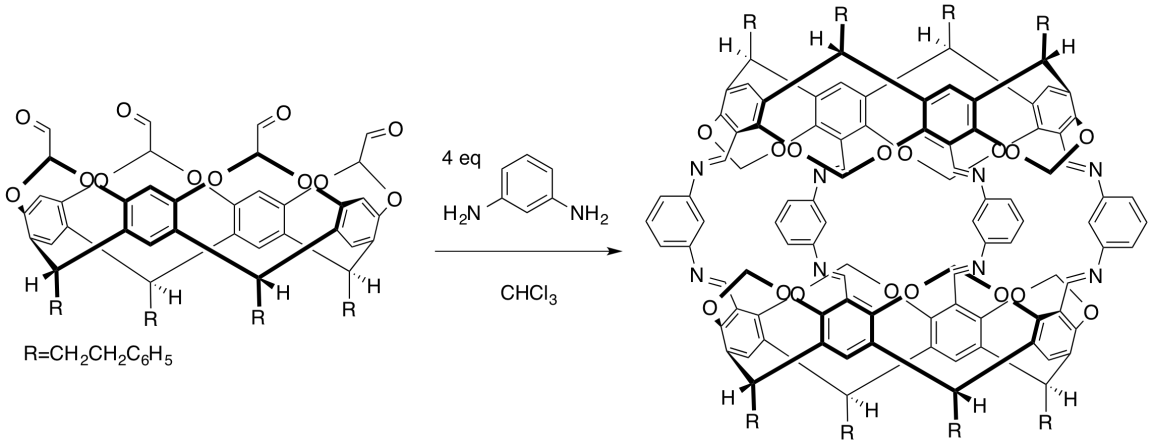

Figure 1.13: Formation of a hemicarcerand cage by imine condensations.

The covalent linkage of two cavitands forms a cage with enclosed space. This class of supramolecules are called "carcerands", from the Latin word *carcer*, to imprison. An example of one entails the imine condensation of four equivalents of 1,3 diaminobenzene with a cavitand with four formyl sites to form the hemicarcerand.[24]

1.3. Practical Applications of Supramolecular Cages with Endohedral Functionality

Enzymes are more effective catalysts than synthetic catalysts in terms of reaction specificity, rate of reaction, and capacity for substrate regulation, largely due to the characteristics (shape, size, electron density, functional groups) of the interior of the enzyme where the catalytic activity takes place. This section will cover some of the supramolecular cages that have been reported in the literature, where their endohedral characteristics play a crucial role on their molecular recognition and catalytic capabilities.[25]

1.3.1. Catalytic Activity of Supramolecular Cages with Endohedral Functionality

A deep cavitand has been shown to undergo the regioselective acid catalyzed epoxide ring opening and cyclization of 1,5 epoxyalcohols in an "open cage-like" deep cavitand with a carboxylic acid group pointing inside as the endohedral functionality.[26] The open-ended cage takes on a bowl type conformation that is stabilized by intramolecular hydrogen bonds between the secondary amides at the opening of the cage. The interior functionality consists of eight electron rich aryl rings, which make up the walls of the cage, where the π surface of the aryl rings can be used to bind substrates.

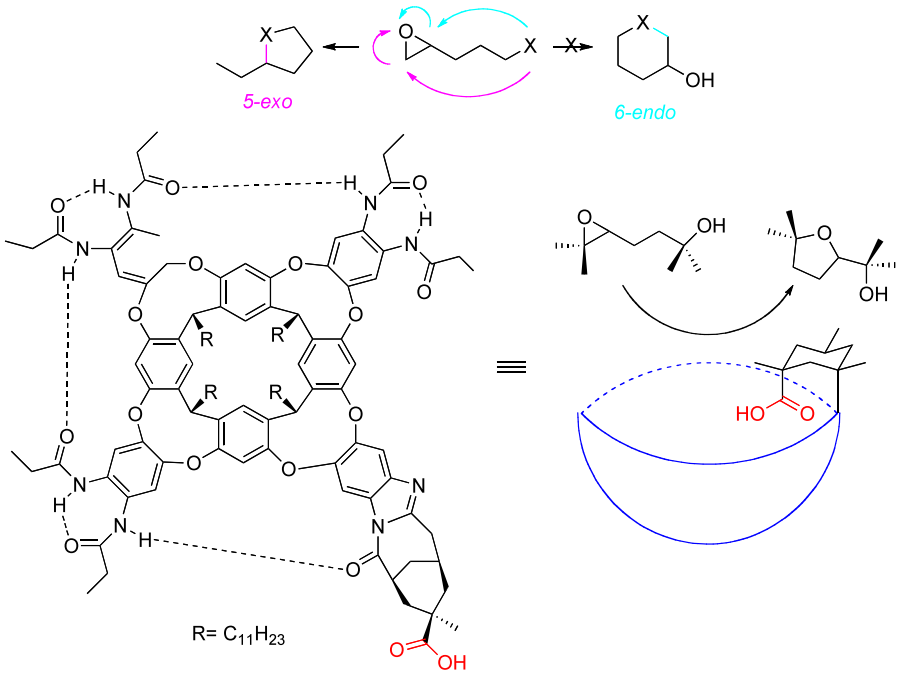

Figure 1.14: Cavitand with a carboxylic acid as an endohedral functional group.

Upon addition of the epoxyalcohol to a solution of the cavitand cage in mesitylene, host-guest binding was immediately observed, and the five-membered ring exo alcohol was exclusively observed, instead of the six membered ring endo alcohol. The reaction was found to be accelerated 50-fold by the endohedral functionalized cage, compared to the reaction using an analogous non-supramolecular acid catalyst. The enhancement of the rate is due to the increase in effective molar concentration between the substrate and the catalytically active Brønsted acid site within the confines of the interior of the cage, coupled with the ability of the alkyl chain of the substrate to coil inside the cavitand, bringing the substrate and catalytic site in closer proximity.[27] The preference in regioselectivity is attributed to the geminal methyl groups of the substrate from multiple CH-π contacts with the aromatic walls of the cage, which in turn restricts

the conformational flexibility of the alkyl chain, thereby stabilizing the five membered ring transition state, which leads to the exclusive formation of the exo alcohol.

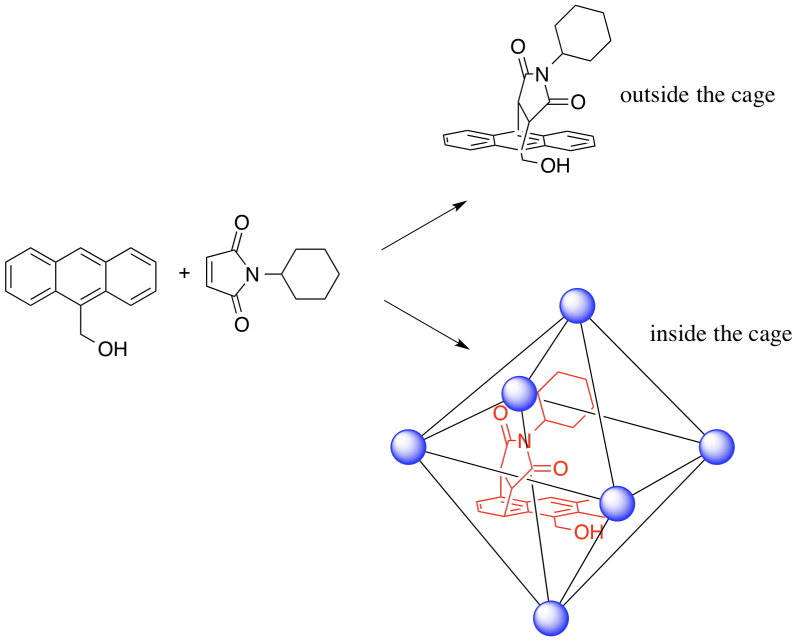

Figure 1.15: Unusual regioselectivity of a Diels-Alder reaction.

The octahedron cage mentioned in **figure 1.9** has been observed to host the formation of an unusual regioselective Diels-Alder product. Even though the cage does not have any interior functionality, it is a good example on how the shape of the cage can force the exclusive formation of what would otherwise be an unfavorable product. The reaction took place in water between 9-hydroxylmethyl anthracene and N-cyclohexylmaleimide in the hydrophobic interior of the cage. Normally, the dienophile undergoes a [4+2] cycloaddition with anthracene to give the 9,10-adduct. Due to spatial constraints in the interior of the cavity, however, cis addition at the terminal site is observed in 98% yield.

1.3.2. Allosteric and Cooperative Catalysis in Macrocyclic Cages

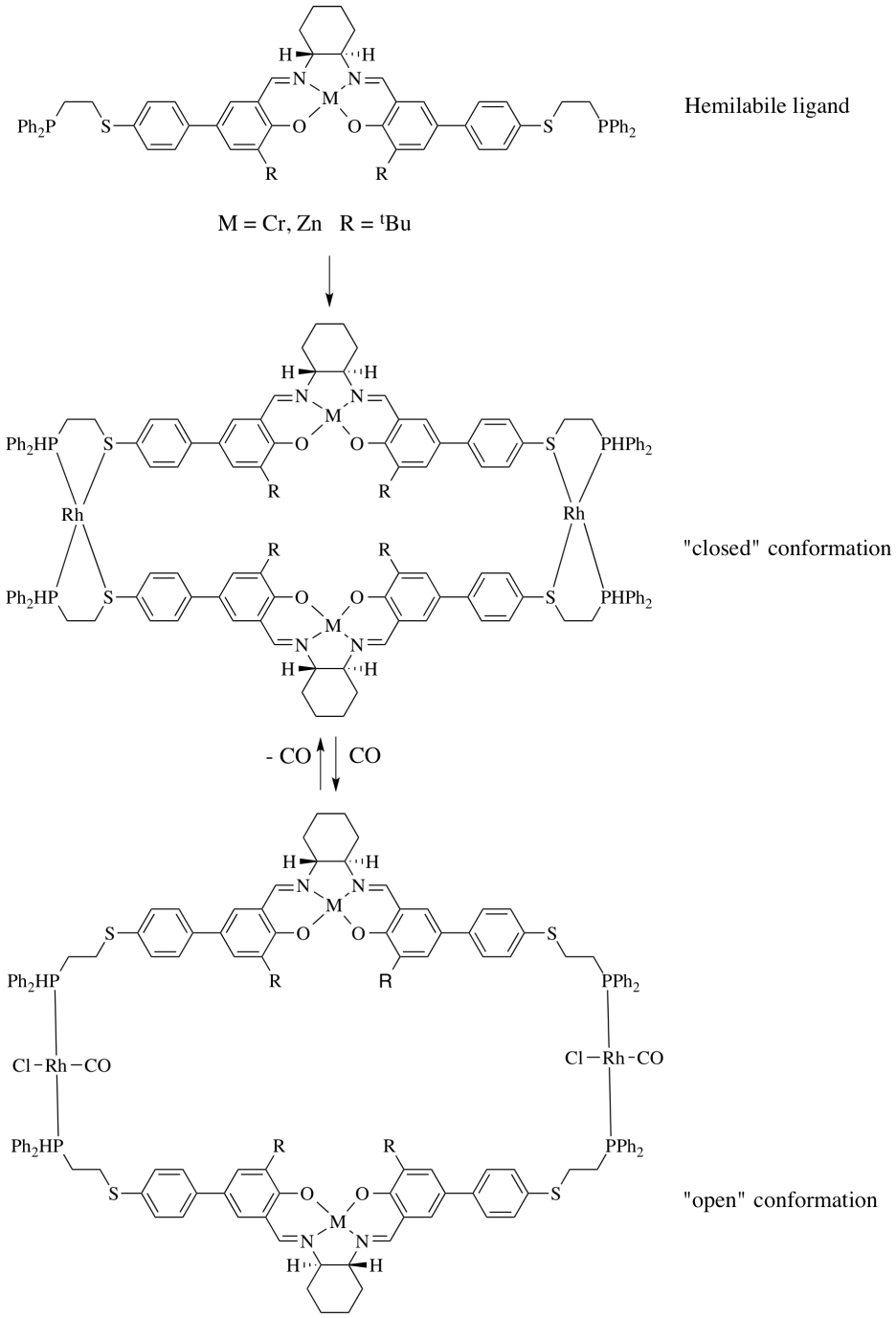

Figure 1.16: A supramolecular allosteric catalyst made via the weak link approach.

An early example of an allosteric supramolecular catalyst was made via the weak-link approach.[28] This is an example of cooperative catalysis taking place in the interior of the supramolecular complex. The formation of an allosteric supramolecular catalyst via the weak-link approach is a useful method yielding cavities that can be "opened" and "closed" in a reversible fashion by an external source (ancillary ligand), thereby regulating the catalytic activity that takes place in the interior of the macrocycle.

This catalyst uses a bimetallic Cr(III) salen complex as the catalytic active sites of the macrocycle.[29] The kinetic product of the macrocycle was obtained in quantitative yield by reacting the Cr(III) salen complex with Rh-(norbornadiene)$_2$BF$_4$ in CH_2Cl_2. At this "closed" state, there is not enough space for a substrate to fit in the interior to undergo cooperative catalysis. Upon addition of an ancillary ligand such as CO and PPNCl as the chloride source in benzonitrile at room temperature, the macrocycle opens via displacement of the weakly binding sulfides on the Rh by the stronger binding CO and Cl^- ligands.

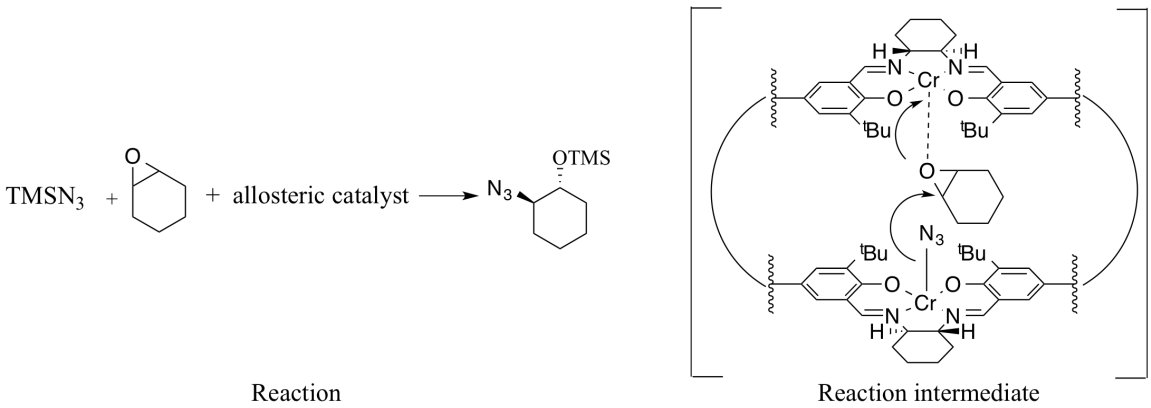

Figure 1.17: Ring opening epoxidation and the proposed intermediate.

The "open" thermodynamic product allows enough space for substrates to undergo catalysis at both Cr(III) sites. This system was found to act as an allosteric catalyst for the ring opening of cyclohexane oxide by $TMSN_3$ to yield *trans* 1-azido-2-(trimethylsiloxy)cyclohexane with 68% ee, and was found to catalyze this reaction 20 times faster than the monomeric analog, which was found to give 12% ee. This principle shows the importance of having two active sites in close proximity. The azide opens the epoxide ring that is held in place via a weak dative bond between the lone pairs on the oxygen and the nearby Cr(III) site. The catalytic activity can be deactivated upon removal of the solvent, in vacuo, resulting in the "closed" conformation of the macrocycle.

A small dinuclear Cu(II) azacryptand cage[30] has been reported to cleave the C-C bond of acetonitrile at room temperature to form a cyanide-bridged complex and methanol as the byproduct. The interested reader can be referred to other (non-cage) allosteric systems that have been developed from the weak-link approach, which are beyond the scope of endohedral cages.[31]

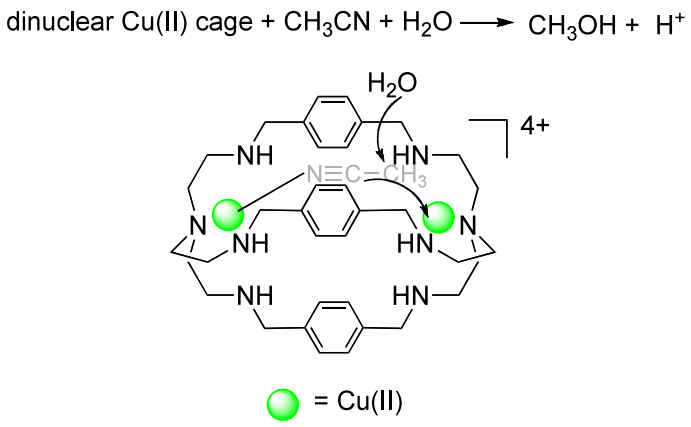

Figure 1.18: C-C bond activation within an azacryptand macrocycle with dinuclear Cu(II) endohedral functionality.

The proposed mechanism entails a nitrogen atom of acetonitrile binding at a Cu(II) site while electron density from the π orbital of the sp-hybridized carbon on the acetonitrile molecule binds to the Cu(II) site on the other side of the cage. This increases the electrophilicity of the terminal carbon, resulting in nucleophilic attack from water to form methanol and the cyanide-bridged complex in the interior of the cage.

Another example of a dinuclear Cu(II) azacryptand cage complex capable of catalytic activity[32] is a luminescent cage[33] containing an anthracene unit that can oxidize water to oxygen via the photoinduced reduction of Cu(II) to Cu(I).

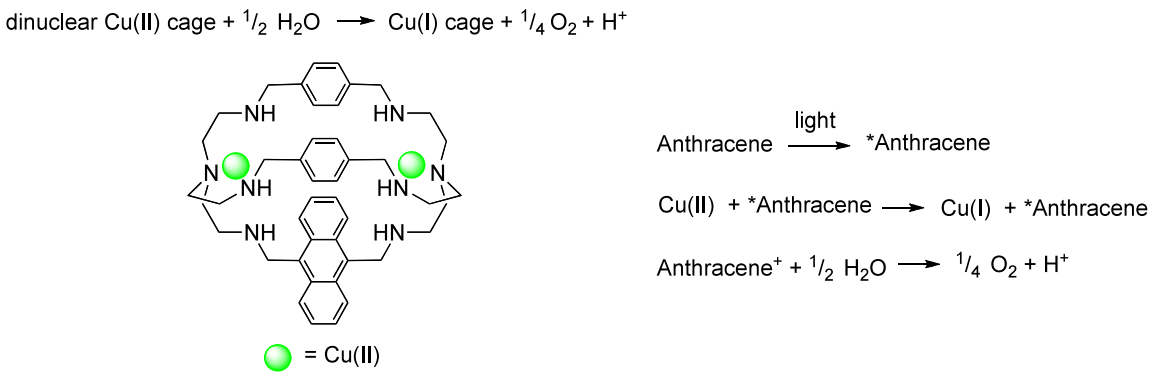

Figure 1.19: Oxidation of water to oxygen from the photoinduced reduction of Cu(II) to Cu(I) within the interior of an azacryptand cage.

Upon IR radiation, the ground state anthracene unit absorbs light, the adjacent Cu(II) sites get reduced to Cu(I) via electron transfer from the excited anthracene unit, and an anthracene radical cation is formed. The cationic anthracene gains an electron from water (the sacrificial electron donor in the process) to reform the neutral anthracene ground state, and water gets oxidized in the process, generating O_2 and H^+. It was also observed that the photocatalytic reaction did not occur when the dinuclear Cu(II) cage

was replaced with anthracene or 9.10-bis(chloromethyl)anthracene. This provides evidence for the importance of the cavity of the molecule, which captures the water molecules and is able to bring them to close proximity to the endohedral catalytically active site.

1.4. Closing Remarks

The ultimate goal in the creation and study of cages with endohedral functionality is to mimic the superior catalytic and molecular recognition properties of enzymes. This thesis takes steps towards achieving that goal by synthesizing, or taking steps to synthesize various cages with endohedral functionality.

Chapter two covers the synthesis of a series of ellipsoidal azacryptand cages of different sizes and shapes, where the interatomic distances of the metal sites are varied. The formation of heterodinuclear coordination complexes with Fe(II)•Cu(I) and Cu(I)•Ni(II) were observed in a polyazacryptand cage with symmetrical binding sites. In addition, the unusual observation of monometallation was observed with Cu(I) and Zn(I). Mixed metal complexes are of interest as models for metalloenzyme active sites.

Chapter three discusses an azacryptand urea system with an interior metal binding site and terminal urea anion binding fragments that were synthesized and found to selectively bind to hydrogen bisulfate. Pre-organization of the azacryptand with Cu(I) as an allosteric effector at the metal binding site brought the three urea sites in closer proximity, thereby increasing the hydrogen bisulfate binding affinity. An allosteric effect was observed where the K_a of hydrogen bisulfate binding is 2.8 times higher with the

metallated azacryptand (3.3 x10^2 M^{-1}) than the unmetallated azacryptand. This allosteric system is reversible upon excess addition of KCN.

Chapter four discusses the self-assembly efforts of C_3 symmetric tripodal ligands with three bidentate metal binding sites and metal ions with tetrahedral and octahedral coordination geometries, and the full characterization of a water soluble M_4L_6 *p*-rosaniline derived pyridine imine tetrahedron cage with Fe(II) and a *p*-rosaniline derived pyridine imine M_3L_2 trigonal bipyramide cage with Cu(I).

Chapter five describes the synthesis and properties of M_2L_4 palladium-pyridyl cages, and M_2L_3 pyridine-imine Fe(II) cages, one with an amino group as the endohedral functionality. And finally, this thesis concludes with chapter six, the experimental section.

References

1.) (a) Leininger, S.; Olenyuk, B.; Stang, P. J. "Self-Assembly of Discrete Cyclic Nanostructures Mediated by Transition Metals" *Chem. Rev.* **2000**, *100*, 853-908; (b) Northrop, B. H.; Zheng, Y. R.; Chi, K. W.; Stang, P. J. "Self-Organization in Coordination-Driven Self-Assembly" *Angew. Chem. Int. Ed.* **2009**, *42*, 1554-1563.

2.) Fujita, M. "Gallery of Our Molecules" http://fujitalab.t.u-tokyo.ac.jp/static/html/res0-e.html (accessed 2013).

3.) Pluth, M.; Raymond, K. "Reversible Guest Exchange Mechanisms in Supramolecular Host-Guest Assemblies" *Chem. Soc. Rev.* **2007**, *36*, 161-171.

4.) (a) Breslow, R.; Dong, S. D. "Biomimetic Reactions Catalyzed by Cyclodextrins and Their Derivatives" *Chem. Rev.* **1998**, *98*, 1997-2011; (b) Vriezema, D.; Aragones, M.; Elemans, J.; Cornelissen, J.; Rowan, A.; Nolte, R. "Self-Assembled Nanoreactors" *Chem. Rev.* **2005**, *105*, 1445-1489.

5.) (a) Schneider, H. J. "Binding Mechanisms in Supramolecular Complexes" *Angew. Chem. Int. Ed.* **2009**, *48*, 2-56; (b) Safont-Sempere, M. M.; Fernández, G.; Würthner, F. "Self-Sorting Phenomena in Complex Supramolecular Systems" *Chem. Rev.* **2011**, *111*, 5784-5814.

6.) Mal, P.; Breiner, B.; Rissanen, K.; Nitschke, J. R. "White Phosphorus is Air-Stable Within a Self-Assembled Tetrahedral Capsule" *Science* **2009**, *324*, 1697-1699.

7.) Yoshizawa, M.; Klosterman, J. K.; Fujita, M. "Functional Molecular Flasks: New Properties and Reactions within Discrete, Self-Assembled Hosts" *Angew. Chem. Int. Ed.* **2009**, *48*, 3418-3438.

8.) Voet, D.; and; Voet, J., *Biochemistry*. 3rd ed.; Wiley: New York, 2004.

9.) Feiters, M. C.; Rowan, A. E.; Nolte, R. J. M. "From Simple to Supramolecular Cytochrome P450 Mimics" *Chem. Soc. Rev.* **2000**, *29*, 375-384.

10.) (a) J., L. "Supramolecular Chemistry-Scope and Perspecetives Molecules, Supermolecules, and Molecular Devices" *Angew. Chem. Int. Ed.* **1998**, *27*, 89-112; (b) Breslow, R. "Biomimetic Chemistry and Artificial Enzymes: Catalysis and Design" *Acc. Chem. Res* **1995**, 146-153; (c) Kirby, A. J. "Enzyme Mechanisms, Models, and Mimics" *Angew. Chem. Int. Ed.* **1996**, *35*, 707-724; (d) Fenton, D. E. "Metallobiosites and Their Synthetic Analogues-A Belief in Synergism" *Chem. Soc. Rev.* **1999**, *28*, 159-168; (e) Zhang, X.; Houk, K. N. "Why Enzymes are Proficient Catalysts: Beyond the Pauling Paradigm" *Acc. Chem. Res.* **2000**, *57*, 4663-4686; (f) Motherwell, W. B.; Bingham, M. J.; Six, Y. "Recent Progress in the Design and Synthesis of Artificial Enzymes" *Tetrahedron* **2001**, *57*, 4663-4686.

11.) Yoshizawa, M.; Miyagi, S.; Kawano, M.; Ishiguro, K.; Fujita, M. "Alkane Oxidation via Photochemical Excitation of a Self-Assembled Molecular Cage" *J. Am. Chem. Soc.* **2004**, *126*, 9172-9173.

12. Steed, J.; Turner, D.; Wallace, K., *Core Concepts in Supramolecular Chemistry and Nanochemistry*. John Wiley & Sons, Ltd.: West Sussex, England, 2007.

13.) (a) Mavroidis, C.; Dubey, A.; Yarmush, M. "Molecular Machines" *Annu. Rev. Biomed. Eng.* **2004**, *6:10*, 10.1-10.33; (b) Fang, L.; Olson, M. A.; Benitez, D.; Tkatchouk, E.; Goddard, W. A.; Stoddart, J. F. "Mechanically Bonded Macromolecules" *Chem. Soc. Rev.* **2010**, *39*, 17-29; (c) Kay, E. R.; Leigh, D. A.; Zerbetto, F. "Synthetic Molecular Motors and Mechanical Machines" *Angew. Chem. Int. Ed. 46*, 72-191.

14.) (a) Caulder, D. L.; Raymond, K. N. "The Rational Design of High Symmetry Coordination Clusters" *J. Chem. Soc. Dalton Trans.* **1999**, 1185-1200; (b) Caulder, D. L.; Bruckner, C.; Powers, R. E.; Stefan, K.; Parac, T. N.; Leary, J. A.; Raymond, K. N.

"Design, Formation and Properties of Tetrahedral M_4L_4 and M_4L_6 Supramolecular Clusters" *J. Am. Chem. Soc.* **2001**, *123*, 8923-8938; (c) Caulder, D. L.; Powers, R. E.; Parac, T. N.; Raymond, K. N. "The Self-Assembly of a Predesigned Tetrahedral M_4L_6 Supramolecular Cluster" *Angew. Chem. Int. Ed.* **1998**, *37*, 1840-1843.

15.) Mal, P.; Schultz, D.; Beyeh, K.; Rissanen, K.; Nitschke, J. R. "An Unlockable-Relockable Iron Cage by Subcomponent Self-Assembly" *Angew. Chem. Int. Ed.* **2008**, *47*, 8297-8301.

16.) Fujita, M.; Oguro, D.; Miyazawa, M.; Oka, H.; Yamaguchi, K.; Ogura, K. "Self-Assembly of Ten Molecules into Nanometre-Sized Organic Host Frameworks" *Nature* **1995**, *378*, 469-471.

17.) Fujita, M.; Umemoto, K.; Yoshizawa, M.; Fujita, N.; Kusukawa, T.; Biradha, K. "Molecular Paneling via Coordination" *Chem. Commun.* **2001**, 509-518.

18.) Yoshizawa, M.; Tamura, M.; Fujita, M. "AND/OR Bimolecular Recognition" *J. Am. Chem. Soc.* **2004**, *126*, 6846-6847.

19.) Tashiro, S.; Tominaga, M.; Kawano, B.; Therrien, T.; Ozeki, M.; Fujita, M. "Sequence-Selective Recognition of Peptides within the Single Binding Pocket of a Self-Assembled Coordination Cage" *J. Am. Chem. Soc.* **2005**, *127*, 4546-4547.

20.) (a) Oliveri, C. G.; Ulmann, P. A.; Wiester, M. J.; Mirkin, C. A. "Heteroligated Supramolecular Coordination Complexes Formed via the Halide-Induced Ligand Rearrangement Reaction" *Acc. Chem. Res.* **2008**, *41*, 1618-1629; (b) Gianneschi, N. C.; Masar, M. S.; Mirkin, C. A. "Development of a Coordination Chemistry-Based Approach for Functional Supramolecular Structures" *Acc. Chem. Res.* **2005**, *40*, 2022-2043; (c) Holliday, B. J.; Mirkin, C. A. "Strategies for the Construction of Supramolecular

Compounds Through Coordination Chemistry" *Angew. Chem. Int. Ed.* **2005**, *38*, 2022-2043.

21.) (a) Höpfl, H.; Roesky, H. W.; Atwood, D. A., *Structure and Bonding*. Springer: Berlin, 2002; Vol. 103; (b) Icli, B.; Sheepwash, E.; Riis-Johannessen, T.; Schenk, K.; Filinchuk, Y.; Scopellti, R.; Severin, K. "Dative Boron-Nitrogen Bonds in Structural Supramolecular Chemistry: Multicomponent Assembly of Prismatic Organic Cages" *Chem. Sci.* **2011**, *2*, 1719-1721; (c) Fujita, N.; Shinkai, S.; James, T. D. "Boronic Acids in Molecular Self-Assembly" *Chem. Asian. J.* **2008**, *3*, 1076-1091; (d) Horng, Y.; Lin, T.; Tu, C.; Sung, T.; Hsieh, C.; Hu, C.; Lee, H.; Kuo, T. "Preparation of a Reversible Redon-Controlled Cage-Type Molecule Linked by Disulfide Bonds" *Eur. J. Org. Chem.* **2009**, 1511-1514; (e) Corbellini, F.; Costanzo, L.; Crego-Calama, M.; Geremia, S.; Reinhoudt, D. N. "Guest Encapsulation in a Water-Soluble Molecular Capsule Based on Ionic Interactions" **2003**, *125*, 9946-9947; (f) Oshovsky, G. V.; Reinhoudt, D. N.; Verboom, W. V. "The Underestimated Role of Counter Ions in Electrostatic Self-Assembly: [1+1] Cavitand-Calix[4]arene Capsules Based on Azinium-Sulfonate Interactions" *Eur. J. Org. Chem.* **2006**, 2810-2816; (g) Cresswell, A. L.; Piepenbrock, M. O.; Steed, J. W. "A Water Soluble, Anion-Binding Zwitterionic Capsule Based on Electrostatic Interactions Between Self-Complementary Hemispheres" *Chem. Commun.* **2010**, *46*, 2787-2789; (h) Anachenko, G. S.; Udachin, K. A.; Dubes, A.; Ripmeester, J. A.; Perrier, T.; Coleman, A. W. "Guest Exchange in Single Crystals of van der Waals Nanocapsules" *Angew. Chem. Int. Ed.* **2006**, *45*, 1585-5618; (i) Anachenko, G. S.; Moudrakovski, I. L.; Coleman, A. W.; Ripmeester, J. A. "A Channel-Free Soft-Walled Capsular Calixarene Solid for Gas Adsorption" *Angew. Chem. Int. Ed.* **2008**, *47*, 5616-5618.

22.) (a) Conn, M. M.; Rebek, J. "Self-Assembling Capsules" *Chem. Rev.* **1997**, *97*, 1647-1668; (b) Atwood, J. L.; Szunma, A. "Hydrogen Bonds Seal Single-Molecule Capsules" *J. Am. Chem. Soc.* **2002**, *124*, 10646-10647; (c) Atwood, J. L.; Barbour, L. B.; Jerga, A. "Hydrogen-Bonded Molecular Capsules are Stable in Polar Media" *Chem. Commun.* **2001**, 2376-2377.

23.) Belowich, M.; Stoddart, F. "Dynamic Imine Chemistry" *Chem. Soc. Rev.* **2012**, *41*, 2003-2024.

24.) Quan, M.; Cram, D. "Constrictive Binding of Large Guests by a Hemicarcerand Containing Four Portals" *J. Am. Chem. Soc.* **1991**, *113*, 2754-2755.

25.) Liu, X.; Yong, L.; Li, G.; Warmuth, R. "One-Pot 18 Component Synthesis of an Octahedral Nanocontainer Molecule" *Angew. Chem. Int. Ed.* **2006**, *45*, 901-904.

26.) Shenoy, S. R.; Pinacho Crisostomo, P. R.; Iwasawa, T.; Rebek, J. "Organocatalysis in a Synthetic Receptor with an Inwardly Directed Carboxylic Acid" *J. Am. Chem. Soc.* **2008**, *130*, 5658-5659.

27.) Purse, B. W.; Rebek, J. "Self-Fulfilling Cavitands: Packing Alkyl Chains into Small Spaces" *PNAS* **2006**, *103*, 2530-2514.

28.) Gianneschi, N. C.; Bertin, P. A.; Nguyen, N. T.; Mirkin, C. A.; Zakharov, L. N.; Rheinhold, A. L. "A Supramolecular Approach to an Allosteric Catalyst" **2003**, *125*, 10508-10509.

29.) Jacobsen, E. "Asymmetric Catalysis of Epoxide Ring-Opening Reactions" *Acc. Chem. Res.* **2000**, *33*, 421-431.

30.) Lu, T.; Zhuang, X.; Li, Y.; Chen, S. "C-C Bond Cleavage of Acetonitrile by a Dinuclear Copper (II) Cryptate" *J. Am. Chem. Soc.* **2004**, *126*, 4760-4761.

31.) (a) Yoon, H. J.; Mirkin, C. A. "PCR-like Cascade Reactions in the Context of an Allosteric Enzyme Mimic" *J. Am. Chem. Soc.* **2008**, *126*, 4760-4761; (b) Yoon, H. J.; Kuwabara, J.; Kim, J.; Mirkin, C. A. "Allosteric Supramolecular Triple-Layer Catalysts" *Science* **2010**, *330*, 66-69.

32.) Hao, H. G.; Zheng, X. D.; Lu, T. B. "Photoinduced Catalytic Reaction by a Fluorescent Active Cryptand Containing an Anthracene Fragment" *Angew. Chem. Int. Ed.* **2010**, *49*, 8148-8151.

33.) Fabbrizzi, L.; Faravelli, I. "A Fluorescent Cage for Anion Sensing in Aqueous Solution" *Chem. Commun.* **1998**, 971-972.

Chapter 2

Azacryptand Cages with Endohedral Functionality

2.1. Introduction

Azacryptands with *tris*(2-aminoethyl)amine (TREN) derived binding units located at the two ends of the structure are capable of dinuclear metal coordination and can act as good receptors for molecular recognition.[1] To date, very few heterodinuclear cryptates have been reported.[2] Mixed metal complexes are of interest as models for metalloenzyme active sites such as the CuZn family of superoxide dismutases and the FeCu active site of Cytochrome P450.[3] Studying how two different metals in the interior of a model cavity interact and influence each other in terms of their electronic, electrochemical, magnetic, catalytic and molecular recognition properties are of interest in understanding how metalloenzymes work.

Herein we synthesized ellipsoidal azacryptands of different sizes and ellipsoidal derived shapes, where the interatomic distances of the metal sites are varied. Using first row transition metals Fe(II), Cu(I) and Ni(II) we report the formation of mixed metal coordination complexes, Fe(II)•Cu(I) and Cu(I)•Ni(II) of a polyazacryptand with symmetrical binding sites, and the unusual observation of monometallated species with Cu(I) and Zn(I).

2.1.1. Synthesis of Azacryptand Cages

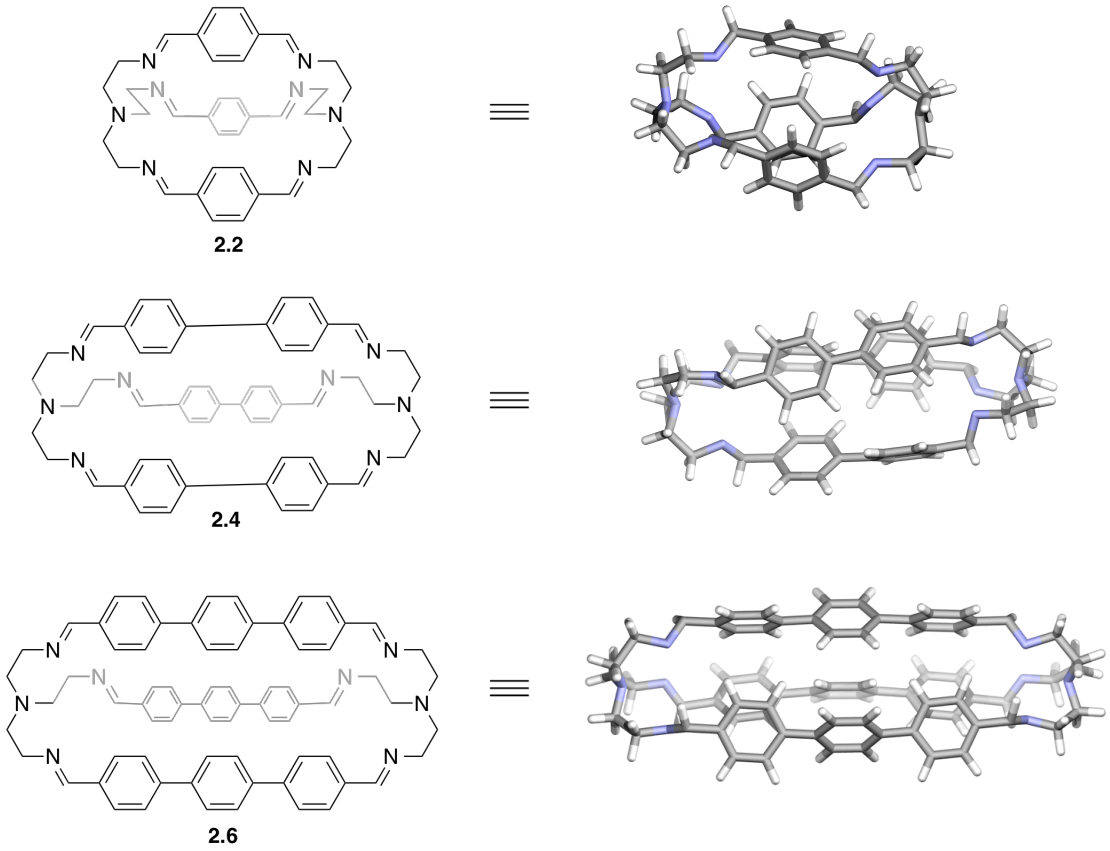

Figure 2.1: Azacryptand cages **2.2**, **2.4** and **2.6** from linear *bis* aldehydes.

The target ellipsoidal azacryptands have two sections; phenyl spacers to vary the length of the azacryptand and metal-metal distance within the cavity and TREN, derived binding units located at the two ends of the cryptand. These cages can be synthesized via the condensation of a *bis* aldehyde and with the commercially available *tris*(2-aminoethyl)amine. The azacryptand cages that form are poorly soluble in most solvents (solubility in methanol is poor, but sufficient to characterize by mass spectrometry), but some of them can be rendered soluble in acetonitrile, methanol and DMSO upon addition

of suitable metal salts. These cages are stable, and show good resistance to hydrolytic decomposition.

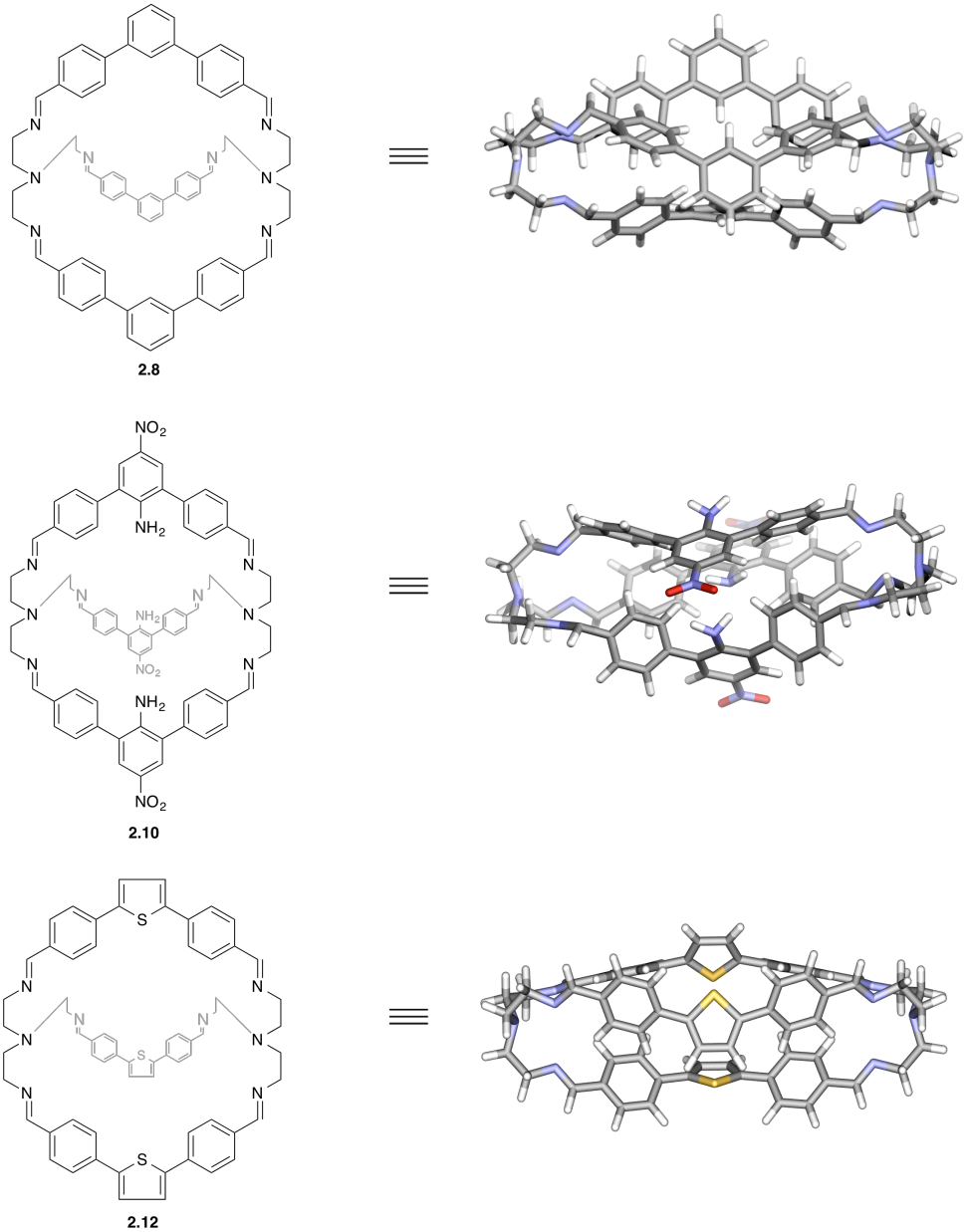

Figure 2.2: Azacryptand cages **2.8**, **2.10** and **2.12** from V-shape *bis* aldehydes.

Six types of ellipsoidal cages were synthesized, three with varying linear spacers, and three different types with V-shaped spacers. Of these six cages, three of them (**2.4**, **2.6** and **2.8**) were suitable for study, for reasons that will be discussed further in this section. The smallest of the cages, **2.2** is well precedented, and its amine analog and its derivatives have been widely studied for its metal binding and anion binding capabilities.[4] Cage **2.4** has biphenyl spacers, and to date appeared in the literature only for its ability to recognize carboxylic acids in water with the dicuprate amine analog of the cage.[5] Cages **2.8** and **2.10** were made to vary the geometry of the interior from the linear analog, to provide additional shape-based selectivity of substrates. Cages **2.10** is made with terphenyl V-shaped spacers and has an endohedral amine group at the central ring of the terphenyl spacer. Cage **2.12** is made with V-shape spacer with a thiophene ring at the center of the spacers. Thiophene derivatives are well known for their interesting photophysical properties, and were made with the intention of being able to incorporate that feature in molecular recognition.

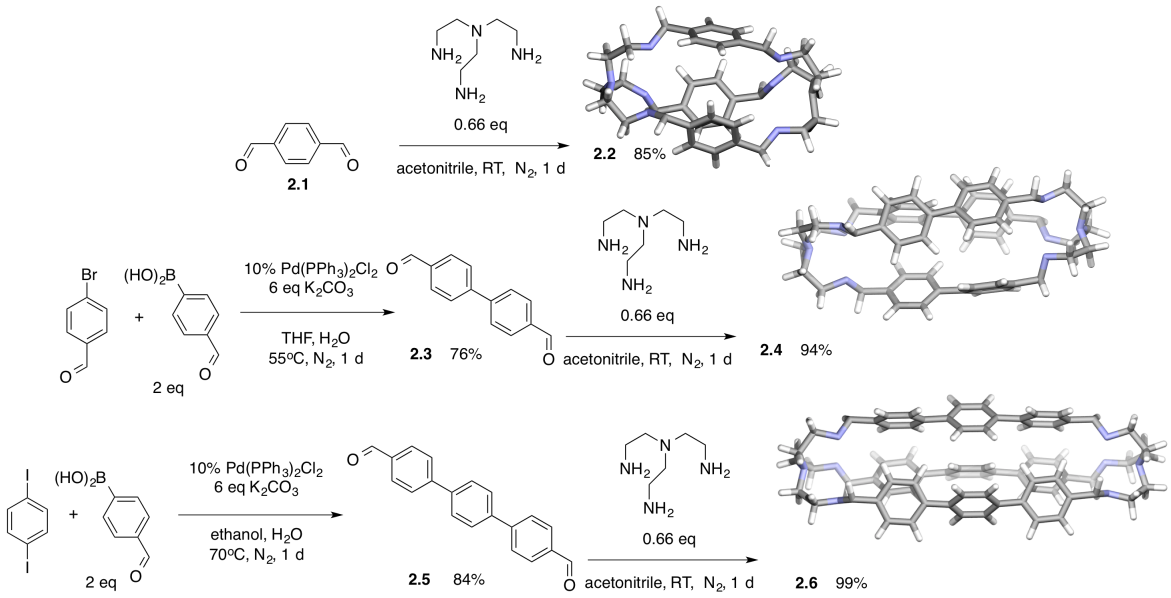

Figure 2.3: Synthesis of ellipsoidal cages with linear spacers.

Cage **2.2** was synthesized via the condensation between **2.1** and *tris*(2-aminoethyl)amine in excellent yield. The interatomic distance between the two nitrogens at opposite ends of the cage is approximately 20 Å. These dimensions provide enough space for the encapsulation of small molecules such as transition metals and small organic molecules.[6]

Cage **2.4** was synthesized via the condensation between **2.3** and *tris*(2-aminoethyl)amine in excellent yield. The *bis* aldehyde precursor, **2.3** was synthesized by Suzuki coupling of 4-bromobenzaldehyde and 4-formylphenyl boronic acid in good yield. The cage has poor solubility; however, upon complexation with a transition metal salt, the metallated cage is soluble in DMSO, acetonitrile and methanol.

Cage **2.6** was synthesized via the condensation between **2.5** and *tris*(2-aminoethyl)amine with previous known methods in excellent yield. The *bis* aldehyde precursor, **2.5** was synthesized by Suzuki coupling of 1,4 diiodobenzene with 4-formyl phenylboronic acid in moderate yield. The cage has poor solubility; again, upon complexation with a transition metal salt, the metallated cage is soluble in DMSO and methanol. This cage can undergo dimetallation with $Cu(CH_3CN)_4PF_6$, $Zn(NO_3)_2 \bullet 6H_2O$, and $Fe(ClO_4)_2 \bullet 6H_2O$.

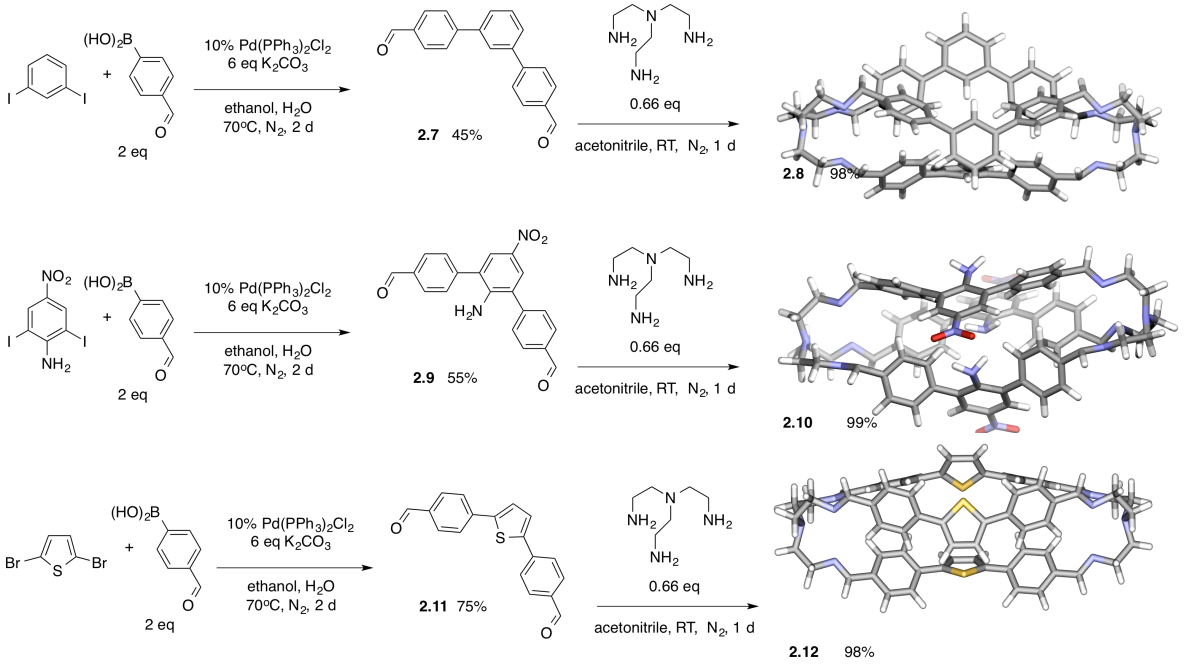

Figure 2.4: Synthesis of ellipsoidal cages with V-shaped spacers.

Cage **2.8** was synthesized via the condensation between **2.7** and *tris*-(2-aminoethyl)amine in excellent yield. The *bis* aldehyde precursor, **2.7** was synthesized by Suzuki coupling of 1,4 diiodobenzene with 4-formylphenyl boronic acid in moderate yield. The cage has poor solubility; once again, upon complexation with $Cu(CH_3CN)_4PF_6$ and $Fe(ClO_4)_2 \bullet 6H_2O$ the metallated cage is soluble in DMSO and methanol.

Cage **2.10** was synthesized via the condensation between **2.9** and *tris*(2-aminoethyl)amine in excellent yield. The *bis* aldehyde precursor, **2.9** and *tris*(2-aminoethyl)amine in excellent yield. The cage has poor solubility, attempts to solubilize the cage via metal complexation led to decomposition, forming the starting material **2.9** and *tris*(2-aminoethyl)amine. The three amine groups pointing towards the interior of the cage can be potentially useful endohedral functionality for molecular recognition and catalysis if solubility were not an issue.

Cage **2.12** was synthesized via the condensation between **2.11** and *tris*(2-aminoethyl)amine in excellent yield. The *bis* aldehyde precursor, **2.11** and *tris*(2-aminoethyl)amine in excellent yield was synthesized by Suzuki coupling of 1,4 diiodobenzene with 4-formylphenyl boronic acid in moderate yield. The cage has poor solubility. Attempts to solubilize the cage via metal complexation led to decomposition, forming the starting material **2.11** and *tris*(2-aminoethyl)amine. Given the interesting photophysical properties inherent in thiophene based compounds, this cage can be potentially useful for sensing applications if solubility problems can be overcome.

2.1.2. Towards TREN Cages with Enhanced Solubility

Most attempts to make cages with enhanced solubility were unsuccessful. Cage **2.2** can be reduced to its amine analog via $NaBH_4$. The interior size of the cage is too small to study binding of guests that have not already been reported. Cage **2.4** can be reduced to its amine analog via $NaBH_4$.

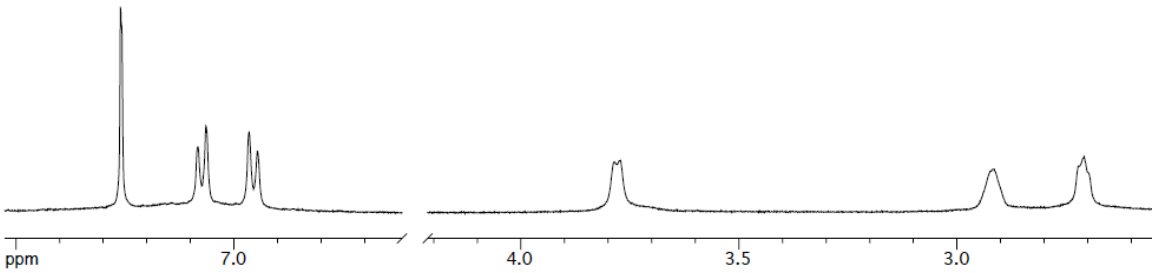

Figure 2.5: ^{1}H NMR spectrum of the reduced analog of **2.4**. ($CHCl_3$-*d*, 400 MHz, 298 K.)

Amine derivatives of Cage **2.2** and **2.4** are soluble in chloroform, methylene chloride, methanol, and water. Cage **2.6**, **2.8**, **2.10** and **2.12** were unable to be reduced to their amine analog. Reduction attempts under various conditions with $NaBH_4$ and $NaBH_3CN$ generally led to unreacted starting material or decomposition of the cage, forming *tris*(2-aminoethyl)amine and the corresponding *bis* aldehyde.

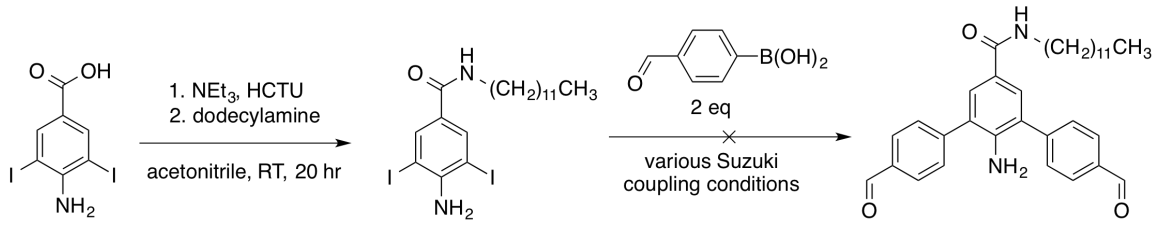

Figure 2.6: Towards synthesis of a *bis* aldehyde with enhanced solubility.

Attempts to enhance the solubility of the imine cages were done by trying to introduce long alkyl chains to the exterior of the cage. Dodecylamine was added to 4-amino 3,5-diiodobenzoic acid with triethylamine and 2-(6-Chloro-1-H-benzotriazole-1-yl)-1,1,3,3-tetramethylaminium hexafluorophosphate (HCTU) to form the corresponding amide. Attempts to make the *bis* aldehyde via various Suzuki coupling conditions did not yield the desired compound.

2.2. Homo Dinuclear Cages

2.2.1. Homo Dinuclear Metallation with Cage 2.4

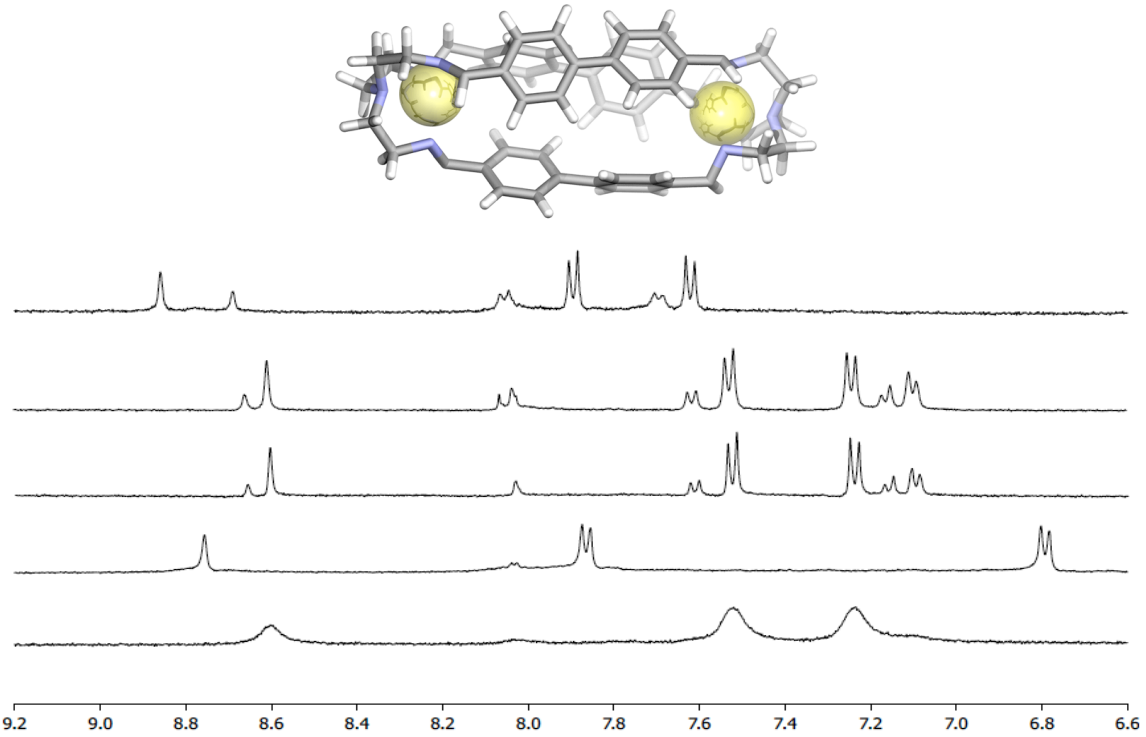

Figure 2.7: ^{1}H-NMR spectra of homonuclear complexes (from top to bottom): (a) **2.4•Ag$_2$•(NO$_3$)$_2$** & **2.4•Ag$_2$⊂(NO$_3$)$_2$**, (b) **2.4•Zn$_2$•(NO$_3$)$_4$** & **2.4·Zn•(NO$_3$)$_2$**, (c) **2.4·Ni$_2$•(NO$_3$)$_4$** & **2.4·Ni•(NO$_3$)$_2$**, (d) **2.4•Cu$_2$•(PF$_6$)$_2$**, (e) **2.4·Fe$_2$•(ClO$_4$)$_2$**. (DMSO-d_6, 400 MHz, 298 K.)

Cage **2.4** can undergo dimetallation with $Cu(CH_3CN)_4PF_6$, $AgNO_3$, and $Fe(ClO_4)_2 \bullet 6H_2O$ at room temperature in methanol or acetonitrile. A mixture of 1/3 monometallation and 2/3 dimetallation has been observed with $Ni(NO_3)_2 \bullet 6H_2O$ and $Zn(NO_3)_2 \bullet 6H_2O$ when let to react in methanol or acetonitrile at 60°C for 16 hr. Upon addition of excess metals, complete formation of the dimetallated species with $Ni(NO_3)_2 \bullet 6H_2O$ and $Zn(NO_3)_2 \bullet 6H_2O$ is not observed.

Evidence of a mixture of **2.4•Ag_2•$(NO_3)_2$** and **2.4•Ag_2⊂$(NO_3)_2$** was observed upon addition of $AgNO_3$ to **2.4** in either methanol or acetonitrile when let to react at 60°C for 16 hr, where nitrate anion binding occurred in the majority of the silver metallated cage (78%) during the course of the reaction. Formation of **2.4•Ag_2•$(NO_3)_2$** is shown by the metal coordinated singlet imine peak at 8.70 ppm, two doublets at 8.07 ppm and 7.71 ppm and alkyl peaks at 3.81 ppm and 2.87 ppm. Evidence of anion binding is observed by the downfield peak at 8.86 ppm that corresponds to the metallated imine peak that is also bound to a nitrate ion, in addition to the downfield shifts of the alkyl peaks at 3.94 ppm and 3.10 ppm. Due to observation of one imine peak that is coordinated to nitrate bound silver, it is likely that two nitrate anions are bound in the interior, otherwise if only one nitrate anion were bound, there would be two imine peaks, one corresponding to a silver metallation, and the other corresponding to silver metallation with a nitrate anion coordinated to the silver in the interior of the cage.

Nitrate anion binding was exclusively observed upon dimetallation of **2.4** with Ag(I) instead of Ni(II) and Zn(II) likely due to Ag(I) being larger in size.

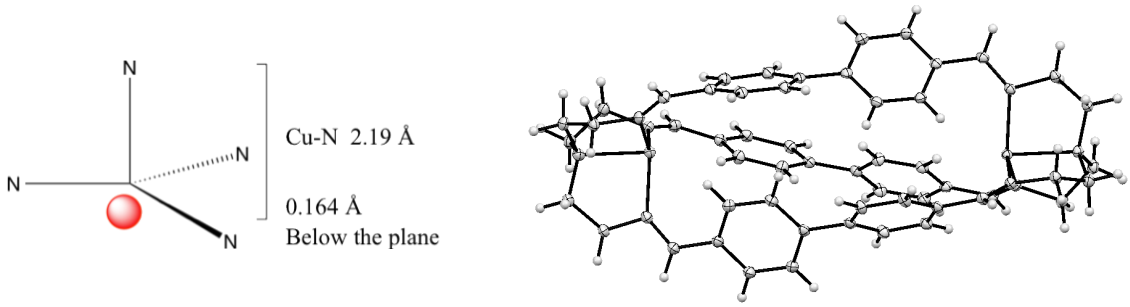

Figure 2.8: X-ray crystal structure of **2.4•Cu$_2$•(PF$_6$)$_2$**. The PF_6 counter anion and disordered DMSO molecules have been removed for clarity. Selected bond lengths [Å] around the Cu(I) metal centers: Cu-N(1) 2.190(11) (axial); and equatorial: Cu-N(2) 2.008(11), Cu-N(3) 2.027(11), and Cu-N(4) 2.0126(11). Cu(2)-N(5) 2.198(12) (axial); and equatorial: Cu(2)-N(6) 2.002, Cu(2)-N(7) 1.992(12), and Cu(2)-N(8) 2.014(12).

X-ray quality crystals of **2.4•Cu$_2$•(PF$_6$)$_2$** were obtained via slow vapor diffusion of methylene chloride in into a solution of **2.4•Cu$_2$•(PF$_6$)$_2$** in DMSO. The structure of the dimetallated cage is shown as an ORTEP plot in **figure 2.8**. Both Cu(I) ions are bound inside the TREN units with trigonal pyramidal geometry around the metal centers. Since both Cu(I) metals are 0.164 Å below the axial plane, they can be considered to be trigonal pyramidal instead of a distorted tetrahedral. If the metal center were to be significantly above the axial plane, the geometry around the metal center can arguably be a distorted tetrahedral.

The average equatorial Cu-N bond lengths around both metal centers are 2.039 Å, which is shorter than the average axial bond length (2.194 Å) of both metal centers. The opposite trend has been observed with a Cu(II) dimetallated analog of the same cage,[5] where the average length of the Cu-N equatorial bond lengths is 2.140 Å, and the average Cu-N axial bond lengths is 2.000 Å, where two water molecules are bound to both interior coppers, in a trans position to the axial nitrogens. Solvent molecules in the crystal

structure of **2.4•Cu$_2$•(PF$_6$)$_2$** were not found bound to the interior coppers, however, one water molecule was found to be hydrogen bonding to the exterior π face of a phenyl ring (omitted from for **figure 2.8** clarity.)

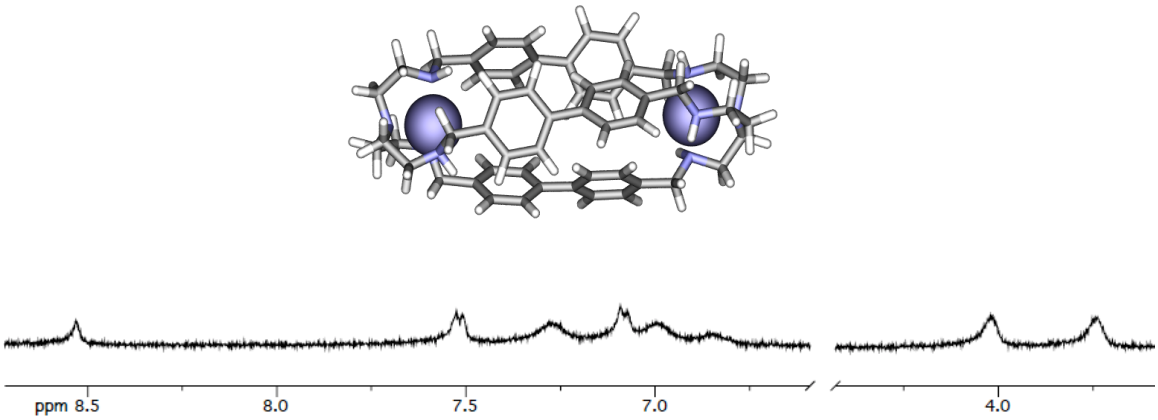

Figure 2.9: ^{1}H-NMR spectra of homonuclear complex **2.4•Fe$_2$•(BPh$_4$)$_2$**. (Acetonitrile-*d$_3$*, 400 MHz, 298 K.)

The di Fe analog with the perchlorate anion of Cage **2.4** can be rendered soluble in acetone and acetonitrile by switching the counter anion with tetraphenyl borate. This cage is also soluble in a solvent mixture of acetonitrile and water, which are suitable solvent conditions for C-H oxidation catalysis.[7] The Fe(II) at both ends of the interior cage should be capable of selectively oxidizing organic substrates of suitable shape and size.

2.2.2. Homo Dinuclear Metallation with Cage 2.6

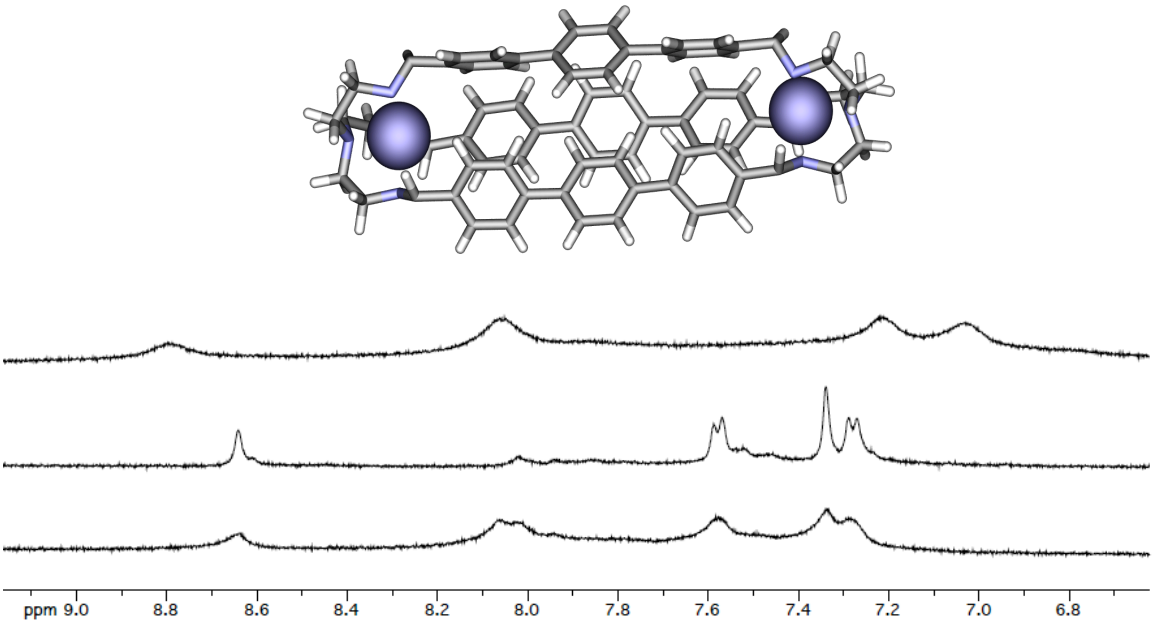

Figure 2.10: ^{1}H-NMR spectra of homonuclear complexes (from top to bottom): (a) **2.6•Cu$_2$•(PF$_6$)$_2$**, (b) **2.6·Fe$_2$•(ClO$_4$)$_4$** (c) **2.6·Zn$_2$•(NO$_3$)$_2$**. (DMSO-d_6, 400 MHz, 298 K.)

Cage **2.6** can undergo dimetallation with $Cu(CH_3CN)_4PF_6$, $Zn(NO_3)_2$•$6H_2O$, and $Fe(ClO_4)_2$•$6H_2O$ upon reflux with methanol. Metallation is not observed at room temperature or with any other solvent. Metallation with Ni(II), and Ag(I) was not observed. Mixtures of mono and di metallation were not observed as they were with Cage **2.4**.

2.2.3. Homo Dinuclear Metallation with Cage 2.8

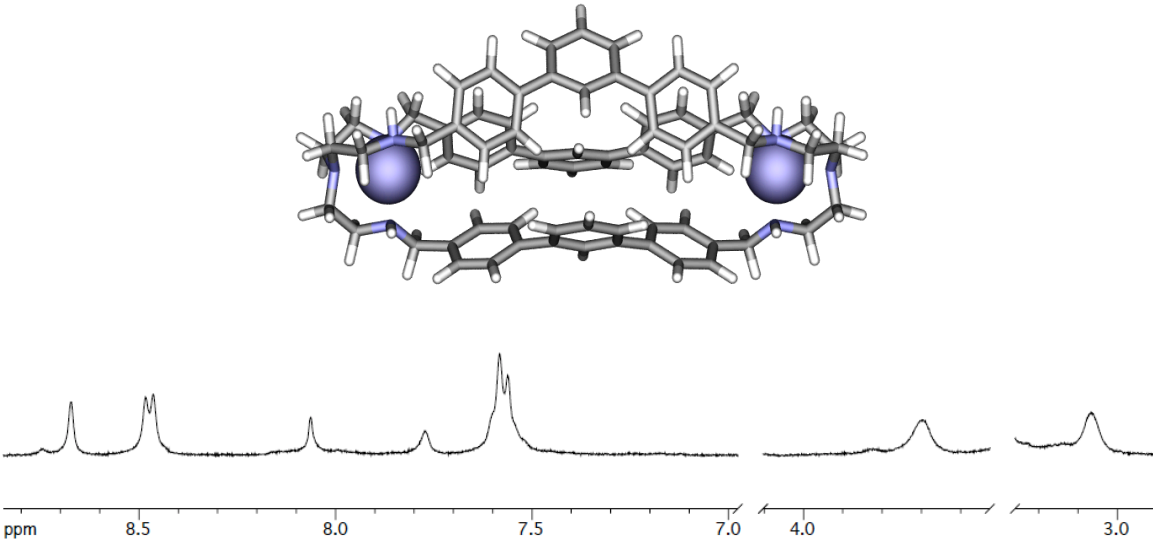

Figure 2.11: ^{1}H-NMR spectra of homonuclear complexes **2.8·Fe$_2$•(ClO$_4$)$_4$**. (DMSO-*d$_6$*, 400 MHz, 298 K.)

Cage **2.8** can undergo dimetallation with $Fe(ClO_4)_2$•$6H_2O$ at room temperature or upon reflux with methanol. Metallation is not observed at room temperature or with any other solvent. Metallation with Ni(II), Cu(I), and Ag(I) was not observed with varying anions; $(ClO_4)_2$, NO_3, OAc_2, PF_6, BF_4, chlorides, iodides and bromides were attempted, with no observable metal coordination. Decomposition of the cage to the *bis* aldehyde ligand and *tris*(2-aminoethyl)amine starting material were observed.

2.2.4. Homo Dinuclear Metallation with Cage 2.10

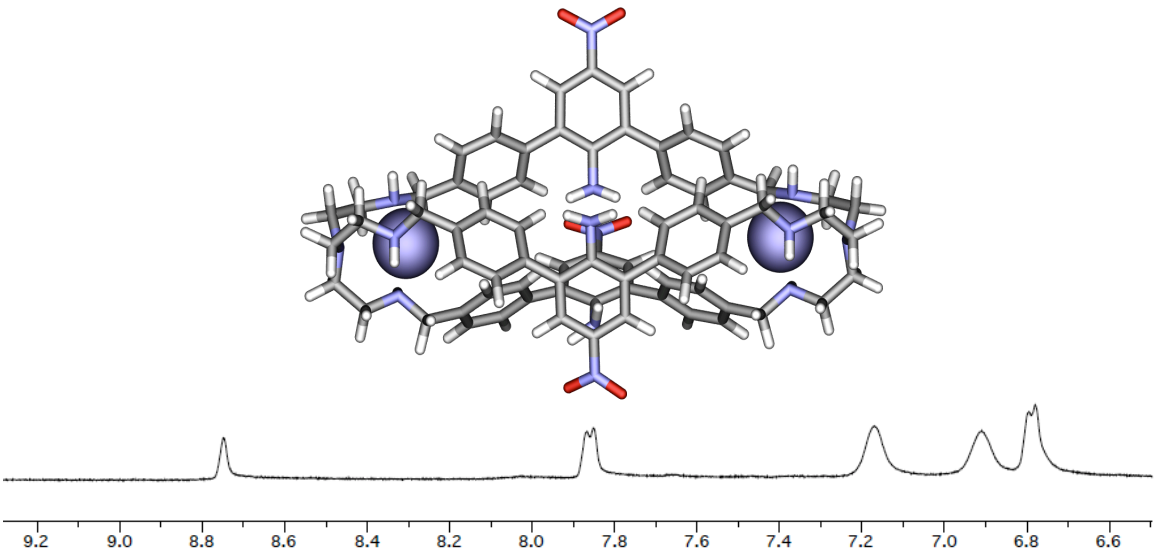

Figure 2.12: ^{1}H-NMR spectrum of homonuclear complex **2.10·Fe$_2$•(ClO$_4$)$_4$**. (DMSO-d_6, 400 MHz, 298 K.)

Cage **2.10** can undergo dimetallation with $Fe(ClO_4)_2$•$6H_2O$ at reflux with acetonitrile. Several coordination attempts at various temperatures, solvents, reaction times and metal salts, such as Fe(II), Cu(I), Zn(II), Ga(II), Mn(II), and Ag(I) with varying anions; $(ClO_4)_2$, NO_3, OAc_2, PF_6, BF_4, chlorides, iodides and bromides were attempted, with no observable metal coordination. Decomposition of the cage to the *bis* aldehyde ligand and *tris*(2-aminoethyl)amine starting material were observed.

2.3. Mononuclear Cages

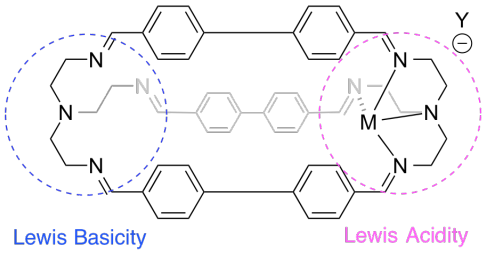

Figure 2.13: Figure of a monometallated azacryptand cage.

Monometallation of symmetrical azacryptands with multiple TREN binding sites are unusual to observe.[8] The design concept behind this monometallated cage was to utilize the Lewis basicity of the TREN binding site, and the Lewis acidity of the metal site to recognize guests cooperatively. Potential guests include alkyl compounds of an appropriate length with carboxylic acids and ketones on one end that would bind to Zn (II), and ammonium functionality on the other end of the alkyl chain that would bind to the Lewis basic site of the cage. Guest binding was not observed with aryl and alkyl carboxylic acids, protonated amines, ketones, and alcohols.

Cage **2.4** was exclusively observed to undergo monometallation. Cage **2.4•Zn•$(NO_3)_2$** was observed via ^{1}H-NMR, and **2.4•Cu•PF_6** was not observed via ^{1}H-NMR, but was observed via X-ray crystallography.

2.3.1. Mononuclear Zn(I) Cage

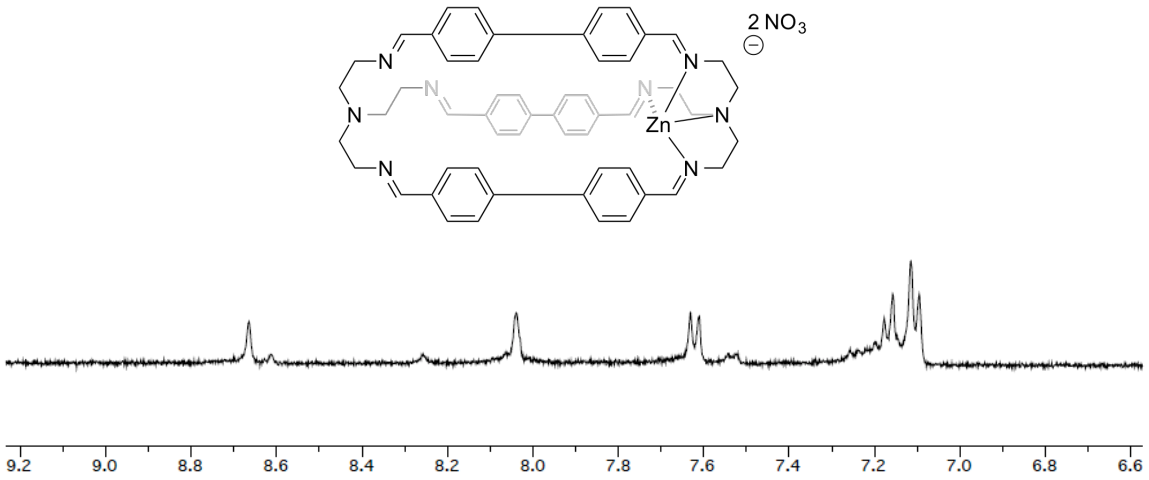

Figure 2.14: ^{1}H NMR spectrum of mononuclear complex **2.4•Zn•(NO$_3$)$_2$**. (DMSO-d_6, 400 MHz, 298 K.)

Upon metallation of Cage **2.4** with one equivalent of $Zn(NO_3)_2$•$6H_2O$, monometallation is observed. The ^{1}H NMR spectrum shows an unsymmetrical metallated cage with the metal, coordinated imine peak shifted downfield at 8.65 ppm, and the unmetallated imine peak at 8.1 ppm. The aryl protons closest to the metallated site occur at 7.6 ppm, while the aryl protons closest to the unmetallated site are found at 7.18 ppm, and the aryl protons towards the center of the cage are found at 7.1 ppm.

2.3.2. Mononuclear Cu(I) Cage

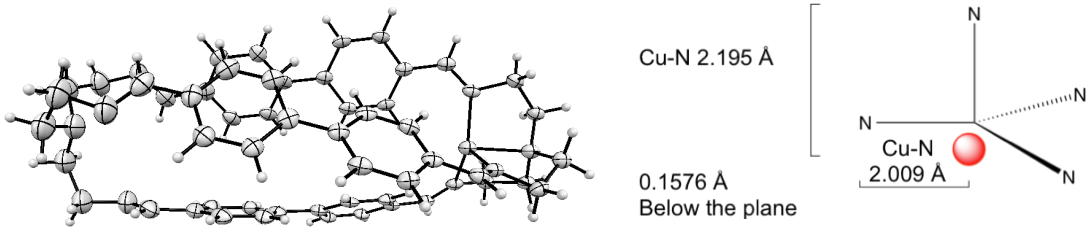

Figure 2.15: X-ray crystal structure of **2.4•Cu•PF$_6$**. The PF_6 counter anion and disordered DMSO molecules have been removed for clarity. Selected bond lengths [Å] around the Cu(I) metal center: Cu-N(1) 2.195(7) (axial); and equatorial: Cu-N(2) 2.009(4), Cu-N(3) 2.009(4), and Cu-N(4) 2.009(4).

Bright orange X-ray quality crystals of **2.4•Cu•PF$_6$** were obtained via slow vapor diffusion of methylene chloride into a solution of **2.4•Cu•PF$_6$** in DMSO. The X-ray crystal structure of the monometallated cage is shown as an ORTEP plot in **figure 2.15**. As observed in **2.4•Cu$_2$•(PF$_6$)$_2$**, the structure exhibits C_3 point symmetry. In the absence of a solvent coordinating molecule, Cu(I) has a trigonal monopyramidal geometry, and the Cu-N axial and equatorial bond lengths are similar. The unmetallated TREN site shows the nitrogens to be further apart in relation to each other, due to not being organized in closer proximity via binding with a metal.

2.4. Hetero Dinuclear Cages

Previous reports on the formation of heterodinuclear complexes from symmetrical azacryptands include transmetallation of a homodinuclear complex with a stronger binding metal,[2a] or by binding a stereochemically discriminating cation on one site which alters the conformation of the host at the other end to prevent the formation of a homodinuclear complex, while still allowing a non-stereochemically demanding cation to bind at the other site. Using first row transition metals Fe(II), Cu(I) and Ni(II) we report the formation of mixed metal coordination complexes, Fe(II)•Cu(I) and Cu(I)•Ni(II) with cage **2.2**.

2.4.1. Introduction

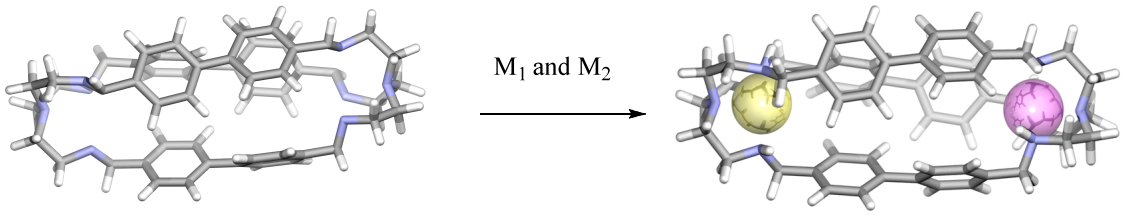

Figure 2.16: Formation of hetero dinuclear species.

Heterodinuclear formation with cages **2.2**, **2.4** and **2.6** was attempted with Fe(II), Cu(I), and Ni(II). Heterodinuclear formation was only observed for cage **2.4**. Heterodinuclear formation attempts with cage **2.2** led to the complete decomposition of the cage to *tris*(2-aminoethyl)amine and 1,4 diformylbenzene. This may be due to the close proximity of the two binding sites imposing too much steric strain along the backbone of the cage, because each of the metal centers have different geometries, (e.g.

Fe(II) is octahedral, Cu(I) is tetrahedral, and Ni(II) is square planar, but can adopt a tetrahedral conformation.)

Heterodinuclear formation was observed with cage **2.4** with Fe(II) and Cu(I), and Cu(I) and Ni(II). Heterodinuclear formation with Fe(II) and Ni(II) was not observed, likely due to the cage's inability to accommodate the differing Fe(II) octahedral geometry at one end, and square planar Ni(II) at the other. Dinuclear formation with Fe(II) was observed, in addition to decomposition of the cage. Dinuclear formation of Ni(II) was not observed.

Heterodinuclear formation with Fe(II) and Cu(I) was observed, likely due to the similarity in geometries between the octahedral Fe(II) and the trigonal pyramidal geometry of the Cu(I) center at the TREN binding site, as observed in the crystal structures discussed in previous sections. Heterodinuclear formation with Cu(I) and Ni(II) was also observed, likely due to the similarities between the trigonal pyramidal geometry of the Cu(I) center at one end, and the square pyramidal geometry of Ni(II) at the other. The octahedral geometry of Fe(II) has an axial binding site that can bind to the tertiary nitrogen of TREN, a binding advantage that the square planar Ni(II) does not have. Therefore, the cage with a biphenyl spacer is sturdy (yet flexible, with more degrees of freedom) enough to be able to provide enough stability for to the cage to accommodate the slightly differing geometries of two different metal centers.

Heterodinuclear formation was not observed with the amine analogs of cages **2.2** and cage **2.4** with mixed variations of Fe(II), Cu(I), Ag(I), Ni(II), and Zn(II) with various counter anions. Mixtures of homodinuclear cages of the respective metals were observed.

Amine analogs of **2.6-2.12** were unable to be isolated, and therefore were not used in heterodinuclear metallation attempts.

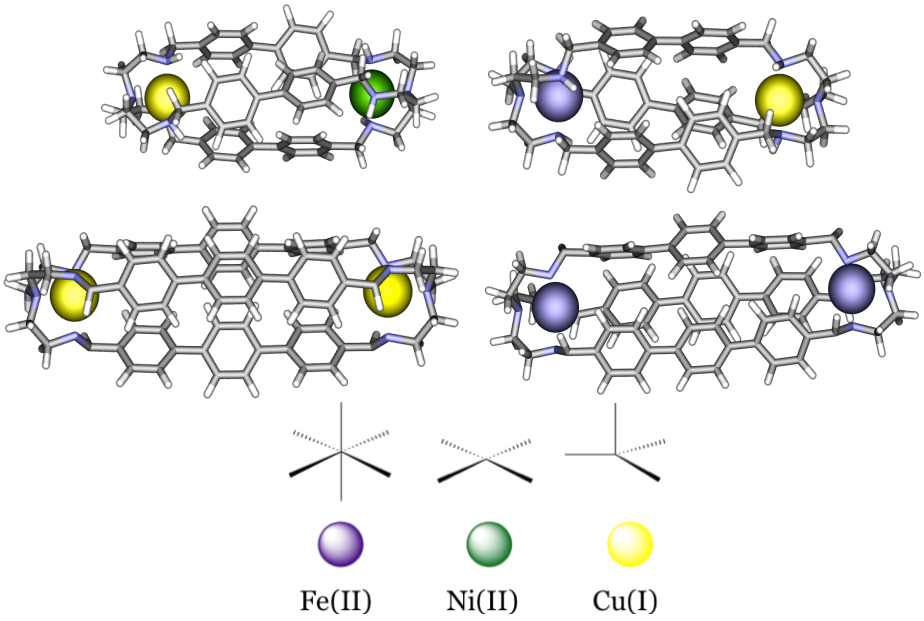

Figure 2.17: Formation of hetero and homo dinuclear species.

Heterodinuclear formation was not observed with cage **2.6**. Despite the argument that additional phenyl units provide the cage with more structural support, cage **2.6** is considerably less soluble than cages **2.2** and **2.4**, therefore solubility likely plays a role. Heterodinuclear formation between Fe(II) and Cu(I) leads to the exclusive formation of dimetallated Cu(I), in addition to decomposition of cage. This is more likely due to the preferential trigonal pyramidal geometry of Cu(I) than that of an octahedral Fe(II) around at the C_3 symmetric TREN binding site. Heterodinuclear formation between Fe(II) and Ni(II) lead to the exclusive formation of dimetallated Fe(II), in addition to decomposition of the cage, as one would expect with their respective geometries in relation to a TREN site. Heterodinuclear formation between Cu(I) and Ni(II) leads to the exclusive

formation of dimetallated Cu(I), in addition to decomposition of cage. This may be due to an issue of solubility, since dinuclear metallation with Ni(II) was not observed with cage **2.6**.

2.4.2. Heterodinuclear Fe (II)•Cu(I) Cage

Evidence for the formation of a heterodinuclear complex using Fe (II) and Ni(II) with cage **2.4** was observed amongst a mixture of di Fe(II) and di Cu(I) complexes. A 1:2 ratio of $Cu(CH_3CN)_4PF_6$, and $Fe(ClO_4)_2•6H_2O$ with cage **2.4**, and is supported by observation NOESY and COSY spectra. Calculating the formation of each species is not feasible due to the broadness of the peaks and spectral overlap.

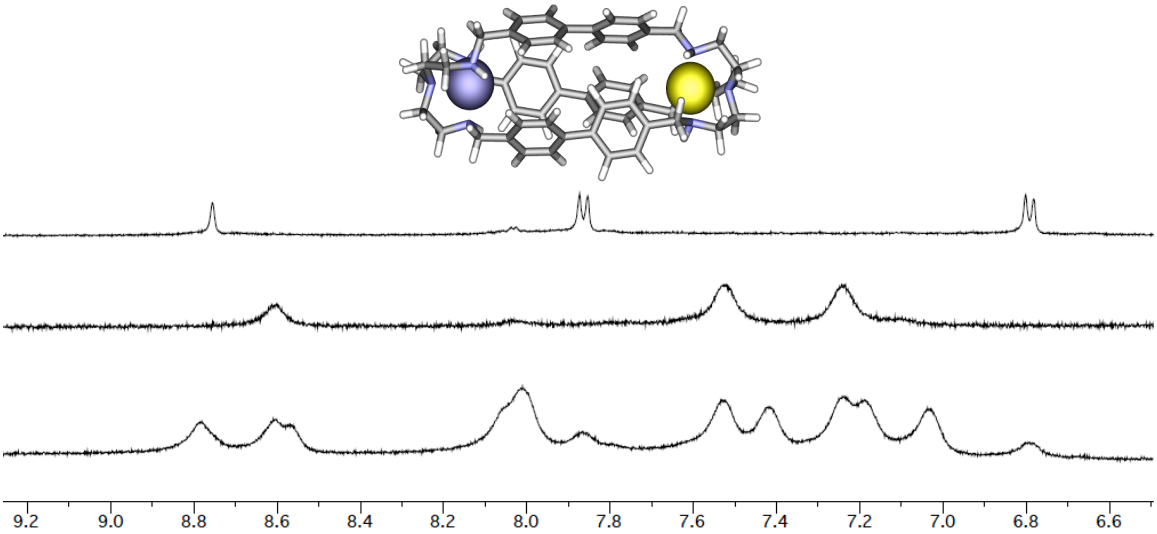

Figure 2.18: ^{1}H-NMR spectra of (from top to bottom): (a) **2.4·Cu$_2$•(PF$_6$)$_2$**, (b) **2.4·Fe$_2$•(ClO$_4$)$_4$**, and (c) **2.4·CuFe•PF$_6$•(ClO$_4$)$_4$**, **2.2·Cu$_2$•(PF$_6$)$_2$**, and **2.4·Fe$_2$•(ClO$_4$)$_4$.** (DMSO-d_6, 400 MHz, 298 K.)

Two unique imine singlet peaks would be expected of a heterodinuclear complex, which are observed at 8.78 ppm, and 8.57 ppm. The imine peak at 8.78 ppm corresponds to Cu(I) metallation, since it is the imine peak closest to the imine peak **2.4·Cu$_2$•(PF$_6$)$_2$** is found at 8.75 ppm. The imine peak found at 8.57 ppm corresponds to Fe(II) metallation, since it is the imine peak closest to the imine peak for the homodinuclear Fe(II) complex found at 8.61 ppm. Due to the presence of the Fe(II) metal, the aryl peaks are broad, similar to **2.4·Fe$_2$•(ClO$_4$)$_4$**. The peak at 8.01 ppm corresponds to the aryl protons adjacent to the Cu(I) binding site, since it is closest to the aryl peaks adjacent to the Cu(I) binding site which is found at 7.87 ppm. The aryl peak at 8.01 ppm has a NOESY and COSY cross peak with the peak at 7.03 ppm, which are the aryl peaks on the same aryl ring that are towards the center of the cage on the same aryl ring.

The aryl peak at 7.42 ppm corresponds to the aryl protons adjacent to the heterodinuclear Fe(II) binding site, since it is a peak that is closest to the aryl protons adjacent to the Fe(II) binding site for the di Fe(II) homodinuclear cage **2.4** complex found at 7.24 ppm. The aryl peak at 7.42 ppm has a NOESY and COSY cross peak with the aryl peak at 7.19 ppm, which are the aryl peaks towards the center of the cage on the same aryl ring.

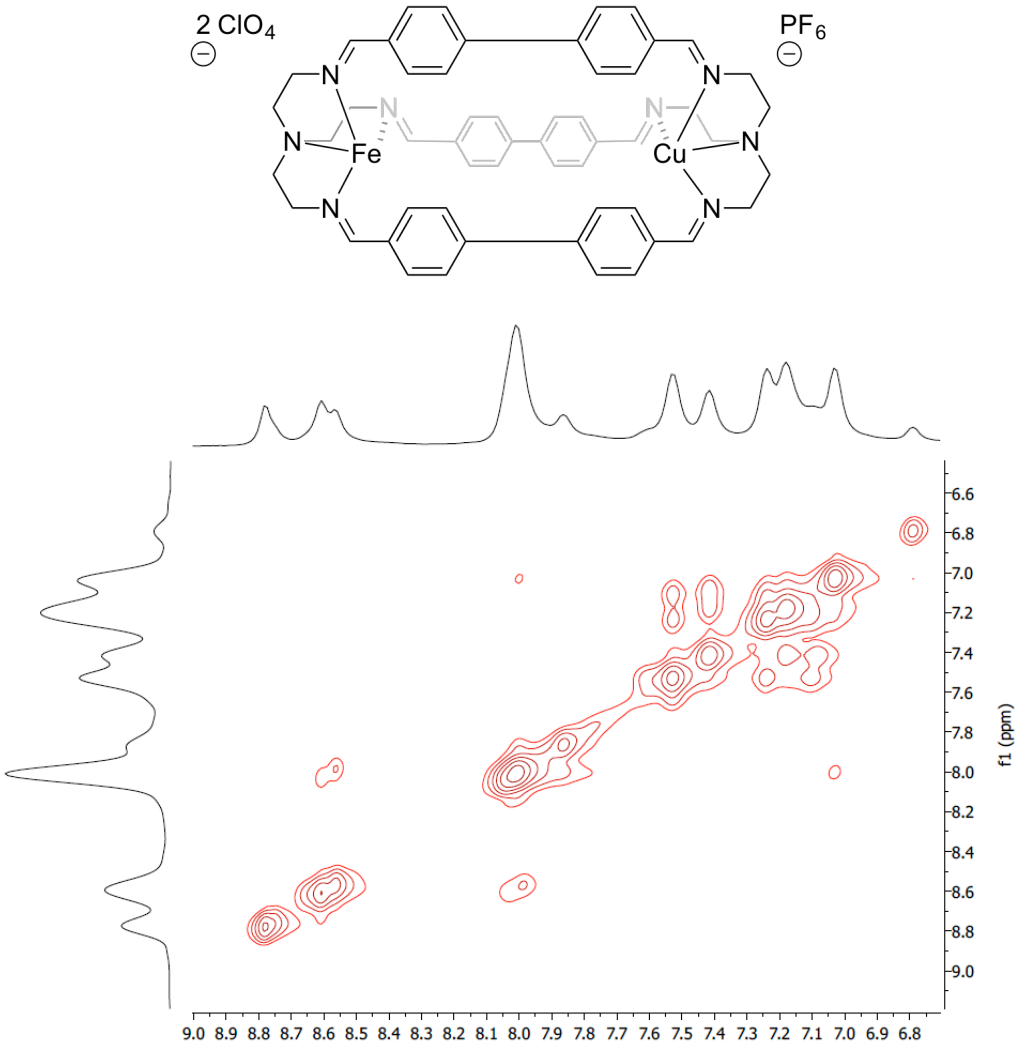

Figure 2.19: NOESY spectrum showing the formation of a **2.4•CuFe•PF_6•$(ClO_4)_2$**. (DMSO-d_6, 400 MHz, 298 K.)

.

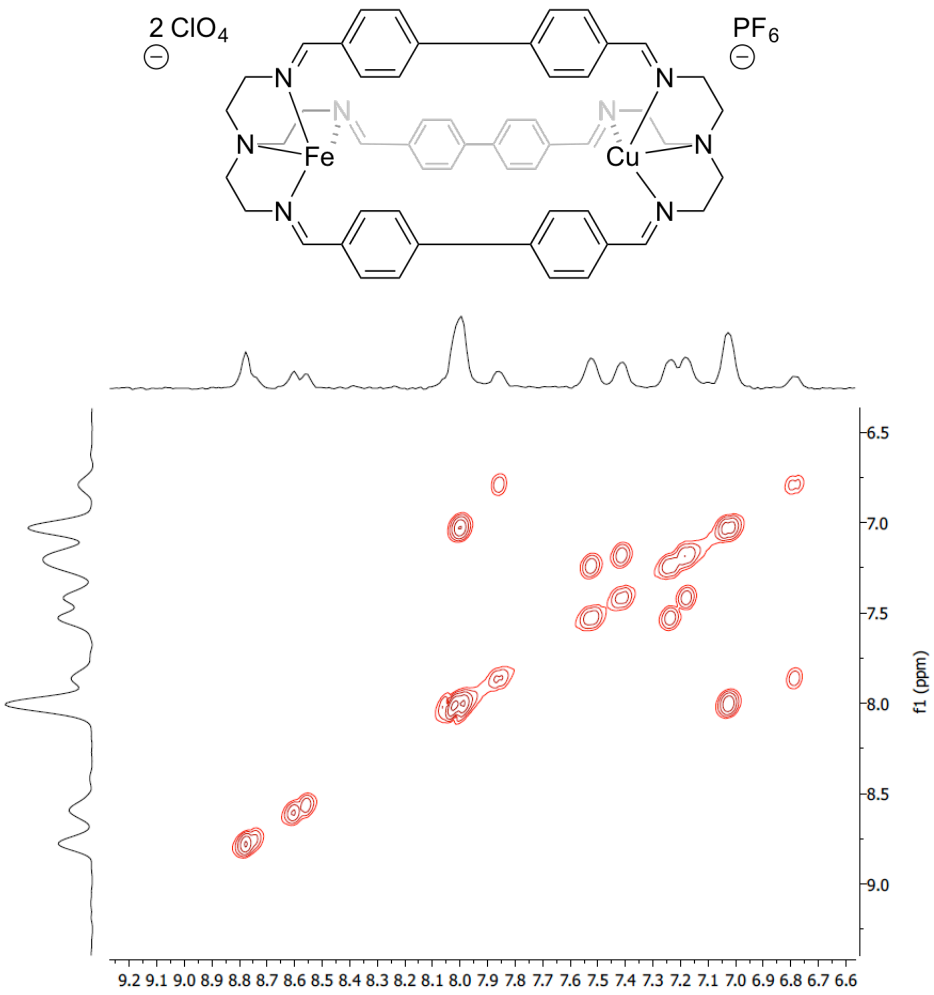

Figure 2.20: COSY spectrum showing the formation of a **2.4•CuFe•PF_6•$(ClO_4)_2$**. (DMSO-d_6, 400 MHz, 298 K.)

2.4.3. Heterodinuclear Cu(I)•Ni(II) Cage

Optimized conditions for the formation of a heterodinuclear complex using Cu (I) and Ni(II) with cage **2.4** was observed amongst a mixture of di Cu(I) and di Ni(II) complexes. A 1:1 ratio of $Cu(CH_3CN)_4PF_6$, and $Ni(NO_3)_2•6H_2O$ with cage **2.4**. With 78% decomposition of cage to the *bis* aldehyde ligand precursor and *tris*(2-aminoethyl)amine, 7% % of the di Cu (I) complex, 4% of the mono Ni (II) complex, and 11% of the mixed metal species were observed. Of the mixture of metallated cages (excluding decomposition), the distribution of metallated cages goes as follows: 32% diCu (I), 16% of the mono Ni (II), and 52% of the heterodinuclear complex.

NOE analysis can be used to analyze hetero dinuclear metallation due to the desymmetrization of the cage. The NOESY in **figure 2.21** shows the formation of a CuNi heterodinuclear complex with cage **2.4**. A 1:1 ratio of $Cu(CH_3CN)_4PF_6$, and $Ni(NO_3)_2•6H_2O$ was added to cage **2.4**, forming a mixture of a homodinuclear complex with Cu(I), and a Cu(I)•Ni(II) heterodinuclear complex. The symmetrical homodinuclear complex shows cross peaks at 7.8 ppm and 6.8 ppm, both corresponding to the aryl peaks. The doublet peak at 7.8 ppm corresponds to the aryl protons closest to the metal binding sites, and the doublet peak at 6.8 ppm corresponds to the aryl protons that are more shielded in the middle of the cage. The cross peak at 8.75 ppm is a singlet that corresponds to the protons to the imine protons that are in close proximity to the binding site.

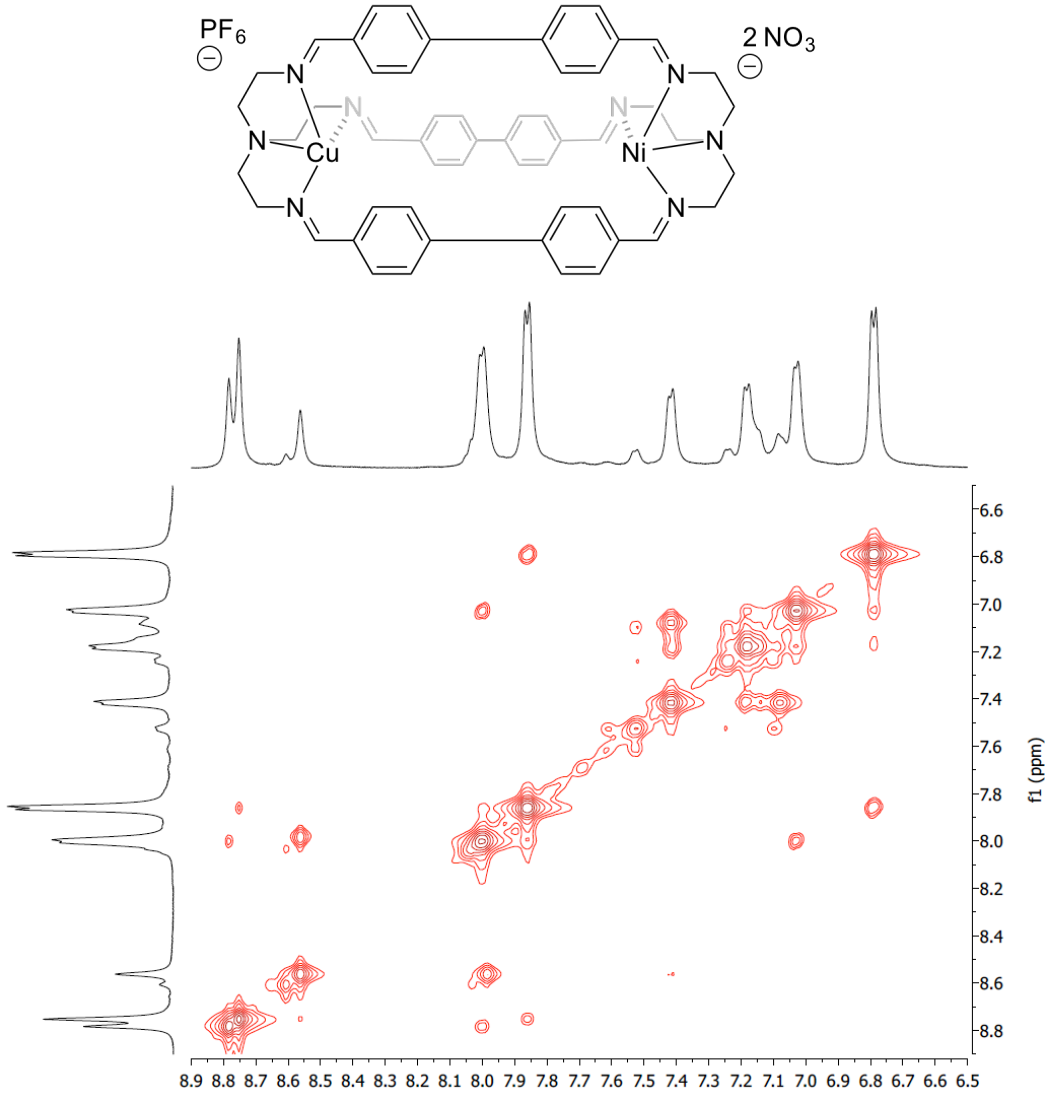

Figure 2.21: NOESY showing the formation of **2.4·CuNi•PF_6•$(NO_3)_2$**. (DMSO-d_6, 400 MHz, 298 K.)

Concerning the formation of the CuNi heterodinuclear complex with cage **2.2**, two different imine peaks are found, one pertains to the binding of Cu(I), and the other to Ni(II). The singlet at 8.75 ppm corresponds to the imine proton adjacent to the Cu(I) binding site, which forms a cross peak with adjacent aryl protons at 7.95 ppm. The singlet at 8.55 ppm corresponds to the imine proton adjacent to the Ni(II) binding site, which

forms a cross peak with adjacent aryl protons at 7.4 ppm. Due to the asymmetric nature of the heterodimetallated cage, distinct aryl protons on the phenyl units adjacent to the different metal binding sites are observed, and can be analyzed with NOESY. Adjacent to the Cu(I) binding site, the doublet aryl peak in closest proximity at 8.0 ppm forms a cross peak with the doublet aryl peak at 7.0 ppm. Adjacent to the Ni(II) binding site, the doublet aryl peak in closest proximity at 7.4 ppm forms a cross peak with the doublet aryl peak at 7.15 ppm. Cross peaks are not observed between the two different sets of doublets (7.2 ppm and 7.0 ppm) that correspond to the aryl protons towards the center of the cage on the two different aryl rings. This is likely due to a torsional twist of the two phenyl rings in relation to each other, as observed in the crystal structures of **2.4·Cu_2•$(PF_6)_2$** and **2.4·Cu•PF_6** shown in **figures 2.8** and **2.15**. Due to the different singlet imine peaks and aryl peaks formed upon metal coordination, the cross peak analysis of the NOESY spectrum is consistent with what one might expect in the formation of a symmetrical cage that has been desymmetrized upon formation of a mixed metal complex.

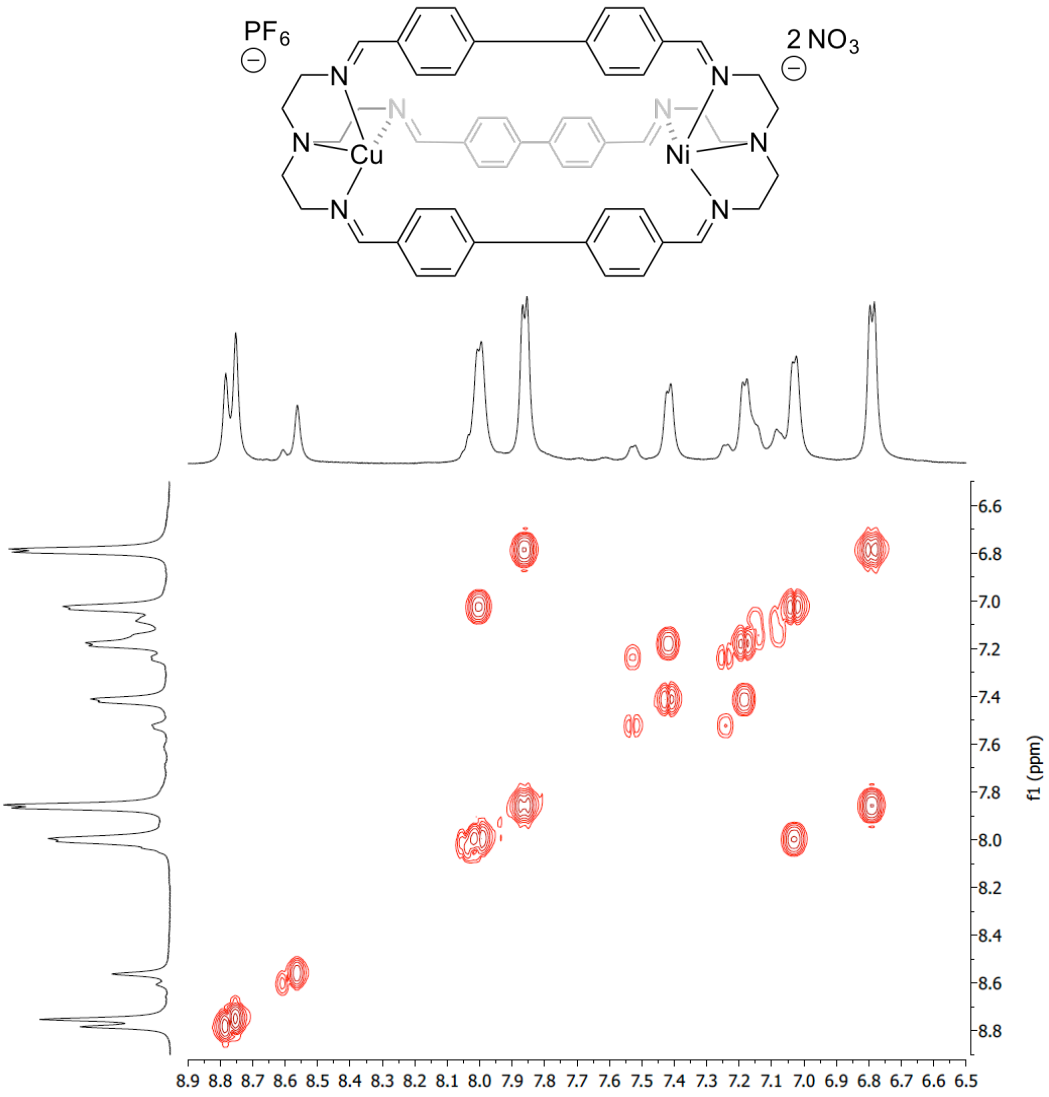

Figure 2.22: COSY spectrum showing the formation of a **2.4·CuNi•PF_6•2$(NO_3)_2$**. (DMSO-d_6, 400 MHz, 298 K.)

The formation of an asymmetric heterodinuclear cage is further supported by a COSY analysis. Cross-peaks between the singlet imine protons and adjacent doublet aryl protons are not observed, however, as in the NOESY spectrum, but cross peaks between adjacent aryl protons are observed. The doublet aryl peaks in closest proximity to the Cu(I) binding site at 8.0 ppm forms a cross peak with the doublet aryl peak at 7.0 ppm.

The doublet aryl peak in closest proximity to the Ni(II) binding site forms a cross peak with the doublet aryl peak at 7.15 ppm, thereby further confirming an asymmetrical heterodimetallated cage.

2.5 Conclusions

In conclusion, six symmetrical ellipsoidal azacryptand cages of differing sizes were synthesized. Most of these cages were observed to be able to bind to Fe(II), Ni(II), Zn(II), Cu(I) and Ag(I). Unusual monometallation was observed with **2.4** and not the other cages.

Heterodinuclear formation with cages **2.2**, **2.4** and **2.6** were attempted with Fe(II), Cu(I) and Ni(II). Heterodinuclear formation was not observed for cage **2.2**, likely due to the close proximity of the two binding sites imposing too much steric strain along the backbone of the cage to be able to accommodate two metals of differing sizes and geometries. Heterodinuclear metallation was observed with cage **2.4** with Fe(II) and Cu(I); and with Cu(I) and Ni(II), likely due to the cage with two phenyl spacing units being able to provide enough stability to the cage to be able to accommodate two metals of different geometries and sizes. Heterodinuclear metallation with Fe(II) and Ni(II) was not observed, likely due to cage being unable to accommodate the differing geometries and sizes of those two metals, thereby resulting in decomposition of cage to *tris*(2-aminoethyl)amine and **2.3**. Heterodinuclear formation was not observed with **2.6**, even though the cage has additional structural support due to the additional phenyl units,

heterodinuclear formation was not observed with cage **2.6**, likely due to the cage's poor solubility.

Future work with this project would entail optimizing synthetic methods to isolate the heterodinuclear cages from the homo dinuclear cages, to study how two different metals of different oxidation states in the interior of a cage interact and influence each other in terms of their electronic, electrochemical, magnetic catalytic and molecular recognition properties.

References

1.) Kang, S. O.; Linares, J. M.; Day, V. W.; Bowman-James, K. "Cryptand-Like Anion Receptors" *Chem. Soc. Rev.* **2010**, *39*, 3980-4003.

2.) (a) Chen, Q. Y.; Luo, Q. H.; Wang, Z. L.; Chen, J. T. "Synthesis and Crystal Structure of the First d-f Heterodinuclear Dy(III)-Cu(II) Cryptate" *Chem. Commun.* **2000**, 1033-1034; (b) Ronson, T. K.; Nelson, J.; Jameson, G. B.; Jeffery, J. C.; Brooker, S. "Controlled Access to Mixed-Metal Pyridazine-Linked Cryptates" *Eur. J. Inorg. Chem.* **2004**, 2570-2584.

3.) Bertini, I.; Gray, H. B.; Valentine, J. S.; Lippard, J., *Bioinorganic Chemistry*. University Science Books: 1994.

4.) (a) Sessler, J. L.; Gale, P. A.; and; Cho, W. S., *Anion Receptor Chemistry*. Royal Society of Chemistry: Cambridge, UK, 2006; (b) Bianchi, A.; Bowman-James, K.; Garcia-Espana, E., *"Supramolecular chemistry of Anions"*. Wiley-VCH: New York, 1987.

5.) Boiocchi, M.; Bonizzoni, M.; Fabbrizzi, L.; Piovani, G.; Taglietti, A. "A Dimetallic Cage with a Long Ellipsoidal Cavity for the Fluorescent Detection of Dicarboxylate Anions in Water" *Angew. Chem. Int. Ed.* **2004**, *43*, 3847-3852.

6.) Drew, M. G.; Harding, C. J.; Howarth, O. W.; Lu, Q.; Marrs, D. J.; Morgan, G. G.; McKee, V.; Nelson, J. "Thiophene-linked Azacryptand Sites for Dicopper and Disilver; Thiophene Sulfur as an Inert Spacer?" *J. Chem. Soc., Dalton Trans* **1996**, 3021-3030.

7.) (a) Chen, M. S.; White, M. C. "A Predictably Selective Aliphatic C-H Oxidation Reaction for Complex Molecule Synthesis" *Science* **2007**, *318*, 783-787; (b) Djernes, K. E.; Padilla, M.; Mettry, M.; Young, M. C.; Hooley, R. J. "Hydrocarbon Oxidation Catalyzed by Self-Folded Metal-Coordinated Cavitands" *Chem. Commun.* **2012**, *48*, 11576-11578.

8.) Tsubomura, T.; Masahiko, E.; Sato, T.; Sakai, K. "A Hexaimino Cryptand Containing Naphthyl Groups; Structural Characterization of Mononuclear Complexes and Catalysis in Hydrolysis of p-Nitrophenyl Phosphate" *Inorg. Chim. Acta* **2000**, *310*, 265-267.

Chapter 3

Allosteric Regulation and Selective Hydrogen Bisulfate Binding in an Azacryptand Urea Host

3.1 Introduction

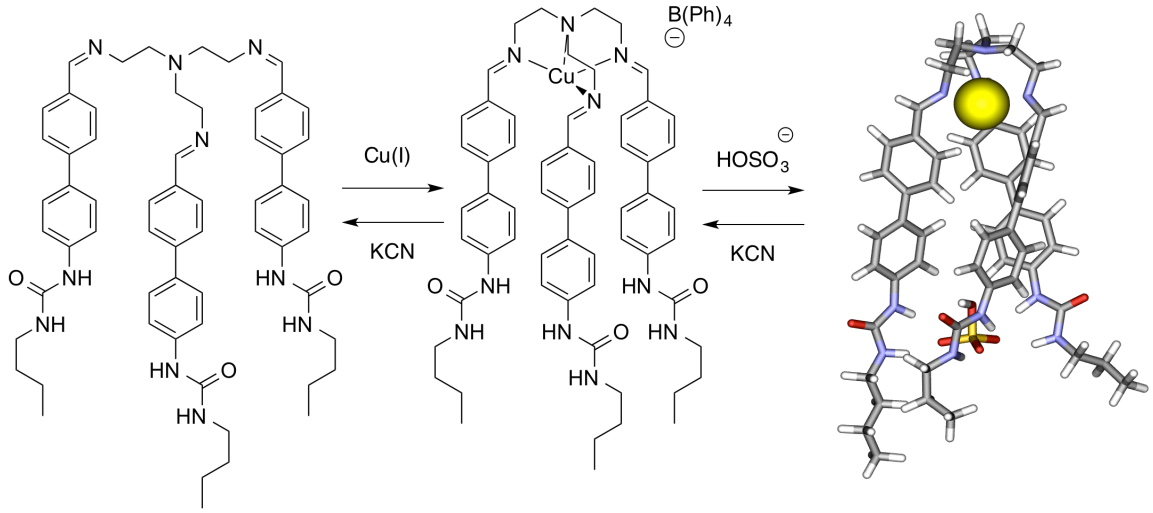

Figure 3.1: Allosteric regulation of hydrogen bisulfate binding.

This chapter describes the formation of tripodal urea azacryptands with *bis*-phenyl spacers and a *tris*(2-aminoethyl)amine (TREN) derived transition metal binding unit located toward the central interior of the structure. This family of urea azacryptands were found to bind to Cu(I), Cu(II), and Ag(I) at the TREN center. Binding at the urea sites with hydrogen bisulfate was observed in the UV-vis.

Hydrogen bisulfate binding at the urea sites was observed with the unmetallated and metallated butyl analog, as well as the phenyl analog in acetonitrile. Pre-organization of the azacryptand with Cu(I) as an allosteric effector at the TREN site brought the three urea sites in closer proximity, thereby increasing the hydrogen bisulfate binding affinity.

An allosteric effect was observed with the butyl analog, where the K_a of hydrogen bisulfate binding is 2.8 times higher with the metallated analog (3.3 x10^2 M^{-1}) than the unmetallated analog (1.2 x 10^2 M^{-1}). The hydrogen bisulfate binding K_a of the metallated phenyl analog was 150 times higher (5.0 x10^4 M^{-1}) than the metallated butyl analog, due to the phenyl analog being more acidic due to the electron withdrawing nature of the phenyl groups, and more sterically hospitable to hydrogen bisulfate binding than the butyl analog which has additional degrees of freedom. The unmetallated phenyl analog was not sufficiently soluble in acetonitrile for study. This allsoteric system is reversible, upon excess addition of KCN.

3.1.1. Design Concept

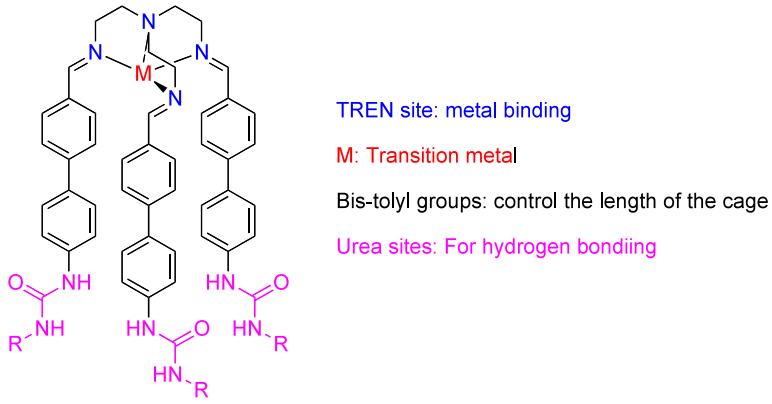

Figure 3.2: Design concept for azacryptand-ureas.

The tripodal cages are ellipsoidal in shape open at one end, and are composed of three main functional parts. The enclosed concave end of the ellipsoidal structure is a TREN imine binding site, capable of binding transition metals. Connected to the TREN imine site are the *bis*-phenyl "arms" that control the length of the cage. At the end are

urea "feet" capable of hydrogen bonding. Metallation at the TREN imine site, efforts towards the formation of dimeric capsules via hydrogen bonding, and anion binding will be further discussed in this chapter.

3.2. Synthesis of Azacryptand Ureas

3.2.1. Synthesis and Metallation of Azacryptand Ureas

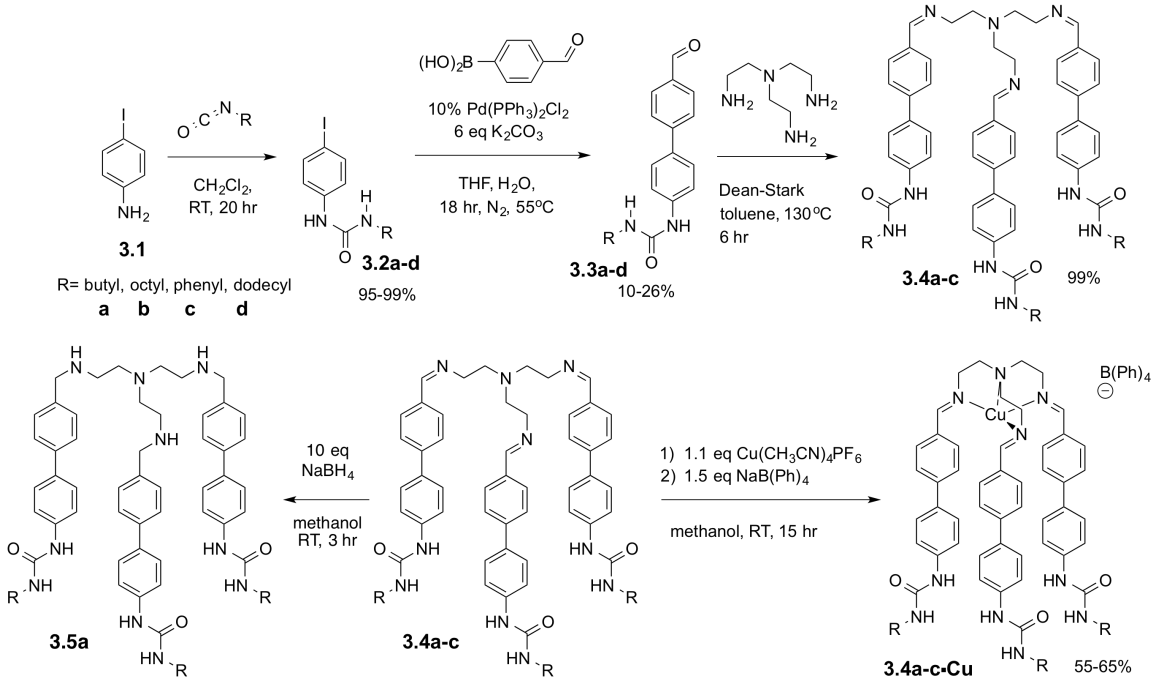

Figure 3.3: Synthesis of Azacryptand-ureas.

The family of azacryptand ureas can be synthesized in three steps, with metallation following as the fourth step. The first step entails the reaction between the commercially available 4-iodoaniline with the appropriate alkyl or phenyl isocyanates in anhydrous methylene chloride to form the corresponding 4-iodo phenyl urea in excellent yields. This is following by Suzuki coupling with the commercially available 4-formyl

phenyl boronic acid to form the urea *bis*-phenyl aldehyde in low yields. Condensation between *tris*(2-aminoethyl)amine and an urea *bis*-phenyl aldehyde forms the tripodal urea azacryptand in high yields. Attempts were made to reduce **3.4a-c** with $NaBH_4$ to its corresponding amine analog, however the product was very difficult to purify.

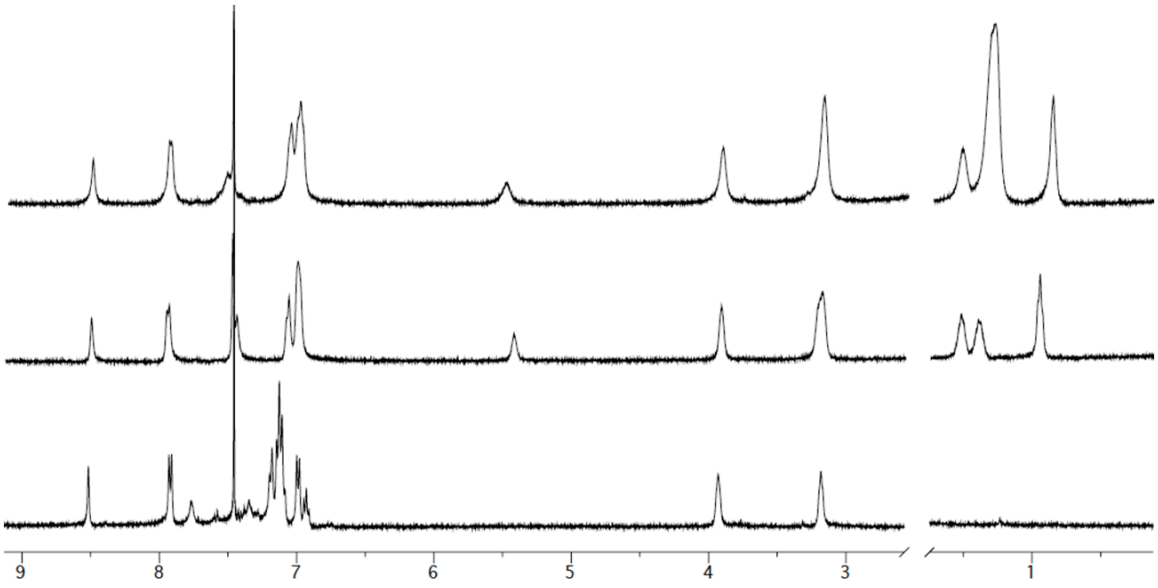

Figure 3.4: ^{1}H NMR of (top to bottom) **4b•Cu**, **4a•Cu**, **4c•Cu**. (50:50 mixture of $CHCl_3$-*d*/Acetonitrile-d_3, 400 MHz, 298 K.)

The family of TREN azacryptand ureas can be metallated with Cu(I), Cu(II), and Ag(I). The **3.4a-c•Cu** analogs with BF_4^- and PF_6^- and Cl_2^{-2} counter anions are soluble in methanol and DMSO, and are insoluble in most common organic solvents. Anion metathesis with sodium tetraphenylborate yields an analog that is soluble in acetonitrile, methanol, DMSO, and is soluble enough in a 50/50 mixture of $CHCl_3$–*d* and acetonitrile-d_3 to be observable via NMR. **3.4c•Ag** with NO_3^- and $B(Ph)_4^-$ were made and were found to have poor solubility in DMSO, and were insoluble in most common organic solvents.

Metallation attempts with various Fe(II), Fe(III), Ga(III) and Zn(II) metal salts under various conditions resulted in complete decomposition of the imine bonds to *tris*(2-aminoethyl)amine and the respective urea *bis*-phenyl aldehyde. Consequently, Fe(II) and Zn(II) metallated analogs were not observed.

Attempts towards enhancing the solubility of the azacryptand scaffold by implementing a lengthy alkyl chain on the urea, thereby increasing the solubility in nonpolar solvents were unsuccessful. The reaction of 4-iodoaniline with dodecylisocyanate led to the formation of **3.2d** in 99% yield. Suzuki coupling with 4-formyl phenyl boronic acid and **3.3d** led to form the urea *bis*-phenyl aldehyde **3.3d** in very low yield, 10%. Several attempts were made using various Pd catalysts, bases and solvents to increase the yield, but these attempts were unsuccessful. Formation of **3.4d** is likely, however it was thoroughly insoluble, and could not be characterized by ^{1}H-NMR or mass spectrometry. Attempts to solubilize of **3.4d** via metallation with Cu(I) were unsuccessful, resulting in either unreacted starting material, or the metallated product was also insoluble.

Attempts towards enhancing the soluble of azacryptand scaffold was also done by reducing **3.4** to its amine analog. Reduction attempts were successful with **3.4a**, resulting in an amine analog soluble in chloroform, methylene chloride, methanol, and acetonitrile. Unfortunately the product could not be purified. Attempts towards synthesizing amine analogs of **3.4b** and **3.4c** were low yielding, and the desired product could not be isolated.

3.2.2. Towards Azacryptand Thioureas

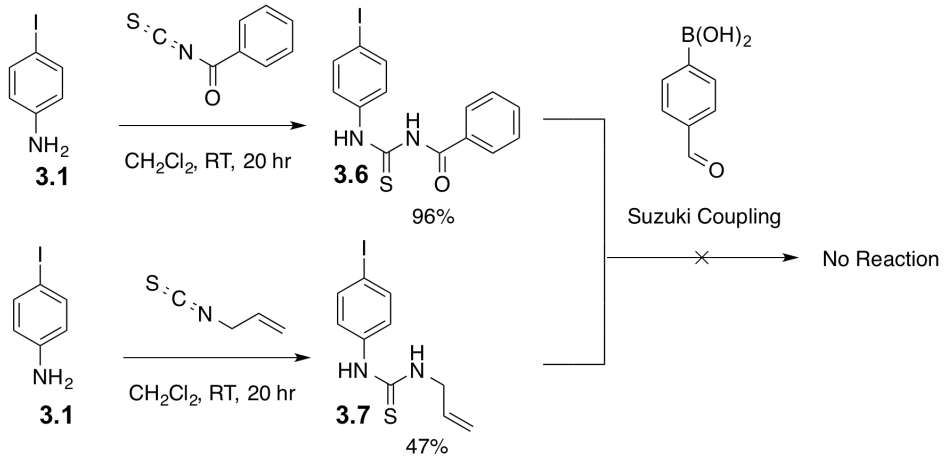

Figure 3.5: Towards the synthesis of azacryptand-thioureas.

In order to enhance the acidity of the uric protons, attempts towards making thiourea analogs of the azacryptand cages was attempted. The acidity of thioureido –NH protons are generally higher than that of ureido –NH protons, with pK_a values in DMSO of 21.1 and 26.9 for thiourea and urea, respectively.[1] Reaction of benzoyl isothiocynate with 4-iodo aniline in methylene chloride at room temperature overnight yielded **3.6** at 98% yield. Reaction of allyl isothiocyanate with 4-iodo aniline in methylene chloride at room temperature overnight yielded **3.7** at 47% yield. Attempts at Suzuki coupling of **3.6** and **3.7** with 4-formyl phenyl boronic acid under various conditions to form the corresponding *bis*-phenyl aldehyde were unsuccessful, resulting in unreacted starting material.

3.3. Towards H-Bonded Urea Self-Assembly

3.3.1. Introduction

The first example of hydrogen bonded dimeric urea capsules was reported in the mid 1990's and was based on the self-assembly of two calix[4]arene scaffolds where the calixarene units dimerize through upper rim interactions with complementary hydrogen bonding patterns based on four urea units per monomer.[2]

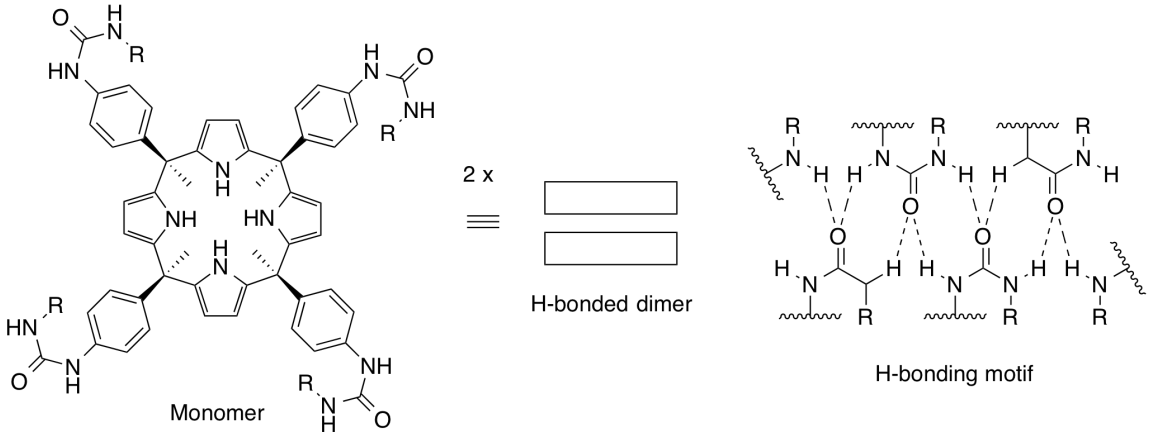

Figure 3.6: Dimeric tetraurea calix[4]pyrrole hydrogen bonded capsules.

To date, there has been one report in the literature of a hydrogen bonded dimeric urea capsule with endohedral functionality, as shown in **Figure 3.6.** The tetraurea calyx[4]pyrrole has a sizable endohedral functionalized cavity consisting of pyrrole units, which are capable of binding a chloride anion in the interior. The tetraurea calix[4]pyrrole undergoes dimerization to form a total of 16 hydrogen bonds from the four urea units located at the upper rim of each monomer. Dimerization is formed in methylene chloride via templation of 4,4'-bipyridine N-N'-dioxide. The encapsulated guest is one molecule of *bis*-N-oxide which is bound to the endohedral pyrrole units via hydrogen bonding.

3.3.2. Efforts Towards H-Bonded Azacryptand Urea Capsules

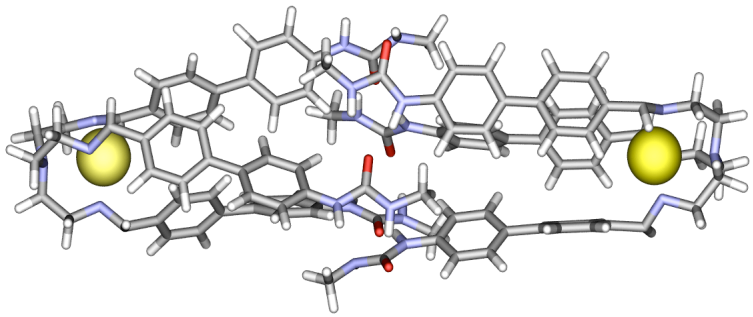

Figure 3.7: Molecular model of an H-bonded azacryptand urea dimer of **5a•Cu**.

The general scaffold for the azacryptand urea consists of three "upper rim" urea units which, *a priori*, should be able to undergo intermolecular dimerization[3] under the right circumstances to form a H-bonded capsule sealed by 12 hydrogen bonds, based on six urea groups.

A molecular model of an azacryptand urea scaffold metallated at the TREN site shows that the three urea subunits in a compatible orientation for the formation of a hydrogen bonded dimeric molecular capsule with two transition metals as endohedral functionality. There is enough space in the interior to encapsulate anions and organic molecules of suitable shapes and sizes. Long chain aliphatic and flat planar molecules could fit in the interior cavity, and depending on the interior metals. For example, the presence of metal coordinating functional groups on the substrate such as carboxylic acids, nitriles and amines would be appropriate to bind to Cu(I) or Cu(II).

Evidence for the formation of a hydrogen bonding cage would be observed via ^{1}H NMR in non polar solutions such as $CHCl_3$-*d* or C_6H_6-d_6 where the hydrogen bonding a

the urea sites would cause the NH protons to shift downfield in relation to the monomer due to the electron withdrawing nature of the carbonyl oxygen atoms that are hydrogen bonded to the NH protons.

There are two methods typically employed to promote the dimerization of hydrogen bonded supramolecular complexes. Either by an increase in concentration in solution or by templation of a guest, where the guest promotes the organization of the two monomers by brining them in close proximity, thereby directing the geometry of the urea units towards intermolecular dimerization.[4]

A thermodynamic benefit to applying templation by guest encapsulation in cavity containing cages is that the displacement of solvent molecular in cage interior is entropically motivated by encapsulation of a larger guest, thereby liberating multiple solvent molecules, resulting in a net gain in the amount of free molecules after encapsulation of a larger guest.[5]

A practical limitation to this family of synthesized azacryptand ureas is the poor solubility in non-polar organic solvents. At best, the copper metallated azacryptands with $B(Ph)_4^-$ counter anions are soluble in a 50/50 mixture of chloroform and acetonitrile. As a consequence, the presence of the polar solvent, acetonitrile in the surrounding medium likely plays a role in inhibiting intermolecular hydrogen bonding and guest encapsulation.

Templation can be promoted by a guest of C_2 symmetry with functional groups compatible to bind to the interior copper at both ends of a lengthy guest (or short chain, where the guest can bounce back and forth from both ends of the enclosed dimeric cage like a ping pong ball in equilibrium) thereby bringing together two azacryptands to guide

the urea moieties for intermolecular dimerization. Several (short and long chain) alkyl and phenyl amines, carboxylic acids, nitriles, ketones and alcohols were screened for either monomeric guest encapsulation or promotion of dimeric formation by way of guest templation. Guest encapsulation was not observed.

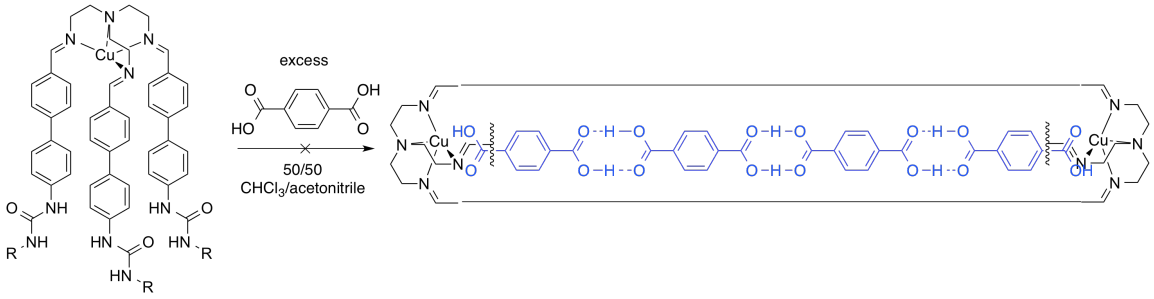

Figure 3.8: Example of intermolecular dimeric hydrogen bond formation via templation with a repeating series of smaller hydrogen bonding guests (terphthalic acid) that bridge together both ends of the cage. The donor azacryptand cage is of suitable size to be able to accommodate four molecules of terphthalic acid.

Another anticipated possibility to promote dimerization via templation was that smaller guests would hydrogen bond with each other in a head to tail fashion thereby acting as a bridge from one end of the cage interior to the other. Neither guest encapsulation nor intermolecular hydrogen bonding was observed.

Further attempts to promote intermolecular hydrogen bonding were performed by increasing the concentration of the azacryptand urea in a 50/50 mixture of chloroform and acetonitrile. Broad and unresolved signals were observed in the aryl region, suggesting the formation of ambiguous aggregates.

3.4. Azacryptand-Urea Anion Binding via Allosteric Regulation

In this section, factors to consider towards the design of anion receptors will be discussed, as well as factors to take in to account in the design of hydrogen bonding anion receptors such as (thio)ureas. This will be followed by an analysis of results of anion binding studies of the family of metallated and unmetallated azacryptand ureas studied.

3.4.1. Introduction to Anion Binding

Cation	*r*[Å]	Anion	*r*[Å]
Na^+	1.16	F^-	1.19
K^+	1.52	Cl^-	1.67
Rb^+	1.66	Br^-	1.82
Cs^+	1.81	I^-	2.06

Figure 3.9: A comparison of the radii of isoelectronic anions and cations in octahedral environments.[6]

Anions are commonplace throughout nature and are involved in a wide variety of biological processes. Much effort in recent years has been spent on anion recognition.[7] Designing anion receptors is challenging for four main reasons: 1) Anions display a wide range of coordination geometries which requires a higher degree of selectivity in the anion receptor. 2) H-bonding anion receptors are limited to functioning within a certain pH frame in order to not protonate the target anion. 3) Compared to other isoelectronic cations, anions have a lower charge to radius ratio. As a consequence of this, electrostatic binding with anions is less effective than cations. 4) Solvent effects are heavily influential

to the strength and selectivity of anion binding. Anions generally have high free energies of solvation, and as a consequence anion hosts compete with solvation from the surrounding environment for anion recognition. Anion binding is generally stronger in non-polar solvents due to the anion's solvophobic properties. Host-anion binding constants generally increase with the following solvent order: H_2O < DMSO < CH_3CN < $CHCl_3$ < CCl_4.[6, 8]

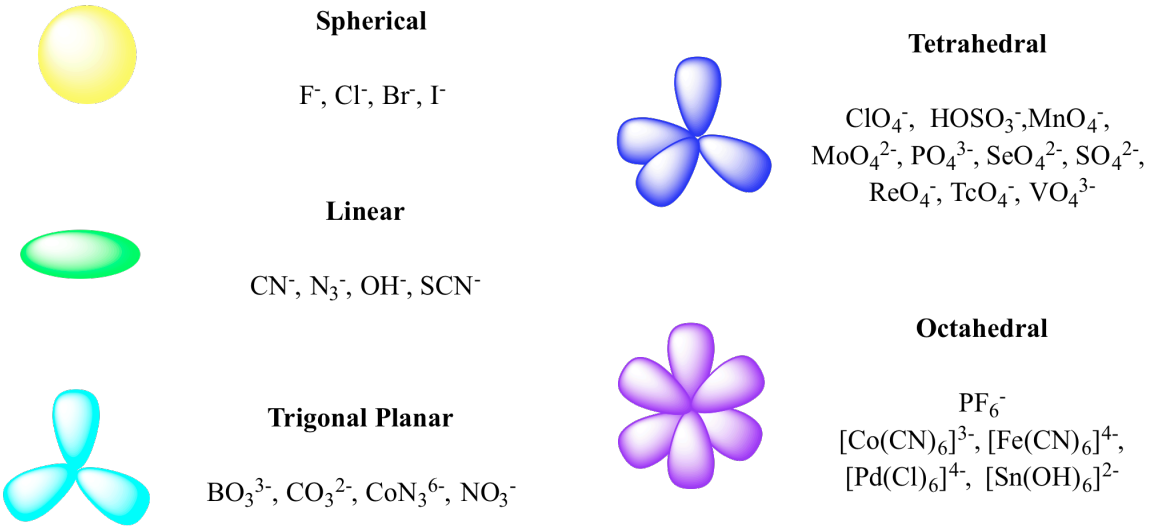

Figure 3.10: The geometric types of anions.[6]

Molecules capable of anion recognition are typically categorized by the type of non covalent interactions used to complex the anions, such as: electrostatic interactions, hydrogen bonding, hydrophobicity, metal-ligand coordination.[6] Molecules containing (thio)urea binding sites are well precedented to be able to hydrogen bond to anions by hydrogen bond donation of the (thio)ureido –NHs.[1]

In addition to taking into account the various factors that go in to the design of anion recognition, other variables to consider which are unique to (thio)urea anion

receptors as hydrogen bond donors include 1) the strength of hydrogen bonding (which is influenced by the presence of electron withdrawing substituents on the receptor.) 2) The *cis* or *trans* conformation of the two (thio)ureido N-H bonds in relation to the C=Z bond (Z=S or O) and, 3) the topology of the (thio)urea binding site(s) in the anion receptor.[1]

3.4.2. Allosteric Regulation of Hydrogen Bisulfate Recognition

Developing a system where the anion binding capability can be controlled by an exterior factor is of interest.[9] This can be done via principles of allosteric regulation, where the binding of a substrate at one site can control enzyme activity at the active site by altering its conformation.[9a]

Given the C_3 symmetric nature of the unmetallated and metallated azacryptand ureas, the three urea groups are well positioned to be able to bind to anions of spherical, tetrahedral, and trigonal planar geometry. Several salts were screened for the anion binding capability of **3.4a-c** and **3.4na-c•Cu** in acetonitrile or a 50/50 mixture of chloroform and acetonitrile via ^{1}H NMR and in the UV-vis in acetonitrile. These salts include F^-, Cl^-, Br^-, I^-, PF_6^-, BF_4^-, NO_3^-, SbF_6^-, PO_4^-, PO_4^{-2}, PO_4^{-3}, NO_3^-, SO_4^{-2}, and $HOSO_3^-$. Binding was not observed via ^{1}H NMR, in most cases, precipitate emerged, likely due to anion metathesis with the tetraphenylborate counter anion. In the UV-vis spectrum, however, anion binding was exclusively observed with $HOSO_3^-$ and both unmetallated and metallated azacryptand urea analogs **3.4a-c** and **3.4a-c•Cu**. Anion recognition of $HOSO_3^-$ was also exclusively observed in the presence of several other anions for both unmetallated and metallated azacryptand analogs. To rule out the

possibility that hydrogen bisulfate binding is occurring at the Cu(I) site instead of the urea sites, a pyridyl analog of the Cu(I) metallated azacryptand was tested for hydrogen bisulfate binding in the UV-vis. Changes in the UV-vis were not observed, confirming the preferential binding of hydrogen bisulfate at the urea sites instead of the Cu(I) site.

$$\frac{1}{\Delta A} = \frac{1}{b\Delta\varepsilon[G]_o[H]_o K_a} + \frac{1}{b\Delta\varepsilon[G]_o}$$

Figure 3.11: The Benesi-Hildebrand equation, where ΔA=change in absorbance upon incremental addition of guest, b=path length of the UV-vis cuvette where the sample is contained, Δε = change in molar absorptivity of the H•G complex, $[G]_o$ = initial concentration of guest, $[H]_o$ = initial concentration of host, K_a = association constant.

Studies measuring the equilibrium constants of host-guest association were done via UV-vis. The Benesi-Hildebrand method was used to calculate the measured K_a values. The Benesi-Hildebrand method, derived from the Beer-Lambert equation, A=εlc, can be used to determine the K_a of a host-guest interaction by studying the donor-acceptor charge transfer bands in the UV-vis as a function of the varying the concentration of the gust. Upon incremental addition of guest in to a solution of a fixed amount of host, the inverse change in absorbance, 1/ΔA is plotted on the y-axis and the inverse concentration of added guest, 1/[G] is plotted in the x-axis. The association constant, K_a can be determined as the inverse slope of the graph, $1/K_a$.

There are three main instrumental methods used in determining K_a values, either by photospectroscopical methods such as UV-vis absorption and fluorescence emission and NMR. Photospectroscopic methods are more sensitive and therefore provide a more accurate means of determining association constants compared to NMR because UV-vis can monitor differences in absorption phenomena on a picosecond time scale and

fluorescence emission can be monitored in a nanosecond time scale. The NMR time scale is considerably slower (ms range) than that of photospectroscopical methods. As a consequence of this, it is often the case that a separate signal for the host-guest complex is not clearly observed. Instead, the signal observed for the guest would be the averaged signal for the guest and host-guest complex. When the host-guest signals can be clearly observed, NMR is beneficial to observe structural information that photospectroscopical methods cannot.

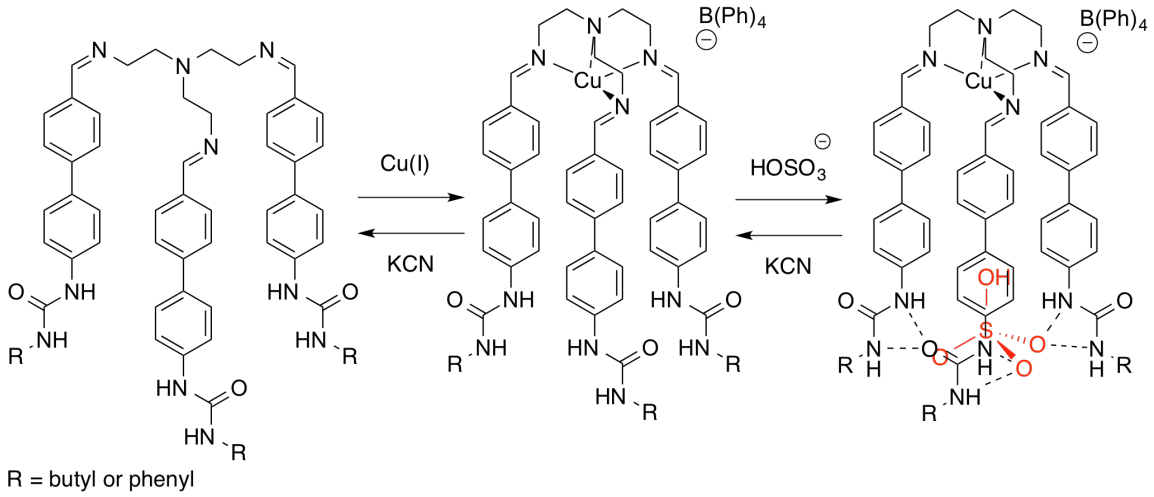

Figure 3.12: Pre-organization of an azacryptand with Cu(I) as an allosteric effector enhances the favorability hydrogen bisulfate binding. The system is reversible with excess addition of KCN.

Entry	ε ($cm^{-1}•M^{-1}$)	λ_{max}(abs)(nm)	K_a (M^{-1})	ΔG (J/mol)
4a	1.4×10^2	300	-	-
4a•$HOSO_3^-$	2.4×10^2	309	1.2×10^2	1.2×10^4
5a	1.0×10^3	318	-	-
5a•$HOSO_3^-$	1.4×10^2	354	3.3×10^2	1.4×10^4
5c	3.1×10^5	312	-	-
5c•$HOSO_3^-$	2.4×10^4	323	5.0×10^4	2.6×10^4

Table 3.1: Molar absorptivity, λ_{max}, K_a and ΔG values for azacryptand ureas.

K_a values were measured and calculated for **3.4a** and **3.4a•Cu** and **3.4c•Cu**. Due to poor solubility in acetonitrile, reliable K_a values were not acquired for **3.4b** , **3.4c** and **3.4b•Cu**.

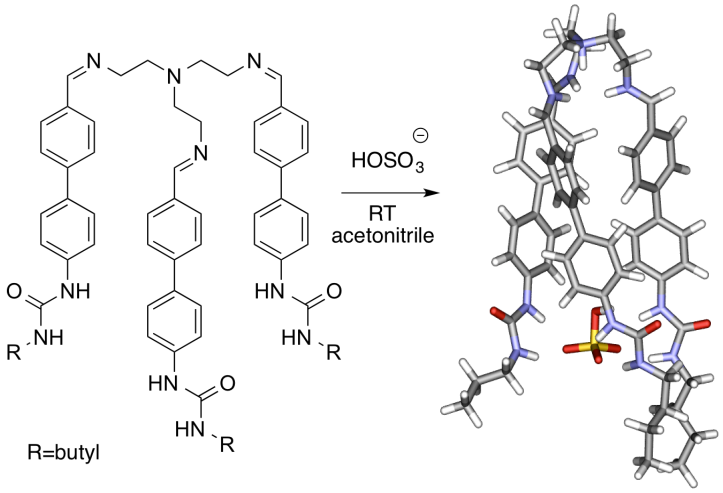

Figure 3.13: 3.4a binding to hydrogen bisulfate.

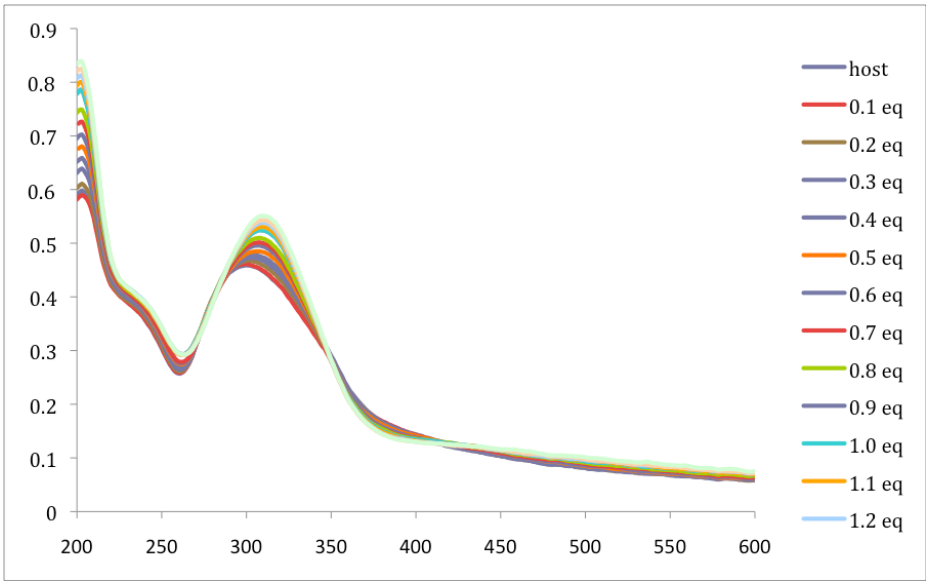

Figure 3.14: Hydrogen bisulfate anion binding with **3.4a**. $\varepsilon_{\lambda=300}$=1.4 x10^2 mol•cm/L of **3.4a** and $\varepsilon_{\lambda=309}$=2.4 x10^2 mol•cm/L for **3.4a•HOSO$_3^-$**.

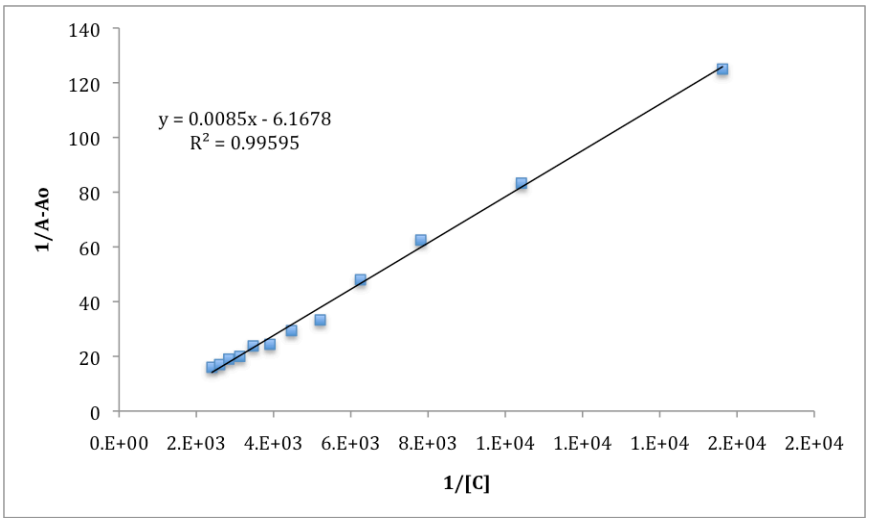

Figure 3.15: Benesi-Hildebrand graph of hydrogen bisulfate anion binding with **3.4a**. K_a=1.2 x 10^2 M^{-1} for **3.4a•HOSO$_3^-$**.

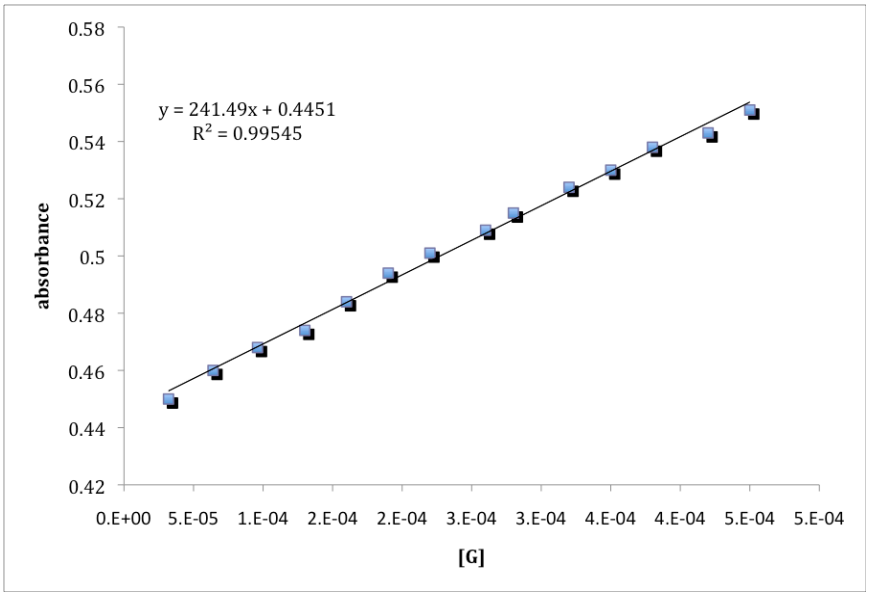

Figure 3.16: Beer-Lambert plot of **3.4a•HOSO$_3^-$**. $\varepsilon_{\lambda=309}$=2.4 x$10^2$ mol•cm/L.

Hydrogen bisulfate binding was observed with the unmetallated butyl analog, **3.4a (see figure 3.14)**, which was found to have a maximum absorption at 300 nm, and a molar absorptivity of 1.4 x 10^2 $cm^{-1}M^{-1}$. Upon hydrogen sulfate binding, at a maximum of the incremental addition of hydrogen bisulfate anion to 1 equivalent, the maximum absorption red shifts to 309 nm, with an increase of molar absorptivity was calculated by way of a Beer-Lambert plot to be 2.4 x 10^2 $cm^{-1}\bullet M^{-1}$. The binding event was found to have a positive equilibrium constant of 1.2 x 10^2M^{-1}.

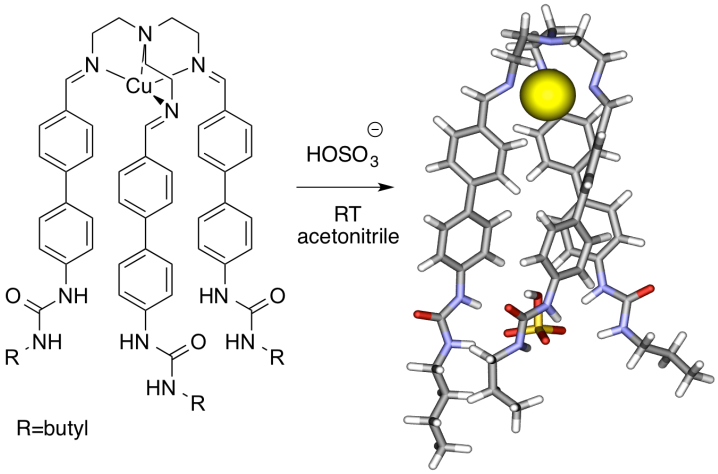

Figure 3.17: 3.4a•Cu binding to hydrogen bisulfate.

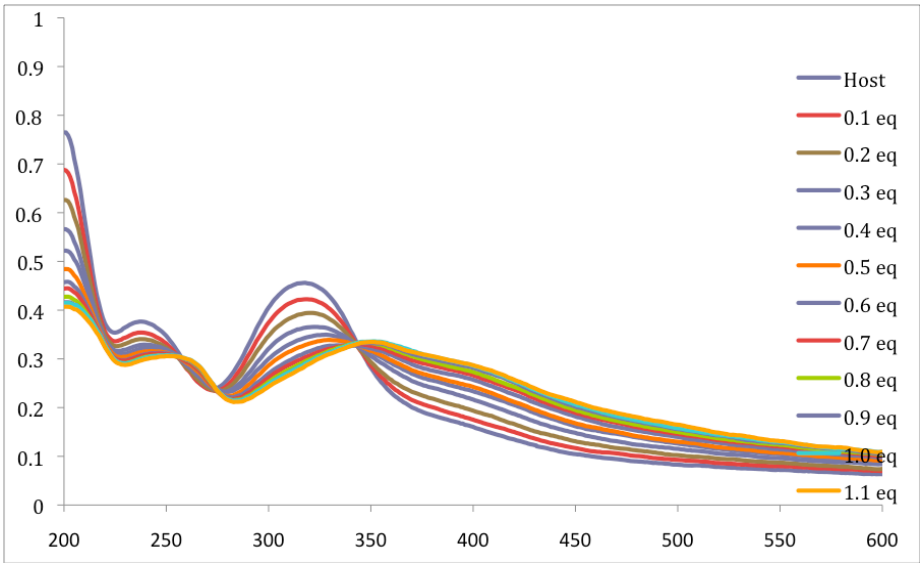

Figure 3.18: Hydrogen bisulfate anion binding with **3.4a•Cu**. $\varepsilon_{\lambda=318}$=1.0 x$10^3$ mol•cm/L and $\varepsilon_{\lambda=354}$=1.4 x$10^2$ mol•cm/L for **3.4a•Cu•HOSO$_3^-$**.

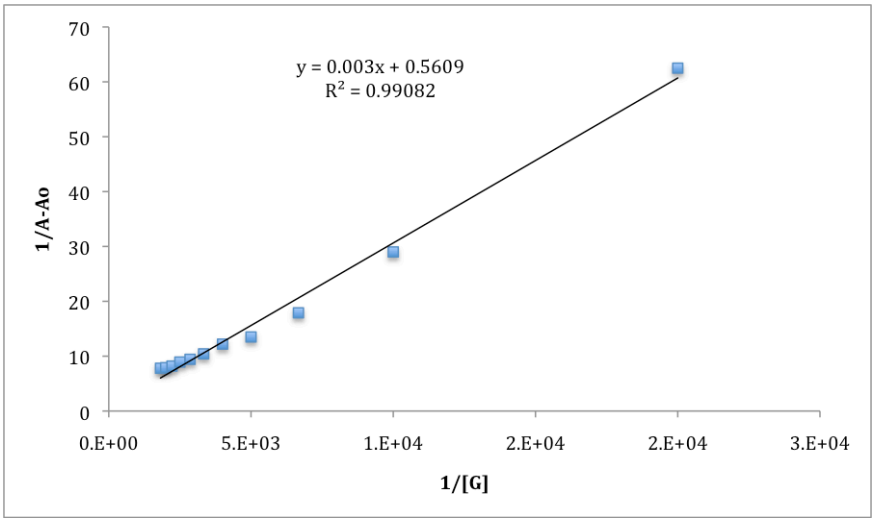

Figure 3.19: Benesi-Hildebrand graph of hydrogen bisulfate anion binding with **3.4a•Cu**. K_a=3.3 x10^2 M^{-1} for **3.4a•Cu•HOSO$_3^-$**.

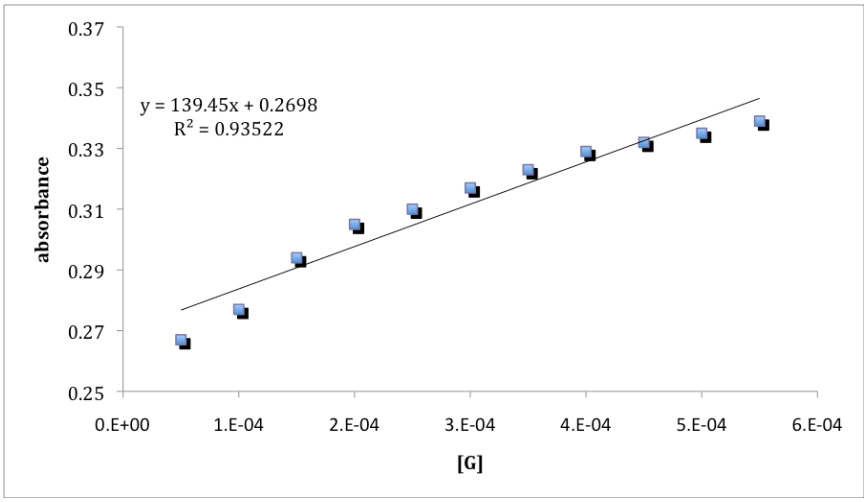

Figure 3.20: Beer-Lambert plot of **3.4a•Cu•HOSO$_3^-$** $\varepsilon_{\lambda=309}$=1.4 x$10^2$ mol•cm/L.

Hydrogen sulfate binding was observed with the metallated butyl analog, **3.4a•Cu (figure 3.18)**, which has a higher molar absorptivity and maximum absorption, both at 1.0 x $10^{23}cm^{-1}M^{-1}$ and 318 nm respectively. Upon hydrogen bisulfate binding, at a maximum of the incremental addition of hydrogen sulfate anion to 1.1 equivalent, the molar absorptivity considerably decreases to 1.4 x 10^2 cm-$1M^{-1}$ and has a sizable red shift to 354 nm. A clear isosbestic point was observed at 345 nm, providing evidence of the formation of a 1:1 species. The K_a value was 3.3 x 10^2 M^{-1}, which is 2.8 times higher than the unmetallated analog. This enhanced K_a value observed with the metallated analog is attributed to the pre-organization Cu(I) as an allosteric effector provides in changing the conformation of the molecule, providing a preformed pocket for hydrogen bisulfate binding. Therefore, the change in conformation of the molecule increases the favorability of hydrogen sulfate binding.

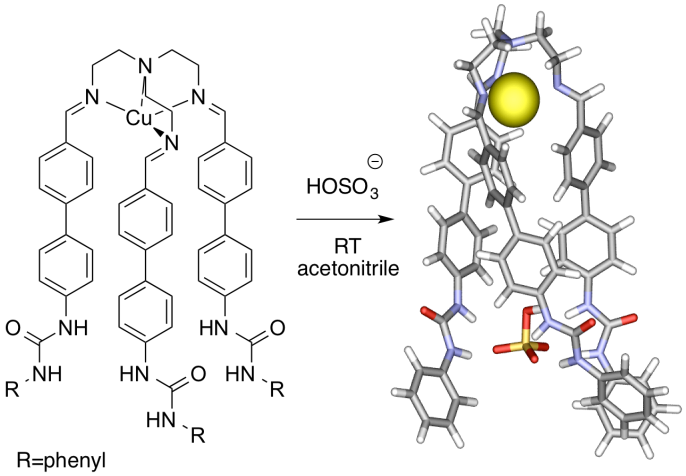

Figure 3.21: 3.4c•Cu binding to hydrogen bisulfate.

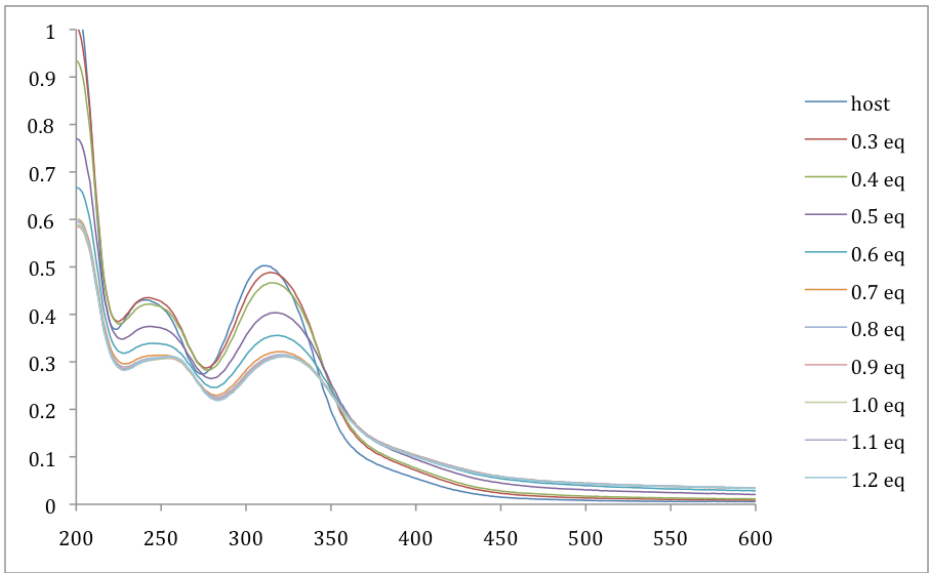

Figure 3.22: Hydrogen bisulfate anion binding with **3.4c•Cu**. $\varepsilon_{\lambda=318}$=3.1 x$10^5$ mol•cm/L and $\varepsilon_{\lambda=352}$=1.2 x$10^5$ mol•cm/L for **3.4c•Cu•$HOSO_3^-$**.

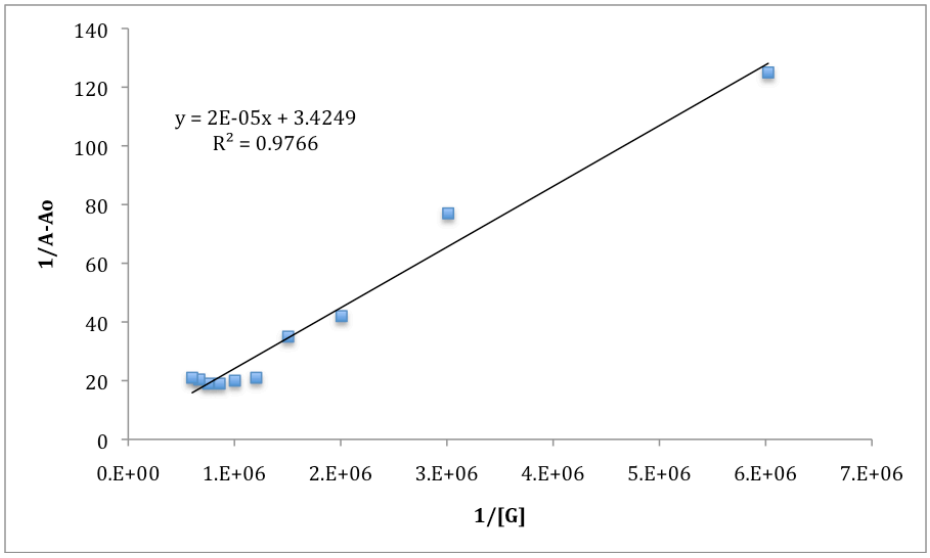

Figure 3.23: Benesi-Hildebrand graph of hydrogen bisulfate anion binding with **3.4c•Cu.** K_a=5.0 x10^4 M^{-1} for **3.4c•Cu•HOSO$_3^-$**.

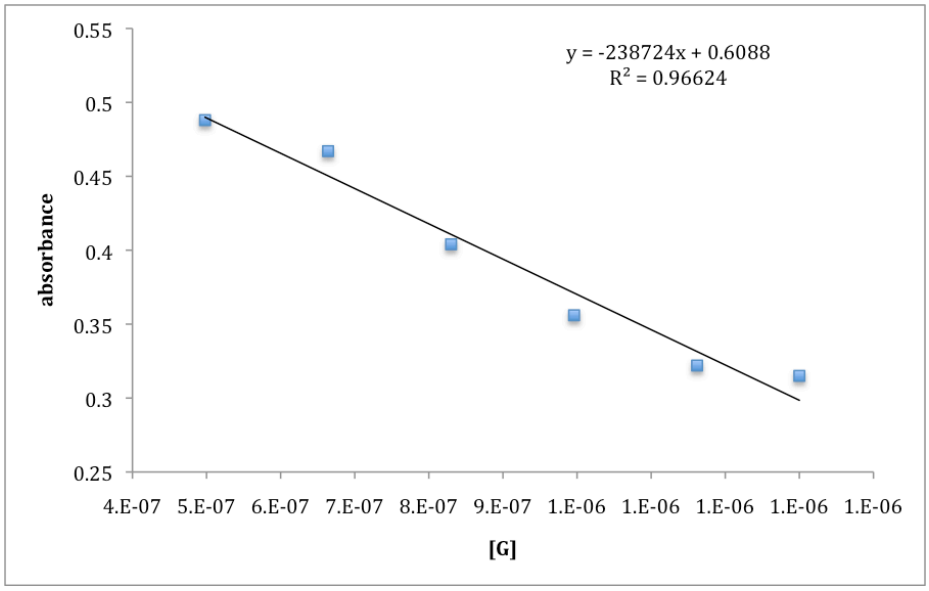

Figure 3.24: Beer-Lambert plot of hydrogen bisulfate anion binding with **3.4c•Cu**. K_a=2.4 x10^4 M^{-1} for **3.4c•Cu•HOSO$_3^-$**.

Hydrogen sulfate binding was observed with **3.4c**, but due to poor solubility in acetonitrile, K_a values were not acquired. Hydrogen bisulfate binding was observed with the metallated phenyl analog, **3.4c•Cu (figure 3.22)**, which has a molar absorptivity of 3.1 x 10^5 cm-1•M^{-1}, higher than the butyl analog, Just like the butyl analog, a red shift was observed upon hydrogen bisulfate binding, although the red shift was slight in relation to the butyl analog. 3.4•c•Cu•$HOSO_3$ has a molar absorptivity value of 2.4 x 10^4 , higher than the butyl analog, but a lower absorption maximum at 323 nm. This is only a difference of 11 nm between unmetallated and metallated phenyl analog. The change in maximum absorption for the butyl analog is much higher, having a difference of 36 nm. Also, the K_a value for the metallated phenyl analog was observed to be 5.0 x 10^2 M^{-1}, 150 times greater than the metallated butyl analog. The higher K_a value is due to the phenyl analog being more acidic due to the electron withdrawing nature of the phenyl groups, and more sterically hospitable to hydrogen bisulfate binding than the butyl analog which has additional degrees of freedom.

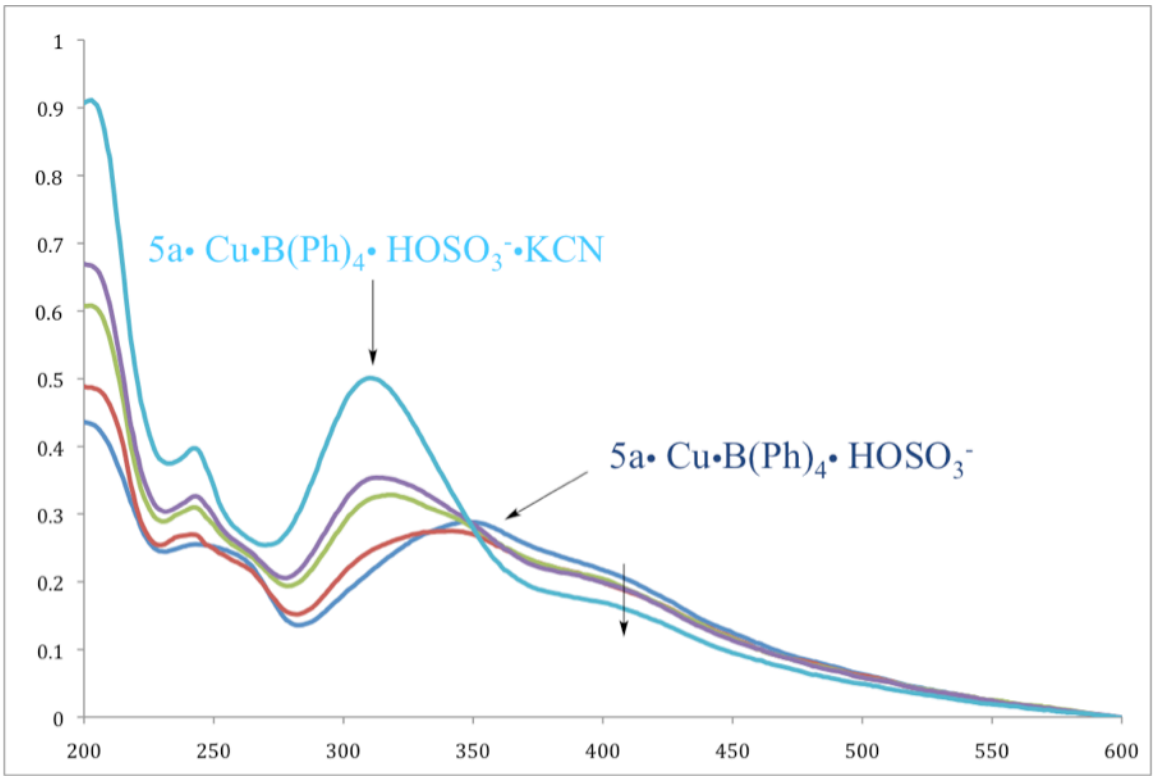

Figure 3.25: UV-vis of **3.4a•Cu•$HOSO_3^-$** incrementally reverting back to **3.4a** upon excess addition of KCN.

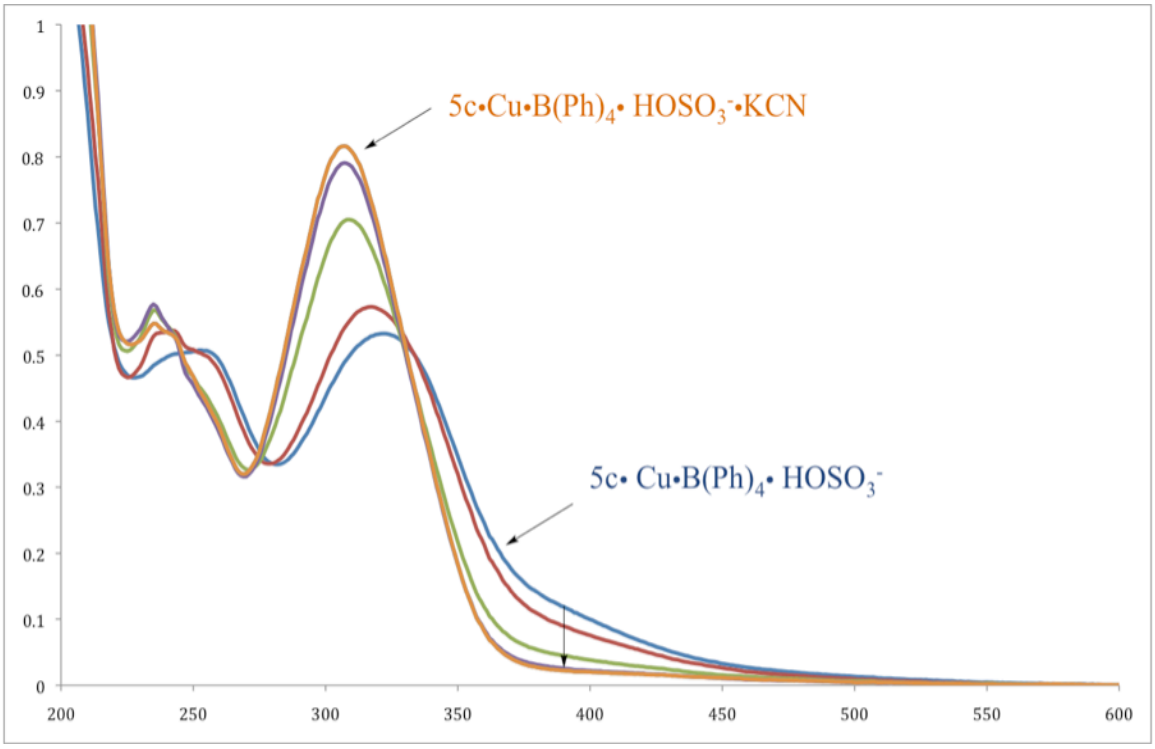

Figure 3.26: UV-vis of **3.4c•Cu•HOSO$_3^-$** incrementally reverting back to **3.4c** upon excess addition of KCN.

Upon excess addition of KCN, both metallated butyl and phenyl analogs bound to hydrogen sulfate will revert back to unmetallated and analog, liberated of hydrogen bisulfate. If both 3.4•a•Cu•$HOSO_3^-$ and 3.4•c•Cu•$HOSO_3^-$ were to stir at room temperature in acetonitrile with excess amounts of KCN for 4 h, the ^{1}H NMR in DMSO of the products would show their respective unmetallated analogs with no evidence of decomposition. To further prove the liberation of hydrogen sulfate, UV-vis titrations (**figures 3.25 and 3.26**) of the incremental excess addition of KCN[10] to **3.4a•Cu•$HOSO_3^-$** and **3.4c•Cu•$HOSO_3^-$** showed the slow reversion back to their respective unmetallated and hydrogen sulfate free analogs. (Due to the poor solubility of KCN in acetonitrile, reliable K_a values were not measured.)

3.5. Conclusions

In conclusion, an allosteric effect was observed in these azacryptand ureas, where Cu(I) as the allosteric effector demonstrated to increase the binding affinity of hydrogen sulfate upon changing the conformation of the molecule by bringing the urea groups in closer proximity upon binding at the TREN site. It was also demonstrated that urea groups with electron withdrawn substituents increase the binding affinity. This system is reversible with excess addition of KCN, where excess CN- is excellent at demetallating Cu(I) from chelating ligands, and the excess presence of KCN is suitable for liberating hydrogen sulfate.

References

1.) Li, A. W., J.; ; Wang, F.; Jiang, Y. "Anion Complexation and Sensing Using Modified Urea and Thiourea-Based Receptors" *Chem. Soc. Rev.* **2010**, *39*, 3729-3745.

2.) Shimizu, K.; Rebek, J. "Synthesis and Assembly of Self-Complementary Calix[4]arenes" *Proc. Natl. Acad. Sci.* **1995**, *92*, 12403-12407.

3.) Alajarin, M.; Orenes, R.; Howard, J.; Spencer, E.; Steed, J.; Pastor, A. "Novel Capsular Aggregates From Flexible Tripodal Triureas with Cs Symmetry" *Chem. Eur. J.* **2012**, *18*, 2389-2397.

4.) Steed, J. W.; Turner, D. R.; Wallace, K. J., *Core Concepts in Supramolecular Chemistry and Nanotechnology*. 1st ed.; Wiley: West Sussex, U.K, 2007.

5.) Steed, J. W.; Atwood, J. L., *Supramolecular Chemistry*. 2nd ed.; Wiley: West Sussex, U.K, 2009; p 643.

6.) Beer, P.; Gale, P. "Anion Recognition and Sensing: The State of the Art and Future Perspectives" *Angew. Chem. Int. Ed.* **2001**, *40*, 486-516.

7.) Llinares, J.; Day, V.; Bowman-James, K. "Cryptand-like Anion Receptors" *Chem. Soc. Rev.* **2010**, *39*, 3980-4003.

8.) Steed, J. W.; Atwood, J. L., *Supramolecular Chemistry*. 2nd ed.; Wiley: West Sussex, U.K, 2009; p 234-235.

9.) (a) Goodey, N.; Benkovic, S. "Allosteric Regulation and Catalysis Emerge via a Common Route" *Nat. Chem. Biol.* **2008**, *4*, 474-482; (b) Anslyn, E. "Signal Amplification by Allosteric Catalysts" *Angew. Chem. Int. Ed.* **2006**, *45*, 1190-1196; (c) Kovbasyuk, L.; Kramer, R. "Allosteric Supramoleular Receptors and Catalysts" *Chem. Rev.* **2004**, *104*, 3161-3187.

10.) Atkinson, I. M.; Lindo, L. F.; Stoddart, J. F., *Self-Assembly in Supramolecular Systems*. 1st ed.; Royal Chemical Society: Cambridge, U.K., 2000.

Chapter 4

Metal-Ligand Self-Assembly from Tripodal Ligands with Endohedral Functionality

4.1. Introduction

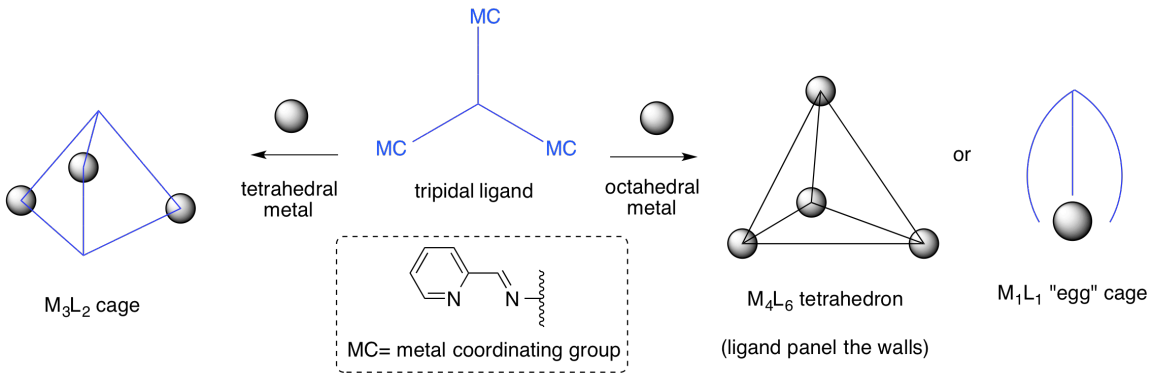

Figure 4.1: Possible self-assembled polyhedra from C_3 symmetric ligands.

This chapter describes the self-assembly efforts of C_3 symmetric tripodal ligands with three bidentate metal binding sites and metal ions with tetrahedral and octahedral coordination geometries. Two different types of C_3 symmetric ligands were explored, *tris*(4-aminophenyl)methanol (*p*-rosaniline) derivatives with salen and pyridine imine metal coordinating groups, and TREN *p*-aniline derived ligands with pyridine imine metal coordinating groups.

This chapter also describes the synthesis of *p*-rosaniline pyridine imine and salicylaldehyde derived ligands and the full characterization of M_4L_6 *p*-rosaniline pyridine imine tetrahedral cage with Fe(II) and M_3L_2 trigonal bipyramide with Cu(I), as

well as the synthesis of *tris*(2-aminoethyl)amine (TREN) amine aniline ligands and self-assembly attempts with tetrahedral and octahedral metals.

4.1.1. General Design Concept for Endohedral Functionality

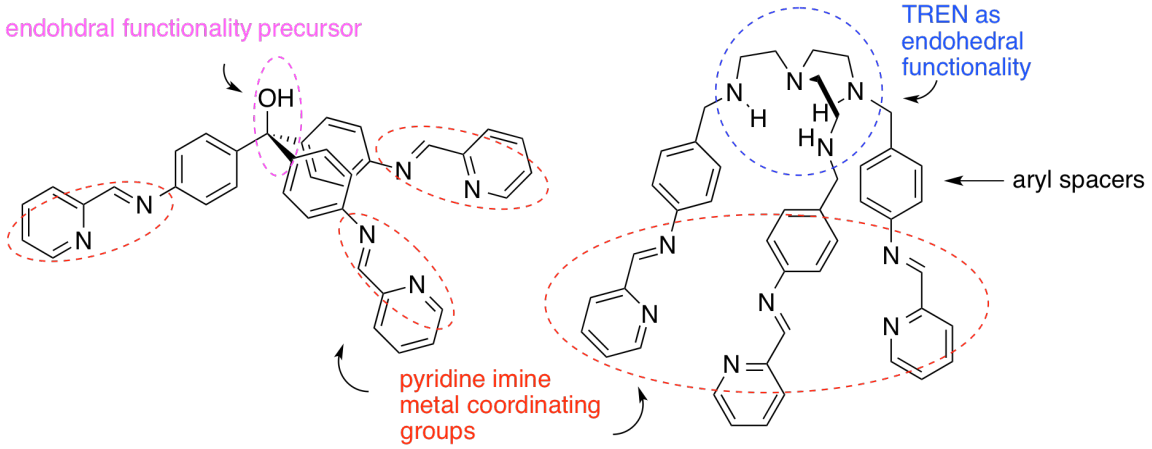

Figure 4.2: C_3 symmetric ligands: *p*-rosaniline derived (left) and TREN amine *p*-aniline derived (right.)

The self-assembly of two different C_3 symmetric ligand scaffolds with pyridine imine metal coordinating groups were explored. One ligand has a *tris* phenyl methanol core, and the other ligand has a TREN amine site for endohedral functionality. Both ligands have pyridine imine metal coordinating groups, which are known to chelate tetrahedral metals such as Cu(I) and Cu(II)[1] and octahedral metals such as Zn(II),[2] Cd(II),[3] Fe(II), Co(II), and Ni(II)[4] in metal-ligand self assembled polyhedra.[1a] Some of these complexes have been reported to be air stable and soluble in water.[5] The most common approach in the metal-ligand self-assembly of pyridine-imine complexes is via multi-component self assembly, an approach that was pioneered in recent years,[1a, 6] where

multiple subcomponents self assemble to form a polyhedron, as opposed to two building blocks, *e.g.* an intact ligand and a metal salt.

4.2. Self-Assembly from *p*-Rosaniline Derivatives

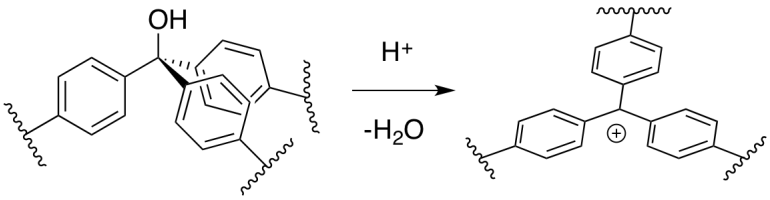

Figure 4.3: Formation of a cation as endohedral functionality in a *p*-rosaniline derived self-assembled complex.

Para-rosaniline was chosen as a ligand precursor because of its commercial availability. It has very high molar absorptivity and is often used as a dye, so its interesting photophysical properties might be of interest for sensing applications if *p*-rosaniline constituted the wall paneling of a self-assembled complex. Endohedral functionality can potentially be generated in the *p*-rosaniline self-assembled complex by acidic elimination of the hydroxy group. The driving force of the reaction is thermodynamically and entropically favored by the formation of water, and the subsequent cation that is generated is resonance stabilized by the tertiary carbon attached to three phenyl groups with *para*-amino functionality.

A carbocation as endohedral functionality can be used to promote fragmentation, or rearrangement reactions with an appropriate substrate, or to render the cage available for post synthetic modification[7] with addition of a nucleophile. Ideally, the self-assembled species would be soluble in water, thereby promoting reactions in the interior of the cavity via hydrophobic effect.

4.2.1. Self-Assembly of an M_4L_4 *p*-Rosaniline Fe(II) Tetrahedron Cage

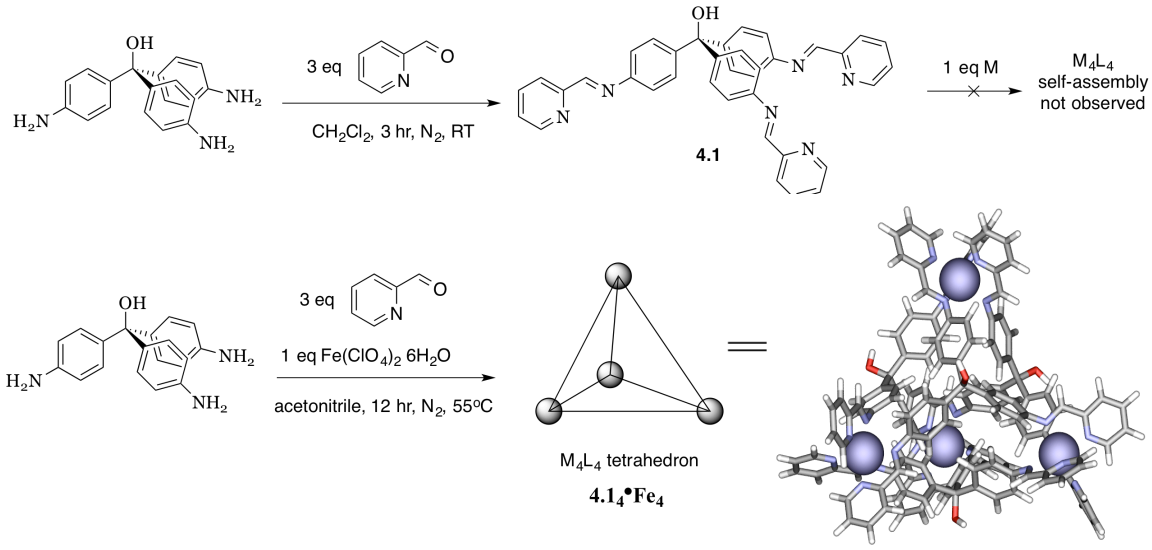

Figure 4.4: Ligand synthesis of *p*-rosaniline pyridine imine (top) and multicomponent self-assembly of M_4L_4 tetrahedron (bottom.)

In principle, a tripodal ligand with bidentate metal coordinating groups having a metal-ligand approach angle close to 35.3° should form a M_4L_4 tetrahedron cage with an octahedral metal.[8] Several attempts towards self-assembly were attempted via "paneling method" and "multicomponent method" under various temperatures (room temperature to 150°C), solvents (acetonitrile, THF, 1,4 dioxane, H_2O, toluene, benzene, toluene, xylenes, ethanol, methanol, diethyl ether, and nitromethane) and octahedral metals ($CoCl_2$, $CoBr_2$, $CoSO_4$, $Ni(NO_3)_2$ $6H_2O$, $Ni(OAc)_2$, $Ni(acac)_2$, $NiBr_2$, $Zn(OAc)_2$, $Al(NO_3)_3$ $6H_2O$, $Ga(acac)_3$, $GaCl_3$, $RuCl_3$, $Fe(OAc)_3$, $Fe(OAc)_2$, $FeCl_3$, $FeCl_2$, $FeBr_3$, $FeSO_4$, $Fe(ClO_4)_2$ $\cdot 6H_2O$.) All self-assembly attempts via "paneling method" resulted in decomposition of ligand to *p*-rosaniline and 2-formylpyridine, or an insoluble and uncharacterizable product.

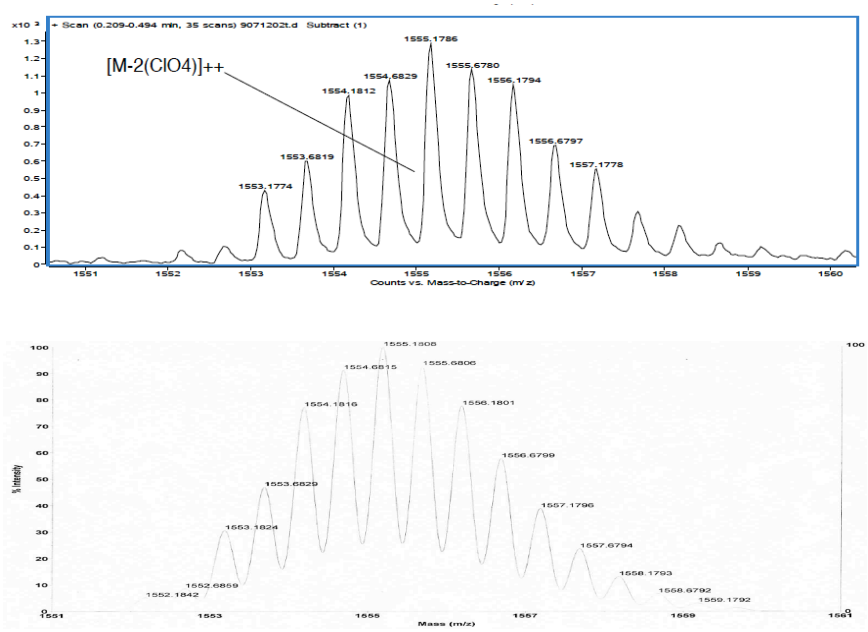

Figure 4.5: ESI mass spectrum of (**4.1$_4$•Fe$_4$•(ClO$_4$)$_6$** as a +2 charge (top). Theoretical isotope distribution pattern (**4.1$_4$•Fe$_4$•(ClO$_4$)$_6$** as a +2 charge modeled in Data Explorer 4.0.)

Most self-assembly attempts via multicomponent self-assembly yielded similar results. Self-assembly of a M_4L_4 tetrahedron was observed to form with $Fe(ClO_4)_2 \bullet 6H_2O$ in H_2O or acetonitrile for 16 hr under nitrogen. Filtration followed by washing with diethyl ether yielded the M_4L_4 tetrahedron cage in 73% yield.

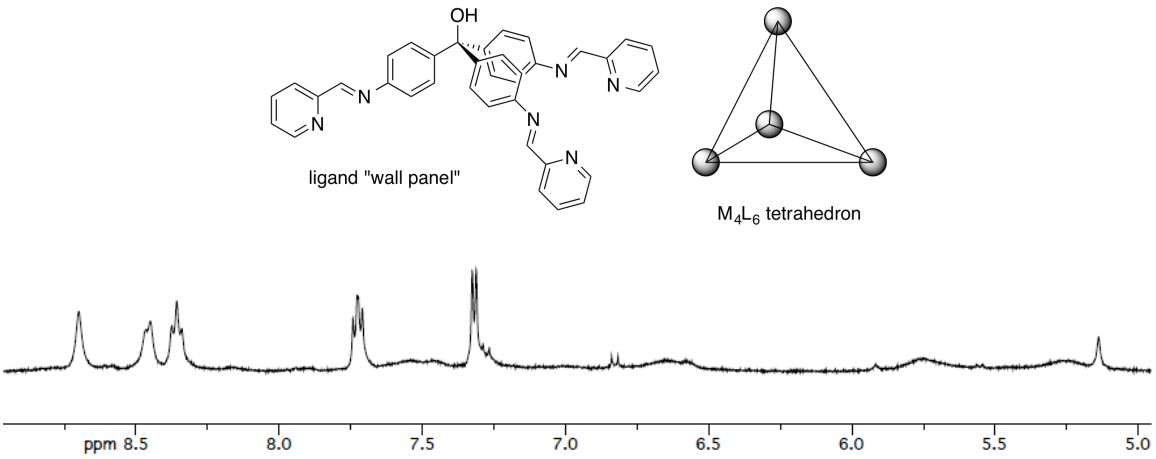

Figure 4.6: ^{1}HNMR of *p*-rosaniline pyridine imine-Fe(II) M_4L_4 tetrahedron, **4.1_4•Fe_4•$(ClO_4)_8$**. (Acetonitrile-d_3, 400 MHz, 298 K.)

The ^{1}H-NMR spectrum in acetonitrile-d_3 of the M_4L_4 tetrahedron showed an imine peak at 8.7 ppm, a characteristic range for a pyridine-imine Fe(II) complex. The peaks at 8.449 ppm, 8.358 ppm, and 7.724 ppm correspond to the protons on the pyridine ring, and the doublet at 7.326 correspond to the protons on the *p*-rosaniline phenyl protons adjacent to the central sp^3 carbon. The peak at 5.139 ppm corresponds to the hydroxy proton. The broad peak at 5.755 ppm corresponds to the *p*-rosaniline phenyl protons adjacent to the imine, and the broad peak at 6.641 ppm corresponds to the protons on the pyridine ring adjacent to the nitrogen. The broadness of these peaks and considerable upfield shift is due to the restricted rotation around the metal center and shielding due to the steric arrangement of the three bidentate chelators around the octahedral metal. The cage is soluble in both acetonitrile and water. Due to the concurrent

publication of this cage (a triflate and sulfate analog) by a different group,[9] this project was no longer pursued.

4.2.2. Self-Assembly of an M_3L_2 *p*-rosaniline Cu(I) Trigonal Bipyramide Cage

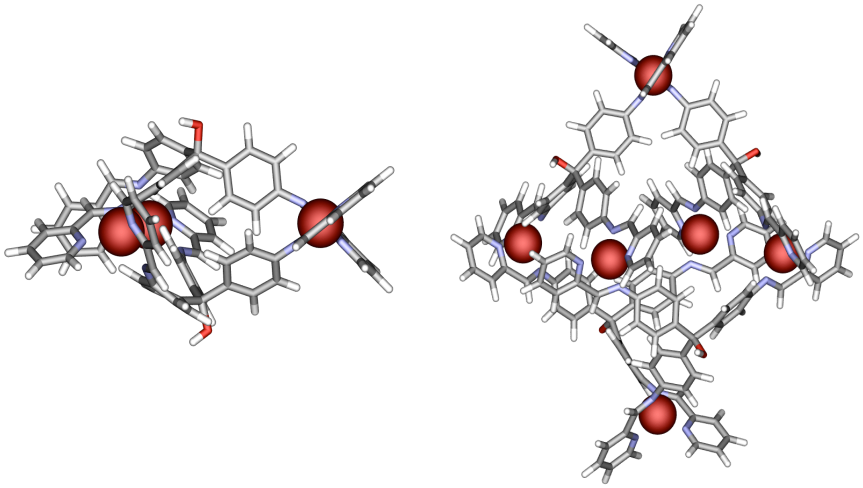

Figure 4.7: Possible self-assemblies between *p*-rosaniline pyridine imine ligand and a tetrahedral metal: M_3L_2 trigonal bipyramide, $\mathbf{4.1_2 \bullet Cu_3 \bullet (PF_6)_3}$ (left) and M_6L_4 octahedron, $\mathbf{4.1_4 \bullet Cu_6 \bullet (PF_6)_6}$ (right).

A tripodal ligand with bidentate metal coordinating groups could form a M_3L_2 trigonal bipyramide cage or a M_6L_4 octahedron with a tetrahedral metal, if mixed in those appropriate ligand:metal ratios.[8]

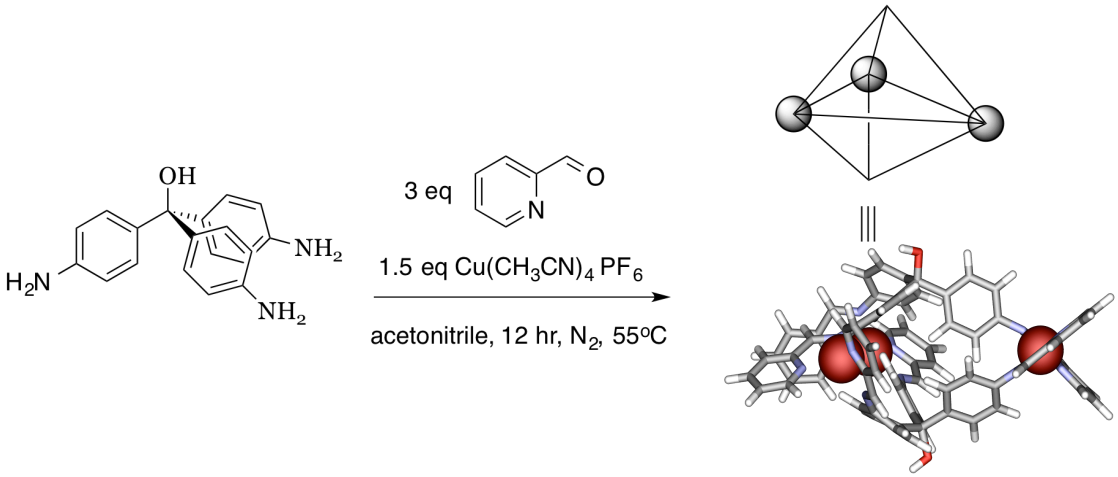

Figure 4.8: Self-assembly of M_3L_2 trigonal bipyramide *p*-rosaniline-Cu(I) cage, **4.1_2•Cu_3•$(PF_6)_3$**.

Several attempts towards self-assembly were attempted via "paneling method" and "multicomponent method" under various temperatures, (room temperature to 150°C), solvents, (acetonitrile, THF, 1,4 dioxane, H_2O, toluene, benzene, toluene, xylenes, ethanol, methanol, diethyl ether, and nitromethane) and tetrahedral metals attempted ($ZnCl_2$, $ZnBr_2$, $Zn(NO_3)_2$ $6H_2O$, $Zn(OTf)_2$, AgCl, AgBr, $AgNO_3$, CuI, CuBr, $CuBr_2$, $Cu(OAc)_2$, $Cu(CH_3CN)_4PF_6$, and $Cu(CH_3CN)_4BF_4$). Most self-assembly attempts via "paneling method" and multi component method resulted in decomposition of ligand to *p*-rosaniline and 2-formylpyridine, or insoluble and uncharacterizable product.

Self-assembly of a M_3L_2 trigonal bipyramide was observed to form with either $Cu(CH_3CN)_4PF_6$ or $Cu(CH_3CN)_4BF_4$ in acetonitrile at 55°C overnight under nitrogen. Filtration of precipitate yielded the self-assembled complex in 95% yield. The ^{1}H-NMR spectrum in acetonitrile-d_3 of the M_3L_2 trigonal bipyramide cage shows a peak at 8.533

ppm, which likely corresponds to the imine peak. The peaks at 9.893 ppm, 9.412 ppm, 8.96 ppm, and 8.87 ppm, correspond to the protons on the pyridine rings, and the peaks at 8.21 ppm and 8.06 ppm correspond to the protons on the *p*-rosaniline core. The peak at 5.40 ppm corresponds to the hydrogen on the alcohol.

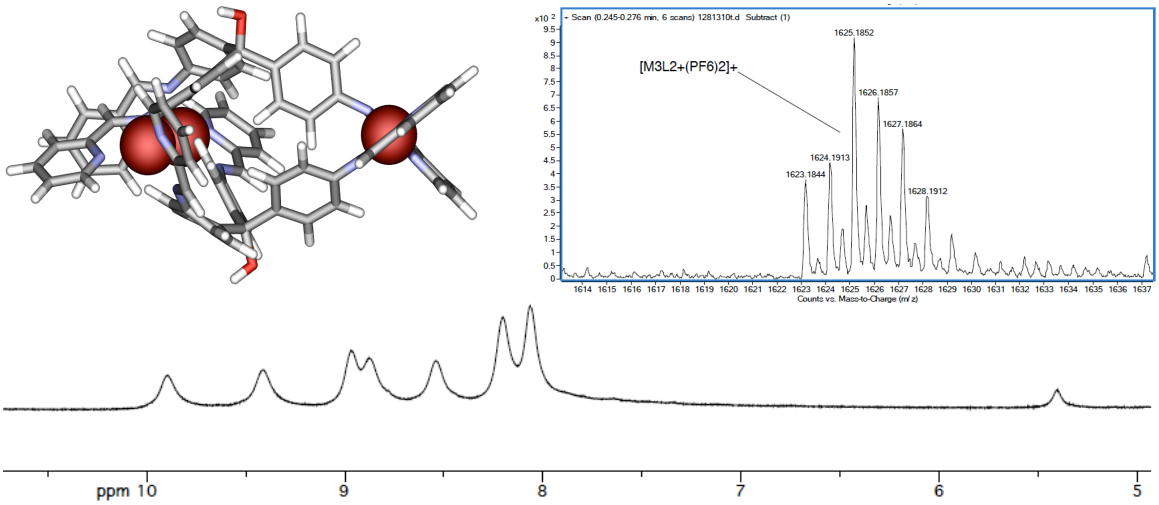

Figure 4.9: Model of M_3L_2 *p*-rosaniline-Cu(I) trigonal bipyramide cage, **4.1_2•Cu_3•$(PF_6)_3$** (top left) and its mass spectrum (top right.) ^{1}H-NMR of M_3L_2 *p*-rosaniline-Cu(I) cage (bottom.) (Acetonitrile-d_3, 400 MHz, 298 K.)

It is also interesting to note that, in contrast to the M_4L_6 Fe(II) tetrahedral cage, broad and upfield peaks are not observed with the M_3L_2 Cu(I) trigonal bipyramide cage. This is due to less steric crowding around the tetrahedral metal center with two bidentate chelating ligands instead of three around an octahedral metal center as observed with M_4L_6 Fe(II) tetrahedron cage. This cage is soluble in acetonitrile and insoluble in water in contrast with its M_4L_6 Fe(II) tetrahedron counterpart. Vapor diffusion of diethyl ether into an acetonitrile solution produced large, X-ray quality crystals.

4.2.3. Attempts towards Self-Assembly with a *p*-Rosaniline-Salen Ligand

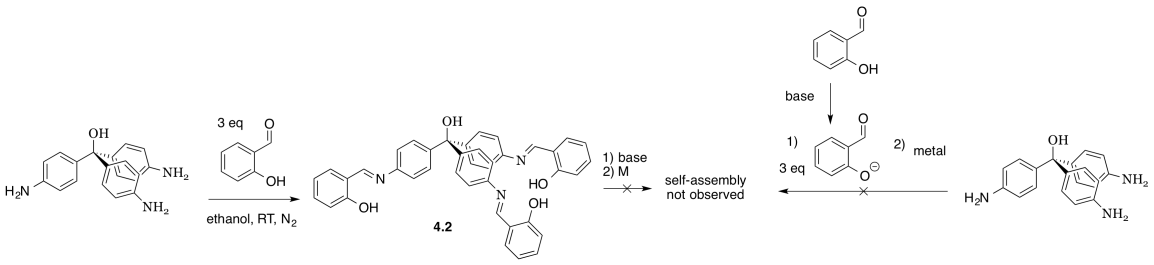

Figure 4.10: Synthesis of, and self-assembly attempts with a *p*-rosaniline salen ligand via the paneling method (left), and multicomponent method (right).

Self-assembly attempts towards formation of a M_3L_2 trigonal bipyramide and M_4L_4 tetrahedron were done with salen metal coordinating groups on a *p*-rosaniline core, via the molecular paneling method and multicomponent self-assembly method using the same octahedral, tetrahedral metals, solvent conditions, and temperatures mentioned previously. Decomposition of ligand to *p*-rosaniline and salicylaldehyde was typically observed via the paneling method, and insoluble products (likely to be polymers, or insoluble discrete metal-ligand complexes) were observed via the multicomponent method with $CuBr_2$, $Cu(CH_3CN)_4PF_6$ $Cu(CH_3CN)_4BF_4$, $CuBr_2$ and $FeCl_3$.

4.3. Towards Metal-Ligand Self-Assembly with Endohedral Functionality from TREN derived Ligands

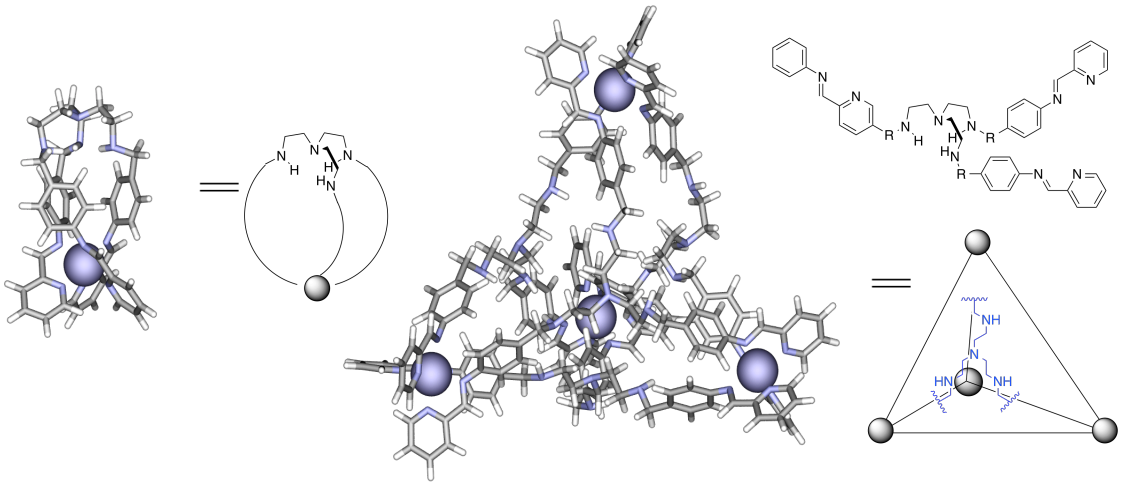

Figure 4.11: Possible metal-ligand self-assembly with TREN amine derivative ligand (top right): M_1L_1, **4.5•Fe** (left), and M_4L_4 tetrahedron, **4.5_4•Fe_4** (right).

A tripodal ligand bearing a TREN amine as an endohedral functional group was chosen due to its multifaceted nature of having four nitrogen lone pairs, and three hydrogens. Because of he flexibility of the ligand due to the sp^3 carbons present, it is likely that efforts towards making a M_4L_4 tetrahedron with an octahedral metal will preferentially undergo intramolecular chelation to form a M_1L_1 cage. Intramolecular chelation has been observed with the multicomponent assembly between *tris*(2-aminoethyl)amine, 2-formylpyridine, and Fe(II). The geometry around the metal was reported to be pseudo octahedral with Fe(II) in a diamagnetic, low spin state over a wide temperature range.[10] Due to the added flexibility with the sp^3 methylene groups in the TREN amine *p*-aniline ligand and the phenyl groups, that broadens the range of metal-ligand approach angles, thereby expanding the number of possibilities of self-assembled

polyhedra formation, since the slightest change in approach angles can have a dramatic effect on the product formed.[11]

Employing the hydrophobic effect[12] and template formation is a strategy to form a M_4L_6 tetrahedron with this ligand is via multicomponent assembly in water. Using an appropriately sized cycloalkane that would be indifferent to the TREN amine unit such as cyclopentane would be a good candidate due to occupying close to 55% percent of the interior space[13] of tetrahedron cages of similar size.[5a]

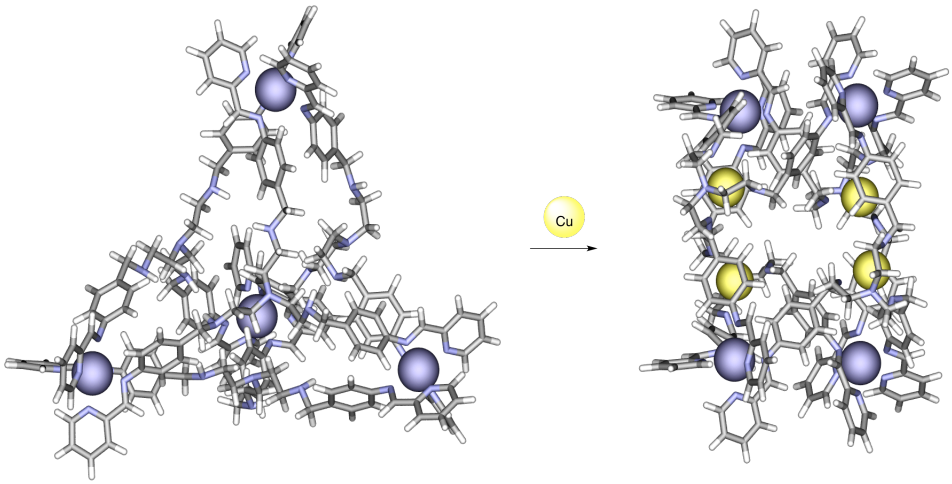

Figure 4.12: M_4L_4 tetrahedron cage with TREN amine endohedral functionality (**4.5_4•Fe_4)** binding to four Cu(I) atoms in the interior of the cage (**4.5_4•Fe_4•Cu_4**).

Self-assembled polyhedra with TREN derived ligands as "wall panels" have the potential for various applications. Despite the cage being overall cationic, it should be able to recognize electrophilic substrates, due to the Lewis basicity of the TREN endohedral functionality. Due to the tetradentate nature of the TREN chelator, the TREN unit is capable of undergoing dative bonds with octahedral, tetrahedral and square planar transition metals. Also, the TREN unit is in its reduced secondary amine form with three

hydrogens available for hydrogen bonding, most notably with halogens or dative bonding with transition metals.[14]

If an M_4L_6 cage were to be formed, the flexibility of the TREN site is due to the alkyl units bridging the central nitrogen to the secondary amines. Any binding to occur at that site would alter the shape and size of the cage, thereby making it possible to control molecular recognition by an allosteric effect, where a halide can act as the allosteric initiator. As a consequence, this will alter the size and shape of the cage, depending on how many equivalents of the allosteric initiator is added.

As shown in **figure 4.12**, the model of single atom binding in the interior of the cage at each of the four TREN amine site shows the conformation of the cage as a rectangular cube in shape, assuming octahedral geometry (as opposed to pseudooctahedral) around the Fe(II) metal centers and trigonal mono pyramidal geometry around the Cu(I) center at each TREN site.

4.3.1. Synthesis of TREN *p*-Aniline Ligand

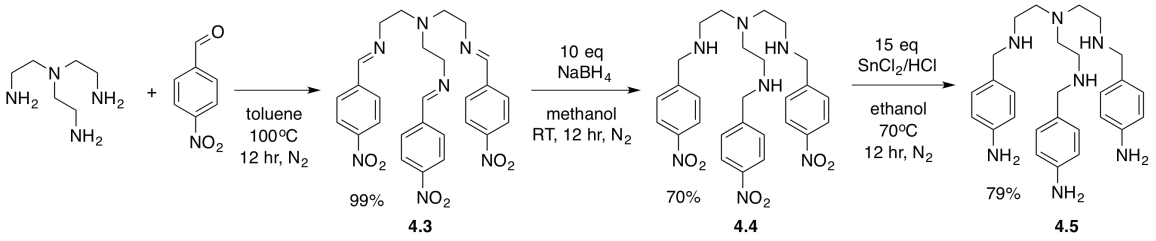

Figure 4.13: Synthesis of TREN amine *p*-aniline.

The synthesis of the TREN amine *p*-aniline ligand precursor required three steps. The first step was the condensation reaction between TREN and 4-formylnitrobenzene to yield the imine product in 99% yield. Subsequent reduction to the amine analog entailed the use of ten equivalents of sodium borohydride in anhydrous methanol at room temperature for 12 hours, resulting in the product being formed at 70% yield. The target ligand precursor can finally be made by reducing the nitro groups to amines with 15 equivalents of tin chloride in a mixture of hydrochloric acid and ethanol at 70'C for twelve hours under nitrogen to yield the product in 77% yield.

4.3.2. Towards Self-Assembly of TREN *p*-Aniline Derived Fe(II) Complexes

As previously mentioned, the multi component self assembly between TREN *p*-aniline, 2-formylpyridine and an octahedral metal, when combined in a metal:ligand 1:1 ratio, have the possibility to self-assemble either a M_1L_1, (**4.5•Fe**) or M_4L_4 tetrahedron, **4.5**$_4$**•Fe**$_4$.

The reaction between 1 equivalent of **4.5**, 3 equivalents of 2-formylpyridine, and 1 equivalent of $FeSO_4 \bullet 7H_2O$ or $Fe(ClO_4)_2 \bullet 6H_2O$ in acetonitrile yield a deep purple

precipitate, due to the intense metal-ligand charge transfer excitations typical with low-spin Fe(II) complex chelated by three pyridine-imine metal coordinating groups.[5a]

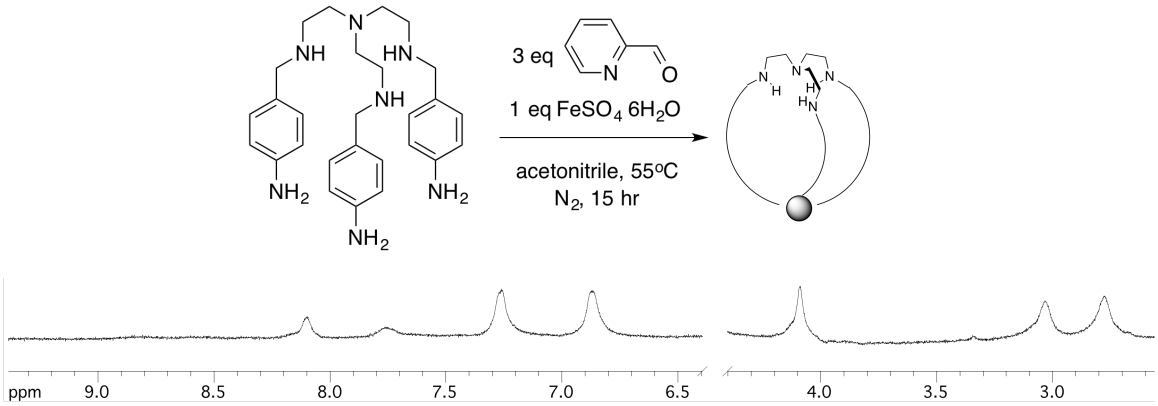

Figure 4.14: ^{1}H-NMR of the proposed M_1L_1 complex, **4.5•Fe•SO$_4$**. (H_2O-d_2, 400 MHz, 298 K.)

The ^{1}H-NMR in D_2O shows that the alkyl peaks branching from the tertiary amine to the secondary amines have shifted downfield from 2.89 ppm and 2.68 ppm to 3.04 ppm and 2.79 ppm. Evidence that the TREN amine pocket is not bound to the Fe(II) comes from the methylene peaks adjacent to the secondary amines, which are present at 4.1 ppm, a modest downfield shift from 3.89 ppm. Typical shifts for methylene units of a metallated TREN amine complex occur are present around 4.5 ppm. The aryl peaks from the TREN amine ligand core appear as broadened doublets at 7.27 ppm and 6.88 ppm, and two more noticeable peaks show up at 8.1 ppm and 7.26 ppm. The peak at 8.1 ppm is likely the imine peak, and the peak at 7.26 ppm is likely from the pyridine rings. The other protons from the aryl ring are perhaps too broadened out to be noticeable. The complex with a ClO_4 counter anions showed a similar ^{1}H-NMR in D_2O, except that all peaks were much broader. The complex (soluble in water and acetonitrile) was not able

to be identified via ESI and MALDI mass spectrometry, nor were X-ray quality crystals obtained. It is likely that the M_1L_1 complex was formed, due to the kinetic ease of intramolecular chelation with the octahedral Fe(II) metal, in addition to the entropic favorability of more solvent being liberated.

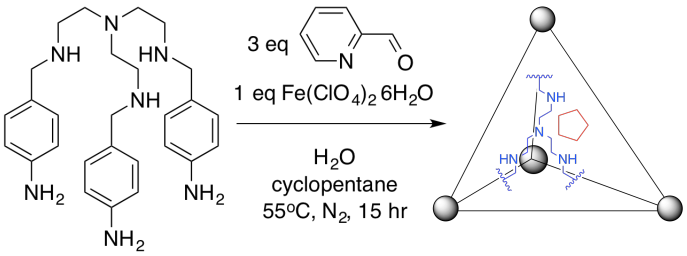

Figure 4.15: Towards template driven self-assembly of a of **4.5** derived M_4L_4 tetrahedron with cyclopentane as a guest, **4.5_4•Fe_4•$(ClO_4)_8$•⊂cyclopentane**.

To increase the probability of the self-assembly of a M_4L_4 tetrahedron, templation with an hydrophobic aliphatic ring of a suitable size was attempted. The reaction between 1 equivalent of **4.5**, 3 equivalents of 2-formyl pyridine, and 1 equivalent of $Fe(ClO_4)_2$•$6H_2O$ in a mixture of cyclopentane and H_2O yielded a deep purple precipitate. The complex was insoluble in all common NMR solvents and other organic solvents, in contrast to **4.5•$FeSO_4$** and **4.5•$Fe(ClO_4)_2$**. It was also not able to be identified via ESI and MALDI mass spectrometry, nor were X-ray quality crystals obtained. The product formed is likely a different complex from the product formed under the similar conditions (without cyclohexane), since **4.5•$Fe(ClO_4)_2$** is soluble in water, and **4.5_4•Fe_4•$(ClO_4)_8$•⊂cyclopentane** is insoluble. The deep purple color of **4.5_4•Fe_4•$(ClO_4)_8$•⊂cyclopentane** that is characteristic of low spin Fe(II) pyridine

imine complexes suggests that a metal-ligand complex was formed, which may very well be a M_4L_4 tetrahedron.

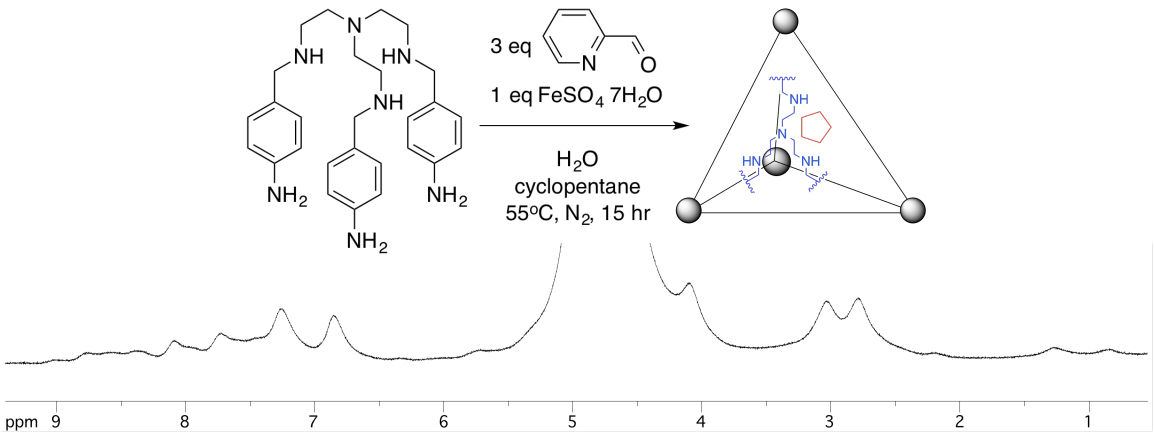

Figure 4.16: ^{1}H-NMR of TREN amine *p*-aniline derived possible M_4L_4 complex with cyclopentane as a guest, **4.5_4•Fe_4•$(SO_4)_4$⊂ cyclopentane**. (D_2O-d_2, 400 MHz, 298 K.)

Self-assembly under the same conditions was attempted using $FeSO_4$, which has a different, weak counter anion, to see if the solubility of self-assembled complex can be enhanced. The product formed again had a deep purple color. In contrast to **4.5_4•Fe_4•$(ClO_4)_8$•⊂cyclopentane**, the ClO_4 analog of this product, which is insoluble, and to the product that was formed without cyclopentane templation, which is soluble in both water and acetonitrile, this product **4.5_4•Fe_4•$(SO_4)_4$ ⊂ cyclopentane** was found to be soluble in water only.

The protons on the alkyl chain that bridge the tertiary amine to the secondary amines, and the singlet peak that corresponds to the methylene protons adjacent to an unmetallated TREN unit uncoordinated TREN amine unit and the phenyl peaks from the

TREN amine core are found to be in the same place as what is believed to be the M_1L_1 analog, **4.5Fe•SO$_4$**. In contrast, this product shows visible, albeit broad peaks between 8.78 ppm-7.39 ppm that correspond to the imine peaks and the protons on the pyridine rings.

Evidence for the formation of a M_4L_4 tetrahedron cage is indicated by the encapsulated cyclopentane peak at 0.509 ppm, an upfield shift of 0.734 ppm from free cyclopentane at 1.243 ppm. The presence of free cyclopentane is likely due to an equilibrium of being free and encapsulated on the NMR time scale. This is congruent with a similar observation reported, where cyclohexane was reported to be encapsulated in a tetrahedron cage of similar size in water, and the change in upfield shift between free and liberated cyclopentane was 1.03 ppm.[5a] Unfortunately, the complex was not able to be identified via ESI and MALDI mass spectrometry, nor were x-ray quality crystals obtained.

4.3.3. Towards Hetero and Homo Dinuclear M_2L_1 Metal-Ligand Self-Assembly with Endohedral Functionality from TREN Derived Ligands

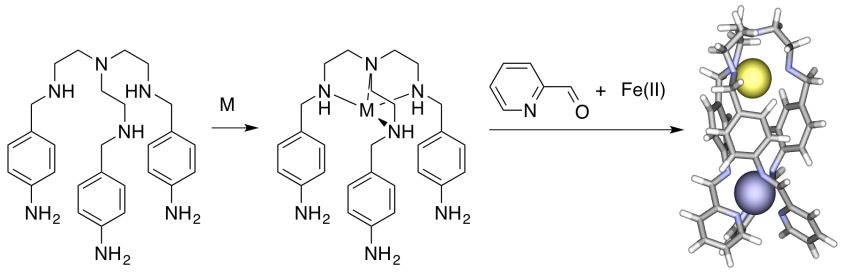

Figure 4.17: Towards the formation of hetero dinuclear TREN derived complexes, where M=Cu(I), **4.5•Fe•SO_4•Cu•PF_6**.

The synthesis of hetero dinuclear M_2L_1 metal-ligand complexes was attempted using via multi component self assembly using similar conditions where Fe(II)-pyridine imine metal-ligand coordination has been observed.

After pre-organization for 3 hr at 50°C at the TREN amine site with $Cu(CH_3CN)_4PF_6$ in acetonitrile (producing a green solution), 2-formylpyridine and Fe(II) (both sulfate and perchlorate anions were separately attempted) was added and let to react overnight under nitrogen. A deep purple precipitate was formed that was soluble in acetonitrile. The ^{1}H-NMR in acetonitrile-d_3 showed very broad peaks that shed little light on the nature of what was formed.

Similar conditions were used to attempt to form a M_2L_1 complex with two equivalents of $FeSO_4$•$7H_2O$. Two conditions were attempted that yielded the same results; one was by adding in one equivalent of Fe(II) for pre-organization at the TREN amine site, followed by multi component self-assembly. The other condition involved adding in two equivalents of Fe(II) during the multi component assembly process. The reaction was allowed to stir at 55°C in acetonitrile overnight. A deep purple precipitate

was formed, which was found to be insoluble in various organic solvents, but is water soluble.

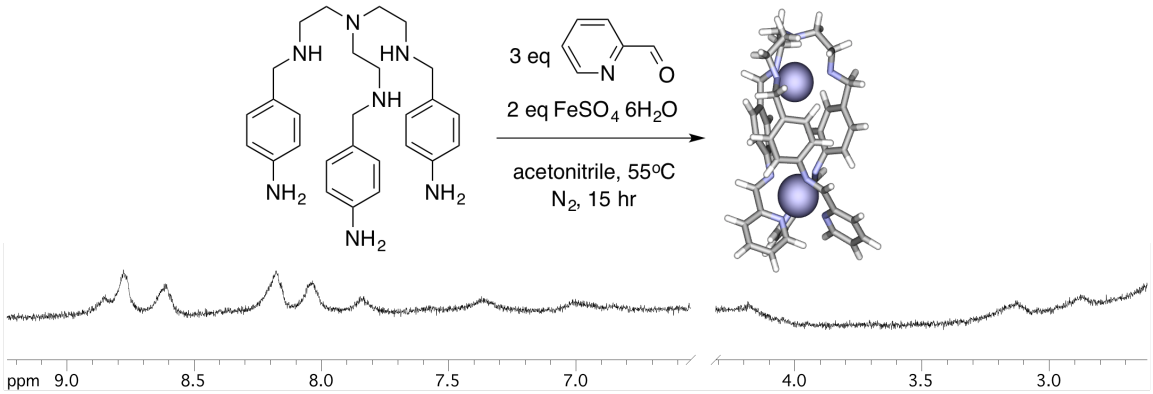

Figure 4.18: ^{1}H-NMR of the likely TREN amine *p*-aniline derived M_2L_1 **4.5• Fe_2• $(SO_4)_2$.** (D_2O-d_2, 400 MHz, 298 K.)

In contrast to complex formed with one equivalent of Fe(II) (see **figure 4.14**), the ^{1}H-NMR spectrum taken in D_2O shows visible peaks that correspond to the protons on the pyridine ring, between 8.8 ppm -7.9 ppm. One of those peaks, either the one at 8.62 ppm or at 8.19 ppm, corresponds to the imine peak adjacent to the Fe(II) pyridine imine site. A pronounced unmetallated methylene peak that corresponds to the sp^3 carbons that bridge the secondary amines and the phenyl units was not observed between the 3.5 ppm-4.1 ppm range (visible in f**igure 4.14**.) Therefore, the metallated methylene peak that characteristically appears around 4.5 ppm is likely buried underneath the D_2O peak. The complex was not identifiable via ESI and MALDI mass spectrometry, nor were X-ray quality crystals obtained.

4.3.4. Towards Self-Assembly of TREN *p*-Aniline Derived Cu(I) M_5L_2 Bridging Dimers

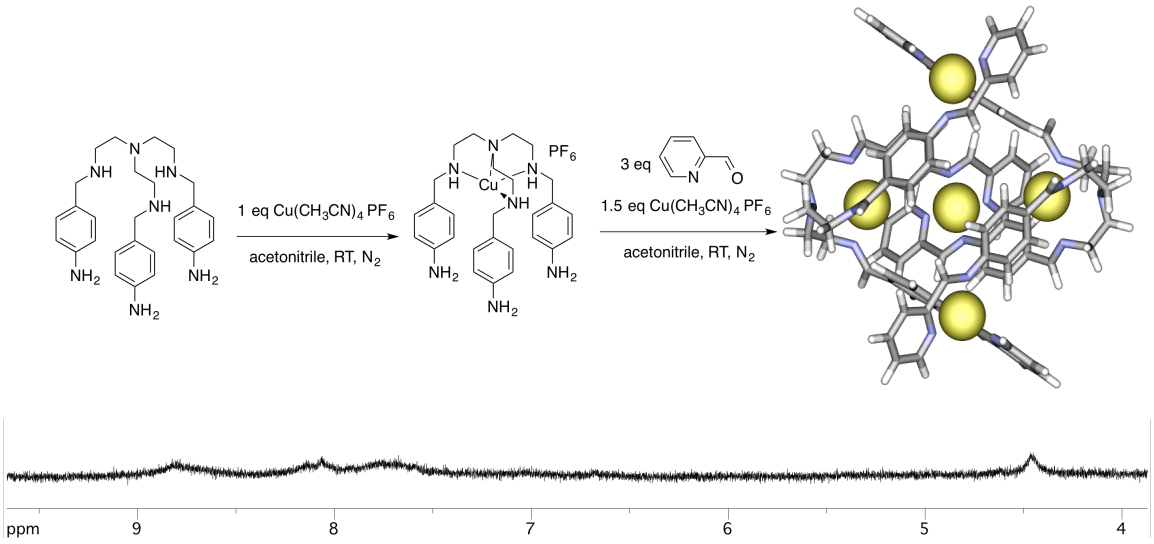

Figure 4.19: ^{1}H-NMR of the possible formation of a M_5L_2 dimer, **4.5_2•Cu_5•$(PF_6)_5$** from **4.5_2** and Cu(I). (Acetonitrile-d_3, 400 MHz, 298 K.)

The synthesis of the M_5L_2 ellipsoidal capsule was attempted via multi component self-assembly using similar conditions where Cu(I)-pyridine imine metal-ligand coordination were observed. To minimize the odds of forming polymers, Cu(I) was added first to pre-organize the ligand, bringing the amine groups in proper orientation. During the formation of metal coordinating groups and the metal-ligand bond, each Cu(I) should bridge each of the ligands together, binding to each pyridine imine units in a tetrahedral fashion.

After pre-organization for 3 hr at 50^{o}C at the TREN amine site with $Cu(CH_3CN)_4PF_6$ in acetonitrile (producing a green solution), three equivalents of 2-formylpyridine and 1.5 equivalents of $Cu(CH_3CN)PF_6$ were added. The reaction was

allowed to stir at 55°C in acetonitrile overnight. A greenish brown precipitate was formed.

The ^{1}H-NMR in of the product (see **figure 4.19**), shows a metallated methylene peak that corresponds to the sp^3 carbons that bridge the secondary amines and the phenyl units at 4.47 ppm. The aryl region between 8.8 ppm and 7.5 ppm shows broad peaks that do not tell much about the nature of the product formed. The complex was not able to be identified via ESI and MALDI mass spectrometry, nor were X-ray quality crystals obtained.

4.4. Conclusions

In conclusion, different types of polyhedra, depending on the geometry of the metal center and the metal-ligand ratio, can be formed via multi component self-assembly with *p*-rosaniline derived C_3 symmetric tripodal ligands. With a 3:2 metal-ligand ratio with a tetrahedral metal such as Cu(I), a trigonal bipyramide cage is formed. With a 1:1 metal-ligand ratio with Fe(II), a M_4L_4 tetrahedron cage is observed. The M_3L_2 cage has a smaller interior cavity with the potential to encapsulate anions. The M_4L_4 cage has an interior cavity of suitable size to encapsulate organic substrates, is water soluble, and should therefore be able to encapsulate organic substrates via hydrophobic effect. The stable formation of a cation generated at the sp^3 center by hydrolysis of the hydroxy units would enhance the potential to encapsulate anions, Lewis basic organic substrates, highly reactive nucleophiles, and selectively promote fragmentation or rearrangement reactions in the interior.

References

1.) (a) Nitschke, J. R. "Construtions, Substitution, and Sorting of Metallo-organic Structures via Subcomponent Self-Assembly" *Acc. Chem. Res.* **2007**, *40*, 103-113; (b) Bibeisi, R. A.; Clegg, J. K.; Elgrishi, N.; de Hatten, X.; Devillard, M.; Breiner, B.; Mal, P.; Nitschke, J. R. "Subcomponent Self-Assembly and Guest-BInding Properties of Face-Capped Fe4L48+ Capsules" *J. Am. Chem. Soc.* **2012**, *134*, 5110-5119.

2.) Li, H.; Eddaoudi, M.; O'Keefe, M.; Yaghi, O. "Design and Synthesis of an Exceptionally Stable and Highly Porous Metal-Organic Framework" *Nature* **1999**, *402*, 276-279.

3.) Meng, W.; Ronson, T. K.; Clegg, J. K.; Nitschke, J. R. "Transformations Within a Network of Cadmium Architectures" *Angew. Chem. Int. Ed.* **2013**, *52*, 1017-1021.

4.) Ronson, T. K.; Giri, C.; Beyeh, N. K.; Minkkinen, A.; Topic, F.; Holstein, J. J.; Rissanen, K.; Nitschke, J. R. "Size-Selective Encapsulation of Hydrophic Guests by Self-Assembled M4L6 Cobalt and Nickel Cages" *Chem. Eur. J.* **2013**, *19*, 3374-3382.

5.) (a) Mal, P.; Schultz, D.; Beyeh, K.; Rissanen, K.; Nitschke, J. R. "An Unlockable-Relockable Iron Cage by Subcomponent Self-Assembly" *Angew. Chem. Int. Ed.* **2008**, *47*, 8297-8301; (b) Browne, C.; Brenet, S.; Clegg, J. K.; Nitschke, J. R. "Solvent-Dependent Host-Guest Chemistry of an Fe_8L_{12} Cubic Capsule" *Angew. Chem. Int. Ed.* **2013**, *52*, 1944-1948; (c) Salvatore, Z.; Clegg, J. K.; NItschke, J. R. "Selective Assembly and Disassembly of a Water-Soluble Fe10L15 Prism" *Angew. Chem. Int. Ed.* **2013**, *52*, 4837-4840.

6.) Smulders, M. M.; Riddel, I. A.; Browne, C.; Nitschke, J. R. "Building on Architectural Principles for Three-Dimensional Metallosupramolecular Construction" *Chem. Soc. Rev.* **2013**, *42*, 1728-1754.

7.) (a) Wang, M.; Lan, W. J.; Zheng, Y. R.; Cook, T. R.; White, H. S.; Stang, P. J. "Post-Self-Assembly Covalent Chemistry of Discrete Multicomponent Metallosupramolecular Hexagonal Prisms" *J. Am. Chem. Soc.* **2011**, *133*, 10752-10755; (b) Tanabe, K.; Cohen, S. "Postsynthetic Modification of Metal-Organic Frameworks- A Progress Report" *Chem. Soc. Rev.* **2011**, *40*, 498-519.

8.) Leininger, S.; Olenyuk, B.; Stang, P. J. "Self-Assembly of Discrete Cyclic Nanostructures Mediated by Transition Metals" *Chem. Rev.* **2000**, *100*, 853-908.

9.) Bilbeisi, R., Clegg, J., Elgrishi, N., de Hatten, X., Devillard, M., Breiner, B., Mal, P., Nitschke, J. Subcomponent Self-Assembly and Guest-Binding Properties of Face-Capped Fe4L48+ Capsules *J. Am. Chem. Soc.* **2012**, *134*, 5110-5119.

10.) Schultz, D.; Nitschke, J. R. "Choices of Iron and Copper: Cooperative Selection During Self-Assembly" *Angew. Chem. Int. Ed.* **2006**, *45*, 2453-2456.

11.) (a) Bunzen, J.; Iwasa, J.; Bonakdrarzadeh, P.; Numata, E.; Rissanen, K.; Sato, S.; Fujita, M. "Self-Assembly of $M_{24}L_{48}$ Polyhedra Based on Empirical Prediction" *Angew. Chem. Int. Ed.* **2012**, *51*, 3161-3163; (b) Sun, Q.; Iwasa, J.; Ogawa, D.; Ishido, Y.; Sato, S.; Ozeki, T.; Sei, Y.; Yamaguchi, K.; Fujita, M. "Self-Assembled M24L48 Polyhedra and Their Sharp Structural Switch Upon Subtle Ligand Variation" *Science* **2010**, *328*, 1144-1147.

12.) (a) Biros, S. M.; Rebek, J. "Structure and Binding Properties of Water-Soluble Cavitands and Capsules" *Chem. Soc. Rev.* **2007**, *36*, 93-104; (b) Biros, S. M.; Bergman, R. G.; Raymond, K. N. "The Hydrophobic Effect Drives the Recognition of Hydrocarbons by an Anionic Metal-Ligand Cluster" *J. Am. Chem. Soc.* **2007**, *129*, 12094-12095; (c) Hooley, R. J.; Van Anda, H. J.; Rebek, J. "Extraction of Hydrophobic Species Into a Water-Soluble Synthetic Receptor" *J. Am. Chem. Soc.* **2007**, *129*, 13464-13473.

13.) Mecozzi, S.; Rebek, J. "The 55% Solution: A Formula for Molecular Recognition in the Liquid State" *Chem. Eur. J.* **1998**, *4*, 1016-1022.

14.) Kang, S. O.; Llinares, J. M.; Day, V. W.; Bowman-James, K. "Cryptand-like Anion Receptors" *Chem. Soc. Rev.* **2010**, *39*, 3980-4003.

Chapter 5

Metal-Ligand Self-Assemblies with Linear and V-Shape Ligands

5.1. Introduction

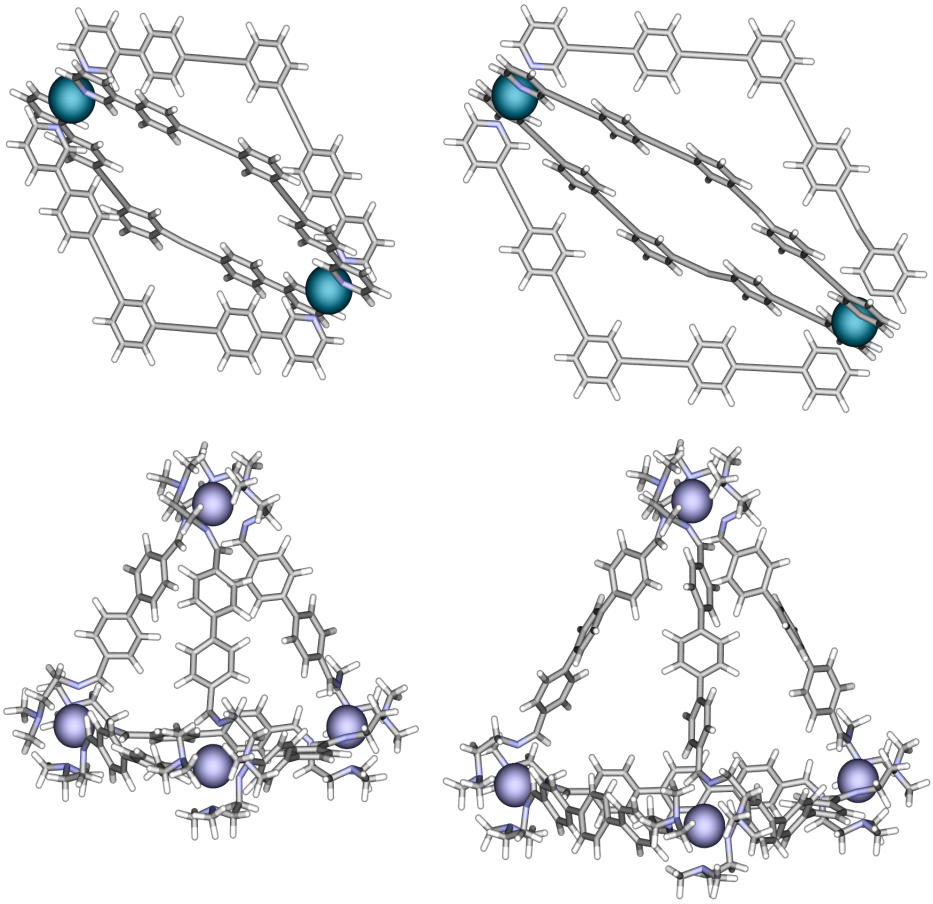

Figure 5.1: M_2L_4 palladium-pyridyl cages (top) and M_4L_6 tertiary amine-imine Fe(II) complexes.

.

This chapter describes the synthesis and properties of M_2L_4 palladium-pyridyl cages and M_2L_3 pyridine-imine Fe(II) cages, one with an amino group as the endohedral functionality. In addition, efforts towards the self-assembly of tertiary amine-imine Fe(II) complexes provide a more flexible metal coordinating group, which have the potential to

provide flexibility around the metal center for ease in adjusting the shape of the self-assembly depending on the endohedral functional group.

5.1.1. Design Concept

The self-assembly of metal-ligand complexes is aided by having planar and rigid ligands. Restricted movement of ligands limits entropic unfavorability. Known rigid ligands often use the face of arene rings as "walls."

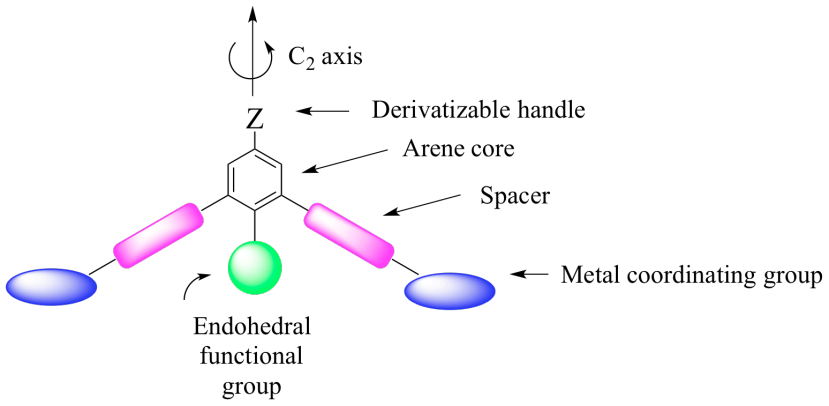

Figure 5.2: Design concept of the modular "V shape" ligand.

The design concept of the building blocks for the self-assembled cages consists of "V shape" ligands with the goal of having an interior functionality as the endohedral functional group. Specifically, the ligands consist of a scaffold that consists of three segments: 1) an arene center with an endohedral functional group that would point toward the interior of the cluster, 2) rigid spacers that help control the size of the cluster, and 3) metal coordinating group that help control self assembly.

From this general terphenyl scaffold, three types of metal-ligand cages are proposed: a M_2L_4 based Pd "paddle wheel" with D_{4h} symmetry, made from pyridine

groups that serve as single point contacts to the metal, an M_4L_6 cage with tetrahedral symmetry, and an M_2L_3 cage with D_3 symmetry. Using the same scaffold, the geometry and size of the cluster can be modulated by varying the metal-ligand contacts.

5.2. M_2L_4 Palladium-Pyridyl Cages with V-shaped Ligands

Self-assembled Pd cages have been reported to noncovalently bind to guests of compatible size,[1] in addition to being able to host catalytic reactions.[2] The use of flat and rigid organic ligands with pyridine metal coordinating groups to self-assemble into a polyhedral structure with Pd(II) as the metal structural units has been shown to form various geometries,[3] depending on the ligand-metal approach angle,[4] and steric availability around the metal center, depending on which ligands are there to help control the self-assembly (*e.g.* ethylenediamine can chelate around Pd(II) or Pt(II) to enforce a 90°C *cis* geometry around these metals of square planar geometry, thereby promoting the self-assembly of octahedral cages instead of a polymer.)[5]

5.2.1. Synthesis of V-shaped Pyridyl Ligands

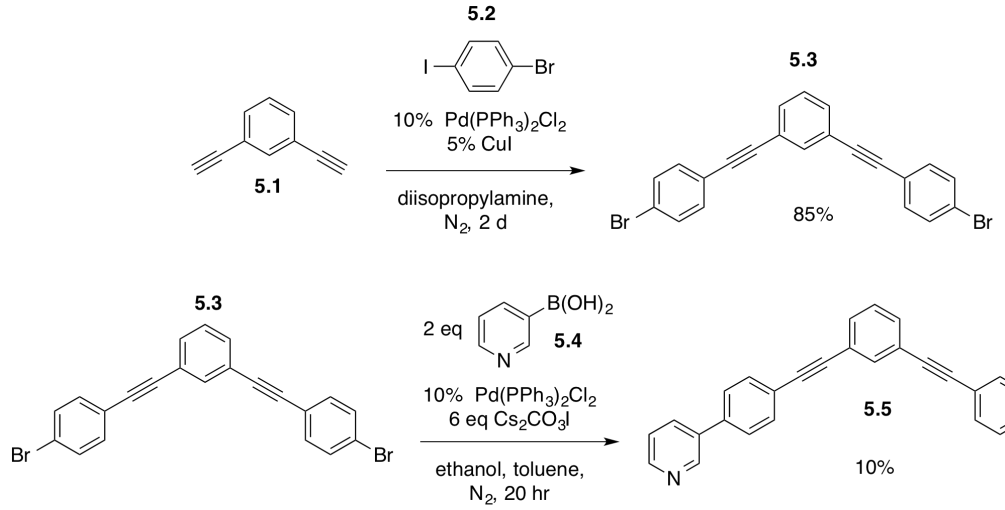

Figure 5.3: Synthesis of ligand **5.5**.

The ligand **5.5** was synthesized by Sonogashira coupling of 1,3-diethynylbenzene and 1,4 bromoiodobenzene yielding **5.3** in high yield, which subsequently underwent Suzuki coupling with **5.4** to yield the target ligand **5.5** low yield.

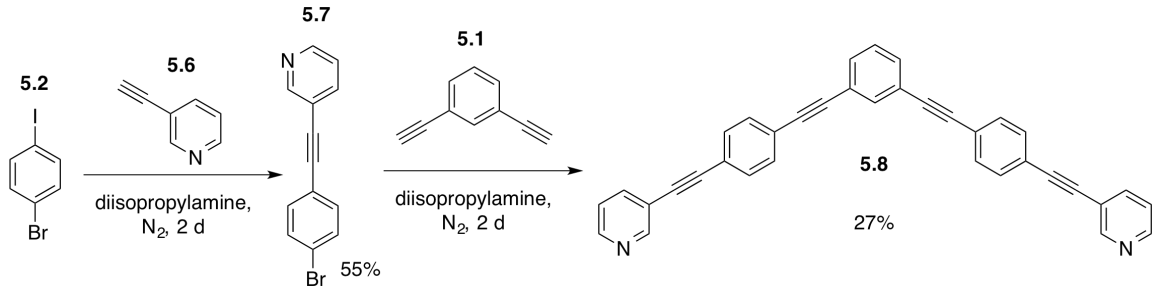

Figure 5.4: Synthesis of ligand **5.8**.

Ligand **5.8** has more extensive conjugation with the additional acetylene units between the central aryl ring and pyridine ring compared to ligand **5.5**. The first step was the Sonogashira reaction between 1,4 bromoiodobenzene and 3-ethynyl pyridine to form **5.8** in 55% yield, followed by Sonogashira coupling with 1,3-diethynylbenzene to form the target ligand **5.8** in 27% yield. The electron rich ligand **5.8** is unstable in solution at room temperature, forming aggregates via π stacking, as observed by the very broad peaks observed in ^{1}H-NMR after sitting in solution for a day or two.[5]

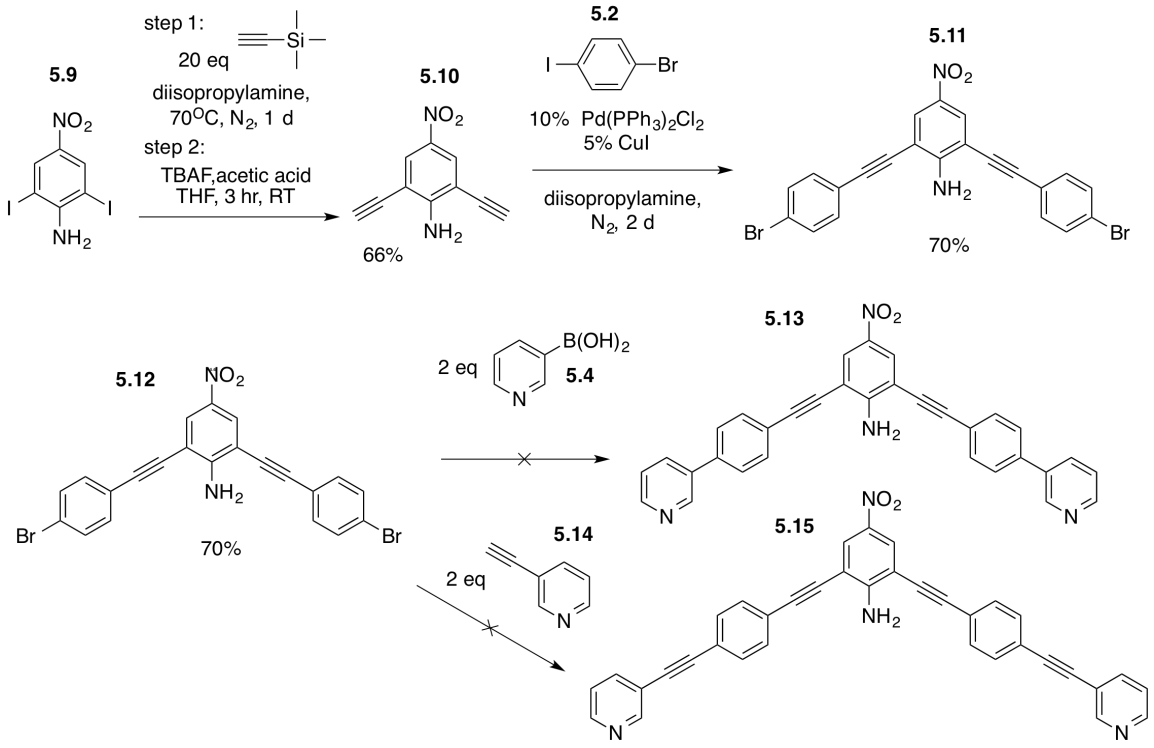

Figure 5.5: Towards the synthesis of ligand **5.11** and **5.15** for Pd_2L_4 cages with endohedral functionality.

Attempts to introduce amines as endohedral functionality were unsuccessful. Precursor **5.9** was treated with an excess amount of trimethylsilylacetylene under

Sonogashira reaction conditions followed by desilylation with tetra-n-butyl ammonium fluoride (TBAF) to yield **5.11** in 66% yield. Sonogashira coupling with 1,4 bromoiodobenzene and **5.10** resulted in the formation of **5.11** in 70% yield. Various Suzuki coupling conditions were attempted to form ligand **5.13** to no avail. Attempts to form a highly conjugated analog by various Sonogashira coupling conditions with **5.11** to yield **5.14** resulted in starting material. Publications on pyridyl-Pd polyhedra with endohedral functionality have been sparse. The interested reader can be referred to the following references.[6]

5.2.2. Synthesis of M_2L_4 Palladium-Pyridyl Cages

Pd_2L_4 cages self-assembled in a few seconds at ambient temperature at millimolar concentration, as monitored by ^{1}H-NMR by addition of 0.5 equivalent of $Pd(NO_3)_2$ to **5.5** and **5.8** respectively, in DMSO-d_6. Molecular modeling of these cages show them to be oval-like "paddle wheels". The formation of these cages were confirmed by ^{1}H-NMR and mass spectrometry, supported by the comparison to smaller and similar cages made in the lab where the crystal structure was determined.[7]

Even though each cage is tetracationic, due to the two Pd(II) centers present in each cage, these cages are stable to air, water, and light, in both solution and the solid state for months. Although the ligand **5.8** by itself is unstable in solution, when self-assembled with Pd to form a M_2L_4 cage, **5.8_4•$Pd_2(NO_3)_4$**, it is as stable as the other cage. Both M_2L_4 cages showed downfield chemical shifts compared to their unmetallated ligand due to the ligand-metal coordination with the cationic Pd(II) centers.

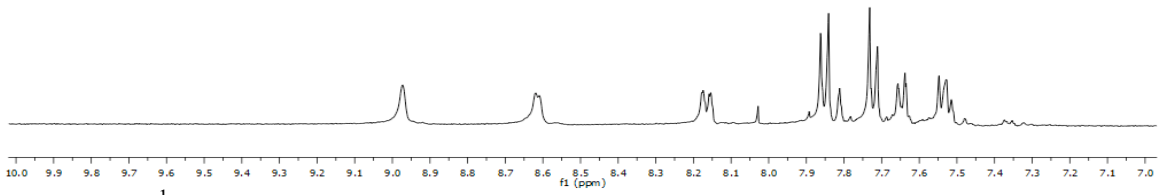

Figure 5.6: ^{1}H NMR spectrum of ligand **5.5** in DMSO-d_6.

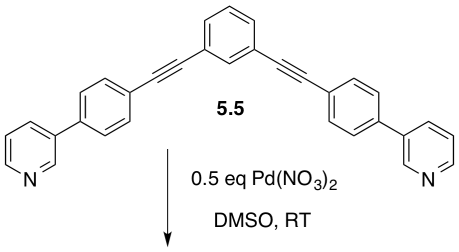

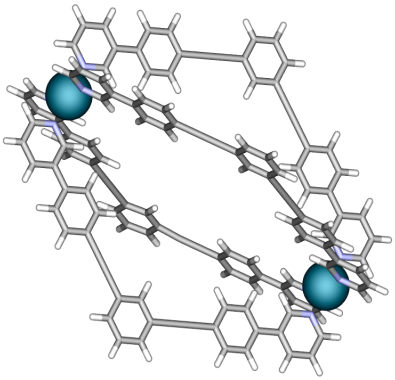

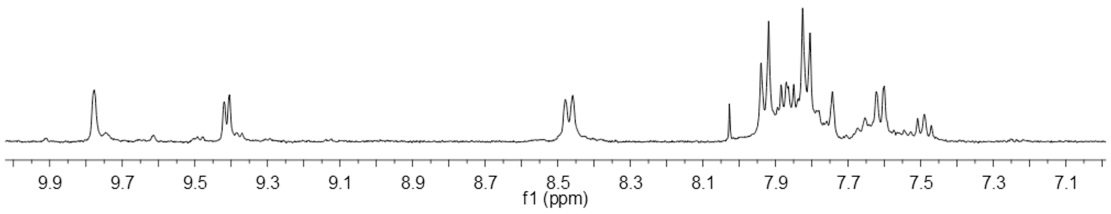

Figure 5.7: ^{1}H NMR spectrum of cage **5.5$_4$•Pd$_2$(NO$_3$)$_4$** in DMSO-d_6.

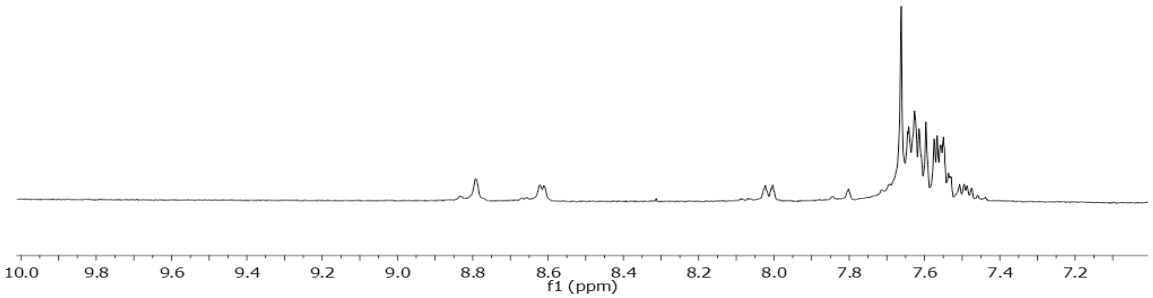

Figure 5.8: ^{1}H NMR spectrum of ligand **5.8** in DMSO-d_6.

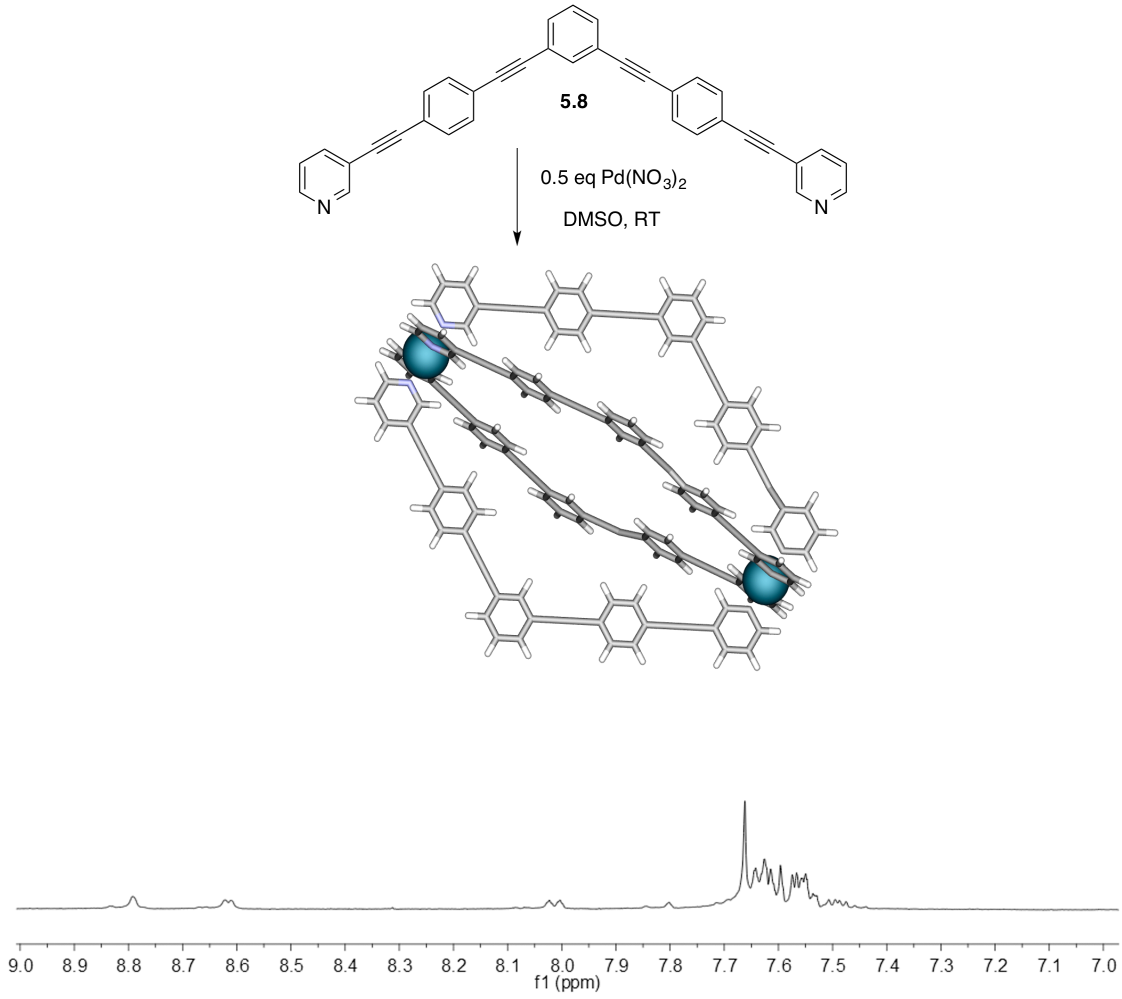

Figure 5.9: ^{1}H NMR spectrum of cage **5.8$_4$•Pd$_2$(NO$_3$)$_4$** in DMSO-d_6.

5.2.3. Photophysical of Properties of M_2L_4 Palladium-Pyridyl Cages

Cage entry	ε ($cm^{-1}•M^{-1}$)	λ_{max}(abs)(nm)	excited @	λ_{max}(emis)(nm)	(%) Φ
$5.5_4•Pd_2(NO_3)_4$	6.23×10^4	309	309	344, 361	21
5.5	6.00×10^4	309	309	344, 361	23
$5.8_4•Pd_2(NO_3)_4$	7.17×10^3	311, 475	311	354, 371, 381	10
5.8	3.69×10^3	325	325	354, 371	38

Table 5.1: UV-vis absorbance and fluorescence emission characteristics of the Pd_2L_4 cages.

The highly conjugated nature of the ligands that make up the "bars" of the cage gives rise to their interesting photophysical properties. The cages absorb strongly in the UV-vis, due to the π-π∗ transitions, suggesting that the nature of the N-Pd dative bond can best be described as a Werner-type complex with relatively little electron density on the metal centers, which is not surprising for the cationic transition metals, each having a 2+ charge for an over all 4+ charge for the Pd_2L_4 cage.

Monodentate Pd(II)-pyridine dative bonds have been reported to be kinetically labile, and dissociate with ease under equilibrium conditions.[8] The possibility of ligand dissociation was probed by observing the UV-vis at varying concentrations from 0.35 x 10^{-7} M to 2.2 x 10^{-5} M. The spectra were found to be identical at the various

concentrations, suggesting that the Pd_2L_4 cages do not dissociate at very low concentrations in DMSO.

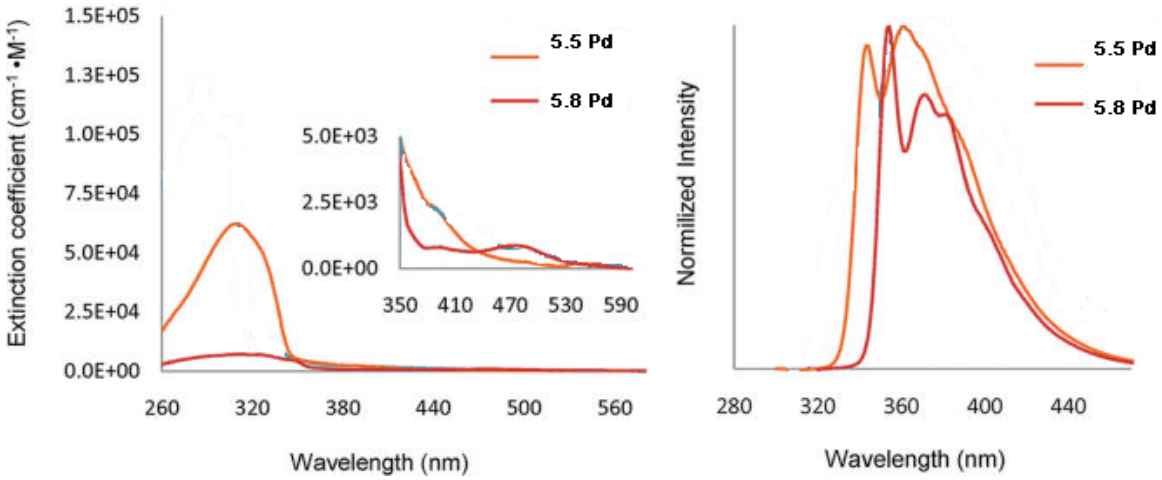

Figure 5.10: UV-vis (left) and emission spectra (right) of **5.5_4•$Pd_2(NO_3)_4$** and **5.8_4•$Pd_2(NO_3)_4$.**

The λ_{max} of **5.5** and **5.5_4•$Pd_2(NO_3)_4$** was found to be at 309 nm. In addition, weak ($\varepsilon = 10^2$-10^3 $cm^{-1}M^{-1}$) metal-ligand charge transfer transitions were observed with **5.5_4•$Pd_2(NO_3)_4$**. The λ_{max} of the free ligand **5.8** was found to be at 325 nm. In contrast to its Pd cage analog, **5.8_4•$Pd_2(NO_3)_4$** was found to have two absorption maxima, one at 311 nm, and a metal-to-ligand-charge-transfer transition at 475 nm. When excited at 309 nm, **5.5_4•$Pd_2(NO_3)_4$** the emission spectra shows two bands, one at 344 nm, and the other at 361 nm. The quantum yield of fluorescence was found to be 21%. In contrast, when **5.8_4•$Pd_2(NO_3)_4$** was excited at 311 nm, the emission spectra was found to have three bands at 354 nm, 371 nm, and 381 nm, with a fluorescence quantum yield of 10%. These two Pd_2L_4 cages show good fluorescence, due to their elongated nature, and they were

found to have considerably higher fluorescence than smaller similar cages with less conjugation.

5.3. Pyridine-Imine Fe(II) Cages

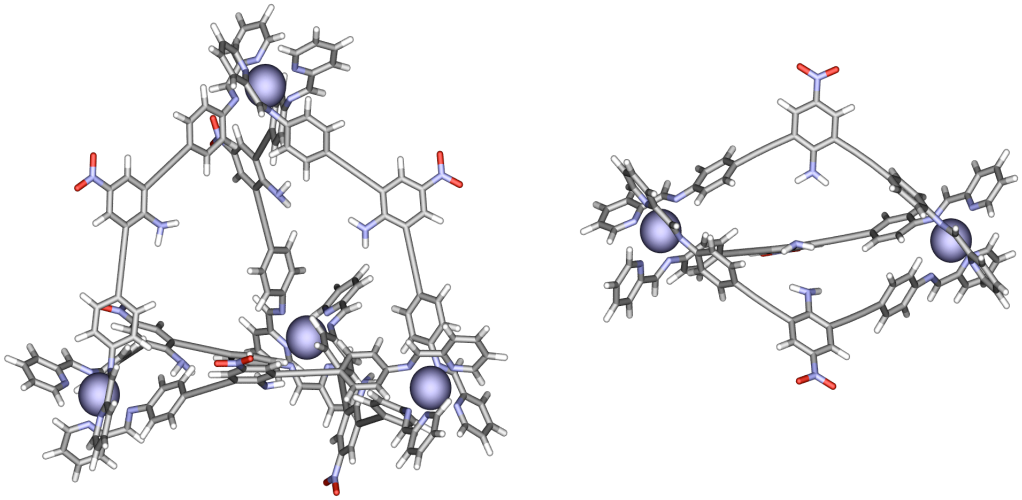

Figure 5.11: Models of possible self-assembled cages from V-shape ligands with amine endohedral functionality, M_4L_6 cage (left) and M_2L_3 cage (right).

Multicomponent self-assembly with aniline derivatives, 2-formyl pyridine, and Fe(II) salts are known to form discrete polyhedra.[9] V-shaped ligands of C_{2v} symmetry with two metal coordinating sites can theoretically form two different polyhedra, a M_4L_6 tetrahedron or a M_2L_3 helicate with an octahedral. The formation of a M_4L_6 tetrahedron cage would be preferable, because the larger size of the interior cavity would expand the scope of possible guests, in comparison to a M_2L_3 helicate. Unfortunately, the M_2L_3 helicate was formed from V-shaped ligands instead of the target M_4L_6 tetrahedron. Following is a description of the synthesis of ligands used for the multicomponent assembly of M_2L_3 cages.

5.3.1. Pyridine-Imine Fe(II) Cages

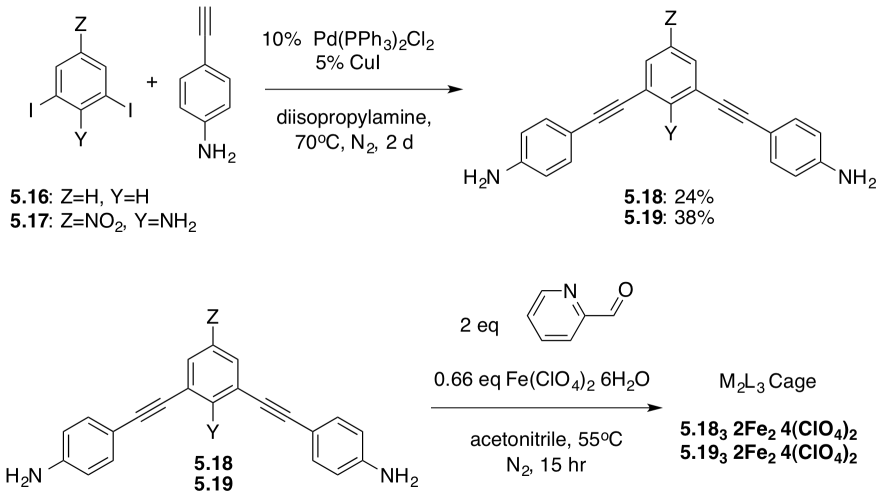

Figure 5.12: Synthesis of ligand precursors for the multicomponent self-assembly of an M_2L_3 cage.

The synthesis of the *bis*-aniline ligands entails the use of a dihalobenzene core where endohedral functionality can be introduced in the interior of the cage. Two *bis*-aniline ligands were made, one without endohedral functionality, **5.18** and one with an amino group as endohedral functionality, **5.19**. The dihalobenzene arene cores **5.16** and **5.17** were allowed to react with 4-ethynylaniline under Sonogashira conditions to yield their particular *bis*-aniline ligands, **5.18** and **5.19**, respectively.

5.3.2. Pyridine-Imine Fe(II) Cages

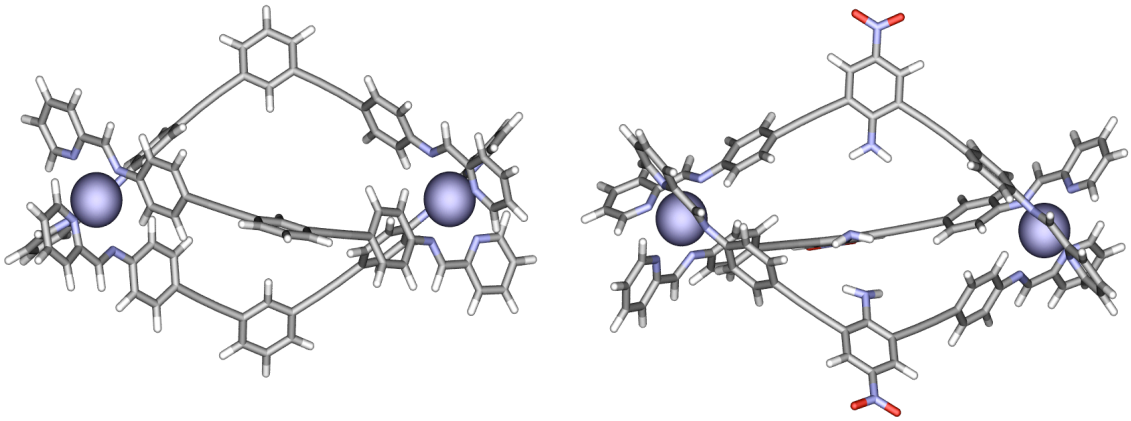

Figure 5.13: M_2L_3 cages **5.18$_3$•2Fe$_4$(ClO$_4$)$_2$** and **5.19$_3$•2Fe$_4$(ClO$_4$)$_2$**, containing three amino groups as endohedral functionality.

Multicomponent self-assembly of ligands **5.18** and **5.19** with 2-formylpyridine and $Fe(ClO_4)_2 \bullet 6H_20$ at 55^{o}C in acetonitrile under nitrogen for 15 hr formed their corresponding M_2L_3 cages, **5.18$_3$•2Fe$_4$(ClO$_4$)$_2$** and **5.19$_3$•2Fe$_4$(ClO$_4$)$_2$**. These cages are stable under inert atmosphere and are sensitive to air and moisture.

These cages were fully characterized and studied by a fellow group member, Mike Young. In short, the introduction of large achiral groups such as *p*-^{t}butyl benzyl ether as endohedral functionality provide diastereochemical control around the octahedral metal center due to the steric bulk of the interior functionality imposing limited flexibility on the ligand during the self-assembly process. Smaller endohedral functionalities yielded mesocate isomers. The interested reader can read the resulting publication for more information on these cage structures.[10]

5.4. Tertiary Amine-Imine Fe(II) Cages

The multicomponent self-assembly of chelating imine-tertiary amine metal coordinating groups was attempted. The alkyl chain between the two chelating nitrogens would provide additional flexibility of the metal coordinating group, thereby broadening the possibility of metal approach angles around the metal. As a consequence, this can broaden the scope of polyhedra formed, and possibly be controlled by the steric demands of the size of the endohedral functional group. For example, V-shaped ligands tend to form M_2L_3 cages. Can V-shaped cages form M_4L_6 cages if they are limited by the size of the endohedral guest, and aided by the additional flexibility of the chelating metal coordinating group? Unfortunately, metal-ligand complexes with V-shaped ligands were insoluble, therefore not characterized by NMR and mass spectroscopy. Evidence of metal-ligand coordination was, however, observed with linear ligands via ^{1}H-NMR.

5.4.1. Synthesis of Tertiary Amine-Imine Ligands

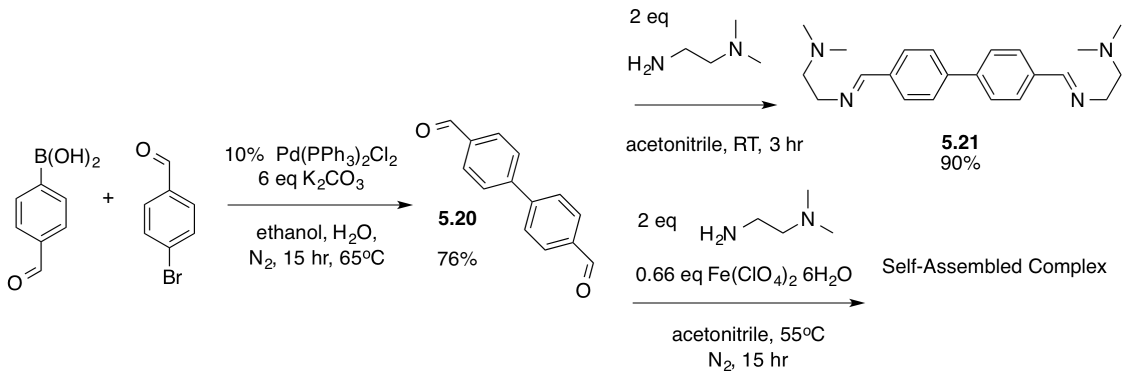

Figure 5.14: Synthesis of *bis*-phenyl tertiary amine-imine ligand **5.20** and **5.21** and multicomponent self-assembly of metal-ligand complex.

The synthesis of ligand **5.20** entails the Suzuki coupling between 4-formylphenyl boronic acid and 4-bromobenzaldehyde to yield **5.20** in 76% yield. Synthesis of **5.21** was done by reacting **5.21** with two equivalents of *N, N'*-dimethylethylenediamine in acetonitrile at room temperature for three hours. Ligand **5.21** was not used in self-assembly attempts, however, but was synthesized for ^{1}H-NMR spectra comparison of any metal-ligand complexes formed.

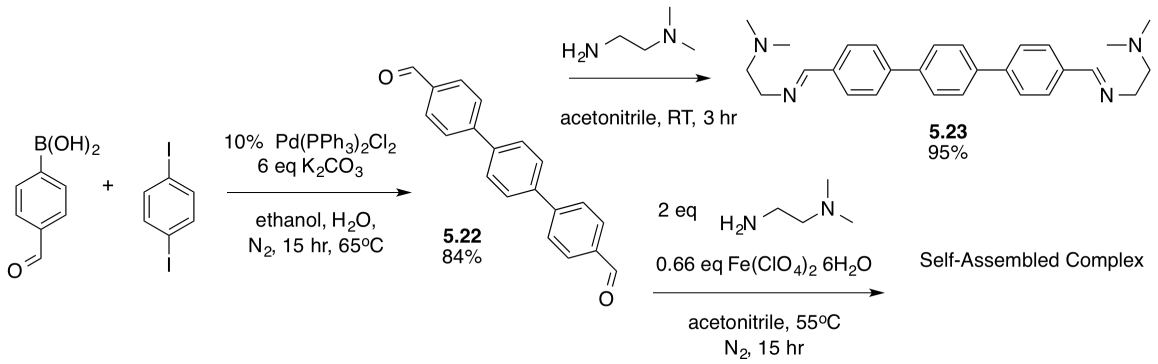

Figure 5.15: Synthesis of *tris* phenyl tertiary amine-imine ligand **5.22** and **5.23** and multicomponent self-assembly of metal-ligand complex.

The synthesis of ligand **5.22** entails the Suzuki coupling between two equivalents of 4-formyl phenylboronic acid and 1,4 diiodobenzene to yield **5.22** in 84% yield. Synthesis of **5.23** was done by reacting **5.22** with two equivalents of *N, N'*-dimethylethylenediamine in acetonitrile at room temperature for three hours. Ligand **5.23** was not used in self-assembly attempts, however, but was synthesized for ^{1}H-NMR spectra comparison of any metal-ligand complexes formed.

5.4.2. Tertiary Amine-Imine Fe(II) Cages with Linear Ligands

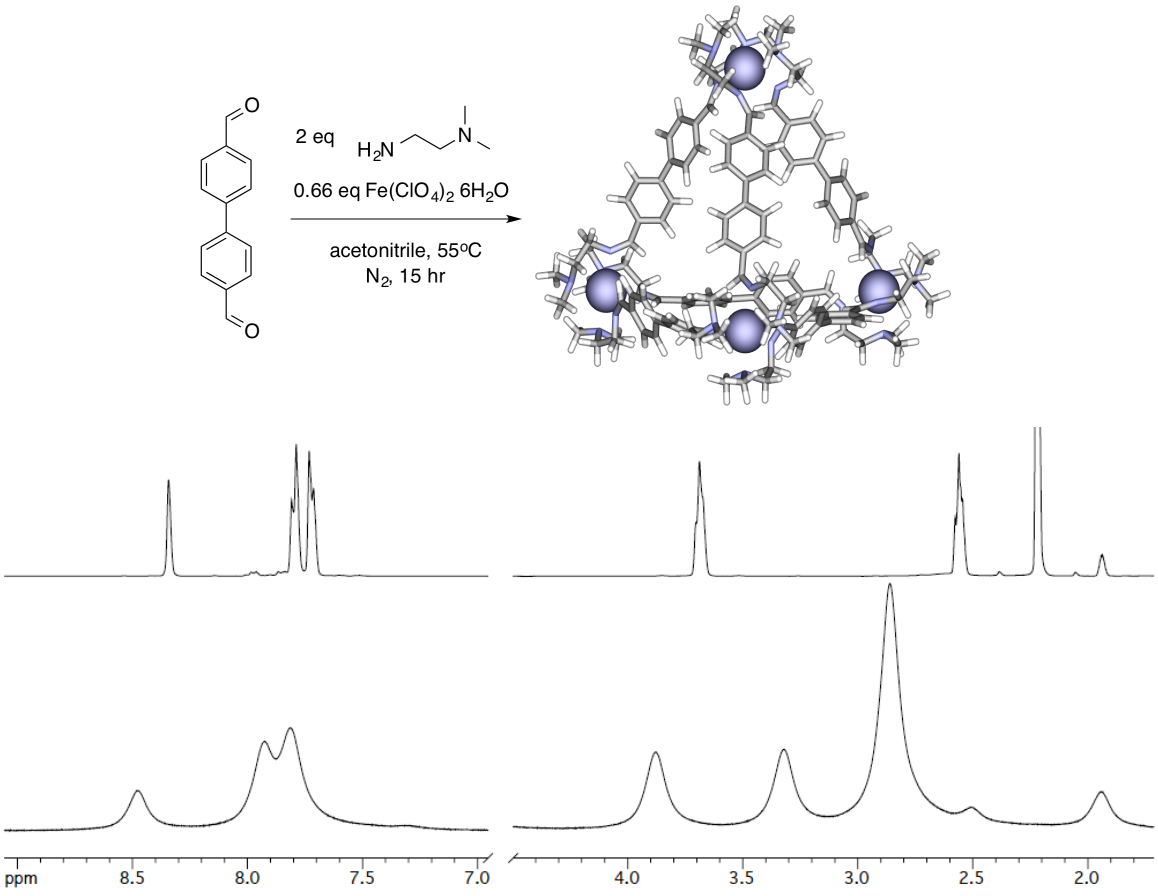

Figure 5.16: ^{1}H-NMR spectrum of **5.21** in acetonitrile-d_3 (top). ^{1}H-NMR spectrum of the analogous metal-ligand complex of **5.21_6•$Fe_4(ClO_4)_2$** in acetonitrile-d_3 (bottom).

Multicomponent self-assembly of ligands **5.20** with two equivalents of *N, N'*-dimethylethylenediamine and 0.66 equivalents of $Fe(ClO_4)_2$•$6H_20$ at 55°C in acetonitrile-d_3 under nitrogen for 15 hr formed a metal-ligand complex, likely to be a M_4L_6.

The ^{1}H-NMR spectrum of **5.21** shows the imine peak at 8.34 ppm, two doublet peaks, one at 7.81 ppm which corresponds to the aryl protons adjacent to the formyl functional group, and the other at 7.73 ppm, corresponding to the aryl protons towards the center. The two triplet peaks at 3.62 ppm and 3.32 ppm correspond to the alkyl peaks

that make up the backbone of the metal coordinators. The large singlet at 2.2 ppm corresponds to the methyl groups on the tertiary amine.

The ^{1}H-NMR spectrum in acetonitrile-d_3 of what is likely to be an M_4L_6 cage, **5.19_6•$Fe_4(ClO_4)_2$** shows a spectrum with broadened peaks, likely due to some paramagnetism or small amounts of spin cross over, as known for Fe(II)-tertiary amine complexes.[11] The aldehyde peak at 10 ppm from the ligand **5.20** is gone, with an imine peak assigned at 8.48 ppm, indicating that the imine was formed. This is a characteristic range where imine-Fe(II) peaks are typically observed,[12] thereby indicating that the imine-nitrogen is bound to an Fe(II) center. The pair of doublets corresponding to the aryl protons are found at 7.93 ppm and 7.82 ppm. In contrast, the aryl proton peaks adjacent to the metal coordination site of pyridine-imine Fe(II) self-assembled cages are shifted upfield around the 6 ppm range due to steric shielding around the Fe(II) center. The aryl protons closest to the Fe(II) center in **5.21_6•$Fe_4(ClO_4)_8$** are farther away compared to pyridine-imine Fe(II) complexes, which accounts for those protons downfield shift.

The peaks corresponding to the alkyl chain of the imine-tertiary amine metal coordinating group show sizable downfield shifts at 3.68 ppm and 3.32 ppm, compared to the free ligand. A sizable downfield shift at 2.86 ppm is also observed for the methyl groups on the nitrogen, due to the ligand-metal coordination with the cationic Fe(II) center. The self-assembled product could not be confirmed by ESI and MALDI mass spectrometry. Large X-ray quality crystals however, can be obtained by the slow evaporation of diethyl ether and acetonitrile.

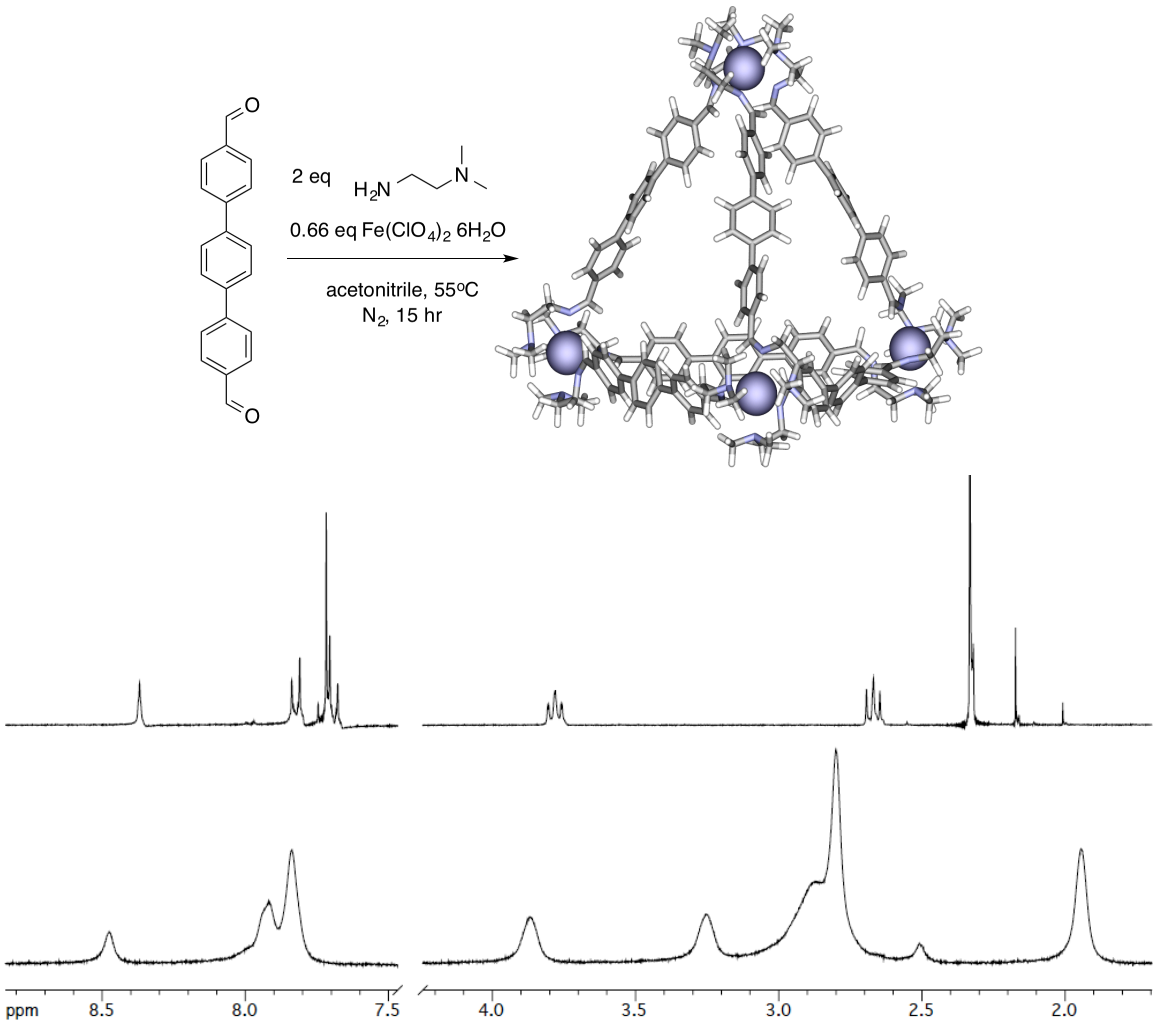

Figure 5.17: ^{1}H-NMR spectrum of **5.23** in chloroform-*d*$_3$ (top). ^{1}H-NMR spectrum of the analogous metal-ligand complex of **5.23**$_6$**•Fe**$_4$**(ClO**$_4$**)**$_2$ in acetonitrile-*d*$_3$ (bottom).

Multicomponent self-assembly of ligands **5.22** with two equivalents of *N, N'*-dimethylethylenediamine and 0.66 equivalents of $Fe(ClO_4)_2 \bullet 6H_2O$ at 55^{o}C in acetonitrile under nitrogen for 15 hr formed a metal-ligand complex, likely to be a M_4L_6 cage.

The ^{1}H-NMR spectrum of **5.23** shows the imine peak at 8.36 ppm, Two doublet peaks, one at 7.92 ppm and the other at 7.70 ppm which corresponds to the aryl protons adjacent to the formyl functional group, and the other at 7.70 ppm corresponding to the

other aryl protons on the same ring. The tall singlet at 7.71 ppm corresponds to the protons on the central ring. Two triplets, one at 3.78 ppm and the other at 2.67 ppm corresponds to the alkyl peaks that make up the backbone of the metal coordinators. And the large singlet at 2.32 ppm corresponds to the methyl groups on the tertiary amine.

Similar to **5.21_6•$Fe_4(ClO_4)_2$**, the ^{1}H-NMR spectrum in acetonitrile-d_3 of what is likely to be an M_4L_6 cage, **5.23_6•$Fe_4(ClO_4)_2$** shows a spectrum with broaden peaks. The aldehyde peak at 10 ppm from the ligand **5.22** is gone, with an imine peak formed at 8.48 ppm, a characteristic range for imine-Fe(II) complexes. The broadened aryl protons are found at 7.92 ppm and 7.83 ppm, a shift downfield shift compared to the unmetallated ligand **5.23**.

The peaks corresponding to the alkyl chain of the imine-tertiary amine metal coordinating group show downfield shifts at 3.87 ppm and 3.80 ppm. A sizable downfield shift at 2.8 ppm is also observed for the methyl groups on the nitrogen. The self-assembled product could not be confirmed by mass spectrometry. Large X-ray quality crystals however, can be obtained by the slow evaporation of diethyl ether and acetonitrile.

5.5. Conclusion

In conclusion, two tetracationic M_2L_4 palladium-pyridyl paddle-wheel cages of different sizes have been self-assembled from C_{2v} symmetric ditopic V-shaped ligands. The formation of the M_2L_4 cages is favored, with no polymeric aggregates observed. Structural analysis is possible via NMR and mass spectrometry, in comparison to other

similar cages where the structural characterization is supported with a crystal structure. These cages with extended conjugation present in the ligands show good fluorescent properties. Unfortunately, synthesis of a family of these cages with amine endohedral functionality was unsuccessful.

Multicomponent self-assembly of V-shape ligands with pyridine-imine metal coordinating groups and octahedral metals such as Fe(II) form M_2L_3 cages. The interior amine group of the V-shape ligand does not compete with the external amines during the self-assembly process, thereby allowing the lone pairs of the external nitrogens to coordinate to the metal vertices to form an enclosed cage. This preferential assembly allows the lone pairs of the interior amines the potential to promote reactivity, catalysis, and sensing. Methods to bias the formation of an M_4L_6 tetrahedron instead of a M_2L_3 helicate by implementing large endohedral functional groups on the interior amine are currently underway.

Attempts to self-assemble a M_4L_6 tetrahedron with V-shape ligands with imine-tertiary amine metal coordinating groups that permit greater geometric flexibility upon coordination to the metal center were inconclusive, due to poor solubility of the metal-ligand complexes formed. Linear analogs like $\mathbf{5.21_6 \bullet Fe_4(ClO_4)_2}$ and $\mathbf{5.23_6 \bullet Fe_4(ClO_4)_2}$, however, were soluble and showed evidence via ^{1}H-NMR of forming a metal-ligand complex.

References

1.) Yoshizawa, M.; Tamura, M.; Fujita, M. "AND/OR Bimolecular Recognition" *J. Am. Chem. Soc.* **2004**, *126*, 6846-6847.

2.) Yoshizawa, M.; Takeyama, Y.; Okano, T.; Fujita, M. "Cavity-Directed Synthesis Within a Self-Assembled Coordination Cage: Highly Selective [2+2] Cross-Photodimerization of Olefins" *J. Am. Chem. Soc.* **2003**, *125*, 3243-3247.

3.) (a) Suzuki, K.; Tominaga, M.; Kawano, M.; Fujita, M. "Self-Assembly of an M6L12 Coordination Cube" *Chem. Commun.* **2009**, 1638-1640; (b) Tominaga, M.; Suzuki, K.; Kawano, M.; Kushukawa, T.; Ozeki, T.; Sakamoto, S.; Yamaguchi, K.; Fujita, M. "Finite, Spherical Coordination Networks that Self-Organize From 36 Small Components" *Angew. Chem. Int. Ed.* **2004**, *43*, 5621-5625; (c) Klosterman, J. K.; Yamauchi, Y.; Fujita, M. "Engineering Discrete Stacks of Aromatic Molecules" *Chem. Soc. Rev.* **2009**, *38*, 1714-1725; (d) Takeda, N.; Umemoto, K.; Yamaguchi, K.; Fujita, M. "A Nanometre-Sized Hexahedral Coordination Capsule Assembled From 24 Components" *Nature* **1999**, *29*, 794-796.

4.) Sun, Q.; Iwasa, J.; Ogawa, D.; Ishido, Y.; Sato, S.; Ozeki, T.; Sei, Y.; Yamaguchi, K.; Fujita, M. "Self-Assembled M24L28 Polyhedra and Their Sharp Structural Switch Upon Subtle Ligand Variation" *Science* **2010**, *323*, 1144-1147.

5.) Yoshizawa, M.; Klosterman, J.; Fujita, M. "Functional Molecular Flasks: New Properties and Reactions Within Discrete, Self-Assembled Hosts" *Angew. Chem. Int. Ed.* **2009**, *48*, 3418-3438.

6.) Sato, S.; Yoshitaka, I.; Fujita, M. "Remarkable Stabilization of $M_{12}L_{24}$ Spherical Framewords Through the Cooperation of 48 Pd(II)-Pyridine Interactions" *J. Chem. Am. Soc.* **2009**, *131*, 6064-6065.

7.) Johnson, A., Moshe, O., Gamboa, A., Langloss, B., Limtiaco, J., Larive, C. Synthesis and Properties of Metal-Ligand Complexes With Endohedral Functionality *Inorg. Chem.* **2011**, *50*, 9430-9942.

8.) Pazderski, L.; Szluk, E.; Sitkowski, J.; Kamienski, B.; Kozerski, L.; Tousek, J.; Marek, R. "Experimental and Quantum-Chemical Studies of 15N NMR Coordination Shifts in Palladium and Platinum Chloride Complexes with Pyridine, 2,2' Bipyridine and 1,10-Phenanthroline" *Mag. Reson. Chem.* **2006**, *44*, 163-170.

9.) Smulders, M.; Riddell, I.; Browne, C.; Nitschke, J. R. "Building on Architectural Principles for Three-Dimensional Metallosupramolecular Construction" *Chem. Soc. Rev.* **2013**, *42*, 1728-1754.

10.) Young, M.; Johnson, A.; Gamboa, A.; Hooley, R. "Achiral Endohedral Functionality Provides Stereochemical Control in Fe(II)-Based Self-Assemblies" *Chem. Commun.* **2013**, *49*, 1627-1629.

11.) Schmidt, M.; Wiedemann, D.; Moubaraki, B.; Chilton, N. F.; Murray, K. S.; Vignesh, K. R.; Rajaraman, G.; Grohmann, A. "Iron(II) Complexes of Two Amine/Imine N5 Chelate Ligands Containing a 1,4-Diazepane Core- To Crossover or Not to Crossover" *Eur. J. Inorg. Chem.* **2013**, 958-967.

12.) (a) Bilbeisi, R. A.; Clegg, J. K.; Elrishi, N.; de Hatten, X.; Devillard, M.; Breiner, B.; Mal, P.; Nitschke, J. R. "Subcomponent Self-Assembly and Guest-Binding Properties of Face-Capped Fe4L48+ Capsules" *J. Am. Chem. Soc.* **2012**, *134*, 5110-5119; (b) Mal, P.; Breiner, K.; Rissanen, K.; Nitschke, J. R. "White Phosphorus is Air-Stable Within a Self-Assembled Tetrahedral Capsule" *Science* **2009**, *324*, 1697-1699; (c) Mal, P.; Nitschke, J. R. "Sequential Self-Assembly of Iron Structures in Water" *Chem. Commun.* **2010**, *46*, 2417-2419.

Chapter 6

Experimental Section

General Information

^{1}H and ^{13}C NMR spectra were recorded on either a Varian Inova 400 or 500 spectrometer. Proton (^{1}H) chemical shifts are reported in parts per million (δ) with respect to tetramethylsilane ($Si(CH_3)_4$, δ = 0), and referenced internally with respect to the protio solvent impurity. Carbon (^{13}C) chemical shifts are reported in parts per million (δ) with respect to tetramethylsilane ($Si(CH_3)_4$, δ=0), and referenced internally with respect to the solvent ^{13}C signal (either $CDCl_3$, acetonitrile-d_3. DMSO-d_6). Deuterated NMR solvents were obtained from Cambridge Isotope Laboratories, Inc., Andover, MA, and used without further purification. Mass spectra were recorded on an Agilent 6210 LC TOF mass spectrometer using electrospray ionization and processed with an Agilent Mass Hunter Operating System. Transition metal salts were obtained from Aldrich Chemical Company, St. Louis, MO and were used as received. Solvents were dried through a commercial solvent purification system (SG Water, Inc.) or were purchased in their anhydrous form from Aldrich Chemical Company. UV-vis titration experiments were performed on a Varian Cary 500 double beam scanning UV/vis spectrophotometer using a quartz cuvette.

Caution: *Even though no problems occurred during the course of these experiments, perchlorate mixtures are potentially explosive and should therefore be handled with appropriate care.*

Computer modeling of molecules were made using Spartan '06, DS Visualizer 2.0 and POV-Ray. ORTEP models were made using Mercury 2.4. Isotope pattern modeling was done in Data Explorer 4.0.

Chapter 2 Characterization

2.3: *[1,1'-biphenyl]-4,4'-dicarboxaldehyde*

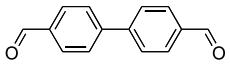

To an oven dried, 100 mL round-bottom flask equipped with a magnetic stirrer was added 4-bromobenzaldehyde (1.00 g, 5.40 mmol), 4-formylphenyl boronic acid (890 mg 6.00 mmol), $Pd(PPh_3)_2Cl_2$ (190 mg, 0.27 mmol), and potassium carbonate (4.48 g, 32.4 mmol). The mixture was placed under nitrogen and degassed ethanol (5.00 mL) and degassed H_2O (3.00 mL) were added by syringe. The reaction was stirred at 73^oC for 20 h. The solvent was removed by rotary evaporation, and product was extracted from the remaining solid with methylene chloride (20.0 mL). The mixture was then filtered through Celite™, and the solvent from the filtrate was removed by rotary evaporation. The crude product was purified by flash column chromatography on silica gel (CH_2Cl_2/methanol=100:1) to yield [1,1'-biphenyl]-4,4'-dicarboxaldehyde (858 mg, 76%) as an off white powder. Characterization has been reported.[1]

2.4: ***Imine of tris-(4,4')-ditolyl-BISTREN***

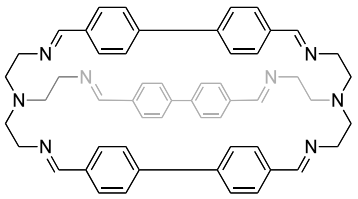

To an oven dried, 100 mL round-bottom flask equipped with a magnetic stirrer was added [1,1'-biphenyl]-4,4'-dicarboxaldehyde (800 mg, 3.80 mmol) in acetonitrile (20.0 mL) and a solution of *tris*(2-aminoethyl)amine (374 mg, 2.60 mmol) in acetonitrile (15.0 mL) drop wise over a period of one hour. The reaction was let to stir for 18 hr and a precipitate formed which was filtered to yield **2.4** (994 mg, 94%) as a yellow powder. Characterization has been reported.[1]

Tris-(4,4')-ditolyl-BISTREN

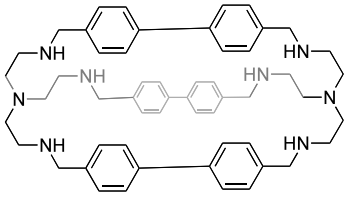

In a 100 mL round bottom flask, **2.4** (0.500 g, 0.61 mmol) was dissolved in 50.0 mL of anhydrous methanol. Sodium borohydride (1.36 g, 36.0 mmol) was added slowly over 30 minutes, and the reaction mixture was stirred for an additional five hours. Methanol was removed *in vacuo*, the solvent was extracted with methylene chloride (50.0 mL) and water (20.0 mL). The organic layer was extracted, and the aqueous layer was washed with 2 x 30.0 mL of methylene chloride. The organic layers were combined and dried with magnesium sulfate. Evaporation of methylene chloride yielded *tris*-(4,4')-ditolyl-BISTREN as a yellow powder, 25.0 mg, 50%. Characterization has been reported.[1]

2.4•Fe_2•$(ClO_4)_2$: ***Imine of tris-(4,4')-ditolyl-BISTREN•Fe_2•$(ClO_4)_4$***

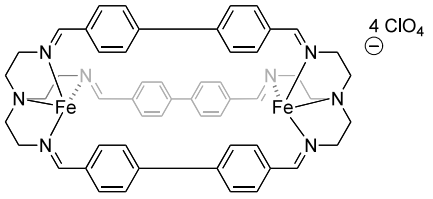

To an oven dried 25 mL round-bottom flask equipped with a magnetic stir bar was added **2.4** (200 mg, 0.25 mmol), $Fe(ClO_4)_2$•$6H_2O$ (131 mg, 0.53 mmol) and anhydrous methanol (4.00 mL). The suspension was let to stir at 65°C under nitrogen for 20 h. The product was separated as precipitate from the filtrate separated via centrifugation to yield **2.4•Fe_2•$(ClO_4)_2$** (214 mg, 76%) as a tan brown powder. ^{1}H NMR (400 MHz, DMSO-d_6): δ 8.62 (s, 6 H), 7.53 (br s, 12H), 7.26 (br s, 12H), 4.07 (br s 12H), 3.82 (br s 12H). MALDI m/z calcd for: $C_{54}H_{54}N_8Fe_2[3ClO_4+6H_2O^+]$ found at 1331.2310.

2.4•Fe_2•$(BPh_4)_4$: ***Imine of tris-(4,4')-ditolyl-BISTREN•Fe_2•$B(Ph_4)_2$***

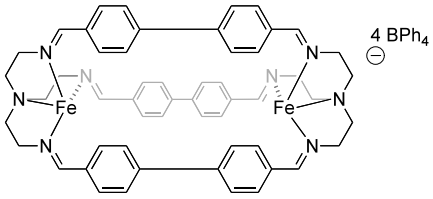

To an oven dried 25 mL round-bottom flask equipped with a magnetic stir bar was added **2.4•Fe_2•$(ClO_4)_2$** (200 mg, 0.18 mmol), $NaBPh_4$ (249 mg, 0.74 mmol) and anhydrous methanol (4.00 mL). The suspension was let to stir at room temperature under nitrogen for 5 h. The product was separated as precipitate from the filtrate separated via centrifugation to yield **2.4•Fe_2•$B(Ph_4)_4$** as a (331 mg, 83%) light brown powder. ^{1}H NMR (400 MHz, DMSO-d_6): δ 8.60 (br s, 6H), 7.71-6.70 (br m, 104H), 4.06 (br s, 12H), and 3.80 (br s, 12H).

2.4•Cu_2•$(PF_6)_2$: ***Imine of tris-(4,4')-ditolyl-BISTREN•Cu_2•$(PF_6)_2$***

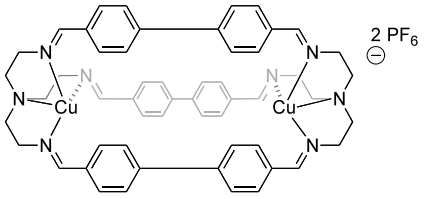

To an oven dried 25 mL round-bottom flask equipped with a magnetic stir bar was **2.4** added (200 mg, 0.25 mmol), $Cu(CH_3CN)_4PF_6$ (194 mg, 0.53 mmol) and anhydrous methanol (4.00 mL). The suspension was let to stir at 65°C under nitrogen for 20 h. The product was separated as precipitate from the filtrate separated via centrifugation to yield **2.4•Cu_2•$(PF_6)_2$** (172 mg, 78%) as an orange powder. ^{1}H NMR (400 MHz, DMSO-d_6): δ 8.75 (s, 6H), 7.84 (d, J = 8.1 Hz, 12H), 6.76 (d, J = 8.1 Hz, 12H), 3.93 (s, 12H), and 3.16 (s, 12H). ^{13}C NMR (125 MHz, DMSO-d_6): δ 162.4, 143.0, 130.2, 128.4, 128.0, 127.3, 58.8, 51.1. HRMS (ESI) *m/z*: calcd for $C_{54}H_{54}N_8F_6PCu_2$ [M-PF_6^+] 1085.2700 found at 1085.2700.

2.4•Ni_2•$(NO_3)_4$ & 2.4•Ni•$(NO_3)_2$: ***Imine of tris-(4,4')-ditolyl-BISTREN•Ni_2•$(NO_3)_4$ & 2.4•Ni•$(NO_3)_2$***

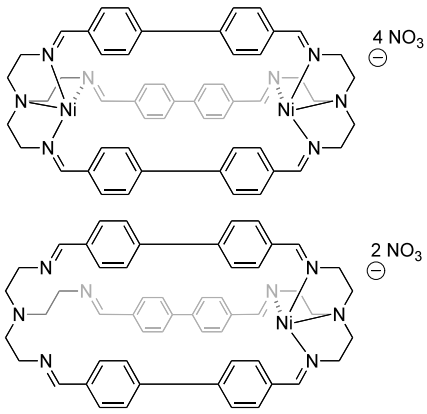

To an oven dried 25 mL round-bottom flask equipped with a magnetic stir bar was added **2.4** (100 mg, 0.12 mmol), $Ni(NO_3)_2$•$6H_2O$ (75 mg, 0.26 mmol and anhydrous methanol (4.00 mL.) The suspension was let to stir at 65°C under nitrogen for 20 h. The product was separated as precipitate from the filtrate separated via centrifugation to yield **2.4•Ni_2•$(NO_3)_4$** (70 mg, 48%) and **2.4•Ni•$(NO_3)_2$** (35 mg, 26%) as a light green powder. ^{1}H NMR of **2.4•Ni_2•$(NO_3)_4$**: (400 MHz, DMSO-d_6): δ 8.61 (s, 6H), 7.54 (d, J = 8.2 Hz, 12H), 7.2 (d,

J = 8.2 Hz, 12H), 4.07 (s, 12H), 3.83 (s, 12H). **2.4•Ni•$(NO_3)_2$**: ^{1}H NMR (400 MHz, DMSO-d_6): δ 8.67 (s, 3H), 8.03 (s, 3H), 7.61 (d, *J* = 8.2 Hz, 6H), 7.17 (d, *J* = 8 Hz, 6H), 7.11 (d, *J*= 7.2 12H), 4.07 (s, 6H).

2.4•Zn_2•$(NO_3)_4$ & 2.4•Zn•$(NO_3)_2$: ***Imine of tris-(4,4')-ditolyl-BISTREN•Zn_2•$(NO_3)_4$ & 2.4•Zn•$(NO_3)_2$***

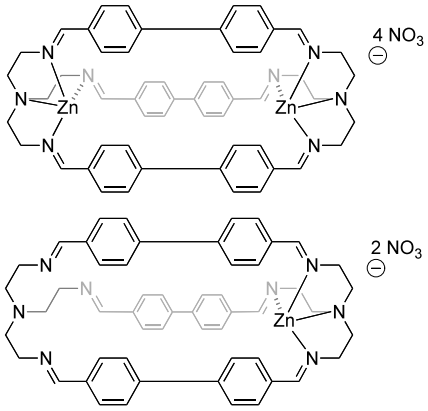

To an oven dried 25 mL round-bottom flask equipped with a magnetic stir bar was added **2.4** (100 mg, 0.12 mmol), $Zn(NO_3)_2$•$6H_2O$ (77 mg, 0.25 mmol) and anhydrous methanol. The suspension was let to stir at 65^{o}C under nitrogen for 20 h. The product was separated as precipitate from the filtrate separated via centrifugation to yield **2.4•Zn_2•$(NO_3)_4$** (74 mg, 50%) and **2.4•Zn•$(NO_3)_2$** (36 mg, 30%). **2.4•Zn_2•$(NO_3)_4$** as a white powder. ^{1}H NMR (400 MHz, DMSO-d_6): δ 8.60 (s, 6H), 7.53 (d, *J*= 8.1 Hz, 12H), 7.25 (d, *J*= 8.1 Hz, 12H), 4.08 (s, 12H), 3.8 (s, 12H). **2.4•Zn•$(NO_3)_2$** ^{1}H NMR (400 MHz, DMSO-d_6): δ 8.66 (s, 3H), 8.04 (s, 3H), 7.62 (d, *J* = 7.6 Hz, 6H), 7.18 (d, *J* = 7.2 Hz, 6H), 7.11 (d, *J* = 7.6 Hz, 12H), 3.69 (s, 6H).

2.4•Zn•$(NO_3)_2$: ***Imine of tris-(4,4')-ditolyl-BISTREN•Zn•$(NO_3)_2$***

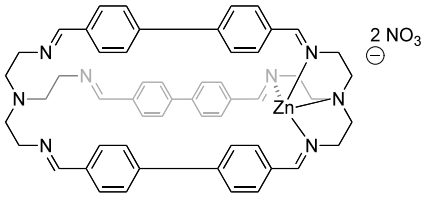

To an oven dried 25 mL round-bottom flask equipped with a magnetic stir bar was added **2.4** (100 mg, 0.12 mmol), $Zn(NO_3)_2•6H_2O$ (39 mg, 0.13 mmol) and anhydrous methanol. The suspension was let to stir at 65°C under nitrogen for 20 h. The product was separated as precipitate from the filtrate separated via centrifugation to yield **2.4•Zn•$(NO_3)_2$** (90 mg, 75%) as a white powder. ^{1}H NMR (400 MHz, DMSO-d_6): δ 8.66 (s, 3H), 8.04 (s, 3H), 7.62 (d, J = 7.6 Hz, 6H), 7.18 (d, J = 7.2 Hz, 6H), 7.11 (d, J = 7.6 Hz, 12H), 3.69 (s, 6H).

2.4•Ag_2⊂$(NO_3)_2$ & 2.4•Ag_2•$(NO_3)_2$: ***Imine of tris-(4,4')-ditolyl-BISTREN• 2.4•Ag_2⊂$(NO_3)_2$ & 2.4•Ag_2•$(NO_3)_2$***

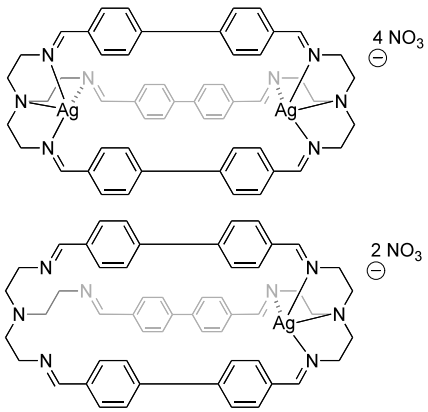

To an oven dried 25 mL round-bottom flask equipped with a magnetic stir bar was added **2.4** (100 mg, 0.12 mmol), $AgNO_3$ (44.0 mg, 26 mmol and anhydrous methanol. The suspension was let to stir at 65°C under nitrogen for 20 h. The product was separated as precipitate from the filtrate separated via centrifugation to yield **2.4•Ag_2⊂$(NO_3)_2$** (101 mg, 78%) and **2.4•Ag_2•$(NO_3)_2$** (29 mg, 21%) as a gray powder. **2.4•Ag_2⊂$(NO_3)_2$** ^{1}H NMR (400 MHz, DMSO-d_6): δ 8.86 (s, 6H), 7.91 (d, J = 8 Hz, 12H), 7.64 (d, J = 8.4 Hz, 12H), 3.95 (s, 12H), 3.09 (s, 12H).

2.4•Ag_2•$(NO_3)_2$ ^{1}H NMR (400 MHz, DMSO-d_6): δ 8.70 (s, 3 H), 8.07 (d, J = 8.8 Hz, 12H), 8.07 (d, J = 8.4 Hz, 12H), 3.81 (s, 12H), 2.87 ppm (s, 12H).

2.5: ***[1,1'-:4',1"-terphenyl]-4,4'-dicarboxaldehyde***

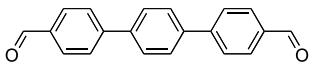

To an oven dried, 50 mL round-bottom flask equipped with a magnetic stirrer was added 1,4 diiodobenzene (400 mg, 1.20 mmol), 4-formyl phenyl boronic acid (382 mg, 2.50 mmol), *bis*(triphenylphosphine)palladium(II) dichloride (84 mg, 0.12 mmol), and K_2CO_3 (995 mg, 7.20 mol). The mixture was placed under nitrogen and degassed ethanol (5.00 mL) and degassed H_2O (3.00 mL) were added by syringe. The reaction was stirred at 73^{o}C for 20 h. The solvent was removed by rotary evaporation, and product was extracted from the remaining solid with methylene chloride (20.0 mL). The mixture was then filtered through Celite™, and the solvent from the filtrate was removed by rotary evaporation to yield compound **2.5** (289 mg, 84%) as an off white powder. ^{1}H NMR (400 MHz, $CDCl_3$): δ 10.08 (s, 2H), 8.00 (d, J = 8.22 Hz, 4H), 7.83 (d, J = 8.20 Hz, 4H), 7.77 (s, 4H). ^{13}C NMR (100 MHz, $CDCl_3$): δ 192.0, 146.4, 139.9, 135.6, 130.5, 128.1, 127.8. HRMS (ESI) *m/z*: calcd for $C_{20}H_{14}O_2$ [M-H$^+$] 287.1067; found at 287.1072.

2.6: ***Imine of [1,1'-:4',1"-terphenyl]-4,4'-BISTREN***

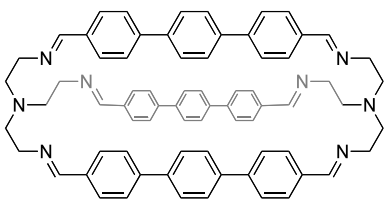

To an oven dried, 100 mL round-bottom flask equipped with a magnetic stirrer was added [1,1'-:4',1"-terphenyl]-4,4'-dicarboxaldehyde (400 mg, 1.40 mmol)

in acetonitrile (20.0 mL) and a solution of *tris*(2-aminoethyl)amine (137 mg, 0.93 mmol) in acetonitrile (15.0 mL) dropwise over a period of one hour. The reaction was let to stir for 18 h and a precipitate formed which was filtered to yield **2.6** (487 mg, 99%) as a yellow powder. HRMS (ESI) *m/z*: calcd for $C_{72}H_{66}N_8$ [M-H^+] 1043.3480; found at 1043.5394.

2.6•Fe_2•$(ClO_4)_2$: ***Imine of [1,1'-:4',1"-terphenyl]-4,4'-BISTREN•Fe_2•$(ClO_4)_4$***

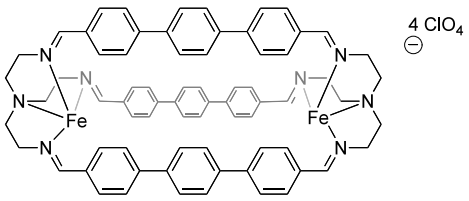

To an oven dried 25 mL round-bottom flask equipped with a magnetic stir bar was added **2.6** (25 mg, 0.025 mmol), $Fe(ClO_4)_2$•$6H_2O$ (18.3 mg, 0.05 mmol) and anhydrous methanol (3.00 mL.) The suspension was let to stir at 65°C under nitrogen for 20 h. The product was separated as precipitate from the filtrate separated via centrifugation to yield **2.6•Fe_2•$(ClO_4)_2$** (33 mg, 89%) as a light brown powder. ^{1}H NMR (400 MHz, DMSO-d_6): δ 8.62 (s, 6H), 7.59 (d, J = 7.2 Hz, 12H), 7.34 (s, 12H), 7.29 (d, J = 8.0 Hz, 12H), 4.09 (s, 12H), 3.84 (s, 12H).

2.6•Cu_2•$(PF_6)_2$: ***Imine of [1,1'-:4',1"-terphenyl]-4,4'-BISTREN•Cu_2•$(PF_6)_2$***

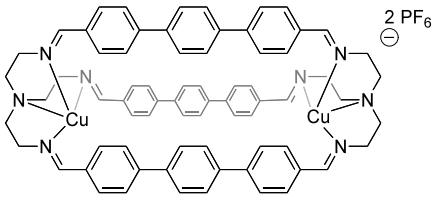

To an oven dried 25 mL round-bottom flask equipped with a magnetic stir bar was added **2.6** (25 mg, 0.02 mmol), $Cu(CH_3CN)_4PF_6$ (18.8 mg, 0.05 mmol and anhydrous methanol. The suspension was let to stir at 65°C under nitrogen for 20 h. The product was separated as precipitate from the filtrate

separated via centrifugation to yield **2.6•Cu$_2$•(PF$_6$)$_2$** (31 mg, 89%) as an orange powder. ^{1}H NMR (400 MHz, DMSO-*d$_6$*): δ 8.78 (br s, 6H), 8.05 (br s, 12H), 7.20 (br s, 12H), 7.012 (br s, 12H), 4.00 (br s, 12H). HRMS (ESI) *m/z*: calcd for $C_{72}H_{66}N_8F_6PCu_2$ [M-PF_6^+] 1315.4048; found at 1315.3650. ^{13}C NMR (125 MHz, DMSO-*d$_6$*): δ 202.2, 164.8, 162.2, 133.5, 130.2, 128.8, 127.3, 127.2, 126.6, 62.8.

2.6•Zn$_2$•(NO$_3$)$_4$: *Imine of [1,1'-:4',1"-terphenyl]-4,4'-BISTREN•Zn$_2$•(NO$_3$)$_2$*

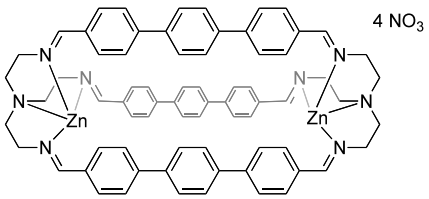

To an oven dried 25.0 mL round-bottom flask equipped with a magnetic stir bar was added **2.6** (25 mg, 0.025 mmol), Zn(NO$_3$)$_2$•6H$_2$O (0.14 mg, 0.05 mmol and anhydrous methanol (3.00 mL.) The suspension was let to stir at 65^{o}C under nitrogen for 20 h. The product was separated as precipitate from the filtrate separated via centrifugation to yield **2.6•Zn$_2$•(NO$_3$)$_4$** (23 mg, 73%) as a white powder. ^{1}H NMR (400 MHz, DMSO-*d$_6$*): δ 8.2 (s, 6H), 8.3 (br d, 12H, 7.58 (br s, 12H), 7.33 (br d, 12H), 4.65 (s, 6H), 4.09 (s, 6H).

2.7: *[1,1'-:3',1"-terphenyl]-4,4'-dicarboxaldehyde*

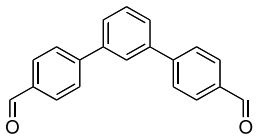

To an oven dried, 50 mL round-bottom flask equipped with a magnetic stirrer was added 1,4 diiodobenzene (400 mg, 1.21 mmol), 4-formyl phenyl boronic acid (382 mg, 2.52 mmol), *bis*(triphenylphosphine)palladium(II) dichloride (84 mg, 0.12 mmol), and K_2CO_3 (995 mg, 7.22 mol). The mixture was placed under nitrogen and anhydrous THF (5.00 mL)

and degassed H_2O (3.00 mL) were added by syringe. The reaction was stirred at 73°C for 2 d. The solvent was removed by rotary evaporation, and product was extracted from the remaining solid with methylene chloride (20 mL). The mixture was then filtered through Celite™, and the solvent from the filtrate was removed by rotary evaporation to yield compound **2.7** (155 mg, 45%) as a brown powder. ^{1}H NMR (400 MHz, $CDCl_3$): 10.07 (s, 2H), 7.99 (d, J = 8.2 Hz, 4H), 7.86, (s, 1H), 7.8 (d, J = 8.16 Hz, 4H), 7.7 (d, J = 8.7, 2H), 7.61 (t, J = 7.67, 2H). ^{13}C NMR (100 MHz, DMSO-d_3): 192.8, 145.5, 139.7, 135.3, 130.128, 129.9, 127.7, 127.3, 126.0. HRMS (ESI) *m/z*:calcd for $C_{20}H_{14}O_2$ [M-H$^+$] 287.1067; found at 287.1072.

2.8: ***[1,1'-:3',1"-terphenyl]-4,4'- BISTREN***

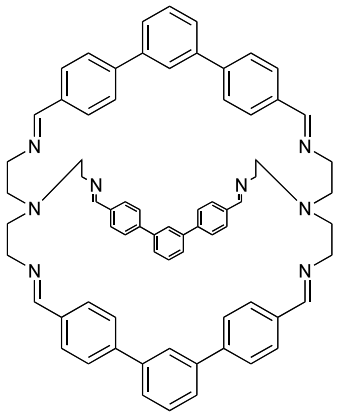

To an oven dried, 100 mL round-bottom flask equipped with a magnetic stirrer was added [1,1'-:3',1"-terphenyl]-4,4'-dicarboxaldehyde (400 mg, 1.4 mmol) in acetonitrile (20.0 mL) and a solution of *tris*-(2-aminoethyl)amine (137 mg, 0.93 mmol) in acetonitrile (15.0 mL) dropwise over a period of one hour. The reaction was let to stir for 18 h and a precipitate formed which was filtered to yield **2.8** (474 mg, 98%) as a white powder. HRMS (ESI) *m/z*:calcd for $C_{72}H_{66}N_8$ [M-H$^+$] 1043.3480; found at 1043.5394.

2.8•Fe_2•$(ClO_4)_4$: *Imine of [1,1'-:3',1"-terphenyl]-4,4'- BISTREN•Fe_2•$(ClO_4)_4$*

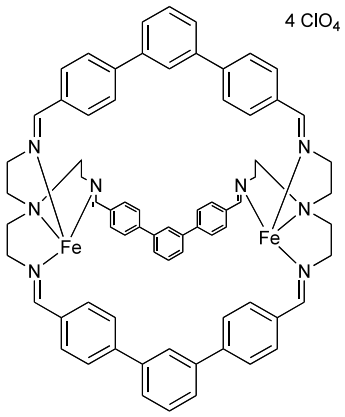

To an oven dried 25 mL round-bottom flask equipped with a magnetic stir bar was added **2.8** (25 mg, 0.025 mmol), $Fe(ClO_4)_2$•$6H_2O$ (18.3 mg, 0.05 mmol and anhydrous methanol. The suspension was let to stir at 65°C under nitrogen for 20 hr. The product was separated as precipitate from the filtrate separated via centrifugation to yield **2.8•Fe_2•$(ClO_4)_4$** (30 mg, 81%) as a light brown powder. ^{1}H NMR (500 MHz, DMSO-d_6): δ 8.540 (br s, 6H), 8.54-7.53 (br m, 33H), 6.807 (br s, 3H).

2.9: *[1,1'-:3',1"-terphenyl-4-nitroaniline]-4,4'-dicarboxaldehyde*

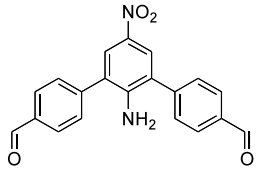

To an oven dried, 50 mL round-bottom flask equipped with a magnetic stirrer was added 2,6 diiodo-4-nitroaniline (468 mg, 1.2 mmol), 4-formyl phenyl boronic acid (382 mg, 2.5 mmol), *bis*(triphenylphosphine)palladium(II) dichloride (84 mg, 0.12 mmol), and K_2CO_3 (995 mg, 7.2 mol). The mixture was placed under nitrogen and anhydrous ethanol (5 mL) and degassed H_2O (3 mL) were added by syringe. The reaction was stirred at 73°C for 2 d. The solvent was removed by rotary evaporation, and product was extracted from the remaining solid with methylene chloride (20 mL). The mixture was then filtered through Celite, and the solvent from the filtrate was removed by rotary evaporation to yield compound **2.9** (229 mg, 55%) as a yellow solid. ^{1}H NMR (400 MHz, $CDCl_3$): δ 10.11 (s, 2H), 8.11 (s, 2H), 8.07 (d, J = 8.3 Hz, 4 H), 7.71 (d, J = 8.2 Hz, 4 H), 4.55 (s, 2H). HRMS (ESI) *m/z*: calcd for $C_{20}H_{14}N_2O_4$ [M-H^+]1223.5363; found at 347.1013.

2.10: ***Imine of [1,1'-:3',1"-terphenyl-4-nitroaniline]-4,4'- BISTREN***

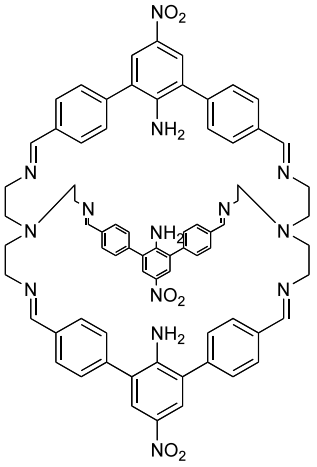

To an oven dried, 100 mL round-bottom flask equipped with a magnetic stirrer was added [1,1'-:3',1"-terphenyl-4-nitroaniline]-4,4'-dicarboxaldehyde (935 mg, 2.70 mol) in acetonitrile (20.0 mL) and a solution of *tris*-(2-aminoethyl)amine (131.6 mg, 0.9 mol) in acetonitrile (15.0 mL) dropwise over a period of one hour. The reaction was let to stir for 18 h and a precipitate formed which was filtered to yield **2.10** (1.09 g, 99%) as a bright yellow powder. HRMS (ESI) *m/z*: calcd for $C_{72}H_{67}N_{14}O_6$ [M-H^+] 1223.5363; found at 1223.5374.

2.10•Fe_2•$(ClO_4)_4$: ***Imine of [1,1'-:3',1"-terphenyl-4-nitroaniline]-4,4'-BISTREN•Fe_2•$(ClO_4)_4$***

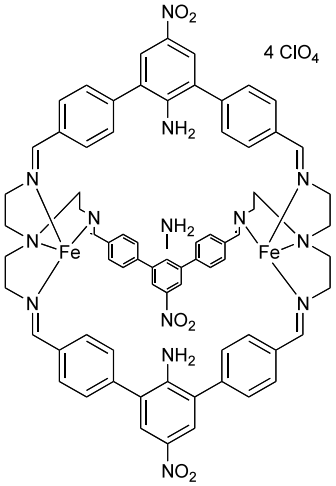

To an oven dried 25 mL round-bottom flask equipped with a magnetic stir bar was added **2.10** (25 mg, 0.02 mmol), $Fe(ClO_4)_2$•$6H_2O$ (16 mg, 0.04 mmol and anhydrous acetonitrile. The suspension was let to stir at 65°C under nitrogen for 20 h. The product was separated as precipitate from the filtrate separated via centrifugation to yield **2.10** (21 mg, 60%). ^{1}H NMR (400 MHz, DMSO-d_6): δ 8.74 (s, 6H), 7.87 (d, J = 6.4 Hz, 12H), 7.17 (s, 6H), 6.91 (s, 6H), 6.78 (d, J=4 Hz, 12H).

2.11: ***4,4'-(2-5-thiophenediyl) bis-benzaldehyde***

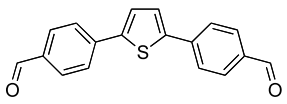

To an oven dried, 50 mL round-bottom flask equipped with a magnetic stirrer was added 2,5 dibromothiophene (580 mg, 2.40 mmol), 4-formyl phenyl boronic acid (1.12 g, 7.50 mmol), *bis*(triphenylphosphine)palladium(II) dichloride (168 mg, 0.24 mmol), and K_2CO_3 (1.90 g, 14.4 mmol). The mixture was placed under nitrogen and anhydrous THF (8.00 mL) and degassed H_2O (3.00 mL) were added by syringe. The reaction was stirred at 53^{o}C for 2 d. The solvent was removed by rotary evaporation, and product was extracted from the remaining solid with methylene chloride (20.0 mL). The mixture was then filtered through Celite™, and the solvent from the filtrate was removed by rotary evaporation. The crude product was purified by flash column chromatography on silica gel (CH_2C_{l2}/methanol=100:1) to yield compound **2.11** (502 mg, 72%) as an orange powder. ^{1}H NMR (400 MHz, $CDCl_3$): δ 10.03 (s, 2H), 7.94 (d, *J* = 8.5 Hz, 4H), 7.82 (d, *J* = 8.4 Hz, 4H), 7.50 (s, 2H). ^{13}C NMR (100 MHz, $CDCl_3$): δ 144.0, 140.0, 130.7, 126.4, 126.1. HRMS (ESI) *m/z*:calcd for $C_{18}H_{12}O_2S$ [M-H$^+$] 1043.3480; found at 1043.5394.

2.12: ***Imine of 4,4'-(2-5-thiophenediyl) - BISTREN***

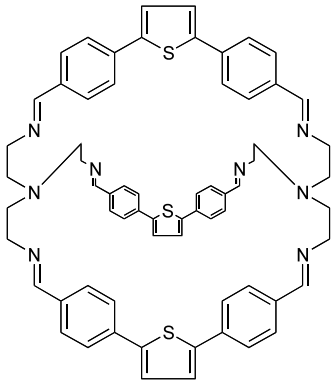

To an oven dried, 100 mL round-bottom flask equipped with a magnetic stirrer was added 4,4'-(2-5-thiophenediyl) *bis*-benzaldehyde (800 mg, 2.74 mmol) in acetonitrile (25.0 mL) and a solution of *tris*(2-aminoethyl)amine (265 mg, 1.8 mmol) in acetonitrile (20.0 mL) dropwise over a period of one hour. The reaction was let to stir for 18 h and a precipitate formed which was filtered to yield **2.12** (950 mg, 98%) as a yellow powder. HRMS (ESI) *m/z*: calcd for $C_{72}H_{65}N_8$ [M-H^+] 1061.4176; found at 1061.4190.

2,6 Diiodo aniline 4-dodecylamide

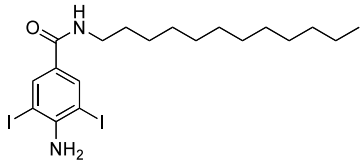

To a 25 mL round-bottom flask equipped with a stir bar was added oxalyl chloride (448 mg, 2.40 mmol), 4-amino-3,5 diiodobenzoic acid (600 mg, 1.55 mmol) and one drop of DMF. The reaction was let to stir at room temperature under nitrogen for 5 h followed by addition of dodecylamine (448 mg, 2.61 mmol). The precipitate was filtered to yield a white powder (376 mg, 50%). ^{1}H NMR (400 MHz, $CDCl_3$): δ 8.05 (s, 2H), 5.88 (s, 1H), 4.93 (s, 2H), 3.40 (q, *J* = 7.2 Hz, 2H), 1.61 (s, 8 H), 1.27 (s, 14H), 0.89 (t, *J* = 7.2 Hz, 2H). HRMS (ESI) *m/z*: calcd for $C_{19}H_{30}I_2N_2O$ [M-H^+] 557.052; found at 557.0531.

Chapter 3 Characterization

3.2a: ***N-(4-iodophenyl)-N)-butyl urea***

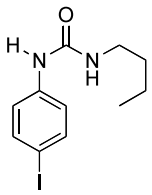

To an oven dried, 25.0 mL round-bottom flask equipped with a magnetic stirrer was added butyl isocyanate (1.36 g, 13.5 mmol) and 4-iodo aniline (2.00 g, 9.13 mmol.) The mixture was placed under nitrogen and anhydrous methylene chloride (8.00 mL) was added by syringe. The reaction was let to stir at room temperature for 24 h. The precipitate was removed by filtration to yield **3.2a** (2.56 g, 89%) as a white powder. ^{1}H NMR (400 MHz, DMSO-d_6) δ 8.50 (s, 1 H), 7.52 (d, J = 8.8 Hz, 2H), 7.24 (d, J = 8.8 Hz, 2H), 6.14 (t, J = 5.5 Hz, 1H), 3.05 (q, J = 5.6 Hz, 2H), 1.40 (p, J = 7.2 Hz, 2H), 1.30 (s, J = 6.8 Hz, 2H), 0.88 (t, J = 7.6 Hz, 3H.) ^{13}C NMR (100 MHz, DMSO-d_6) δ 155.4, 140.9, 137.5, 120.3, 39.1, 32.2, 19.9, and 14.1. HRMS (ESI) *m/z*: calcd for $C_{11}H_{15}IN_2O$ ($M+H^+$) 319.0302; found at 319.0297.

3.2a-Br***: N-(4-bromophenyl)-N)-butyl urea***

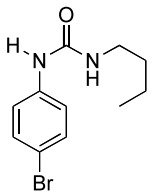

To an oven dried, 25 mL round-bottom flask equipped with a magnetic stirrer was added butyl isocyanate (1.73 g, 17.5 mmol) and 4-bromo aniline (2 g, 11.6 mmol.) The mixture was placed under nitrogen and anhydrous methylene chloride (8.00 mL) was added by syringe. The reaction was let to stir at room temperature for 24 h. The precipitate was removed by filtration to yield **3.2a-Br** (1.73 g, 86%) as a white powder. ^{1}H NMR (400 MHz, DMSO-d_6) δ 8.53 (s, 1H), 7.36 (s, 4H), 6.15 (t, J = 5.6 Hz, 1H), 3.07 (q, J = 6 Hz, 2H), 1.42 (p, J = 5.5 Hz, 2H), 1.30 (s, J = 7.6

Hz, 2H), 0.89 (t, J = 7.2 Hz, 3H.) ^{13}C NMR (100 MHz, DMSO-d_6) δ 155.2, 140.2, 131.5, 119.6, 112.3, 38.9, 32.0, 19.7, 13.9. HRMS (ESI) *m/z*: calcd for $C_{11}H_{15}BrN_2O$ ($M+H^+$); 269.0284; found at 271.0503.

3.2b: ***N-(4-iodophenyl)-N)-octyl urea***

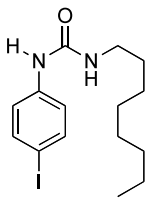

To an oven dried, 25 mL round-bottom flask equipped with a magnetic stirrer was added octyl isocyanate (1.10 g, 11.1 mmol) and 4-iodo aniline (2.00 g, 9.13 mmol.) The mixture was placed under nitrogen and anhydrous methylene chloride (8.00 mL) was added by syringe. The reaction was let to stir at room temperature for 24 h. The precipitate was removed by filtration to yield **3.2b** (1.62 g, 82%) as a white powder. ^{1}H NMR (300 MHz, DMSO-d_6) δ 8.49 (s, 1H), 7.53 (d, J = 8.7 Hz, 2H), 7.25 (d, J = 9.0 Hz, 2H), 7.25 (t, J = 9.0 Hz, 2H), 6.13 (t, J = 5.1 Hz, 1H), 3.06 (q, J = 6 Hz, 2H), 1.43 (t, J = 6.3 Hz, 2H), 1.43 (s, 10H), 0.86 (t, J = 6.6 Hz, 3H.) ^{13}C NMR (100 MHz, DMSO-d_6) δ 154.9, 140.5, 137.1, 119.8, 83.3, 39.0, 31.2, 29.7, 28.7, 26.4, 22.1, and 13.9. HRMS (ESI) *m/z*: calcd for $C_{15}H_{23}IN_2O$ ($M+H^+$): 375.0928; found at 375.0942.

3.2c: ***N-(4-iodophenyl)-N)-phenyl urea***

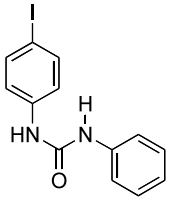

To an oven dried, 25 mL round-bottom flask equipped with a magnetic stirrer was added phenyl isocyanate (408 mg, 3.43 mmol) and 4-iodo aniline (500 mg, 2.28 mmol.) The mixture was placed under nitrogen and anhydrous methylene chloride (5.00 mL) was added by syringe. The

reaction was let to stir at room temperature for 24 h. The precipitate was removed by filtration to yield **3.2c** (745 mg, 96%) as a white powder. ^{1}H NMR (400 MHz, DMSO-d_6) δ 8.76 (s, 1H), 8.67 (s, 1H), 7.60 (d, J = 8.8 Hz, 2H), 7.44 (d, J = 7.66 Hz, 2H), 7.31 (d, J=8.71 Hz, 2H), 7.25 (d, J = 8.15 Hz, 2H), 6.97 (s, J = 7.2 Hz, 1H). ^{13}C NMR (100 MHz, DMSO-d_6) δ 152.4, 139.7, 139.5, 128.8, 122.1, 120.5, 118.4. HRMS (ESI) *m/z*: calcd for $C_{13}H_{11}IN_2O$ ($M+H^+$): 338.9989 found at 339.0001.

3.2d: ***N-(4-iodophenyl)-N)-octyldodecyl urea***

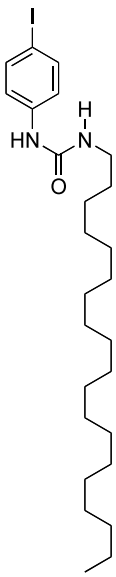

To an oven dried, 25 mL round-bottom flask equipped with a magnetic stirrer was added octyldodecyl isocyanate (1.01 g, 2.30 mmol) and 4-iodo aniline (500 mg, 2.28 mmol.) The mixture was placed under nitrogen and anhydrous methylene chloride (8.00 mL) was added by syringe. The reaction was let to stir at room temperature for 24 h. The precipitate was removed by filtration to yield **3.2d** (524 mg, 45%) as a white powder. ^{1}H NMR (400 MHz, DMSO-d_6) δ 8.5 (s, 1H), 7.52 (d, J = 8.7 Hz, 2H), 7.32 (d, J = 7.06 Hz, 2 H), 6.13 (s, 1H), 1.53 (s, 2H), 1.23 (s, 32H), 0.85 (s, 3H). ^{13}C NMR (1205 MHz, DMSO-d_6) δ 155.0, 140.0, 137.0, 119.9, 113.1, 31.4, 29.7, 29.0, 28.8, 26.2, 22.0, 14.0. HRMS (ESI) *m/z*: calcd for $C_{25}H_{43}IN_2O$ ($M+H^+$)+[-H]); 514.2415; found at 515.24.

3.6: ***N-[[(4-iodophenyl)amino] thioxomethyl]-benzamide***

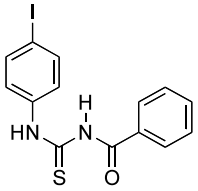

To an oven dried, 25 mL round-bottom flask equipped with a magnetic stirrer was added benzoyl thioisocynate (1.01 g, 3.40 mmol) and 4-iodo aniline (500 mg, 3.40 mmol.) The mixture was placed under nitrogen and anhydrous methylene chloride (8.00 mL) was added by syringe. The reaction was let to stir at room temperature for 24 h. The precipitate was removed by filtration to yield **3.6** (633 g, 72%) as a white powder. ^{1}H NMR (300 MHz, $CDCl_3$) δ 12.62, (s, 1H), 9.07 (s, 1H), 7.89 (d, *J* = 5.4 Hz, 2H), 7.74 (d, *J* = 8.62 Hz, 2H), 7.67 (t, *J* = 7.43 Hz, 1H), 7.57 (d, *J* = 6 Hz, 1H), 7.5 (d, *J* = 6 Hz, 2H). ^{13}C NMR (100 MHz, $CDCl_3$) δ 178.3, 167.1, 138.1, 137.5, 134.0, 131.6, 129.4, 127.6, 125.8, 91.3. HRMS (ESI) *m/z*: calcd for $C_{14}H_{11}IN_2OS$ $(M+NH_4)+[-H])$; found at 382.9889.

3.7: ***N-(4-iodophenyl)-N)-allyl thio urea***

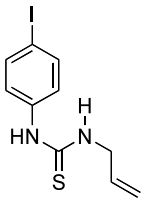

To an oven dried, 25 mL round-bottom flask equipped with a magnetic stirrer was added allyl thioisocyanate (340 mg, 3.38 mmol) and 4-iodo aniline (500 mg, 2.28 mmol.) The mixture was placed under nitrogen and anhydrous methylene chloride (8 mL) was added by syringe. The reaction was let to stir at room temperature for 24 h. The precipitate was removed by filtration and was recrystalized in methylene chloride to yield **3.7** (344 mg, 47%) as white crystals. ^{1}H NMR (300 MHz, $CDCl_3$) δ 7.75 (d, *J* = 8.5 Hz, 2H), 7.00 (d, *J*=8.4 Hz, 2H), 6.0 (s, 1H), 5.9-5.8 (m, *J* = 6 Hz, 1H), 5.19 (t, *J* = 8.8 Hz, 1H), 4.27 (t, *J* = 75.6 Hz, 1H), 4.14 (dd, *J* = 3.3 Hz, 1H). ^{13}C NMR (100 MHz, $CDCl_3$) δ 180.7, 139.5, 136.2, 133.2, 127.213, 117.8,

92.1, 82.0, 77.8, 77.3, 76.9, 48.1. HRMS (ESI) *m/z*: calcd for $C_{10}H_{12}IN_2S$ ($M+H^+$): 318.976; found at 318.9765.

3.3a: ***N-butyl-N'(4'-formyl[1,1'-biphenyl]-4-yl])-urea***

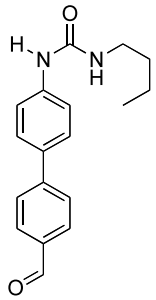

To a 50 mL round-bottom flask equipped with a stir bar and reflux condenser was added **3.2a** (400 mg 1.26 mmol) 4-formyl phenyl boronic acid (283 mg, 1.89 mmol), *bis*(triphenylphosphine)palladium(II) dichloride (88 mg 0.126 mmol) and Cs_2CO_3 (2.5 g, 7.56 mmol). The mixture was placed under nitrogen and degassed THF (5 mL) and degassed H_2O (2.00 mL) were added. The reaction was heated at 55^{o}C for 18 h. The solvent was removed my rotary evaporation and product was extracted from the remaining solid from a mixture of methylene chloride (25.0 mL) and methanol (10.0 mL). The mixture was then filtered through Celite™ and the solvent from the filtrate was removed by rotary evaporation. The crude product was purified by flash column chromatography on silica gel (CH_2Cl_2:methanol = 95:5) to yield **3.3a** (97 mg, 26%) as a white powder. ^{1}H NMR (400 MHz, $CDCl_3$) δ 10.04, 7.9 (d, *J* = 8.4 Hz, 2H), 7.7 (t, *J* = 8 Hz, 2H), 7.60 (t, *J* = 8.4 Hz, 2H), 7.45 (t, *J* = 8.8 Hz, 2H), 6.40 (s, 1H), 4.73 (s, 1H), 3.28 (q, *J* = 5.6 Hz, 2H), 1.53 (p, *J* = 7.2 Hz, 2H), 1.39 (s, *J* = 8 Hz, 2H), 0.96 (t, *J* = 7.6 Hz, 3H). ^{13}C NMR (100 MHz, $CDCl_3$) δ 192.1, 155.7, 146.6, 139.5, 135.3, 130.5, 128.3, 127.3, 120.7, 40.4, 32.3, 20.2, 13.9. HRMS (ESI) *m/z*: calcd for $C_{18}H_{20}N_2O_2$ ($M+H^+$); 297.1603; found at 297.1603.

3.3b: ***N-octyl-N'(4'-formyl[1,1'-biphenyl]-4-yl])-urea***

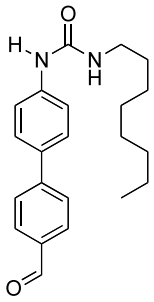

To a 50 mL round-bottom flask equipped with a stir bar and reflux condenser was added **3.2b** (708 mg, 1.89 mmol), 4-formyl phenyl boronic acid (425 mg, 2.84 mmol), *bis*(triphenylphosphine)palladium(II) dichloride (132 mg 0.189 mmol) and K_2CO_3 (1.57 g, 11.3 mmol). The mixture was placed under nitrogen and degassed THF (5.00 mL) and degassed H_2O (2.00 mL) were added. The reaction was heated at 55^oC for 18 h. The solvent was removed my rotary evaporation and product was extracted from the remaining solid from a mixture of methylene chloride (25.0 mL) and methanol (10.0 mL). The mixture was then filtered through Celite™ and the solvent from the filtrate was removed by rotary evaporation. The crude product was purified by flash column chromatography on silica gel (CH_2Cl_2:methanol = 95:5) to yield **3.3b** (145 mg, 23%) as a white powder. ^{1}H NMR (300 MHz, $CDCl_3$) δ 10.0 (s, 1H), 8.0 (d, *J* = 9.0 Hz, 2H), 7.73 (d, *J* = 6.9 Hz, 2H), 7.61 (d, *J* = 8.7 Hz, 2H), 7.5 (d, *J* = 8.7 Hz, 2H), 6.35 (s, 1H), 4.70 (br s, 1H), 3.28 (t, *J* = 6.9 Hz, 2H), 1.27 (m, 12H), 0.88 (t, *J* = 6.9 Hz, 3H). ^{13}C NMR (100 MHz, $CDCl_3$) δ 192.1, 155.7, 146.6, 139.6, 130.5, 128.2, 127.3, 120.6, 40.7, 32.0, 30.3, 29.5, 27.1, 22.8, 14.2. HRMS (ESI) *m/z*: calcd for $C_{22}H_{28}N_2O_2$ (M-H$^-$) 351.2089; found at 351.2078.

3.3c: ***N-phenyl-N'(4'-formyl[1,1'-biphenyl]-4-yl])-urea***

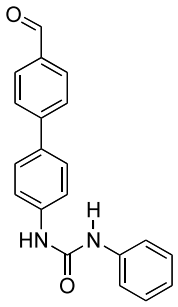

To a 50 mL round-bottom flask equipped with a stir bar and reflux condenser was added **3.3c** (600 mg, 1.80 mmol), 4-formyl phenyl boronic acid (400 mg, 2.60 mmol), *bis*(triphenylphosphine)palladium(II) dichloride (124 mg 0.18 mmol) and Cs_2CO_3 (3.40 g, 10.7 mmol). The mixture was placed under nitrogen and degassed THF (6.00 mL) and degassed H_2O (2.00 mL) were added. The reaction was heated at 55^oC for 18 h. The solvent was removed by rotary evaporation and product was extracted from the remaining solid from a mixture of methylene chloride (25.0 mL) and methanol (10.0 mL). The mixture was then filtered through Celite™and the solvent from the filtrate was removed my rotary evaporation. The crude product was recrystalized with methylene chloride (twice) to yield **3.3c** (145 mg, 26% yield) as an off white powder. ^1H NMR (400 MHz, $CDCl_3$) δ 10.05 (s, 1H), 7.95 (d, *J* = 8.4 Hz, 2H), 7.74 (d, *J* = 8.26 Hz, 2H), 7.63 (d, *J* = 8.6 Hz, 2H), 7.51 (d, *J* = 8.68 Hz, 2H), 7.39 (7.388, *J* = 3.9 Hz, 4H), 7.18 (t, *J* = 3.9 Hz, 1H), 6.68 (s, 1H), 6.55 (s, 1H). ^{13}C NMR (125 MHz, DMSO-d_6) δ 193.0, 152.7, 145.8, 140.6, 139.7, 140.6, 139.7, 134.7, 132.1, 130.5, 129.1, 127.8, 126.8, 122.4, 122.4, 118.8, 118.6. HRMS (ESI) *m/z*: calcd for $C_{20}H_{16}N_2O_2$ (M+H-) 316.1206; found at 316.1205.

3.3d: ***N-octyldodecyl-N'(4'-formyl[1,1'-biphenyl]-4-yl])-urea***

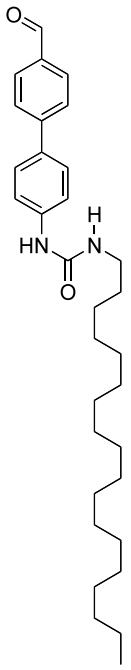

To a 50 mL round-bottom flask equipped with a stir bar and reflux condenser was added **3.2d** (300 mg, 0.58 mmol), 4-formyl phenyl boronic acid (131 mg, 0.87 mmol), *bis*(triphenylphosphine)palladium(II) dichloride (41 mg 0.06 mmol) and K_2CO_3 (480 mg, 3.48 mmol). The mixture was placed under nitrogen and degassed THF (5.0 mL) and degassed H_2O (2.0 mL) were added. The reaction was heated at 55^{o}C for 18 h. The solvent was removed my rotary evaporation and product was extracted from the remaining solid from a mixture of methylene chloride (25.0 mL) and methanol (10.0 mL). The mixture was then filtered through Celite™ and the solvent from the filtrate was removed by rotary evaporation. The crude product was purified by flash column chromatography on silica gel (CH_2Cl_2:methanol = 95:5) to yield **3.3d** (60 mg, 10%) as a white powder. ^{1}H NMR (400 MHz, $CDCl_3$) δ 10.05 (s, 1H), 7.95 (d, *J* = 7.5 Hz, 2H), 7.74 (d, *J* = 7.8 Hz, 2H), 7.62 (d, *J* = 3 Hz, 2H), 7.59 (d, *J* = 3.6 Hz, 2H), 7.46 (d, *J* = 8.4 Hz, 2H), 7.12 (d, *J* = 8.1 Hz, 2H), 6.35 (s, 1H), 6.22 (s, 1H), 4.70 (s, 1H), 4.62 (s, 1H), 3.28 (sx, *J* = 6.6 Hz, 2H), 3.16 (t, *J* = 6.6 Hz, 2H), 1.55 (s, 2H), 1.26 (s, 28H), 0.89 (t, *J* = 6.3 Hz, 2H). ^{13}C NMR (100 MHz, $CDCl_3$) δ 192.0, 146.6, 139.2, 138.3, 135.1, 130.5, 128.4, 127.3, 122.6, 121.0, 40.8, 32.1, 30.2, 29.9, 29.8, 29.7, 29.5, 29.5, 27.1, 22.9, 14.3. HRMS (ESI) *m/z*: calcd for $C_{32}H_{48}N_2O_2$ ($M+Na^+$) 515.3608; found at 515.3628.

3.4a: ***Schiff's base of N-butyl-N'-biphenyl-urea TREN***

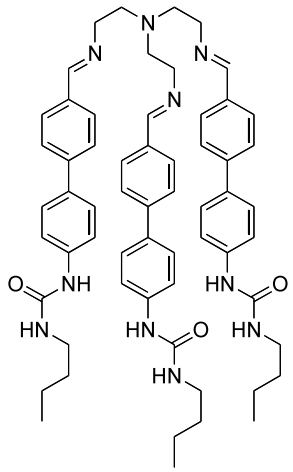

To a 100 round-bottom flask equipped with a stir bar and a Dean-Stark apparatus was added **3.3a** (200 mg, 0.67 mmol) and *tris*(2-aminoethyl)amine (33 mg, 0.22 mmol). The mixture was placed under nitrogen and anhydrous toluene was added. The reaction was heated at 175°C for 15 h. The solvent was removed by rotary evaporation to yield **3.4a** (214 mg, 99%) as a yellow powder. ^{1}H NMR (300 MHz, DMSO-d_6) δ 8.54 (s, 3H), 8.20 (s, 3H), 7.62 (s, 12H), 7.58 (d, J = 8.7 Hz, 6H), 7.50 (d, J = 8.7 Hz, 6H), 6.16 (t, J = 4.2 Hz, 6H), 3.64 (t, J = 5.1Hz, 6H) 2.86 (t, J = 5.1 Hz, 6H), 1.42 (p, J = 3.9 Hz, 6H), 1.31 (p, J = 5.7 Hz, 6H), 0.90 (t, J = 5.4 Hz, 9H). ^{13}C NMR (125 MHz, DMSO-d_6) 141.7, 140.7, 131.6, 128.3, 126.9, 125.9, 59.4, 55.2, 31.9, 19.5, 13.7. HRMS (ESI) *m/z*: calcd for $C_{72}H_{106}N_{11}O_3$ ($M+NH_4^+[-H]$) 983.5292; found at 983.5858.

3.4a•Cu•PF_6: ***Imine of N-butyl-N'-biphenyl-urea TREN•Cu•PF_6***

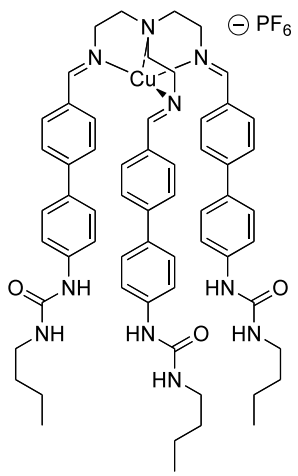

To a 25 mL round-bottom flask equipped with a stir bar was added $Cu(CH_3CN)_4PF_6$ (8.30 mg, 0.022 mmol) and **3.4a** (20 mg, 0.02 mmol). The mixture was placed under nitrogen and anhydrous methanol (2.00 mL) was syringed in through a Teflon® septum. The reaction was heated at 50°C for 5 h. The product was filtered to yield **3.4a•Cu•PF_6** (20.2 mg, 85%) as a yellow solid. ^{1}H NMR (400 MHz, DMSO-d_6) δ 8.70 (s, 3H), 8.57 (s, 3H), 8.16 (d, J = 8.4 Hz, 6H), 7.23 (d, J = 6.4 Hz, 12H), 7.11 (d, J = 8.4 Hz, 6H), 6.13 (t, J = 5.6 Hz, 6H), 3.92 (s, 6H), 3.17 (s, 6H), 3.17 (q, J = 6 Hz, 6H), 1.44 (p, J = 5.2 Hz, 6H), 1.33 (p, J = 8.0 Hz, 6H), 0.90 (t, J = 7.2 Hz, 9H). ^{13}C NMR (125 MHz, DMSO-d_6) 164.6, 161.9, 154.7, 143.0, 140.6, 133.3, 131.9, 130.5, 129.4, 128.8, 126.3, 125.4, 117.8, 58.9, 51.4. HRMS (ESI) *m/z*: calcd for $CuC_{60}H_{72}N_{10}O_3$ ($M+H^+$) 11043.5079; found at 1043.5089.

3.4a•Cu•B(Ph)$_4$: ***Imine of N-butyl-N'-biphenyl-urea TREN•C•B(Ph)$_4$***

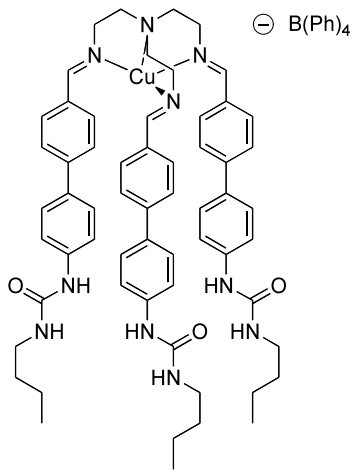

To a 5 mL round-bottom flask equipped with a stir bar was added $Cu(CH_3CN)_4PF_6$ (21.0 mg, 0.05 mmol) and **3.4a** (50 mg, 0.05 mmol). The mixture was placed under nitrogen and anhydrous methanol (2.00 mL) was syringed in through a Teflon® septum. The reaction was heated at 50^{o}C for 5 h. Sodium tetraphenylborohydride (26 mg, 0.08 mmol) was added and the reaction was let to go at room temperature for 15 h. The product was filtered to yield **3.4a•Cu•B(Ph)$_4$** (26 mg, 66%) as a yellow solid. ^{1}H NMR (400 MHz, acetonitrile-d_3) δ 8.53 (s, 3H), 8.00 (d, J = 8 Hz, 6H), 7.47 (s, 3H), 7.13 (d, J = 8 Hz, 6H), 7.13 (d, J = 8.4Hz, 6H), 7.03 (m, 12H), 5.46 (s, 3H), 3.93 (s, 6H), 3.19 (m, 12H), 1.53 (p, J = 7.2 Hz, 6H), 1.41 (p, J = 7.6 Hz, 6H), 0.99 (t, J = 7.2 Hz, 9H). ^{13}C NMR (125 MHz, acetonitrile-d_3): 163.3, 156.8, 144.3, 140.8, 133.5, 132.9, 130.0, 127.9, 127.9, 127.1, 120.6, 59.8, 53.0, 40.4, 32.5, 20.7, 14.2. HRMS (ESI) *m/z*: calcd for $CuC_{60}H_{72}N_{10}O_3$ ($M+H^+$) 11043.5079; found at 1043.5098.

3.5a: ***N-butyl-N'-biphenyl-urea TREN***

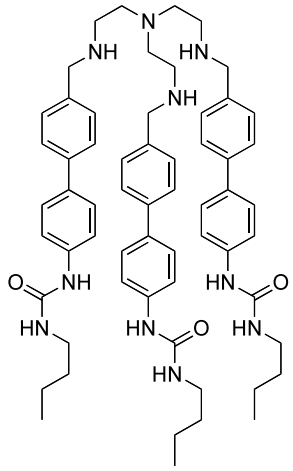

To a 50 mL round-bottom flask equipped with a stir bar, **3.4a** (100 mg, 0.1 mmol) and anhydrous methanol, $NaBH_4$ (57 mg, 1.5 mmol) was added in portions at 0°C and then was let to stir at room temperature for 3 h. The solvent was removed by rotary evaporation and the crude product was then dissolved in 5.00 mL of H_2O and 10.0 mL of CH_2Cl_2. The solution was then transferred to an extraction funnel, and the product was extracted with two additional 10.0 mL portions of CH_2Cl_2. The organic layers were combined and dried with $MgSO_4$ for 30 min, $MgSO_4$ was then filtered, the filtrate was evaporated via rotary evaporation to yield **3.5a** (64 mg, 61% yield.) ^{1}H NMR (300 MHz, $CDCl_3$) δ 7.59 (d, *J* = 8.3 Hz, 6H), 7.56 (d, *J* = 9.1 Hz, 6H), 7.48 (d, *J* = 8.8 Hz, 6H), 7.40 (d, *J* = 8.1 Hz, 6H), 7.18 (s, 3H), 5.20 (s, 3H), 4.56 (s, 6H), 3.17 (q, *J* = 5.7 Hz, 6H), 1.48 (p, *J* = 7.1 Hz, 6H), 1.37 (p, *J* = 7.1 Hz, 6H), 0.92 (t, *J* = 11 Hz, 9H). ^{13}C NMR (125 MHz, acetonitrile-d_3) δ 156.7, 141.9, 141.0, 140.5, 135.2, 128.5, 128.3, 127.5, 119.9, 64.5, 33.1, 20.7, 14.0. GCMS (EI) *m/z*: calcd for $C_{72}H_{106}N_{11}O_3$ ($M+NH_4^+[-H]$) 986.6253; found at 986.6280.

3.4b: ***Imine of N-octyl-N'-biphenyl-urea TREN***

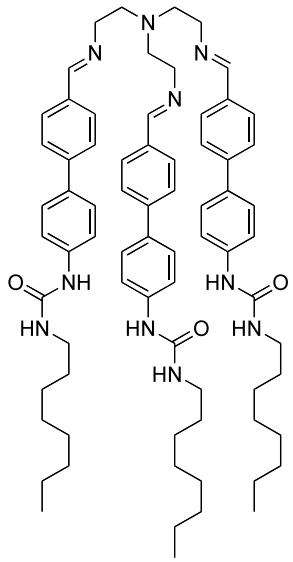

To a 100 mL round-bottom flask equipped with a stir bar and a 20 mL Dean-Stark apparatus was added *tris*(2-aminoethyl)amine (27 mg, 0.19 mmol and **3.4b** (200 mg, 0.57 mmol). The mixture was placed under nitrogen and anhydrous toluene (30.0 mL) was added. The reaction was heated at 145°C for 8 h. The solvent was removed by rotary evaporation to yield **3.4b** (216 mg, 99%) as a yellow powder. ^{1}H NMR (300 MHz, DMSO-d_6) δ 8.53 (s, 3H), 8.34 (s, 3H), 7.77 (d, J = 7.7 Hz, 6H), 7.70 (d, J = 7.8 Hz, 6H), 7.60 (d, J = 8.3 Hz, 6H), 7.49 (d, J = 8.1 Hz, 6H), 6.15 (s, 3H), 1.61 (s, 6H), 1.43 (s, 6H), 1.27 (s, 12H), 0.86 (t, J=2.7 Hz, 9H). ^{13}C NMR (125 MHz, DMSO-d_6) δ 155.1, 134.4, 131.7, 131.0, 130.2, 128.4, 127.5, 127.0, 126.4, 126.1, 117.9, 60.6, 31.3, 28.8, 26.7, 22.1, 14.1. HRMS (ESI) *m/z*: calcd for $C_{72}H_{96}N_{10}O_3$ ($M+H^-$) 1149.7740; found at 1149.7794.

3.4c: ***Imine of N-phenyl-N'-biphenyl-urea TREN***

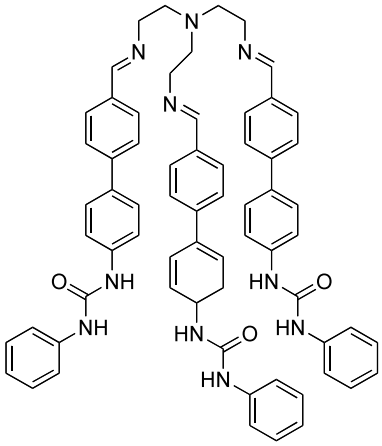

To a 50 mL round-bottom flask equipped with a stir bar and a 20 mL Dean-Stark apparatus was added *tris*(2-aminoethyl)amine (24 mg, 0.16 mmol) and **3.3c** (155 mg, 0.49 mmol). The mixture was placed under nitrogen and anhydrous toluene (20.0 mL) was added. The reaction was heated at 145°C for 8 h. The solvent was removed by rotary evaporation to yield **3.4c** (170 mg, 99%) as a yellow powder. ^{1}H NMR (300 MHz, DMSO-d_6) δ 8.90 (s, 3H), 8.77 (s, 3H), 8.23 (s, 6H), 7.66 (m, J = 8.7 Hz, 18H), 7.60 (d, J = 8.7 Hz, 6H), 7.50 (d, J = 7.7 Hz, 6H), 7.29 (t, J = 7.9 Hz, 6H), 7.00 (t, J = 7.3 Hz, 3H), 3.70 (t, J = 5.7 Hz, 6H), 2.89 (t, J = 5.0 Hz, 6H). ^{13}C NMR (125 MHz, DMSO-d_6) δ 161.0, 152.6, 141.8, 139.9, 139.8, 134.8, 132.7, 128.9, 128.508, 127.2, 126.3, 122.0, 118.7, 118.7, 118.4, 59.6, 55.4. HRMS (ESI) *m/z*: calcd for $C_{66}H_{61}N_{10}O_3$ ($M+H^-$) 1041.4923; found at 1041.4970.

3.4c•Cu•PF_6: ***Imine of N-phenyl-N'-biphenyl-urea TREN•Cu•PF_6***

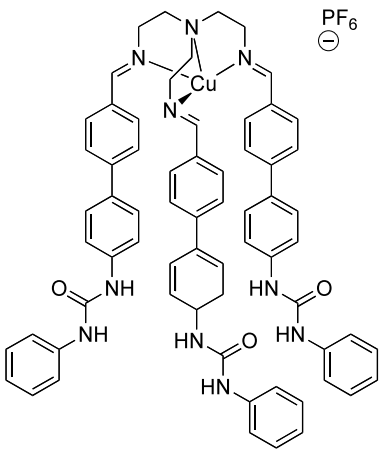

To a 25 mL round-bottom flask equipped with a stir bar was added $Cu(CH_3CN)_4PF_6$ (36 mg, 0.11 mmol) and **3.4c** (100 mg, 0.10 mmol). The mixture was placed under nitrogen and anhydrous methanol (2.00 mL) was syringed in through a Teflon® septum. The reaction was heated at 50°C for 8 h. The product was filtered to yield **3.4c•Cu•PF_6** (83.3 mg, 70%) as a yellow-green solid. ^{1}H NMR (400 MHz, DMSO-*d_6*) δ 8.75 (s, 3H), 8.73 (s, 6H), 8.63 (s, 3H), 8.17 (d, *J* = 7.4 Hz), 7.43 (d, *J* = 7.7 Hz, 6H), 7.32 (m, *J* = 10.2 Hz, 12H), 7.21 (t, *J* = 7.2 Hz, 6H), 7.13 (d, *J* = 7.4 Hz, 6H), 6.93 (t, *J* = 7.2 Hz, 3H), 3.94 (s, 6H), 3.18 (s, 6H). ^{13}C NMR (125 MHz, DMSO-*d_6*) δ 162.2, 152.4, 143.1, 140.2, 139.7, 132.4, 131.7, 129.2, 128.9, 126.9, 125.9, 121.995, 118.5, 118.4, 59.2, 52.2. HRMS (ESI) *m/z*: calcd for $CuC_{66}H_{60}N_{10}O_3$ (M+H)+[-H] 1103.4140; found at 1103.4181.

3.4c•Cu•B(Ph)$_4$: ***Imine of N-phenyl-N'-biphenyl-urea TREN•Cu•B(Ph)$_4$***

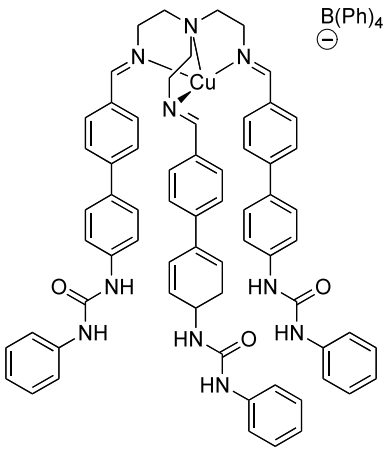

To a 25 mL round-bottom flask equipped with a stir bar was added $Cu(CH_3CN)_4PF_6$ (36 mg, 0.11 mmol) and **3.4c** (100 mg, 0.10 mmol). The mixture was placed under nitrogen and anhydrous methanol (2 mL) was syringed in through a Teflon® septum. The reaction was heated at 50^{o}C for 5 h. Sodium tetraphenylborohydride (49 mg, 0.14 mmol) was added and the reaction was let to go at room temperature for 15 h. The product was filtered to yield **3.4c•Cu•B(Ph)$_4$** (63.5 mg, 46%) as a yellow solid. ^{1}H NMR (400 MHz, DMSO-*d$_6$*) δ 8.52 (s, 6H), 7.93 (d, *J* = 8 Hz, 6H), 7.76 (s, 3H), 7.35 (s, 3H), 7.20 (d, *J* = 7.6 Hz, 6H), 7.13 (m, 18H), 7.00 (d, *J* = 8 Hz, 6 H), 6.93 (t, *J* = 7.2 Hz, 3H), 3.93 (s, 6 H), 3.18 (s, 6H). ^{13}C NMR (125 MHz, DMSO-*d$_6$*) δ 154.6, 145.4, 144.3, 143.4, 142.2, 141.3, 140.1, 134.3, 131.4, 131.0, 130.9, 130.9, 130.4, 130.3, 130.2, 129.2, 129.1, 128.8, 128.4, 128.3, 127.6, 124.2, 121.8, 121.6, 120.9, 120.6, 120.5, 116.7, 114.7, 61.2, 56.7, 53.3, 50.4. HRMS (ESI) *m/z*: calcd for $CuC_{66}H_{60}N_{10}O_3$ ($M+H^+$) 1103.4140; found at 1103.4170.

3.4c•Cu•BF_4: ***Imine of N-phenyl-N'-biphenyl-urea TREN•Cu•BF_4***

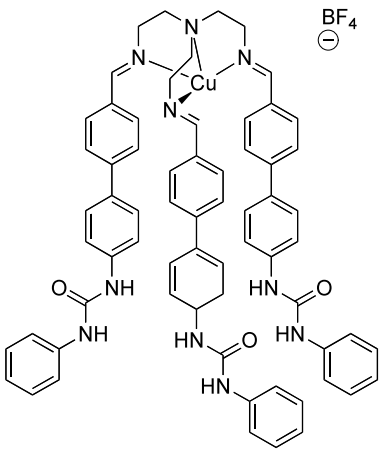

To a 25 mL round-bottom flask equipped with a stir bar was added $Cu(CH_3CN)_4PF_6$ (16.6 mg, 0.053 mmol) and **3.4c** (50 mg, 0.05 mmol). The mixture was placed under nitrogen and anhydrous methanol (2.00 mL) was syringed in through a Teflon® septum. The reaction was heated at 50°C for 5 h. The product was filtered to yield **3.4c•Cu•BF_4** (42.3 mg, 79%) as a yellow solid. ^{1}H NMR (400 MHz, 50:50 acetonitrile-d_3:$CDCl_3$) δ 8.72 (s, 6H), 8.61 (s, 3H), 8.17 (d, J = 7.2 Hz, 6H), 7.42 (d, J = 6.0 Hz, 6H), 7.32 (s, 12H), 7.22 (t, J = 4.4 Hz, 6H), 7.14 (d, J = 7.4 Hz, 6H), 6.93 (t, J = 2.9 Hz, 3H), 3.93 (s, 6H), 3.18 (s, 6H). ^{13}C NMR (125 MHz, DMSO-d_6) δ 162.0, 142.24, 142.9, 140.0, 139.5, 132.3, 131.5, 129.0, 128.8, 128.7, 126.7, 125.7, 121.8, 118.5, 118.3, 118.3, 118.2, 59.3, 51.6. HRMS (ESI) *m/z*: calcd for $CuC_{66}H_{60}N_{10}O_3$ ($M+H^+$) 1103.4140; found at 1103.4168.

3.4c•Ag•NO_3: ***Imine of N-phenyl-N'-biphenyl-urea TREN•Ag•NO_3***

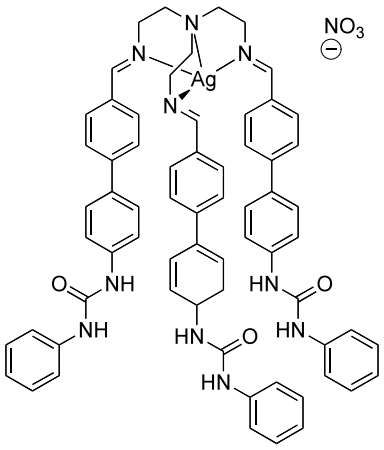

To a 25 mL round-bottom flask equipped with a stir bar was added $AgNO_3$ (9.00 mg, 0.05 mmol) and **3.4c** (50 mg, 0.05 mmol). The mixture was placed under nitrogen and anhydrous methanol (2.00 mL) was syringed in through a Teflon® septum. The reaction was heated at 50°C for 5 h. The product was filtered to yield **3.4•Ag•NO_3** (58 mg, 96%) as a gray solid. ^{1}H NMR (400 MHz, DMSO-d_6) δ 8.83 (s, 3H), 8.70 (s, 3H), 8.66 (s, 3H), 8.01 (d, J = 7.6 Hz, 12H), 7.69 (d, J = 10.4 Hz, 6H), 7.61 (d, J = 10.8 Hz, 6H), 7.54 (d, J = 10.8 Hz, 6H), 7.46 (d, J = 6.4 Hz, 6H), 7.25 (t, J = 6 Hz, 6H), 6.95 (d, J = 8.4 Hz, 6H), 3.85 (s, 6H), 3.03 (s, 6H). ^{13}C NMR (125 MHz, DMSO-d_6) δ 162.0, 142.2, 142.9, 140.0, 139.5, 132.3, 131.5, 129.0, 128.8, 128.7, 126.7, 125.7, 121.8, 118.5, 118.3, 118.3, 118.2, 59.3, 51.6. HRMS (ESI) *m/z*: calcd for $AgC_{66}H_{60}N_{10}O_3$ ($M+H^+$) 1147.3896; found at 1147.3873.

3.4c•Ag•(BPh)$_4$: ***Schiff's base of N-phenyl-N'-biphenyl-urea TREN•Ag•(BPh)$_4$***

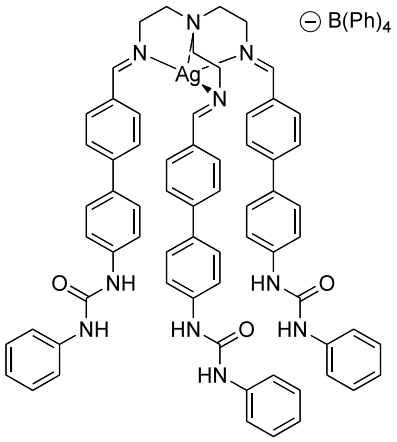

To a 25 mL round-bottom flask equipped with a stir bar was added $AgNO_3$ (9 mg, 0.05 mmol) and **3.4c** (50 mg, 0.05 mmol). The mixture was placed under nitrogen and anhydrous methanol (2.00 mL) was syringed in through a Teflon® septum. The reaction was heated at 50^{o}C for 5 h. Sodium tetraphenylborohydride (27.2 mg, 0.08 mmol) was added and the reaction was let to go at room temperature for 15 h. The product was filtered to yield **3.4c•Ag•(BPh)$_4$** (67 mg, 96%) as a yellow solid. HRMS (ESI) *m/z*: calcd for $AgC_{66}H_{60}N_{10}O_3$ ($M+H^+$) 1149.3924 found at 1149.3924.

Chapter 4 Characterization

p-rosaniline salen

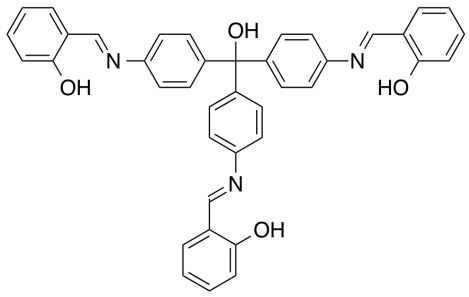

To a 25 mL round-bottom flask equipped with a stir bar containing a solution of salicylaldehyde (248 mg, 2 mmol) in 2 mL of ethanol, *p*-rosaniline base (200 mg, 0.66 mmol) was slowly added and was let to stir for 2 h at room temperature. The product was then filtered to yield a pink solid (92% yield, 408 mg.) ^{1}H NMR (400 MHz, $CDCl_3$) δ 13.17 (s, 3H), 8.63 (s, 3H), 7.39 (d, *J* = 8.0 Hz, 6H), 7.26 (d, *J* = 7.2 Hz, 6H), 7.02 (d, *J* = 8.0 Hz, 3H), 6.93 (t, *J* = 8.0 Hz, 3H), 2.90 (s, 1H). ^{13}C NMR (100 MHz, $CDCl_3$) δ 163.7, 163.5, 146.9, 146.4, 132.7, 129.0, 120.9, 119.5, 119.3, 116.8, 116.7, 113.1, 80.3.

4.1_2•Cu_3•$(PF_6)_3$: ***M_3L_2 p-rosaniline-Cu(I) trigonal bipyramide cage***

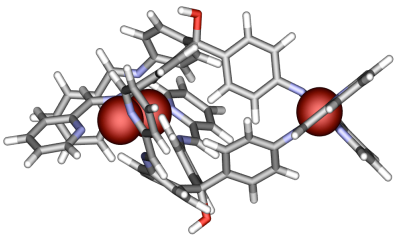

To a 25 mL round-bottom flask equipped wit ha stir bar containing a solution of 2-formyl pyridine (210 mg, 1.95 mmol) in 2.00 mL of anhydrous acetonitrile was added *p*-rosaniline base (200 mg, 0.65 mmol) and $Cu(CH_3CN)_4PF_6$ (363 mg, 0.98 mmol). The reaction was let to stir at 55^{o}C for 15 h. The product was then filtered and washed with diethyl ether to yield **4.1_2•Cu_3•$(PF_6)_3$** (547 mg, 95%) a dark red solid. ^{1}H NMR (400 MHz, acetonitrile-d_3) δ 9.89 (br s, 6H), 9.41 (br s, 6H), 8.96 (br s, 6H), 8.87 (br s, 6H), 8.53 (br s, 6H), 8.21 (br s, 6H), 8.06 (br s, 6H),

5.40 (br s, 2). ^{13}C NMR (100 MHz, acetonitrile-d_3) δ 163.9, 162.2, 159.8, 152.43, 150.4, 139.8, 129.6, 123.2 and 40.6. HRMS (ESI) *m/z*: calcd for $C_{74}H_{56}N_{12}O_2F_{12}P_2Cu_3$ [PF6+]2 1623.1815; found at 1625.1852.

4.1$_4$•Fe$_4$•(ClO$_4$)$_6$: ***M$_4$L$_4$ p-rosaniline-Fe(II) tetrahedron cage***

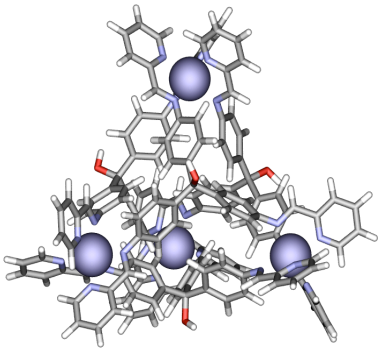

To a… The reaction was let to stir at 55°C for 15 h. The product was then filtered and washed with diethyl ether to yield **4.1$_4$•Fe$_4$•(ClO$_4$)$_6$** (305 mg, 63%) a dark red solid. ^{1}H NMR (400 MHz, acetonitrile-d_3) δ 8.70 (s, *J* = 8.7 Hz, 12H), 8.40 (d, *J* = 6.4 Hz, 12H), 8.35 (t, *J* = 6.8 Hz, 12H), 7.72 (d, *J* = 7.2 Hz, 12H), 7.32 (d, *J* = 5.6 Hz, 24H), 6.64 (br s, 12H), 5.76 (br s, 6H), 5.14 (s, 4H). ^{13}C NMR (100 MHz, acetonitrile-d_3) δ 117.3, 159.2, 156.869, 150.9, 147.6, 141.0, 132.4, 130.7, 81.9. HRMS (ESI) *m/z*: calcd for $C_{146}H_{112}{}^{13}C_2N_{24}O_{28}{}^{35}Cl_5{}^{37}Cl_{56}Fe_4$(M-[$Cl0_4^{++}$]) 1555.1817; found at 1555.1786.

4.3: ***N^2-[4-nitrophenyl)methylene]-N^1,N^1-bis[2-[[(4-nitrophenyl)methylene]amino]ethyl]-1,2-ethanediamine***

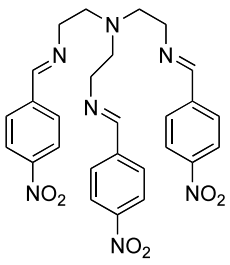

To a 100 mL round-bottom flask equipped with a stir bar and a Dean-Stark apparatus was added 4-formyl nitrobenzene (931 mg, 6.2 mmol) and *tris*(2-aminoethyl)amine (27 mg, 2.06 mmol). The mixture was placed under nitrogen and anhydrous toluene was added. The reaction was heated at 175°C for 15 h. The solvent was removed by rotary evaporation to yield **4.3** (1.14 g, 99%) as a yellow powder. ^{1}H NMR (500 MHz, DMSO-d_6) δ 8.35 (s,

3H), 8.19 (d, J = 8.65 Hz, 6H), 7.82 (d, J = 8.65 Hz, 6H), 3.70 (t, J = 6.0 Hz, 6H), 2.89 (t, J = 6.0 Hz, 6H). ^{13}C NMR (100 MHz, DMSO-d_6) δ 159.8, 148.3, 141.6, 128.7, 123.8, 59.140, 54.5. HRMS (ESI) *m/z*: calcd for $C_{27}H_{27}N_7O_6$ (M+[-H$^-$]) 544.1939; found at 544.1955.

4.4: ***Tris(2-((4-nitrophenyl)amino)ethyl)amine***

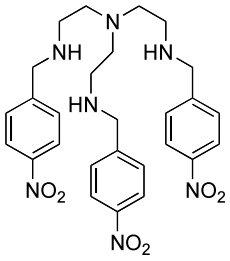

To a 50 mL round-bottom flask equipped with a stir bar, **4.3** (350 mg, 0.64 mmol) and anhydrous methanol, $NaBH_4$ (720 mg, 19.0 mmol) was added in portions at 0^{o}C and then was let to stir at room temperature for 5 h. The solvent was removed by rotary evaporation and the crude product was then dissolved in 10 mL of H_2O and 20.0 mL of CH_2Cl_2. The solution was then transferred to an extraction funnel, and the product was extracted with two additional 10.0 mL portions of CH_2Cl_2. The organic layers were combined and dried with $MgSO_4$ for 30 min, $MgSO_4$ was then filtered, the filtrate was evaporated via rotary evaporation to yield (248 mg, 70%). ^{1}H NMR (400 MHz, $CDCl_3$) δ 8.06 (d, J = 7.96 Hz, 6H), 7.94 (d, J = 8.3 Hz, 6H), 3.84 (s, H), 2.67 (t, J = 5.2 Hz, 6H), 2.60 (t, J = 5.2 Hz, 6H) ^{13}C NMR (100 MHz, $CDCl_3$) δ 148.3, 146.9, 128.5, 123.5, 54.0, 53.2, 47.1. HRMS (ESI) *m/z*: calcd for $C_{27}H_{33}N_7O_6$ (M+H$^+$) 550.2409; found at 552.2558.

4.5: ***Tris(2-((4-aminophenyl)amino)ethyl)amine***

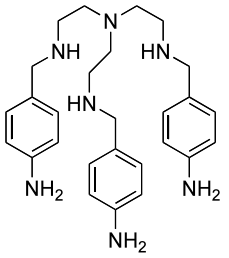

To a 100 mL round bottom flask equipped with a stir bar was added **4.4** (400 mg, 0.73 mmol) and 3 mL of ethanol, followed by a solution of $SnCl_2 \bullet 2H_2O$ (2.46 g (11 mmol) in 12.1 M HCl (4.00 mL). The reaction mixture was placed under nitrogen and was let to stir at 73°C for 18 h. The organic solvent was removed via rotary evaporation, and water (10.0 mL) was added to the residue. Solid KOH was added until the mixture was strongly basic. Product from the mixture was extracted with CH_2Cl_2 (3 x 20 mL), the combined organic layers were dried with $MgSO_4$ for 15 minutes, the $MgSO_4$ was filtered off, and the filtrate was concentrated via rotary evaporation to yield **4.5** (268 mg, 79%) as a tan oil. ^{1}H NMR (400 MHz, $CDCl_3$) δ 7.05 (d, J = 8.3 Hz, 6H), 6.60 (d, J = 8.4 Hz, 6H), 3.61 (s, 6H), 2.64 (t, J = 2.6 Hz, 6H), 2.55 (t, J = 2.6 Hz, 6H). ^{13}C NMR (100 MHz, $CDCl_3$) δ 145.6, 130.4, 129.6, 115.4, 54.5, 53.7, 47.2. HRMS (ESI) *m/z*: calcd for $C_{27}H_{39}N_7$ ($M+H^+$) 462.3350; found at 462.3340.

4.5•Fe•SO_4

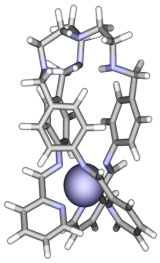

To a 25 mL round-bottom flask equipped with a stir bar containing a solution of 2-formyl pyridine (19 mg, 0.18 mmol) in 2.00 mL of anhydrous acetonitrile was added **4.5** (25 mg, 0.06 mmol) and $FeSO_4$•$7H_2O$ (22 mg, 0.06 mmol). The reaction was let to stir at 55°C for 15 h. The product was then filtered and washed with diethyl ether (10.00 mL) to yield a deep purple product (63 mg, 40%.) ^{1}H NMR (400 MHz, H_2O-d_2) δ 8.10 (s, 3H), 7.75 (s), 2.88 (br s, 6H), 6.88 (br s, 6H), 4.10 (s, 6H), 3.05 (s, 6H), 2.78 (s, 6H).

4.5_4•Fe_4•$(SO_4)_4$⊂ Cyclopentane

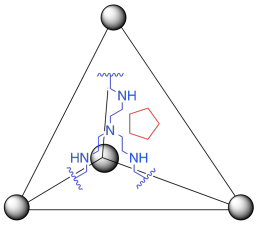

To a 25 mL round-bottom flask equipped with a stir bar containing a solution of 2-formyl pyridine (19 mg, 0.18 mmol) in 2.00 mL of water was added 100 μL of cyclopentane, **4.5** (25 mg, 0.06 mmol) and $FeSO_4$•$7H_2O$ (22 mg, 0.06 mmol). The reaction was let to stir at 55°C for 15 h. The product was then filtered and washed with diethyl ether to yield a deep purple product. ^{1}H NMR (400 MHz, H_2O-d_2) δ 8.99-7.25 (m) 7.35 (s, 24 H), 6.90 (s, 24 H), 4.12 (s, 24 H), 3,12 (s, 24 H), 2.80 (s, 24 H), 0.73 (s, 12 H).

4.5•Fe• SO_4•Cu•PF_6

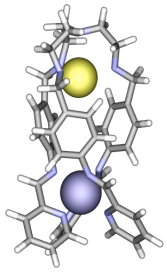

To a 25 mL round-bottom flask equipped with a stir bar was added **4.5** (25 mg, 0.06 mmol), $Cu(CH_3CN)_4PF_6$ (22 mg, 0.06 mmol), and anhydrous acetonitrile. The reaction was let to stir at 55°C under nitrogen for 2 h. Afterwards, 2-formyl pyridine (19 mg, 0.18 mmol) and $Fe(ClO_4)_2$•$6H_2O$ (22 mg, 0.06 mmol) was added and was let to stir at 55°C for 15 h. The product was then filtered and washed with diethyl ether to yield a deep purple product (60 mg, 84%.)

4.5•Fe_2•$(SO_4)_2$

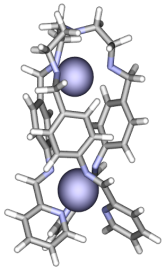

To a 25 mL round-bottom flask equipped with a stir bar was added **4.5** (25 mg, 0.06 mmol), $Fe(ClO_4)_2$•$6H_2O$ (22.0 mg, 0.06 mmol), and anhydrous acetonitrile. The reaction was let to stir at 55°C under nitrogen for 2 h. Afterwards, 2-formyl pyridine (19.0 mg, 0.18 mmol) and $Fe(ClO_4)_2$•$6H_2O$ (22 mg, 0.6 mmol) was added and was let to stir at 55°C for 15 h. The product was then filtered and washed with diethyl ether to yield a deep purple product. ^{1}H NMR (400 MHz, acetonitrile- d_3) δ 8.85 (s, 3H), 8.78 (s, 3H), 8.62 (s, 3H), 8.18 (s, H)), 7.83 (s, 3H), 7.38 (s, 6H), 7.00 (s, 6H), 3.15 (s, 6H), 2.85 (s, 6H).

4.5•Cu_5•$(PF_6)_5$

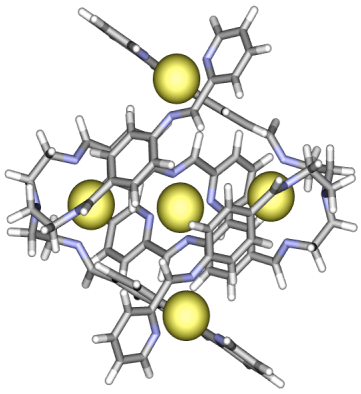

To a 25 mL round-bottom flask equipped with a stir bar was added **4.5** (25 mg, 0.06 mmol), $Cu(CH_3CN)_4PF_6$ (22 mg, 0.06 mmol), and anhydrous acetonitrile. The reaction was let to stir at 55°C under nitrogen for 2 h. Afterwards, 2-formyl pyridine (19 mg, 18 mmol) and $Cu(CH_3CN)_4PF_6$ (33 mg, 0.09 mmol) was added and was let to stir at 55°C for 15 h. The product was then filtered and washed with diethyl ether to yield a greenish brown product (93 mg, 62%).

Chapter 5 Characterization

5.3: *1,3-Bis(4-(pyridin-3-yl)phenyl)ethynyl)benzene*

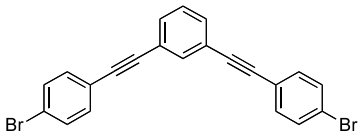

To an oven-dried, 50 mL round-bottom flask equipped with a magnetic stirrer was added 1,3-diethynylbenzene (300 mg, 0.24 mmol), 1-bromo-4-iodobenzene (1.37 g, 0.48 mmol), *bis*(triphenylphosphine)palladium(II) dichloride (168 mg), and CuI (23 mg). The mixture was placed under nitrogen and anhydrous diisopropylamine (20.0 mL) was added by syringe. The reaction was let to stir at room temperature for 30 h. The solvent was removed by rotary evaporation and the remaining solid was dissolved in methylene chloride (10.0 mL). The mixture was then filtered through Celite™, and the solvent from the filtrate was removed by rotary evaporation. Recrystallization from methylene chloride gave **5.3** (880 mg, 85%) as an off white powder. ^{1}H NMR (300 MHz, $CDCl_3$) δ 7.69 (br s, 1H), 7.51-7.45 (m, J = 8.67 Hz, 4H), 7.40 (d, J = 8.23 Hz, 4H), 7.34 (d, J = 7.68 Hz, 1H). ^{13}C NMR (400 MHz, $CDCl_3$) δ 135.3, 134.6, 133.2, 131.7, 131.6, 123.5, 122.8, 122.0, 89.6. GCMS (EI) *m/z*: calcd for $C_{22}H_{12}Br_2$ ($M+H^+$) 433.9300; found 433.9283.

5.5: ***1,3-bis(4-(pyridin-3-ylethynyl)phenyl)ethynyl)benzene***

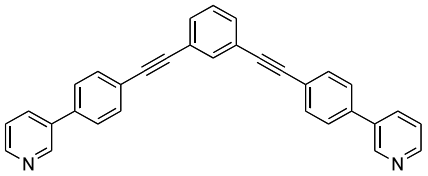

To an oven-dried, 25 mL round-bottom flask equipped with a magnetic stirrer was added **5.3** (100 mg, 0.23 mmol) and 3-pyridine boronic acid (59 mg, 0.48 mmol), *bis*(triphenylphosphine)palladium(II) dichloride (16 mg), and Cs_2CO_3 (450 mg, 1.4 mmol). The mixture was placed under nitrogen and degassed ethanol (4.00 mL) and anhydrous toluene (2.00 mL) were added by syringe. The reaction was stirred at 73°C for 24 h. The solvent was removed by rotary evaporation and the remaining solid was dissolved in methylene chloride (10.0 mL). The mixture was then filtered through Celite™, and the solvent from the filtrate was removed by rotary evaporation. The crude product was purified by flash column chromatography on silica gel (CH_2Cl_2:methanol = 100:1) to yield compound **5.5** (30 mg, 10%) as a light brown solid. ^{1}H NMR (400 MHz, DMSO-d_6): δ 8.97 (s, 2H), 8.61 (d, J = 3.8 Hz, 2H), 8.16 (d, J = 8.6 Hz, 2H), 7.85 (d, J = 8.4 Hz, 4H), 7.81 (s, 1H), 7.73 (d, J = 8.5 Hz, 4H), 7.65 (d, J = 7.4 Hz, 2H), 7.55-7.51 (m, J = 6.6 Hz, 3H). ^{13}C NMR (100 MHz, $CDCl_3$): δ 148.7; 148.1; 137.8; 134.8; 134.5; 132.5; 132.1; 131.6; 129.8; 128.7; 127.2; 123.6; 123.1; 89.9; 89.7. HRMS (ESI) *m/z*: calcd for $C_{32}H_{20}N_2$ ($M+H^+$) 432.1621; found at 432.1614.

5.5_4•Pd_2•$(NO_3)_4$: ***1,3-bis(4-(pyridin-3-ylethynyl)phenyl)ethynyl)benzene M_2L_4 Cage***

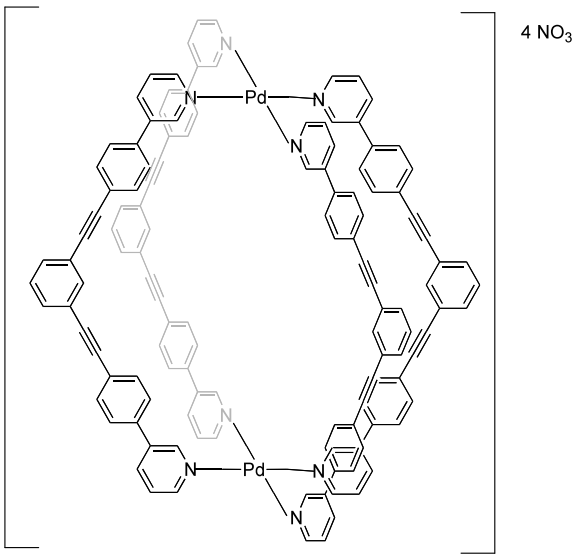

To a mixture of **5.5** (8 mg, 0.038 mmol) and $Pd(NO_3)_2XH_2O$ (4.4 mg, 0.0184 mmol) in DMSO (2.00 mL) was stirred at room temperature for 30 min, then precipitated by addition of acetone and hexane. The precipitate was washed with acetone (2.00 mL) to yield **5.5_4•Pd_2•$(NO_3)_4$** (10 mg, 93%) as a yellow solid. (^{1}H NMR (100 MHz, DMSO-d_6): δ 9.98 (s, 8H), 9.42 (d, J = 5.9 Hz, 8H), 8.48 (d, J = 8.3 Hz, 8H), 7.94 (d, J = 8.4 Hz, 16H), 7.88 (m, J = 6.9 Hz, 8H), 7.81 (d, J = 8.2 Hz, 18H), 7.74 (s, 4H), 7.62 (d, J = 1.1 Hz, 8H), 7.51 (t, J = 7.2 Hz, 4H). ^{13}C NMR (125 MHz, DMSO-d_6): δ 149.9, 148.6, 138.4, 137.6, 134.4, 133.8, 131.9, 129.6, 127.4, 127.3, 123.2, 122.6, 90.1, 89.5. HRMS (ESI) *m/z*: calcd for $C_{130}H_{81}N_8O_6F_6S_2{}^{106}Pd^{108}Pd$ ($M+H^+$) 1120.6844; found at 1120.6888.

5.8: ***1,3-bis((4-(pyridin-3-ylethynyl)phenyl)ethynyl)benzene***

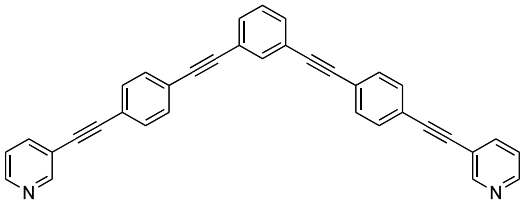

To an oven-dried, 25 mL round-bottom flask equipped with a magnetic stirrer was added 1.3 diethynyl benzene (40 mg, 0.32 mmol), 3-((4-bromophenyl)ethynyl)pyridine **5.3** (166 mg, 0.64 mmol), *bis*(triphenylphosphine)palladium(II) dichloride (2.2 mg), and CuI (3 mg). The mixture was placed under nitrogen and anhydrous diisopropylamine (3.00 mL) were added by syringe. The reaction was stirred at room temperature for 24 h. The solvent was removed by rotary evaporation and the remaining solid was dissolved in methylene chloride (10.0 mL). The mixture was then filtered through Celite™, and the solvent from the filtrate was removed by rotary evaporation to yield **5.8** (42 mg, 27%) as a yellow solid. ^{1}H NMR (400 MHz, $CDCl_3$): δ 8.78 (s, 2H), 8.58 (d, J = 4.8 Hz, 2H), 7.83 (d, J = 7.9 Hz, 2H), 7.72 (s, 1H), 7.53 (s, 8H), 7.51 (d, J = 7.8 Hz, 2H), 7.382 (t, J = 7.1 Hz, 1H), 7.32 (m, J = 7.8 Hz, 2H). LIFDI-MS *m/z*: calcd for $C_{36}H_{20}N_2$ ($M+H^+$) found at 480.

5.8_4•Pd_2•$(NO_3)_4$: ***1,3-bis((4-(pyridin-3-ylethynyl)phenyl)ethynyl)benzene M_2L_4 Cage***

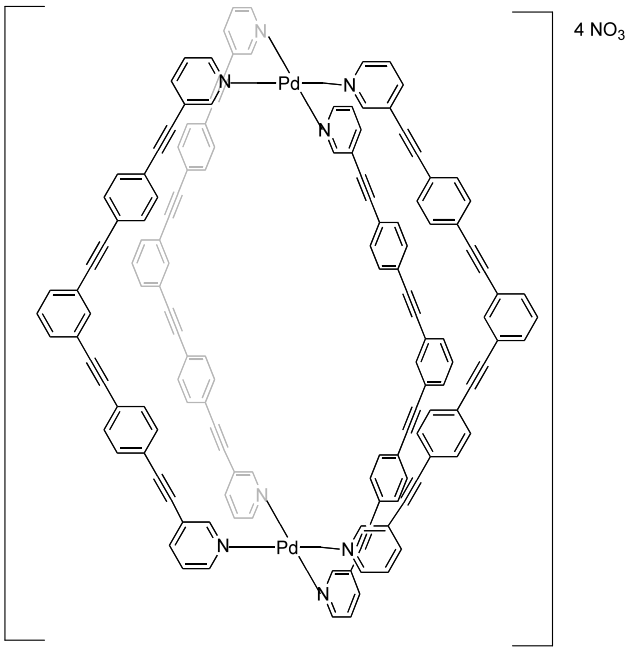

To a mixture of **5.8** (8 mg, 0.0017 mmol) and $Pd(NO_3)_2XH_2O$ (2.0 mg, 0.000083 mmol) in DMSO (2.00 mL) was stirred at room temperature for 30 min, then precipitated by addition of acetone and hexane. The precipitate was washed with acetone (2.00 mL) to yield **5.8_4•Pd_2•$(NO_3)_4$** (8 mg, 83%) as a yellow solid. ^{1}H NMR (400 MHz, DMSO-d_6): δ 9.60 (s, 8H), 9.29 (d, J = 8.52, 8H), 7.82-7.43 (m, 60H).

5.18: ***1,3-Bis[(4-aminophenyl)ethynyl]benzene***

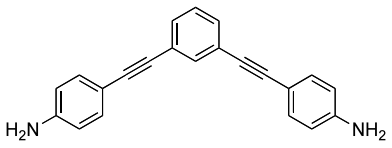

To a 2-neck 25 mL round-bottom flask equipped with a stir bar and reflux condenser was added 1,3 diiodobenzene(100 mg, 30.3 mmol), 4-ethynyl aniline (75 mg, 63.7 mmol), $Pd(PPh_3)_2Cl_2$ (21 mg 0.30 mmol) and CuI (2.5 mg 1.3 mmol). The mixture was placed under nitrogen and anhydrous diisopropylamine (5.00 mL) was added. The reaction was let to stir at room temperature for 40 h. The solvent was removed by rotary evaporation and the remaining solid was dissolved in a mixture of methylene chloride and methanol. The mixture was then filtered through Celite™, and the solvent from the filtrate was removed my rotary evaporation. The product was recrystalized with methylene chloride twice to yield **5.18** as a red-brown powder (32.5 mg, 34%). Collection of fractions and evaporation of solvent *in vacuo* gave product as a dull yellow solid (35 mg, 34%). ^{1}H NMR (400 MHz; $CDCl_3$) δ 7.63 (s, 1H), 7.39 (dd, J = 7.5, 1.1 Hz, 2H), 7.33 (d, J = 8.6 Hz, 4H), 7.28 (d, J = 7.5 Hz, 1H), 6.64 (d, J = 8.6 Hz, 4H), 3.82 (br, 4H). ^{13}C NMR (100 MHz, $CDCl_3$) δ 146.9, 134.2, 133.2, 130.6, 128.4, 124.3, 114.9, 90.7, 86.9. HRMS (ESI) m/z calcd for $C_{22}H_{16}N_2$ ($[M+H]^+$) 309.1386, found 309.1389.

5.19: ***2,6-Bis[(4-aminophenyl)ethynyl]4-nitroaniline***

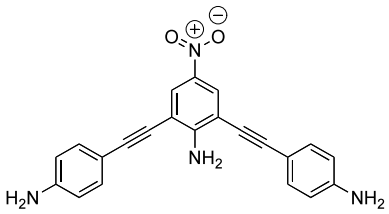

To a 2-neck 25 mL round-bottom flask equipped with a stir bar and reflux condenser was added 2,6-diiodo 4-nitro aniline (100 mg, 25 mmol), 4-ethynyl aniline (58 mg, 50 mmol), $Pd(PPh_3)_2Cl_2$ (17.5 mg 2.5 mmol) and CuI (2.5 mg 1.3 mmol). The mixture was placed under nitrogen and anhydrous diisopropylamine (5.00 mL) was added. The reaction was let to stir at room temperature for 40 h. The solvent was removed by rotary evaporation and the remaining solid was dissolved in a mixture of methylene chloride and methanol. The mixture was then filtered through Celite™, and the solvent from the filtrate was removed my rotary evaporation. The product was recrystalized with methylene chloride twice to yield **5.19** as a red-brown powder (32.5 mg, 34%). ^{1}H NMR (400 MHz, DMSO-d_6) δ 8.00 (s, 2H), 7.36 (d, J = 8.8 Hz, 4H), 6.69 (d, J = 8.4 Hz, 4 H), 5.64 (s, 4H). ^{13}C NMR (100 MHz, DMSO-d_6) δ 153.8, 150.2, 136.5, 133.4, 126.9, 113.8, 108.0, 107.4, 98.3, 81.5, 46.8, 19.2.

5.21: ***N,N'-([1,1'-biphenylene]-4,4'-dimethylidyne)bis[N',N]'-dimethyl-1,2-ethanediamine***

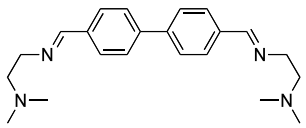

To a 25 mL round-bottom flask equipped with a stir bar was added N,N, dimethyl ethylene diamine (33.5 mg, 0.38 mmol) and [1,1'-biphenyl]-4,4'-dicarboxaldehyde (40 mg, 0.19 mmol). The mixture was placed under nitrogen and anhydrous acetonitrile (2 mL) was added via syringe. The reaction was let to stir at room temperature for 3 h. The solvent was removed by rotary evaporation to yield **5.21** as a white solid (49 mg 88%.) ^{1}H NMR (400 MHz, acetonitrile-d_3) δ 8.34 (s, 2H), 7.81 (d, J = 8.0 Hz, 4H), 7.73 (d, J = 8.9 Hz, 4 H), 3.69 (t, J = 85.5 Hz, 4H), 2.56 (t, J = 6.4 Hz, 4H), 2.22 (s, 12H). ^{13}C NMR (100 MHz, $CDCl_3$) 163.0, 144.16, 138.3, 130.6, 129.3, 119.5, 62.0, 61.5, 47.2, 2.6. HRMS (ESI) *m/z*: calcd for $C_{22}H_{30}N_4$ ($M+H^+$) 351.2543; found at 351.2543.

5.21_6• $Fe_4(ClO_4)_2$

To a 25 mL round-bottom flask equipped with a stir bar was added N,N, dimethyl ethylene diamine (33.5 mg, 0.38 mmol), [1,1'-biphenyl]-4,4'-dicarboxaldehyde (40 mg, 0.19 mmol) and and iron (II) perchlorate hexahydrate (46 mg, 0.12 mmol). The mixture was placed under nitrogen and anhydrous acetonitrile (2 mL) was added via syringe. The reaction was let to stir at room temperature for 3 h. The solvent was removed by rotary evaporation to yield product as a white solid (103 mg, 83%). ^{1}H NMR (400 MHz, acetonitrile-d_3) δ 8.50 (s, 12H), 7.94 (br s, 24H), 7.826 (br s, 24H), 3.90 (br s, 24H),

3.381 (br s, 24H), 2.907 (s, 72H). ^{13}C NMR (100 MHz, acetonitrile-d_3) δ 165.6, 144.2, 137.1, 131.6, 130.5, 129.1, 59.5, 54.4, 44.4.

5.23: ***N,N'-[1,1'-:4',1"-terphenylene] 4,4'-dimethylidyne)bis[N',N]'-dimethyl-1,2-ethanediamine***

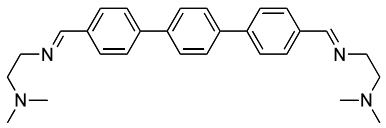

To a 25 mL round-bottom flask equipped with a stir bar was added N,N, dimethyl ethylene diamine (25 mg, 0.28 mmol) and [1,1'-:4',1"-terphenyl]-4,4'-dicarboxaldehyde (40 mg, 0.14 mmol). The mixture was placed under nitrogen and anhydrous acetonitrile (2 mL) was added via syringe. The reaction was let to stir at room temperature for 3 h. The solvent was removed by rotary evaporation to yield product as a white solid (59 mg , 99% yield.) ^{1}H NMR (75 MHz, $CDCl_3$) δ 8.37 (s, 2 H), 7.84 (d, *J* = 8.8 Hz, 4H), 7.72 (s, 4H), 7.71 (d, *J* = 8.4 Hz, 4H), 3.8 (t, *J* = 86.9 Hz, 4H), 2.67 (t, *J* = 7.3 Hz, 4H), 2.33 (s, 12H).

$5.23_6 \bullet Fe_4(ClO_4)_2$

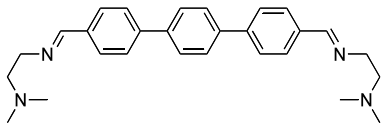

To a 25 mL round-bottom flask equipped with a stir bar was added N,N, dimethyl ethylene diamine (25 mg, 0.28 mmol), [1,1'-:4',1"-terphenyl]-4,4'-dicarboxaldehyde (40 mg, 0.14 mmol) and iron (II) perchlorate hexahydrate (34 mg, (0.09 mmol). The mixture was placed under nitrogen and anhydrous acetonitrile (2.00 mL) was added via syringe. The reaction was let to stir at room temperature for 24 hr. The precipate was filtered to

yield a brown powder (92 mg, 93%.) ^{1}H NMR (400 MHz, acetonitrile-d_3) δ 8.47 (s, 24H), 7.92 (br s, 24H), 7.84 (br s, 32H), 3.85 (s, 24H), 3.25 (br s, 24H), 2.80 (br s, 72H).

2,2'-(1,3-phenylene)bis[4,4,5,5-tetramethyl-1,3,2-dioxaborolane

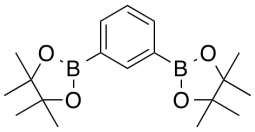

To a 50 mL round-bottom flask equipped with a stir bar and reflux condenser was added 3,5 dibromo benzene (500 mg, 2.1 mmol), *bis*(pinacolato)diboron (1.49 g, 4.4 mmol), [1,1'-*bis*(diphenylphosphino)ferrocene]dichloropalladium(II)dichloromethane (85 mg, 0.08 mmol) and potassium acetate (620 mg, 6.30 mmol). The mixture was placed under nitrogen and degassed 1,4 dioxane (5.00 mL) was added. The reaction was heated at 100^{o}C for 10 hr. The solvent was removed by rotary evaporation and product was extracted from the remaining solid from a mixture of methylene chloride (25 mL) and methanol (10 mL). The mixture was then filtered through Celite™ and the solvent from the filtrate was removed my rotary evaporation to yield a white solid (660 mg, 95% yield.) ^{1}H NMR (400 MHz, DMSO-d_6): δ 8.04 (s, 1 H), 7.79 (dd, J = 7.4 Hz, 2H), 7.4 (t, J = 7.2 Hz, 1H), 1.29 (s, 24H). ^{13}C NMR (100 MHz, DMSO-d_6): δ 141.4, 137.5, 128.0, 84.0, 24.9.

3,5-bis(4,4,5,5-tetramethyl-1,3,2-dioxaborolan-2-yl)-benzoic acid

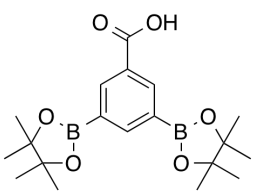

To a 50 mL round-bottom flask equipped with a stir bar and reflux condenser was added 3,5 dibromo benzoic acid (585 mg, 1.6 mmol), *bis*(pinacolato)diboron (1.05 g, 4.1 mmol), [1,1'-

bis(diphenylphosphino)ferrocene]dichloropalladium(II)dichloromethane (85 mg, 0.08 mmol) and potassium acetate (620 mg, 6.3 mmol). The mixture was placed under nitrogen and degassed 1,4 dioxane (5.00 mL) was added. The reaction was heated at 100^{o}C for 10 hr. The solvent was removed by rotary evaporation and product was extracted from the remaining solid from a mixture of methylene chloride (25.0 mL) and methanol (10.0 mL). The mixture was then filtered through celite and the solvent from the filtrate was removed my rotary evaporation to yield a white solid (486 mg, 83% yield.) ^{1}H NMR (400 MHz, $CDCl_3$): δ 8.64 (s, 2H), 8.47 (1H), 1.36 (s, 24H). ^{13}C NMR (400 MHz, $CDCl_3$): δ 172.0, 146.5, 139.4, 84.7, 25.2. HRMS (ESI) *m/z*: calcd for $C_{19}H_{28}B_2O_6$ ($M+NH_4^+$) 390.2483; found at 390.2388.

Experimental Procedures and Data Tables for X-ray Diffraction Studies of 2.8

An orange fragment of a prism (0.14 x 0.11 x 0.02 mm^3) was used for the single crystal x-ray diffraction study of $[C_{54}H_{54}N_8Cu]^+[PF_6]^-$. The crystal was coated with paratone oil and mounted on to a glass fiber. X-ray intensity data were collected at 100(2) K on a Bruker APEX2 version 2010.11-3 platform-CCD x-ray diffractometer system (fine focus x-ray tube, Mo-radiation, λ = 0.71073 Å, 50KV/30mA power). The CCD detector was placed at a distance of 5.0600 cm from the crystal.

A total of 3600 frames were collected for a sphere of reflections (with scan width of 0.3° in ω, starting ω and 2θ angles at –28°, ϕ angles of 0°, 90°, 120°, 180°, 240°, and 270° for every 600 frames, 120 sec/frame exposure time). The frames were integrated using the Bruker SAINT software package version V7.60A and using a narrow-frame integration algorithm. Based on a hexagonal crystal system, the integrated frames yielded a total of 24810 reflections at a maximum 2θ angle of 22.21° (0.94 Å resolution), of which 2068 were independent reflections (R_{int} = 0.1145, R_{sig} = 0.0478, redundancy = 12.0, completeness = 100%) and 1514 (73.2%) reflections were greater than 2σ(I). The unit cell parameters were, **a** = **b** = 12.436(3) Å, **c** = 54.758(12) Å, $\alpha = \beta = 90^o$, $\gamma = 120^o$, V = 7334(3) $Å^3$, Z = 6, calculated density D_c = 1.444 g/cm^3. Absorption corrections were applied (absorption coefficient μ = 0.573 mm^{-1}; max/min transmission = 0.9864/0.9256) to the raw intensity data using the SADABS program version 2008/1.

The Bruker SHELXTL software package version 2008/4 was used for phase determination and structure refinement. The distribution of intensities (E^2-1 = 0.924) and

systematic obverse absent reflections indicated two possible space groups, R-3 and R3. The space group R-3 (#148) was later determined to be correct. Direct methods of phase determination followed by two Fourier cycles of refinement led to an electron density map from which most of the non-hydrogen atoms were identified in the asymmetry unit of the unit cell. With subsequent isotropic refinement, all of the non-hydrogen atoms were identified. There were one PF_6-anion, one $C_{54}H_{54}N_8Cu$ cation and half a disordered-DMSO solvent molecule present in the asymmetry unit of the unit cell. The PF_6-anion was located at the 3-fold screw-axis, the disordered-DMSO solvent molecule and the $C_{54}H_{54}N_8Cu$ cation were located at the 3-fold inversion symmetry. The disordered DMSO molecule is refined isotropically using a rigid-body geometry and with DFIX, DELU, SIMU and SUMP restraints. All the Ueq of the DMSO atoms were restrained using two FVAR variables for the two disordered-DMSO components. The crystal sample is very small where it only diffracted to a maximum angle of 22.21^o in the theta range giving the Alert A warning in the checkcif validation procedure. The short H…H contact Alerts A and B warnings are mainly due to the disordered positions of the DMSO atoms. The Alerts C and G warnings are mainly because of the small crystal size and the disordered DMSO molecule. Although the data quality is marginal because of the small crystal size and disordered-DMSO, giving rise to higher standard uncertainty in the bond-lengths and angles, the accuracy of the crystal structure is correct.

Atomic coordinates, isotropic and anisotropic displacement parameters of all the non-hydrogen atoms were refined by means of a full matrix least-squares procedure on F^2. The H-atoms were included in the refinement in calculated positions riding on the

atoms to which they were attached. The refinement converged at R1 = 0.0484, wR2 = 0.1119, with intensity, $I>2\sigma(I)$. The largest peak/hole in the final difference map was 0.519/-0.437 e/Å^3.

Table 6.1 Crystal data and structure refinement for **2.8**.

Empirical formula	$CuC_{55}H_{57}PF_6N_8$
Formula weight	1062.63
Temperature, K	100(2)
Wavelength, Å	0.71073
Crystal system	Rhombohedral
Space group	*R*-3
Unit cell dimensions:	
a, Å	2.436(3)
b, Å	*b* = 12.436(3)
c, Å	*c* = 54.758(12)
Volume, $Å^3$	7334(3)
α, °	90
β, °	90
γ, °	120
Z	6
Calculated density, mg/m^3	1.444
Absorption coefficient, mm^{-1}	0.573
F(000)	3318
Crystal size, mm^3	0.14 x 0.11 x 0.02
Theta range for data collection, °	1.93 to 22.21
Index ranges	-13<=*h*<=13, -13<=*k*<=13, -58<=*l*<=58
Reflections collected	24810
Independent reflections	2068 [R_{int} = 0.1145]
Completeness to θ = 22.21°	100.0 %
Absorption correction	Semi-empirical from equivalents
Max. and min. transmission	0.9864 and 0.9256
Refinement method	Full-matrix least-squares on F^2
Data / restraints / parameters	2068 / 20 / 239
Goodness-of-fit on F^2	1.034
Final R indices [I>2σ(I)]	*R*1 = 0.0484, *wR*2 = 0.1119
R indices (all data)	*R*1 = 0.0772, *wR*2 = 0.1279
Largest diff. peak and hole, $e.Å^{-3}$	0.519 and -0.437

Experimental Procedures and Data Tables for X-ray Diffraction Studies of 2.15

An orange prism fragment (0.33 x 0.25 x 0.19 mm^3) was used for the single crystal x-ray diffraction study of $[C_{54}H_{54}N_8Cu_2]^{2+}[PF_6]_2^-$. The crystal was coated with paratone oil and mounted on to a cryo-loop glass fiber. X-ray intensity data were collected at 100(2) K on a Bruker APEX2 version 2012.2.2 platform-CCD x-ray diffractometer system (fine focus Mo-radiation, l = 0.71073 Å, 50KV/35mA power). The CCD detector was placed at a distance of 5.0800 cm from the crystal.

A total of 2400 frames were collected for a hemisphere of reflections (with scan width of 0.3^o in w, starting w and 2q angles at -30^o, and f angles of 0^o, 90^o, 180^o, and 270^o for every 360 frames, 30 sec/frame exposure time). The frames were integrated using the Bruker SAINT software package version V8.18C and using a narrow-frame integration algorithm. Based on a monoclinic crystal system, the integrated frames yielded a total of 91824 reflections at a maximum 2q angle of 60.06^o (0.71 Å resolution), of which 17406 were independent reflections (R_{int} = 0.0253, R_{sig} = 0.0189, redundancy = 5.3, completeness = 100%) and 14990 (86.1%) reflections were greater than 2s(I). The unit cell parameters were, **a** = 18.4499(4) Å, **b** = 18.7445(4) Å, **c** = 18.9098(4) Å, **b** = $114.604(1)^o$**,** V = 5945.9(2) $Å^3$, Z = 4, calculated density D_c = 1.566 g/cm^3. Absorption corrections were applied (absorption coefficient m = 0.930 mm^{-1}; max/min transmission = 0.8424/0.7490) to the raw intensity data using the SADABS program version 2008/1.

The Bruker SHELXTL software package verion 2008/4 was used for phase determination and structure refinement. The distribution of intensities (E^2-1 = 0.955) and systematic absent reflections indicated one possible space group, P2(1)/n. The space group P2(1)/n

(#14) was later determined to be correct. Direct methods of phase determination followed by two Fourier cycles of refinement led to an electron density map from which most of the non-hydrogen atoms were identified in the asymmetric unit of the unit cell. With subsequent isotropic refinement, all of the non-hydrogen atoms were identified. There was one cation of $C_{54}H_{54}N_8Cu_2$, two anion of PF_6, one partially occupied (76% occupied) water molecule, and two molecules of DMSO present in the asymmetric unit of the unit cell. One of the two DMSO molecules was modeled with disorder (DMSO disorder site occupancy ratio was 60%/40%). Hydrogen bond distances and angles of the partially occupied water is given in Table 7. The B-level alert was due to the model of the disordered-DMSO molecule.

Atomic coordinates, isotropic and anisotropic displacement parameters of all the non-hydrogen atoms were refined by means of a full matrix least-squares procedure on F^2. The H-atoms were included in the refinement in calculated positions riding on the atoms to which they were attached, except the H-bonding hydrogen atoms were restrained with DFIX command. The refinement converged at R1 = 0.0304, wR2 = 0.0780, with intensity I>2s (I). The largest peak/hole in the final difference map was 0.573/-0.582 e/$Å^3$.

Table 6.2 Crystal data and structure refinement for **2.15**.

Empirical formula	$Cu_2C_{55}H_{57}PF_6N_8$
Formula weight	1402.02
Temperature, K	100(2)
Wavelength, Å	0.71073
Crystal system	Monoclinic
Space group	*P*2(1)/*n*
Unit cell dimensions:	
a, Å	18.4499(4)
b, Å	*b* = 18.7445(4)
c, Å	*c* = 18.9098(4)
α, °	90
β, °	114.604(1)
γ, °	90
Volume, $Å^3$	5945.9(2)
Z	4
Calculated density, mg/m^3	1.566
Absorption coefficient, mm^{-1}	0.930
F(000)	2886
Crystal size, mm^3	0.33 x 0.25 x 0.19
Theta range for data collection, °	1.61 to 30.03
Index ranges	-25<=*h*<=25, -26<=*k*<=26, -26<=*l*<=26
Reflections collected	91824
Independent reflections	17406 [R_{int} = 0.0253]
Completeness to θ = 30.03°	100.0 %
Absorption correction	Semi-empirical from equivalents
Max. and min. transmission	0.8424 and 0.7490
Refinement method	Full-matrix least-squares on F^2
Data / restraints / parameters	17406 / 68 / 834
Goodness-of-fit on F^2	1.027
Final R indices [I>2σ(I)]	*R*1 = 0.0304, *wR*2 = 0.0780
R indices (all data)	*R*1 = 0.0381, *wR*2 = 0.0819
Largest diff. peak and hole, *e*.$Å^{-3}$	0.573 and -0.582

References

1.) Boiocchi, M.; Bonizzoni, M.; Fabbrizzi, L.; Piovani, G.; Taglietti, A. "A Dimetallic Cage with a Long Ellipsoidal Cavity for the Fluorescent Detection of Dicarboxylate Anions in Water" *Angew. Chem. Int. Ed*. **2004**, *43*, 3847-3852.